

**LATE CARBONIFEROUS CYCLOTHEMS AND ORGANIC FACIES
IN THE PHALEN-BACKPIT SEAM INTERVAL, SYDNEY
COALFIELD, NOVA SCOTIA**

By: Judith Christine White

submitted in partial fulfillment of the requirements
for the degree of MASTER OF SCIENCE at Dalhousie
University, Halifax, Nova Scotia

© Copyright by Judith C. White, 1992

DALHOUSIE UNIVERSITY
DEPARTMENT OF EARTH SCIENCES

The undersigned hereby certify that they have read and recommended to the Faculty of Graduate Studies for acceptance a thesis entitled "LATE CARBONIFEROUS CYCLOTHEMS AND ORGANIC FACIES IN THE PHALEN-BACKPIT SEAM INTERVAL, SYDNEY COALFIELD, NOVA SCOTIA" by Judith C. White in partial fulfillment of the requirements for the degree of Master of Science.

Dated 18 August 1992

External Examiner

DALHOUSIE UNIVERSITY

Date August 18, 1992

Author Judith Christine White
Title Late Carboniferous cyclothems and organic facies
in the Phalen-Backpit seam interval, Sydney
Coalfield, Nova Scotia
Department or School Department of Earth Sciences
Degree: M. Sc. Convocation October Year 1992

Permission is herewith granted to Dalhousie University to circulate and to have copied for non-commercial purposes, at its discretion, the above title upon the request of individuals or institutions.

THE AUTHOR RESERVES OTHER PUBLICATION RIGHTS, AND NEITHER THE THESIS NOR EXTENSIVE EXTRACTS FROM IT MAY BE PRINTED OR OTHERWISE PRODUCED WITHOUT THE AUTHOR'S WRITTEN PERMISSION.

THE AUTHOR ATTESTS THAT PERMISSION HAS BEEN OBTAINED FOR THE USE OF ANY COPYRIGHTED MATERIAL APPEARING IN THIS THESIS (OTHER THAN BRIEF EXCERPTS REQUIRING ONLY PROPER ACKNOWLEDGMENT IN SCHOLARLY WRITING) AND THAT ALL SUCH USE IS CLEARLY ACKNOWLEDGED.

DEDICATION

In loving memory of
George Vallis Pilgrim

Table of Contents

	Page
List of Figures	viii
List of Tables	x
List of Plates	xi
Abstract	xii
Acknowledgements	xiii
1. Introduction	
1.1. Introduction	1
1.2. Aim and Scope of Thesis	4
1.3. Geological Setting and Background	7
1.4. Tectonic Setting	9
1.5. Stratigraphy	12
2. Cyclothem Facies Successions Within the Phalen- Backpit Interval	
2.1. Introduction	15
2.2. Cyclothem Recognition Within the Phalen- Backpit Interval	16
2.3. Sedimentary Facies	19
2.3.1. Channels	
2.3.1.1. Major Channel	20
2.3.1.2. Abandoned Channel-fill	25
2.3.2. Vegetated Floodplain	
2.3.2.1. Levee/Crevasse Splay	26
2.3.2.2. Minor Channel	26
2.3.2.3. Poorly-drained Floodplain Soil	27
2.3.2.4. Well-drained Floodplain Soil	28
2.3.3. Calcareous Paleosol	29
2.3.4. Lacustrine/Bay-fill	
2.3.4.1. Organic-poor lacustrine/bay-fill	30

	Page
2.3.4.2. Organic-rich lacustrine/bay-fill	30
2.3.4.3. Delta	31
2.3.5. Mire	32
2.4. Sedimentary Patterns	
2.4.1. Vertical Distribution	33
2.4.2. Lateral Distribution	34
2.5. Controls on Cyclothem Patterns in the PBI.	36
2.6. Summary	39
3. The Backpit Seam: A Record of Peat Accumulation and Termination in a Late Westphalian Paleomire	
3.1. Introduction	41
3.2. The Backpit Seam	42
3.3. Summary of Methods	45
3.4. Results	
3.4.1. Mineral Matter: Occurrence and Distribution	47
3.4.2. Lithotypes	
3.4.2.1. Character and Distribution	49
3.4.2.2. Fusain: A Distinctive Lithotype	52
3.4.2.3. Lithotype Successions	52
3.4.3. Macerals and Microlithotypes	
3.4.3.1. Introduction	53
3.4.3.2. Automated Image Analysis	54
3.4.3.3. Group Maceral Composition	57
3.4.3.4. Detailed Maceral Composition	63
3.4.3.5. Microlithotype Composition	65
3.4.4. Coal Facies Analysis	
3.4.4.1. Seam Intervals	67
3.4.4.2. Microlithotype-derived Coal Facies	69
3.4.4.3. Maceral-derived Coal Facies	72
3.5. Discussion	
3.5.1. Paleogeographic Setting	75

	Page
3.5.2. Backpit Mire Evolution	76
3.5.3. Fusain: A Fire Origin	79
3.5.4. Ombrotrophic Versus Rheotrophic Mires	81
3.5.5. Significance of Vertical Coal Facies	83
3.6 Summary	84
4. The Backpit Roof Unit: A Zone of Maximum Transgression Within a Cyclothem Package	
4.1. Introduction	87
4.2. The Backpit Roof Unit	89
4.3. Summary of Methods	89
4.4. Results	
4.4.1. Megascopic Facies	
4.4.1.1. Description	91
4.4.1.2. Vertical Facies Trends	96
4.4.2. Mineral Matter	
4.4.2.1. Ash and Sulphur	98
4.4.2.2. Minerals	98
4.4.3. Organic Matter	
4.4.3.1. Organic Components	102
4.4.3.2. Source Rock Character	104
4.4.4. Fossil Content	110
4.5. Discussion	
4.5.1. Environmental Significance of Fossils	117
4.5.2. Interpretation of Facies	121
4.5.3. Lepositional Setting	125
4.5.4. Source Rock Potential	126
4.6. Summary	127

	Page
5. Economic Significance of the Phalen-Backpit Interval	
5.1. Introduction	129
5.2. Energy Resource	129
5.3. Associated Facies	130
5.4. Summary	131
6. Conclusions	132

List of Figures

Figure 1.1. The extent of the Sydney Basin within the larger Maritimes Basin.	2
Figure 1.2. The onshore distribution of the Morien Group.	3
Figure 1.3. Schematic representation of the Phalen-Backpit Interval (PBI), in stratigraphic context ..	5
Figure 1.4. Generalized stratigraphy of the Phalen to lower Bouthillier seam interval from a section roughly parallel to depositional strike.	6
Figure 1.5. Stratigraphy of the Sydney Basin.	10
Figure 2.1. Detailed cross-section of measured coastal sections and cores.	enclosure
Figure 2.2. Generalized stratigraphy of the study interval, highlighting channels and laterally extensive coals, limestones, red mudstones and calcareous paleosol horizons.	17
Figure 2.3. Profiles of selected depositional facies assemblages a)Cyclothem 2, Victoria Mines, b)Cyclothem 3, Victoria Mines, c)Cyclothem 3, Longbeach, d)Cyclothem 1, Donkin West.	23
Figure 2.4. The distribution of a)sediment groups and b)depositional facies, in the PBI.	35
Figure 3.1. Frequency histograms generated from manual Ro analyses (random measurements).	43

	Page
Figure 3.2. Distribution of the Backpit seam and Backpit roof unit and lateral correlation of facies.	44
Figure 3.3. Sulphur and ash distribution in the Backpit seam and associated strata.	48
Figure 3.4. Lithotype logs for the Backpit seam: A- Bras d'Or; B-Sydney Mines; C-Victoria Mines; E-Glace Bay West; G-Donkin West.	50
Figure 3.5. Distribution of lithotypes, pyrite and coaly shale in the Backpit seam.	51
Figure 3.6. Average group maceral composition, by lithotype, for each Backpit seam section.	58
Figure 3.7. Group maceral composition profiles, by lithotype and seam interval for a) B-Sydney Mines (IBAS-2) and b) C-Victoria Mines (IBAS-2). ..	61
Figure 3.8. Group maceral composition profiles, by lithotype and seam interval for a) E-Glace Bay West (IBAS-2) and b) E'-Glace Bay West (Manual). ..	62
Figure 3.9. Average microlithotype composition for each lithotype, Glace Bay West seam section.	66
Figure 3.10. Microlithotype compositional variation, by lithotype, for the Glace Bay West seam section.	68
Figure 3.11. Microlithotype group composition of the Backpit seam, Glace Bay West; plotted on a modified facies diagram of Hacquebard and Donaldson (1969). a. lithotypes; b. seam intervals.	71
Figure 3.12. Facies characterization of the Backpit seam, Glace Bay West; plotted on a modified facies diagram of Diessel (1986). a. lithotypes; b. seam intervals.	74
Figure 4.1. Vertical and lateral distribution of facies in the Backpit roof unit (BRU), from a section roughly parallel to depositional strike. ..	90
Figure 4.2. Stereonet plot of poles to bedding and crenulation lineations for the study area.	95

	Page
Figure 4.3. Summary of vertical facies trends for the BRU.	97
Figure 4.4. BRU mineral, organic matter and fossil trends for: a. Sydney Mines (B) and b. Glace Bay West (E).	99
Figure 4.5. Thin section abundance estimates from the BRU - a)C-136; b)C-137.	100
Figure 4.6. Rock-Eval trends for coastal sections: A-Bras d'Or; B-Sydney Mines; C-Victoria Mines; E-Glace Bay West; G-Donkin West; H-Donkin East and J-Longbeach.	105
Figure 4.7. Rock-Eval trends for offshore cores: C-136; C-137.	106
Figure 4.8. Hydrogen Index-Oxygen Index (HI-OI) plots for: A-Bras d'Or; B-Sydney Mines; C-Victoria Mines; E-Glace Bay West; C-136; C-137; G-Donkin West; H-Donkin East; J-Longbeach and BRU Avg-average per section studied.	108
Figure 4.9. Classification of isolated fish fossils from the BRU.	116
 List of Tables	
Table 1.1. Stratigraphic summary of the Morien Group, Sydney Basin.	13
Table 2.1. Sediment groups in the PBI.	20
Table 2.2. Depositional facies in the PBI.	21
Table 3.1. Lithotype classification scheme.	46
Table 3.2. Detailed maceral/minerals included in manual counts.	55
Table 3.3. Microlithotypes included in manual counts.	56
Table 4.1. Backpit roof unit (BRU) facies description.	92

	Page
Table 4.2. Fossil distribution in the BRU - Sydney Mines section.	111

Table 4.3. Fossil distribution in the BRU - Glace Bay West section.	112
---	-----

List of Plates

Plate 1. Sedimentary structures and facies	136
Plate 2. Sedimentary structures and facies	138
Plate 3. Paleosol horizons	140
Plate 4. The Backpit seam	142
Plate 5. Coal photomicrographs	144
Plate 6. Slabbed core C-136	146
Plate 7. Slabbed core C-137.....	147
Plate 8. <u>Anthraconauta phillipsii</u> , plan view and slabbed section	148
Plate 9. BRU photomicrographs	149

APPENDICES

Appendix 1 - Sedimentology - Field Measurements and Core Description.	151
Appendix 2 - Backpit Coal - Sample Collection and Analysis	158
Appendix 3 - Backpit Roof Unit - Sample Collection and Analysis	236
References	260

ABSTRACT

Three Westphalian D cyclothems were studied from the coal-bearing Sydney Mines Formation, Cape Breton Island, Nova Scotia. Allogenic (glacioeustatic?) processes, and superimposed autogenic processes, were responsible for cyclothem facies successions: 1)lake/bay-fill and distributary channel, 2)well-drained floodplain, 3)poorly-drained floodplain to coastal plain and 4)extensive mire. Major coal seams, organic-rich limestone/shale units, red mudstone and nodular carbonate layers are laterally extensive which suggests regional controls on their formation.

The Backpit seam and limestone/shale roof unit (top of Cyclothem 2) contain a detailed record of basinal processes over an extended period. The Backpit seam is a high volatile B to A bituminous coal ($R_o = 0.69-0.76\%$), with moderate to high ash (avg- $15.3 \pm 6\%$) and sulphur (avg- $5.2 \pm 2\%$). Banded lithotypes constitute a major portion of the seam; vitrinite macerals and vitrinite-rich microlithotypes predominate. Distinct fusain bands are common and represent the charred remains of ancient fires. Some dull to coaly shale layers can be correlated across the onshore portion of the basin for more than 45 km.

The Backpit peat accumulated in a rheotrophic mire, elongated parallel to depositional strike. Coal facies patterns indicate a wetting upward trend in the upper portion of the seam that culminated in the flooding of the mire and the formation of a broad, shallow lake or bay. Agglutinated foraminifera extracted from the underclay and the roof strata support a coastal setting for the mire. The abundance of fresh to brackish tolerant fauna such as bivalves, ostracods, serpulids, sharks and other fish in the Backpit roof unit and the paucity of open marine fauna suggest that the area was protected from open marine inundation.

ACKNOWLEDGEMENTS

I thank Dr. Martin Gibling for excellent supervision and helpful suggestions that improved the final text. Thanks go to Dr. David Scott, for his interest and comments on an earlier draft, Dr. Paul Schenk for helpful advice and Dr. Wolfgang Kalkreuth for guidance in organic petrology and review of the text. Dr. Kalkreuth also provided access to the Institute of Sedimentary Geology (ISPG) facilities, including an automated image analysis system (IBAS-2). Ken Pratt gave technical assistance using this system and discussed potential problems of the technique. Rock-Eval pyrolysis data was generated by the Geochemistry Laboratory, ISPG.

Jim Wilson, Environmental Services Laboratory, provided unlimited use of a petrographic microscope and Steve Forgeron, Cape Breton Development Corporation (CBDC), provided access to offshore cores. Richard Nearing and his staff at the Coal Laboratory, CBDC, completed ash and sulphur analyses.

The thesis benefited from discussions with Nova Scotia Department of Natural Resources geologists, including Robert Naylor, Don MacNeil and John Calder. Core NC-87-1, logged by Don MacNeil, was included in some diagrams. Access to core SMS-91-29B, drilled by the Department, was arranged by Robert Naylor, and his interest in this project is greatly appreciated. Black-and-white plates were photographed and reproduced by Reg Morrison.

Gordon Brown, Dalhousie University, prepared thin sections and Bill Parkins, Brock University, provided valuable data on the fossil distributions in the Backpit roof unit. Discussions with Winton Wightman, Dalhousie University, provided useful information on foraminifera assemblage distributions and their significance in the study interval.

Johannes Paul and Mai Nguyen are thanked for field

assistance and insightful discussions. Mai also drafted several diagrams and this is greatly appreciated. Chris White provided much needed support, both technical and emotional, during my term as a graduate student.

Financial support was provided by a Natural Science and Engineering Research Council (NSERC) postgraduate scholarship, a Texaco Research Scholarship, and a NSERC operating grant to Dr. Martin Gibling.

1. INTRODUCTION

1.1. INTRODUCTION

The Late Carboniferous Sydney Mines Formation (SMF), of the Sydney Coalfield, Nova Scotia (Figs. 1.1 and 1.2), has long been eastern Canada's major resource of economic coal. The formation consists of stacked intervals of clastic strata and coal, referred to as cyclothems in this study, based on the original definition of the term (Wanless and Weller, 1932, p. 1003). The SMF cyclothems, about 30 m thick on average, include repeated sequences of sandstone, shale, limestone and coal that represent alternate continental and marginal marine conditions within a sedimentary package (Gibling and Bird, submitted). Cyclothem development during the Pennsylvanian period has been attributed to allogenic mechanisms such as glacioeustatic sea-level fluctuation driven by climate change (Wanless and Shepard, 1936; Heckel, 1986; Veevers and Powell, 1987); tectonic activity (Weller, 1930; 1956; Tankard, 1986); or a combination of the two processes (Klein and Willard, 1989; Chesnut and Cobb, 1989; Klein and Kupperman, 1992). Other workers have invoked autogenic processes such as differential compaction of underlying sediment, channel avulsion, crevasse progradation and delta switching (Heide, 1964; Beerbower, 1969; Ferm, 1970, 1979).

The uncertain paleogeographic position of the SMF has remained a problem for geologists working in the basin for the last 150 years. The lack of diagnostic "open marine" bands has led many workers to question the possibility of a marine connection for the basin, although sedimentology and coal seam geometry would suggest such a connection (Hacquebard et al., 1967). The recent documentation of cyclothems (Gibling and Bird, submitted) and agglutinated foraminifera in strata associated with the coals (Thibaudeau and Medioli, 1986; Thibaudeau et al., 1987; Wightman et al., 1992) supports a paralic setting for the basin and provides

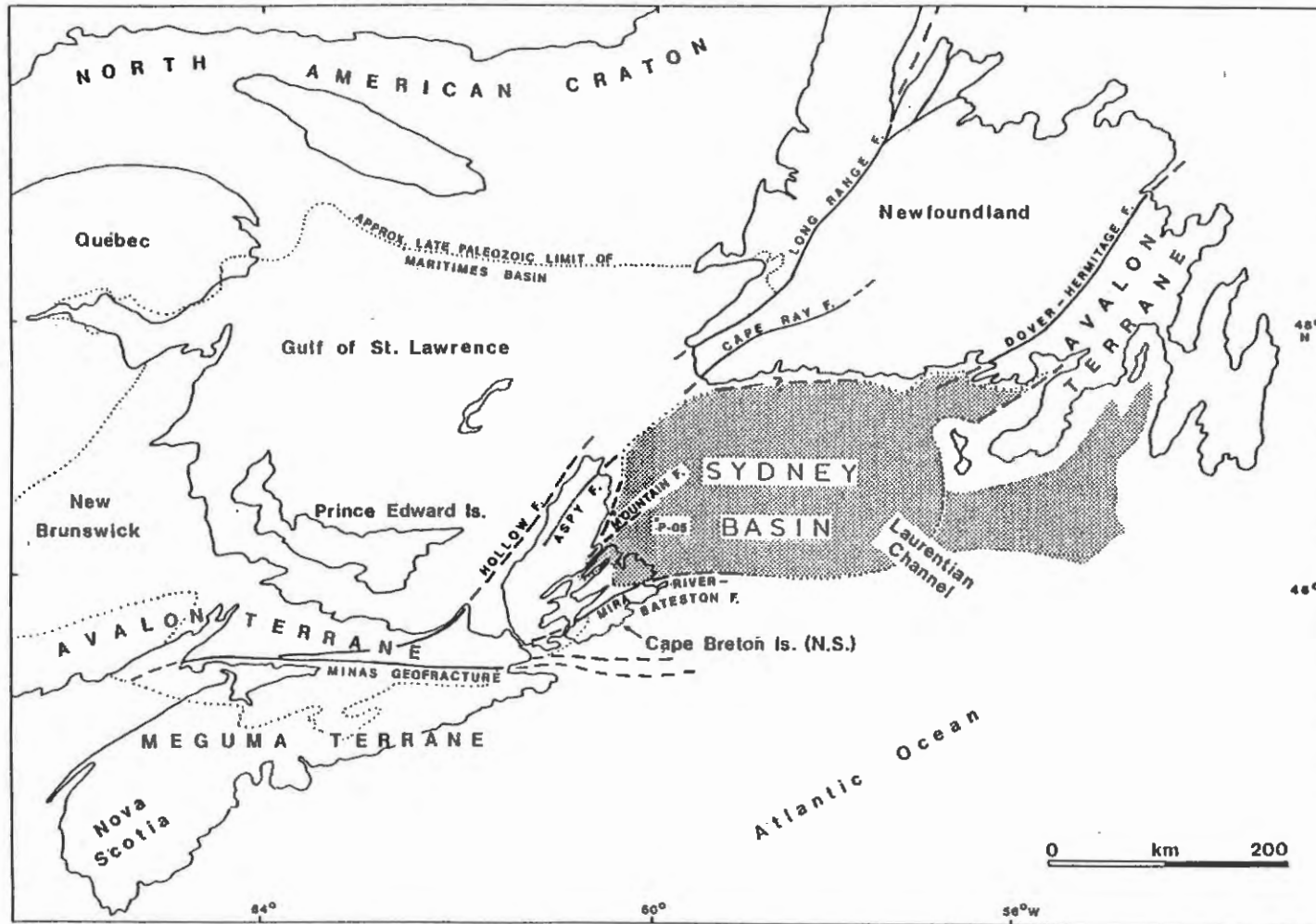


Figure 1.1. The extent of the Sydney Basin (shaded) within the larger Maritimes Basin (dotted outline). (From Gibling *et al.*, 1987).

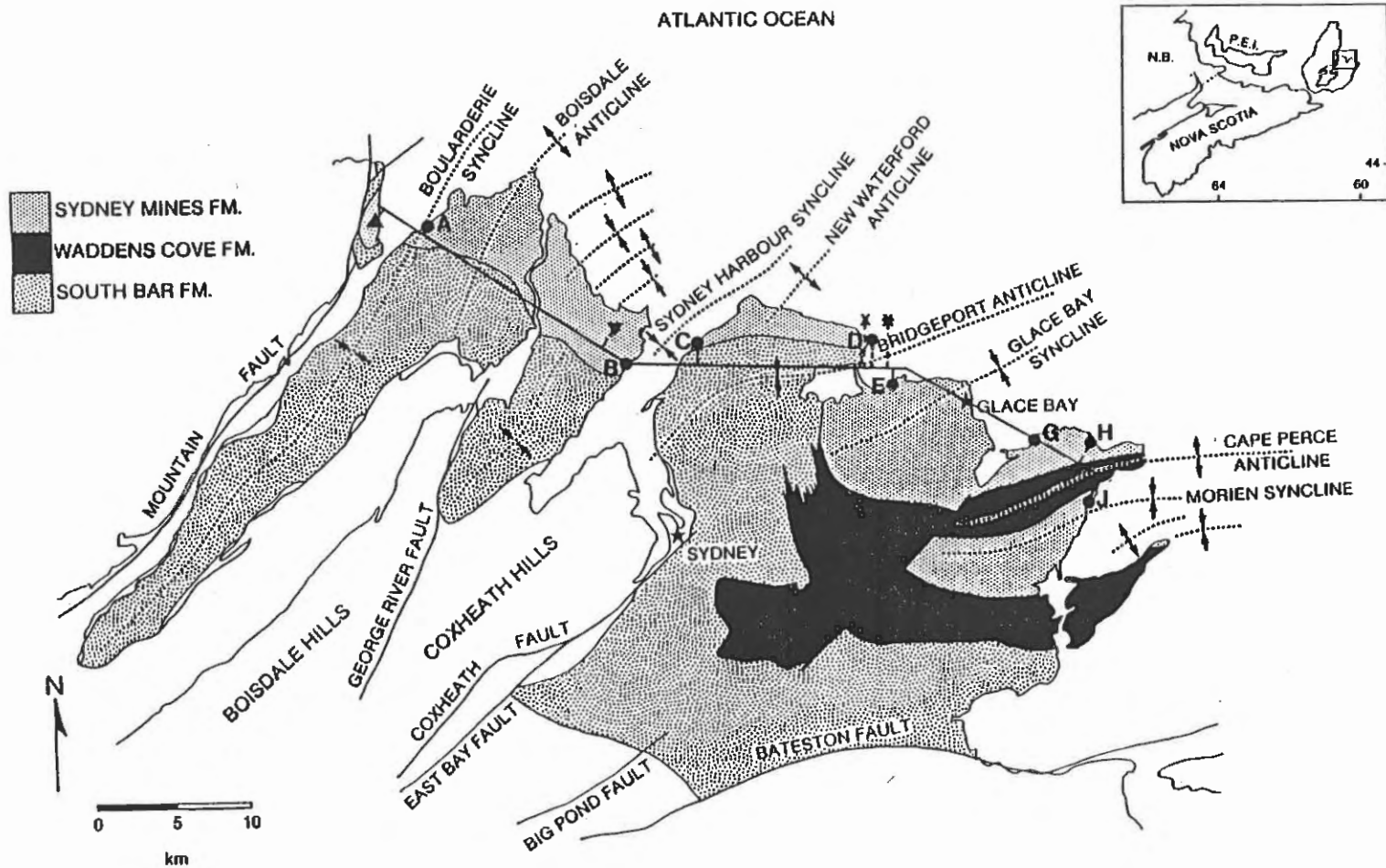


Figure 1.2. The onshore distribution of the Morien Group. Letters represent coastal outcrops of the Phalen-Backpit Interval (PBI) as follows (from west to east): A- Bras d'Or; B-Sydney Mines; C-Victoria Mines; D-New Waterford; E-Glace Bay W; G- Donkin W; H- Donkin E; J-Longbeach. Symbols represent core locations as follows (from west to east): ▲-NC-87-1; ▼-SMS-91-29B; x-C-137; ✕-C-136.

a conceptual framework for the more detailed facies analysis reported in this thesis.

Cliff sections along the northeast coast of Cape Breton Island provide an excellent natural laboratory for the study of these coal-bearing cyclothem. Coeval stratigraphic intervals are exposed in a series of coastal sections, from northwest to southeast, parallel to depositional strike (Fig. 1.2). This project studies the vertical and lateral distribution of siliciclastic and organic facies within two cyclothem packages and relates these patterns to base-level fluctuations and basinal processes.

1.2. AIM AND SCOPE OF THESIS

The study interval, within the SMF, ranges in thickness from 20 to 40 m and is defined stratigraphically by two major coal seams - from the top of the Phalen seam to the top of the Backpit seam (referred to as the Phalen-Backpit interval, PBI, Fig. 1.3). An unnamed seam between the Phalen and Backpit seams divides the PBI into two cyclothem packages (1 and 2, Fig 1.4), the base of each being placed at the top of the relevant coal seam or its organic-rich roof rock. The unnamed seam can be traced from the western basin margin to the Glace Bay area but cannot be traced farther east as the Donkin West section (G) is affected by faulting (Fig. 1.4). General locations for coastal sections (letters) and core (symbols) examined in this study are found on Figure 1.2, with detailed location maps in Appendix 1.

Integration of the disciplines of sedimentology and organic petrology has enabled the characterization of the PBI both laterally and vertically within the basin. Field measurements, core descriptions and laboratory analyses were used to address the major questions considered in this thesis:

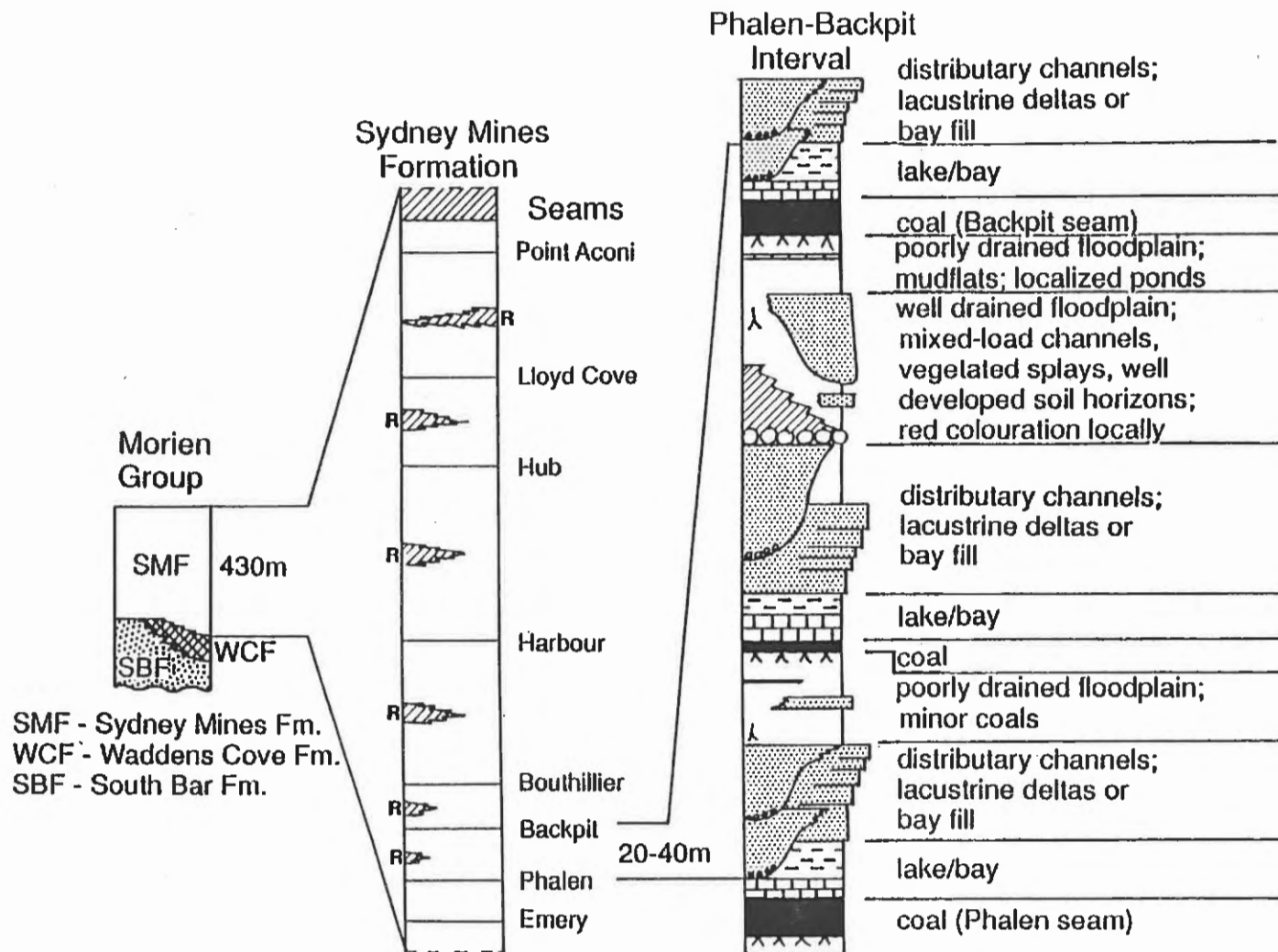


Figure 1.3. Schematic representation of the Phalen-Backpit Interval (BPI) in stratigraphic context. R - red mudstone interval.

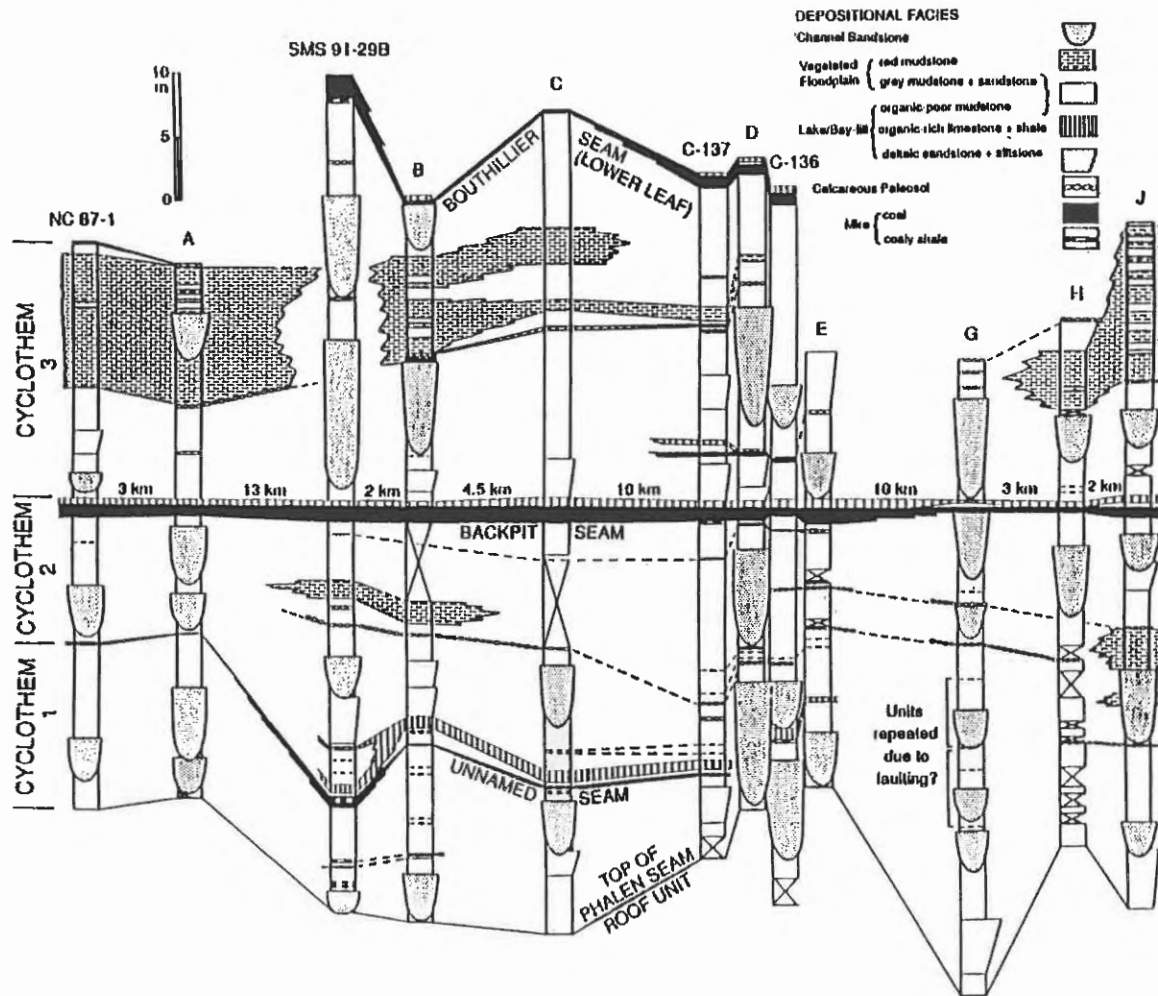


Figure 1.4. Generalized stratigraphy of the Phalen to lower Bouthillier seam interval from a section roughly parallel to depositional strike (see map, Fig. 1.2).

1. What are the sedimentary patterns and lateral facies variations within the cyclothem packages? (Chapter 2)
2. What base-level trends can be established from the succession of interseam strata? (Chapter 2)
3. What compositional trends can be documented for the Backpit seam and how do these relate to base-level variation and paleomire evolution? (Chapter 3)
4. What is the paleoenvironmental significance of the Backpit limestone/shale roof unit? (Chapter 4)

The thesis is presented as three main chapters (2-4), each of which forms the basis for a scientific paper to be submitted following completion of the thesis. Consequently, most data tables and accounts of detailed methodology are included in the attached Appendices to which reference will be made as appropriate. Each Appendix is assigned a number preceded by an 'A'; text, figures or tables from Appendices will be noted with this prefix (e.g. Table A3.12). Chapter 1 serves as a general introduction to the thesis, with an overview of the regional geology. Chapter 5 is a brief account of the economic implications and Chapter 6 summarizes the main conclusions of the thesis.

1.3. GEOLOGICAL SETTING AND BACKGROUND

The Sydney Basin, a fault-bounded Carboniferous basin in Atlantic Canada, is at least 36,000 km² in area (Hacquebard, 1983). It is an erosional remnant of the extensive Maritimes Basin that covered much of the Atlantic region during the Late Paleozoic (Fig. 1.1).

More than 95% of the Sydney Basin is currently submarine. Shipboard seismic, acoustic techniques and drilling have outlined an elongate easterly trending basin (Fig. 1.1) that extends under the Laurentian Channel, almost as far as the coast of Newfoundland (King and MacLean, 1976; Avery and Bell, 1985; King *et al.*, 1986). Loncarevic *et al.* (1989) outlined a more confined, elongate basin, based

on gravity data, although no attempt was made to define basin margins. They recognised a basement high across the Laurentian Channel off the tip of northern Cape Breton Island, which separates the Sydney Basin from the larger Late Paleozoic depocentre in the Gulf of St. Lawrence. The coal-bearing Sydney Mines Formation terminates against this basement high in the offshore region (Grant, 1992).

The first written accounts of the geology of the Sydney Basin are found in 19th century reports such as those of Brown (1871) and Robb (1876). W. A. Bell and co-workers made significant contributions to the fields of stratigraphy and paleobotany (Hayes and Bell, 1923; Bell, 1927, 1938, 1944). Detailed maps of the Sydney Basin were published based on years of field work by Hayes, Bell and Goranson (Hayes and Bell, 1923; Hayes et al., 1938a, b; Bell and Goranson, 1938). These maps formed the basis for a more recent mapping project by the Nova Scotia Department of Mines and Energy (NSDME) (Boehner and Giles, 1986).

As underground mining practices developed, a series of reports on the geology from a sedimentological and structural viewpoint were published, with emphasis on implications for mining (e.g. Gray and Gray, 1941; Haites, 1950, 1951, 1952; Duff et al., 1982; Forgeron et al., 1986). Hacquebard and co-workers published detailed coal compositional studies from both a microscopic and regional perspective (e.g. Hacquebard et al., 1964, 1967; Hacquebard and Donaldson, 1969; Hacquebard and Avery, 1982). Coal maceral and spore compositional data were used to interpret depositional environment and aid in regional correlation.

Recent investigations in the Sydney Basin include a refinement of the stratigraphy (Boehner and Giles, 1986) and a focus on sedimentological processes and tectonic influences (Gibling et al., 1987; Rust et al., 1987; Gibling and Rust, 1990 a, b; Rust and Gibling, 1984, 1990; Masson and Rust, 1990). Other workers have concentrated on faunal,

floral and palynological studies (Copeland, 1957; Zodrow and McCandlish, 1978, 1980; Vasey and Zodrow, 1983; Vasey, 1983; Masson and Rust, 1983, 1984; Dolby, 1988, 1989; Thibaudeau and Medioli, 1986; Thibaudeau et al., 1987; Wightman et al., 1992). Zodrow and Cleal (1985) have published correlations with Europe based on paleobotany.

1.4. TECTONIC SETTING

The Sydney Basin occupied a position near the equator during most of the Carboniferous (Ziegler, 1981; Scotese and McKerrow, 1990). The basin contains up to 4 km of sedimentary fill and is divided into two fining upward megasequences separated by a major hiatus (Gibling et al., 1987) (Fig. 1.5). Regional tectonics associated with orogenesis in the Appalachian region played a major role in the style of deposition within these megasequences. Sedimentation was initiated following the mid to late Devonian Acadian Orogeny, the result of oblique collision of the North American Craton with the European/African plate (Schenk, 1978, 1981; Bradley, 1982; Keppie, 1985). Mountain building continued from the late Devonian to Permian in various parts of the Appalachian Orogen (Bradley, 1983; Slingerland and Furlong, 1989) and both local and distant uplands provided the source for thick sediment accumulations within numerous depocentres in the Atlantic Provinces (Gibling et al., 1992).

A regional phase of dextral strike-slip movement (Webb, 1969; Arthaud and Matte, 1977), a component of the Maritimes Disturbance (Poole, 1967), took place within the Maritimes Basin mainly from the mid-Carboniferous onward. Figure 1.1 illustrates the distribution of major northeast-to east-trending fault systems, some of which are splays from the Minas Geofracture (the junction between the "Meguma Terrane" of mainland Nova Scotia and the "Avalon Terrane" of northern Nova Scotia).

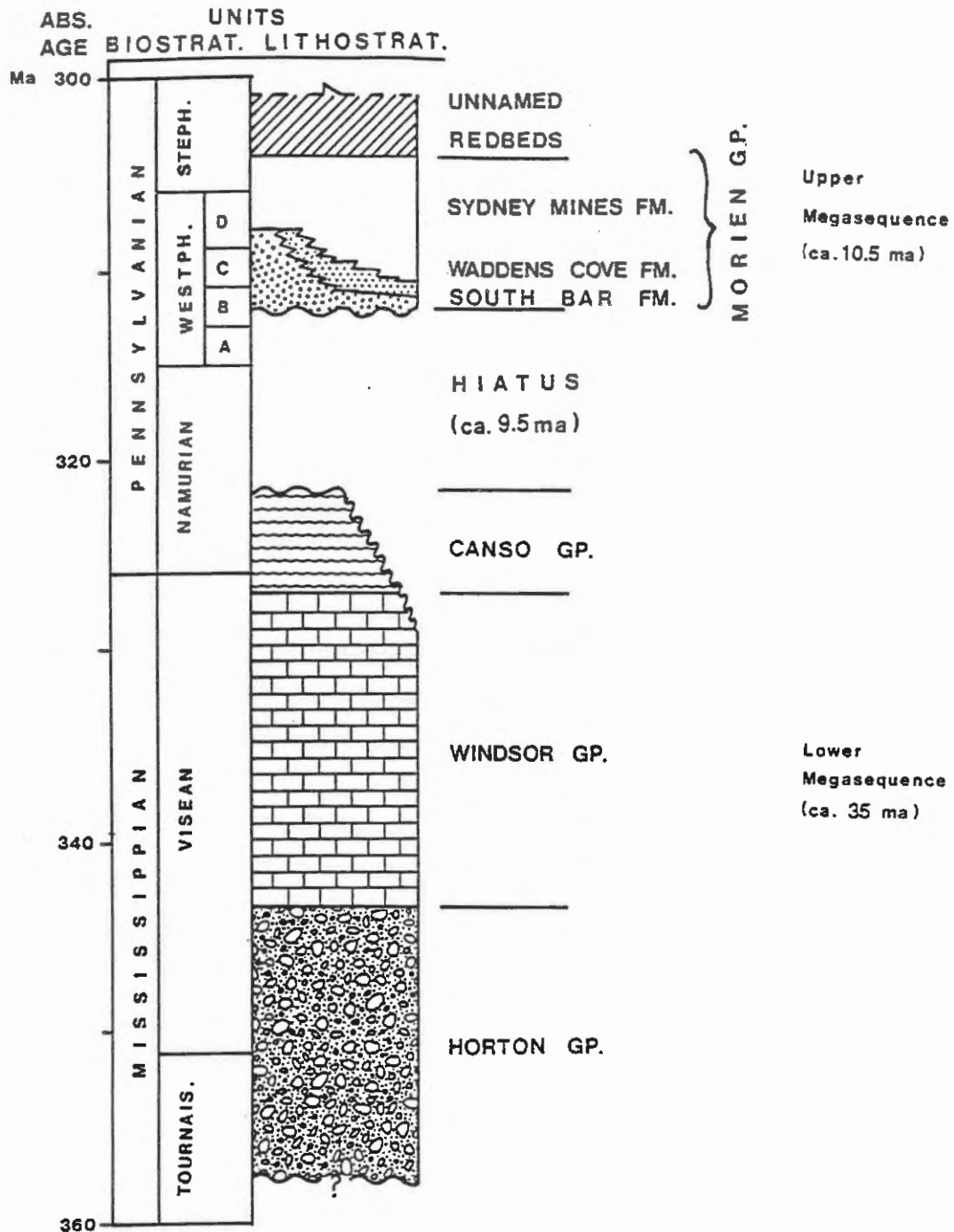


Figure 1.5. Stratigraphy of the Sydney Basin. Geology from Boehner and Giles (1986), biostratigraphic ages from Barss and Hacquebard (1967) and Zodrow and McCandlish (1978). Radiometric time-scale from Lippolt *et al.* (1984) and Hess and Lippolt (1986). (Modified from Gibling *et al.* (1987)).

The Mountain and Mira River-Bateston faults form the northern and southern boundaries of the Sydney Basin, respectively, but their most recent phase of movement postdated Late Carboniferous sedimentation.

A 9.5 m.y. hiatus separates the megasequences and represents a time of renewed uplift, deformation and erosion. This hiatus may correlate with a widespread mid-Carboniferous unconformity recognised in North America by Sloss (1963) and worldwide by Saunders and Ramsbottom (1986). A series of northeast- to east-trending faults underlie the basin (Giles, 1983, see Fig. 1.2) and were probably active during this period. The region was tectonically active as suggested by the discordance in dip between the megasequences as well as a widespread thermal event recorded within the Meguma Group (ca. 300 - 320 Ma.: Reynolds et al., 1987). The Canso (Mabou) Group was eroded locally during this hiatus. Evidence of karst weathering within the Windsor Group (at the unconformity between the two megasequences) has been documented by Boehner (1985), suggesting prolonged exposure of the strata.

The upper megasequence (Morien Group and unnamed red beds) blankets the faulted lower megasequence. There is no evidence for major fault activity locally, although coeval strike-slip activity took place elsewhere in the Maritime Basin. A quiet, tectonically stable phase in the history of the basin is suggested by the relatively simple structural style of the Morien Group. The basin continued to subside providing accommodation space for thick sequences of fluviolacustrine to marginal marine deposits. Evidence for differential subsidence of basement blocks is suggested by the character of the cyclic deposits across the basin (Gibling and Rust, 1990b). Gentle seaward plunging folds mimic the dominant northeast to easterly structural trends of the region (Fig. 1.2). Dips are generally shallow but locally can be as high as 45°. Dominant paleoflow direction

for the Morien Group parallels these structural trends (e.g. Duff et al., 1982; Gibling et al., 1987, 1992).

Rocks studied in this thesis occur within the Morien Group (upper megasequence: Fig. 1.5) and are of Westphalian D age (Barss and Hacquebard, 1967). Time stratigraphic equivalents of the Morien Group include rocks of the Pictou Group in the Cumberland and Stellarton Basins (Bell, 1944); in parts of New Brunswick and Prince Edward Island (van de Poll, 1973; van de Poll and Forbes, 1984); and in the Gulf of St. Lawrence Basin (Hacquebard, 1986). Ryan et al. (1991) have revised the Upper Carboniferous stratigraphy in the Cumberland Basin, Nova Scotia, and equate the upper part of the Cumberland Group with the Morien Group (see their Fig. 4). They redefined the Pictou Group to represent red-bed sequences with minor coals that lie above the Cumberland Group. This work has major implications for regional correlation; however, established stratigraphy for the Sydney Basin will be retained in this study.

The increased reddening of the strata in the Stephanian to Permian, in the Sydney Basin and regionally within the Maritimes Basin, may be attributed to a progressive increase in the effect of continental climatic conditions as continental blocks amalgamated into one landmass.

1.5. STRATIGRAPHY

During the long history of geological investigation in the Sydney Basin there have been numerous subdivisions of the strata based on sedimentology, megaflora and palynology (Table 1.1). The Morien Group was divided into three formations based on mapping by Boehner and Giles (1986), namely (from oldest to youngest):

1. South Bar Formation (SBF) - predominantly sandstone, minor pebbly conglomerate, rare coal; interpreted as a braided river deposit (Rust et al., 1987; Rust and Gibling, 1990).

Table 1.1. Stratigraphic summary of the Morien Group, Sydney Basin.

		SEDIMENTOLOGY			MEGAFLORA		PALYNOLOGY		
		Brown (1871) Robb (1876)	Rust et al. (1983) Best (1984)	Boehner and Giles (1986)	Bell (1938)	Zodrow and McCandish (1978)	Barss and Hacquebard (1967)	Dolby (1988, 1989)	
W e s t p h a l l i a n	D	Productive Coal Measures	Upper Morien	M O R I E N E F o r m a t i o n	Sydney Mines Formation	Ptychocarpus unitus E	Hu Linopteris obliqua	Potoniesispore	Hu
								Thymospora	
	C	Millstone Grit	Lower Morien	G R O U P F m	Maddens Cove South Bar Fm	Linopteris obliqua	Tr Lonchopteris eschuileriana	Torispora	Mu
								Vestispora	
A		Mid-Carboniferous Hiatus					Hu - Hub seam		
Namur- ian							E - Emery seam		Mu - Mullins seam
								Tr - Tracy seam	

2. Waddens Cove Formation (WCF) - red and grey mudstone, sandstone, pedogenic limestone, silcrete and minor coal; (lateral reddened equivalent of the upper SBF and the basal SMF in the southeast portion of the basin, Rust et al., 1987; Gibling and Rust, 1990a).
3. Sydney Mines Formation (SMF) - coal-bearing formation with mudstone, limestone and sandstone intervals; interpreted as a meandering fluvial to fluviolacustrine deposit (Gibling et al., 1987; Rust et al., 1987; Masson and Rust, 1990).

The onshore distribution of these formations is illustrated in Figure 1.2. The fining upward nature of the Morien Group and the transition from braided to meandering alluvial styles possibly reflects a progressive decrease in the source elevation and a decrease in the basin-floor gradient with time (Rust et al. 1987).

2. CYCLOTHEM FACIES SUCCESSIONS WITHIN THE PHALEN- BACKPIT INTERVAL

2.1. INTRODUCTION

Cyclic deposits have been recognised from Carboniferous coal-bearing strata in Europe and North America (e.g. Udden, 1912; Weller, 1930; Wanless and Shepard, 1936; Moore, 1950; Duff and Walton, 1962; Heckel, 1977, 1984; Leeder and Strudwick, 1987) and have been termed cyclothems: "a series of beds deposited during a single sedimentary cycle of the type that prevailed during the Pennsylvanian period" (Wanless and Weller, 1932, p. 1003). Their typical Illinois cyclothems consist of repeated packages of sandstone, underclay, coal, limestone and shale, in upward succession, that can be traced over areas of thousands of square kilometres.

A key element in cyclothem analysis is the relationship between facies successions and relative sea-level change. Glaciation was active in the southern hemisphere throughout the Pennsylvanian (Veevers and Powell, 1987) and glacioeustasy (controlled by climate change induced by orbital-forcing Milankovitch cycles) is considered by many workers to be the dominant mechanism for generating marine influenced cyclothems (Wanless and Shepard, 1936; Heckel, 1977, 1984, 1986; Fischer, 1986). Tectonism also affects relative sea-level and is invoked by other workers (e.g. Weller, 1930, 1956; Tankard, 1986) as a driving mechanism, especially in tectonically active basins. Alluvial and deltaic dominated cyclothems are much more problematic because autogenic processes such as relocation of channels and delta lobes (Beerbower, 1969; Ferm, 1970, 1979; Ghosh, 1987) may preclude recognition of systematic, regional facies changes.

The Sydney Basin of Nova Scotia contains eastern Canada's major economic coal field. The principal coal-bearing unit is the Sydney Mines Formation (SMF), about 400

m thick onshore, and dated as Westphalian D to Stephanian (Barss and Hacquebard, 1967; Dolby, 1988, 1989). The SMF onshore comprises eleven alluvial-dominated stratal packages bounded by coal seams and described as cyclothems by Bird (1987). The cyclothems range from 11 to 72 m thick at Bras d'Or (A, Fig. 1.2) (Gibling and Bird, submitted) and can be traced over an area of at least 2500 km², and possibly tens of thousands of square kilometres. Cyclothems were first recognised at Sydney by Wanless and Shepard (1936) based on review of an earlier study by Hayes and Bell (1923), but the concept received little subsequent attention in the basin. Unlike most Illinois cyclothems, red mudstone beds form a regionally extensive layer within most Sydney cyclothems, a feature shared with some cyclothems of the Appalachian Basin (Beerbower, 1961, 1969), Texas (Boardman and Heckel, 1989) and Kansas-Nebraska (Moore, 1950).

Excellent coastal exposures and drill cores intersect three cyclothems near the base of the SMF (Figs. 1.2, A1.1 and A1.2) and yield a line of section roughly parallel to depositional strike (Fig. 2.1, enclosure). This database has enabled facies distributions to be documented in both a vertical and lateral sense and has permitted identification of local and regional (basin-scale) events. Base-level fluctuations and basin-fill processes are integrated into an overall depositional model for two cyclothems in the Phalen-Backpit seam interval (PBI, Section 1.2, Fig. 1.3) and inferences are also drawn from sedimentological patterns in the overlying cyclothem (Cyclothem 3, Fig. 2.1), where data are available.

2.2. CYCLOTHEM RECOGNITION WITHIN THE PHALEN-BACKPIT INTERVAL

The three cyclothems studied are detailed in Figure 2.1 and summarized in Figure 2.2. Methods are outlined in Appendix 1. The Phalen-Backpit interval (PBI) includes

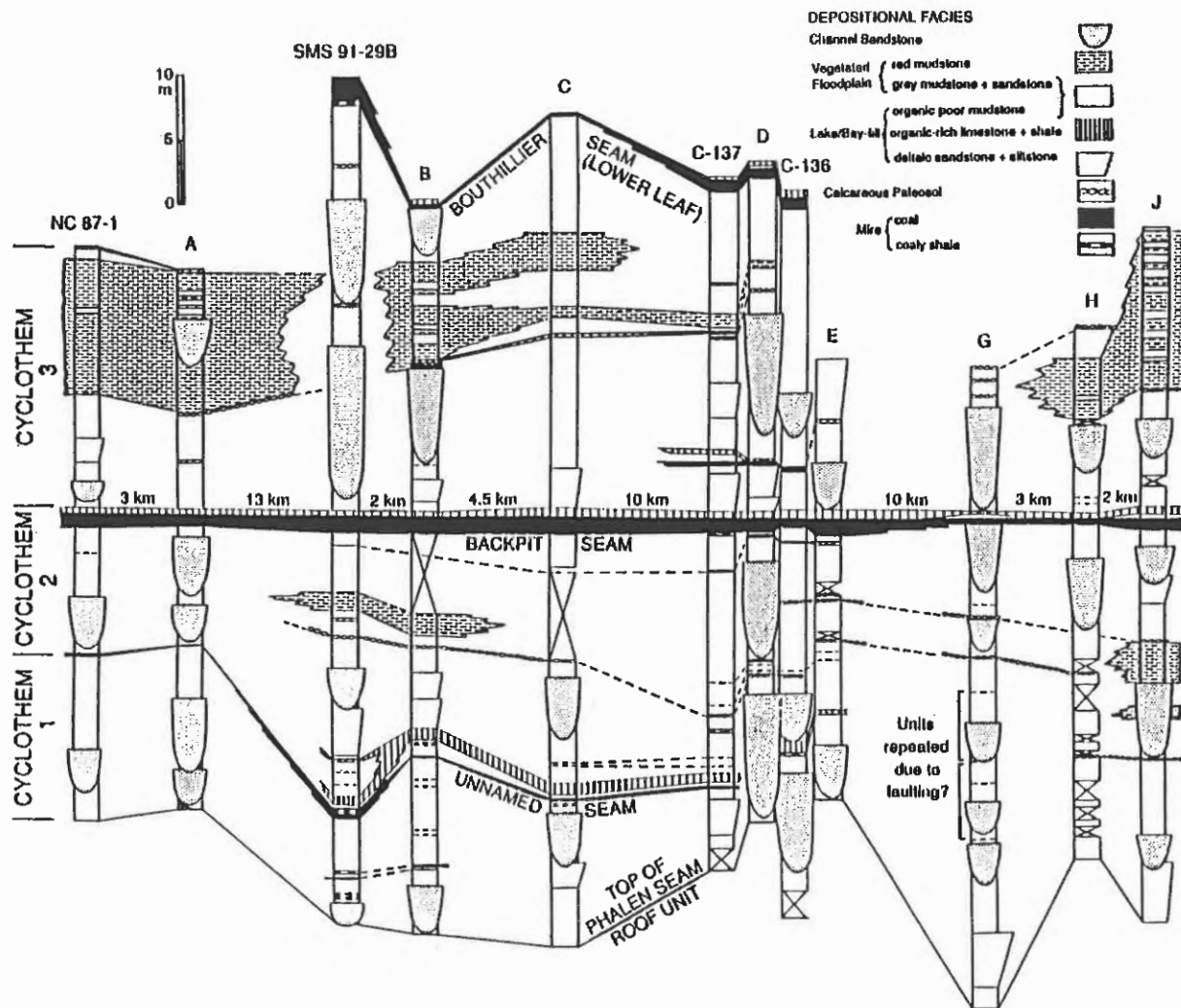


Figure 2.2. Generalized stratigraphy of the study interval, highlighting channels and laterally extensive coal, limestone, red mudstone and calcareous paleosol horizons. Cross-section shortened from map, Figure 1.2.

Cyclothem 1 and 2. Four lithofacies form regionally extensive units within this study interval: coals, limestone/shale roof units, red mudstone and nodular carbonate. Of these, the coal and organic-rich roof unit couplet are the most widespread. Cyclothem bases are placed at the top of the roof unit, an easily recognised level that marks the return of abundant clastic sediment to the basin. Where such a roof unit is missing locally, the cyclothem base is placed at the top of the coal seam. No attempt was made to correlate channel sandstones or crevasse splay and delta deposits due to the distance between measured sections and their potential for lateral variability.

Cyclothem bases in studies elsewhere usually correspond to the most continuous marker horizon (Duff and Walton, 1962). Some American workers (e.g. Weller, 1930; Moore, 1936; Wanless *et al.*, 1963) placed the base of a cyclothem at an erosive channel base ("unconformity") above the coal, although this boundary is difficult to identify where channel units are missing from the package. Udden (1912) chose the bases of extensive coal seams as bounding surfaces for cyclic packages in Illinois. Many workers in Britain and northwestern Europe (e.g. Trueman, 1954; Duff and Walton, 1962; Westoll, 1968) placed cyclothem bases at the change from coal to widespread limestone or shale; where the limestone/shale unit is missing, the top of the coal seam was used.

Cyclothem 1, from the Phalen roof unit to the unnamed seam roof unit, is best developed in the mid- to western portion of the basin where it ranges from 7 to 15.5 m thick (Fig. 2.2). At New Waterford (D) a major sandstone channel cuts completely through this package. It is difficult to trace this interval eastward from Glace Bay due to localized faulting and covered intervals. Red mudstone and calcareous paleosols are not present and this package corresponds to a "poorly developed" cyclothem as described by Gibling and

Bird (submitted).

Cyclothem 2, from the unnamed seam roof unit to the Backpit roof unit, can be traced across the study area for more than 45 km, parallel to depositional strike. The interval ranges from 10.5 to 20 m thick but it is difficult to place the lower boundary in the east for reasons noted above. Thin red mudstones are present near the faulted basin margins, and associated calcareous paleosols can be traced for more than 20 km. This package corresponds to a "well developed" cyclothem as described by Gibling and Bird (submitted).

Data from Cyclothem 3, the Backpit roof unit to the lower Bouthillier roof unit, were collected from some localities to provide additional facies information, but are not discussed in detail due to incomplete coverage of the complex, split Bouthillier seam interval across the study area. Red strata are thickest near the faulted basin margins and can be traced laterally for considerable distances (Fig. 2.2). As in Cyclothem 2, calcareous paleosols are associated with the reddened intervals.

2.3. SEDIMENTARY FACIES

Many of the cyclothem patterns in the SMF are complicated by splits in coal seams. The PBI provides a concisely bounded interval, unaffected by seam splits, from which depositional patterns were quantified. This interval was divided into five major sediment groups based primarily on grain size, as outlined in Table 2.1. Such sediment groups are important for comparing the present results with older published reports (e.g. Hacquebard and Donaldson, 1969) and mine data.

A more interpretative approach was used to identify depositional facies, based on a combination of lithology, sedimentary structures, unit geometry, fossils and biogenic structures (Table 2.2, discussion to follow). Unit geometry

and large-scale sedimentary structures were not applicable criteria when interpreting drill core.

Table 2.1. Sediment groups in the PBI.

COARSE CLASTIC	FINE CLASTIC	NODULAR CARBONATE	ORGANIC-RICH
conglomerate, vfg to cg sandstone; interbedded sandstone/ siltstone	grey/red siltstone; mudstone; claystone	carbonate nodules	1) coals, coaly shale 2) limestone, black shale

Sediment groups and depositional facies occur in specific patterns across the study area and their distribution is considered in Section 2.4, after a description of the facies.

2.3.1. Channels

2.3.1.1. Major Channel

Channel bodies average approximately 4.5 m thick (maximum: 11.7 m) and consist predominantly of fine- to medium-grained sandstone. Thick bodies are multistoried (up to 4 storeys) with erosive surfaces separating and within storeys. Paleochannel margins are commonly observed incised through associated bay-fill or floodplain deposits (Plate 1a), which suggests that the bodies are inextensive laterally. The paleochannel margin above the Backpit rider seam at New Waterford (D) cuts through 6 m of lacustrine/bay-fill strata (Fig. 2.1).

Most channels have an erosive, concave-up base, with lag deposits generally less than 10 cm thick (Fig. 2.3a, Plate 1b), but locally up to 2 m thick (New Waterford-D). Trough cross-beds are abundant in the lower portions of the channel bodies and are excellent paleoflow indicators when

Table 2.2. Depositional facies in the PBI.

DEPOSITIONAL FACIES	THICKNESS + GEOMETRY	LITHOFACIES/ LITHOLOGY	SEDIMENTARY STRUCTURES	ORGANIC MATERIAL	COMMENTS
1. Channel					
a. major channel	2.5-11.7m concave-up base	Coarse Clastic: vfg to cg sandstone; lag common	trough, planar, cross-beds; IHS; planar beds; ripple cross-lamination	peat mats; detrital organics	commonly fining upward, meandering-fluvial; multistoreyed; ridge-and-swale
b. abandoned channel-fill	1.0-5.0m concave-up base	Fine Clastic: interbedded silt-mudstone, minor sandstone	ripple cross-lamination; mm scale horizontal laminae	roots locally; detrital organics	vertical aggradation
2. Vegetated Floodplain					
a. levee/ crevasse splay	0.3-4.0m sheet	Coarse Clastic: vfg to mg sandstone, siltstone	ripple cross-lamination; minor graded bedding	roots common; detrital organics; rare <u>in situ</u> trees	variably fine and coarsen upward
b. crevasse channel	0.6-1.8m concave-up base	Coarse Clastic: vfg to mg sandstone	planar, minor trough cross-beds; ripple cross-lamination	roots rare	minor channel associated with splay sequence
c. poorly-drained soil	<0.5-3.1m sheet	Fine Clastic: grey mudstone, minor sand, siltstone	bioturbated; horizontal laminae rare	carbonaceous root traces; rhizoconcretions	immature hydromorphic soils
c. well-drained soil	0.8-1.8m sheet	Fine Clastic: red to mottled red/grey mudstone	concave-up joints, rare horizontal laminae, mudcracks	calcareous rhizoconcretions	oxidized vertisols

Table 2.2. Depositional facies in the PBI (con't).

DEPOSITIONAL FACIES	THICKNESS + GEOMETRY	LITHOFACIES/ LITHOLOGY	SEDIMENTARY STRUCTURES	ORGANIC MATERIAL	COMMENTS
3. Calcareous Paleosol	0.2-0.85m discrete layers	Nodular Carbonate: carbonate nodules	obliterated by vegetation	calcareous, sideritic rhizo-concretions	competent, resistant to erosion; calcrete?
4. Lacustrine/Bay-fill					
a. delta	0.4-4.0m tabular	Coarse Clastic: siltstone, f to mg sandstone	ripple cross-lamination; parting lamination; convolute bedding	roots near top; large <u>Stigmaria</u> ; detrital organics	planar bedded; coarsens up
b. organic-poor lake/bay	<0.5-4.0m sheet	Fine Clastic: siltstone, mudstone, minor sandstone	ripple cross-lamination; mm scale horizontal laminae; mud-cracks	carbonaceous plant fossils; detrital organics; rare roots	platy beds; siderite bands common
c. organic-rich lake/bay	<0.05-0.82m discrete layers	Organic-Rich: limestone, black shale	dewatering structures	terrestrial organics (up to 20 % TOC); plant fossils	bivalves, serpulids, ostracods, sharks, other fish, foraminifera
5. Mire	<0.5-1.5m discrete layers	Organic-Rich: coal, coaly shale	predominantly banded with continuous dull layers	predominantly vitrinite; discrete fusain layers common	moderate to high ash(15.3%) sulphur(5.2%); 0.69-0.76% Ro onshore

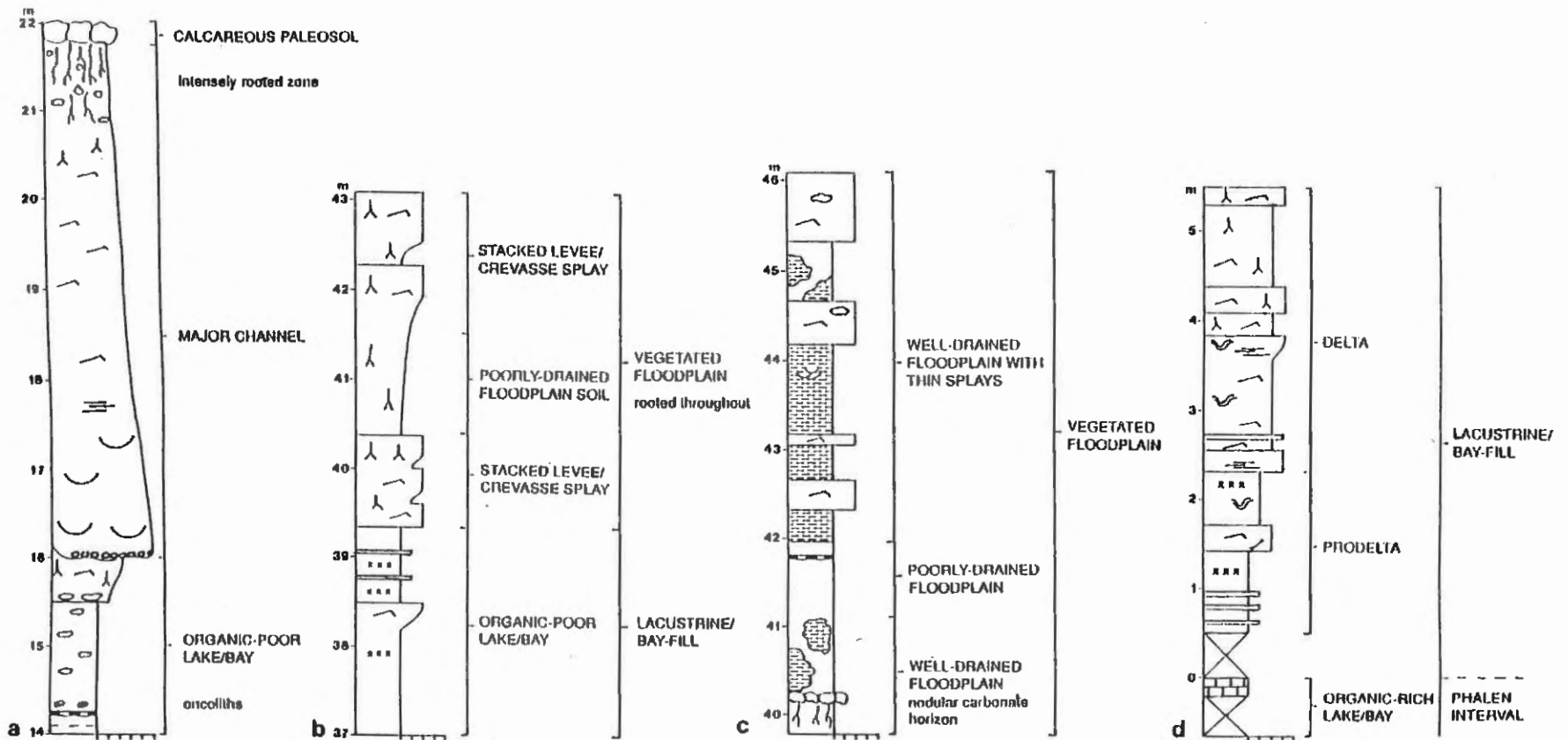


Figure 2.3. Profiles of selected depositional facies assemblages: a) Cyclothem 2, Victoria Mines, b) Cyclothem 3, Victoria Mines c) Cyclothem 3, Longbeach and d) Cyclothem 1, Donkin West. Measurements represent metres above the top of the Phalen interval. Symbols in legend of Figure 2.1.

exposed in three dimensions on wave cut platforms (Plate 1c). Trough sets are 20 cm to 2 m wide and 10 cm to greater than 1 m thick, with an upward decrease in set size within individual channel deposits. Trough bases are commonly lined with pebbles and/or organic debris. Trough cross-beds represent three-dimensional dunes that migrated within the deeper portions of sandy channels (Cant, 1978; Ashley, 1990).

Planar cross-sets from 5 to 20 cm thick, with common reactivation surfaces (Plate 1d), are minor constituents of these channel deposits. Planar cross-beds generally occur at mid-levels of PBI channel bodies and represent the migration of two-dimensional dunes, commonly termed sand waves or bars (Jackson, 1976; Ashley, 1990). Plane-bedded sandstones with primary current lineation (Plate 2a), are locally present at the mid-levels of some channel bodies and indicate periodic upper flow-regime conditions (Harms and Fahnstock, 1965; Stear, 1983), probably related to seasonal fluctuation in stage.

Inclined heterolithic stratification (IHS: Thomas et al., 1987; epsilon cross-stratification of Allen, 1963) was noted in several channel bodies. These beds consist of gently-dipping (up to 25°) sandstone beds, up to 20 cm thick, draped by mudstone beds up to 5 cm thick. The IHS sets are 2 to 5 m thick and indicate minimum water depths for the paleochannels. Paleoflow is parallel to strike of the beds, indicating formation by lateral accretion. Similar fine sediment drapes have been described from low-gradient, tidally influenced rivers (Smith, 1986) and may indicate tidal influence for the SMF (Rust et al., 1987), although they are also known from channel deposits in continental interiors (Taylor and Woodyer, 1978).

Ridge and swale topography is commonly associated with IHS, and is especially well exposed at the top of channel deposits at Bras d'Or (A). This topography, typical of

meandering channels, probably formed by the migration of scroll bars on point bar tops (Gibling, in prep).

Ripple cross-stratification is common in the upper strata of the channel deposits (Fig. 2.3a). Ripple amplitudes range from 0.5 cm to 3 cm and ripple cross-stratified beds are up to 2 m thick. Ripples exposed in plan view (Plate 2b) are asymmetric and sinuous-crested. Ripple-drift cross lamination is common, indicative of rapid deposition. Ripples commonly form during falling stage and are a characteristic feature of typical fining upward channel deposits (Allen, 1964, 1970; Miall, 1985).

Meandering channels have been identified as the predominant channel form in the SMF by previous workers (Haite, 1951; Gibling and Rust, 1987; Gibling *et al.*, 1987). The presence of inclined heterolithic stratification, commonly formed by point bar accretion within a meandering channel (Moody-Stuart, 1966; Leeder, 1973a,b; Walker and Cant, 1976) and ridge-and-swale topography support this interpretation. The multistoried architecture of many channels suggests migration and switching of channels within a channel belt.

2.3.1.2. Abandoned Channel-fill

Abandoned channel deposits commonly occur in the upper portion of channel bodies and retain the concave-up form of the original channel. Their thickness (1 to 5 m) is indicative of the original channel depth. Aggradation was predominantly vertical, with alternate siltstone and mudstone beds that conform to the channel shape. Thin limestone beds, coaly layers and laterally continuous siderite bands are common locally. Sedimentary structures include horizontal laminae and rare ripple cross-lamination. Roots are commonly represented by rhizoconcretions and carbonaceous traces. The assemblage of features indicates a fluctuating water level.

Abandoned channels are especially common in meandering river deposits and represent abandoned reaches that were eventually filled with finer sediments (Allen, 1965).

2.3.2. Vegetated Floodplain

2.3.2.1. Levee/Crevasse Splay

Levee and crevasse splay deposits form sheets of coarsening or fining upward sandstone and siltstone (Fig. 2.3b) up to 4 m thick. These lithologies are often interbedded, indicating fluctuations in flow. Sedimentary structures, commonly obliterated by bioturbation, include ripple cross-stratification, wavy and horizontal lamination. Vertically oriented root casts (sediment or cement-infilled root molds) and/or rhizoconcretions are especially common at unit tops where they reflect the abandonment of the splay or levee. Upright trees are locally preserved in growth position.

Rare matrix-supported conglomerate sheet deposits, up to 0.7 m thick, with sharp basal and upper contacts are associated with levee/splay deposits near the faulted basin margins in the study area (A, J, Fig. 2.1). At Bras d'Or (A) a conglomerate unit thickens laterally into a crevasse channel deposit and probably represents a catastrophic flood event.

The PBI levee/splay deposits formed during the breaching of a major channel bank during flood stage, as described by Farrell (1987) for overbank deposits of the Mississippi River. Coarsening and fining upward packages indicate that the river was approaching or migrating away from the site, respectively (Kraus, 1987).

2.3.2.2. Minor Channel

Minor channel deposits of fine-grained sandstone, up to 1.8 m thick and 5 m wide, locally erode crevasse splay deposits. Basal lags are rare and the most common

sedimentary structures are ripple and minor trough cross-stratification. Paleoflow direction, where measurable, is commonly perpendicular to that observed in associated channel deposits. These minor channel deposits resemble those of modern crevasse splay feeder channels (e.g. Smith, 1983).

2.3.2.3. Poorly-drained Floodplain Soil

Floodplain deposits form extensive sheets of clay- and mudstone up to 5 m thick. Within the PBI, grey floodplain deposits (Fig. 2.3b) are associated with calcite and siderite nodules and rhizoconcretions, organic debris and carbonaceous root traces, indicative of poor drainage, a reducing environment and the development of hydromorphic soils (Coleman, 1966; Buurman, 1980). Roots commonly obscure primary sedimentary structures, but ripple cross-lamination and horizontal laminae are preserved locally in slightly coarser sand/silt layers that may represent distal splays. Concave-up joints occur locally. Although rooted vegetation is common, soil profiles are poorly developed (immature) probably because minor detrital incursions led to cumulative soil development (Bown and Kraus, 1981; Retallack, 1988) and profile accretion (Birkeland, 1984).

Rooted underclays, generally less than 1 m thick, commonly occur below coal seams. They consist of light grey, kaolinite-rich mudstones and claystones commonly with abundant well-preserved carbonaceous root traces and rhizoconcretions. All sedimentary structures have been obliterated by bioturbation and possible leaching from acid swamp waters during peat accumulation (Huddle and Patterson, 1961). Agglutinated foraminifera, dominated by coiled forms, were extracted from several underclay sites below the Backpit seam and indicate a marine-influenced high marsh environment for the original sediment (W. Wightman, pers. comm., 1992).

2.3.2.4. Well-drained Floodplain Soil

Red to red-green mottled mudstone units (Plate 3a) up to 1.8 m thick, are commonly interbedded with laterally extensive, light brown to grey sandy splay deposits (0.2 to 1 m thick), with abrupt lower and upper contacts (Fig. 2.3c). This assemblage is best developed in Cyclothem 3, near the basin margins of the study area (Figs. 2.1, 2.2). The red mudstones are generally slightly calcareous and carbonate rhizoconcretions and desiccation cracks are common in some intervals. Discrete calcareous paleosol horizons are commonly associated with these red intervals, as discussed below. Mineral assemblages for the red mudstone are similar to the grey mudstone with the addition of hematite, which gives this lithofacies its diagnostic colour (Gibling *et al.*, 1985). Detrital organic debris and carbonaceous plant impressions are rarely preserved in this assemblage and abrupt contacts with splay deposits suggests limited root turbation.

Concave-up joints, common in the more massive units resemble the pseudo-anticlinal structures described by Allen (1974, 1986). They form due to shrinking and swelling of clays during alternate wet and dry conditions. Allen compared the structures to gilgai (micro-relief) formed pedogenetically in some clay-rich alluvial soils under conditions of seasonal deep-soil wetting.

Red units in the study area are interpreted as well-drained floodplain soils (vertisols) developed in areas of higher Eh (oxidation) due to a lower water table and improved drainage. Similar inferences were drawn by Besly and Turner (1983) for red-bed sequences in the British Westphalian. They attributed the colour mottling to a fluctuating water table and alternate oxidation and reduction.

2.3.3. Calcareous Paleosol

Roots are a common feature of approximately 20 to 60% of each PBI section measured and may suggest some degree of paleosol development. The term "calcareous paleosol" is reserved for rooted units that consist predominantly of nodular carbonate (Fig. 2.3a). Sedimentary structures are completely obliterated from these units due to root activity and carbonate precipitation. Nodules vary greatly in size (2-30 cm long axis) and locally coalesce to form a single nodular zone (> 70% nodules) typically 30 cm thick (up to 85 cm thick) (Plates 3b, 3c). Nodular layers are locally stacked to form intervals up to 2 m thick. Rhizoconcretions and root casts are abundant in the nodular zone (Plates 3c, 3d) and subjacent strata (Fig. 2.3a). Some of the best developed calcareous paleosols underlie red mudstone intervals and this is particularly common in Cyclothem 3 (Fig. 2.2).

Wanless *et al.* (1963, p. 447) described from Illinois cyclothems similar calcareous layers that had a "very uneven knobby surface which may have numerous calcite-filled veins". These distinctive units were interpreted as corrosive subaerial surfaces, indicative of extended periods of non-deposition. Such nodular zones may represent B soil horizons (illuvation zone, Bk) where calcium carbonate leached from upper horizons is reprecipitated (Retallack, 1988). Similar deposits in ancient strata, referred to as calcretes, have been described in the literature (e.g. Allen, 1973, 1974; McPherson, 1979; Parnell, 1983). In modern settings, these deposits commonly occur in regions with pronounced seasonality. Leeder (1975) suggested that even the least mature calcareous horizons required non- to minimal deposition for at least 1000 years and the more mature, nodular zones required tens of thousands of years to develop.

2.3.4. Lacustrine/Bay-fill

2.3.4.1. Organic-poor Lacustrine/Bay-fill

Organic-poor lake/bay deposits consist of finely laminated siltstones, mudstones and minor claystones up to 4 m thick. The units commonly weather orange-brown, diagnostic of high siderite content. Beds are platy and show horizontal lamination (< 1 cm thick) and minor ripple cross-lamination. Carbonized plant fossils, detrital organic matter and continuous siderite bands up to 3 cm thick are common (Plate 2d), suggesting a reducing environment. Rare roots are typically preserved as carbonaceous traces.

Organic-poor lake/bay deposits represent overbank fines deposited during splay events in standing water on floodplains adjacent to fluvial systems (Fig. 2.3b) or prodelta sequences (Fig 2.3d) deposited as part of a coarsening upward package in lakes and/or bays. These two types of occurrences are distinguished by the associated facies.

2.3.4.2. Organic-rich Lacustrine/Bay-fill

Organic-rich lake/bay deposits (Fig. 2.3d) include bituminous limestones and associated fissile shale units less than 1 m thick that can be traced parallel to depositional strike for more than 20 km. The Backpit roof unit (BRU, Fig. 2.2) is one such interval that occurs above the Backpit seam, and is described in detail in Chapter 4. The BRU contains a fresh to brackish assemblage of shark and fish remains, ostracods, bivalves, serpulids and agglutinated foraminifera (lower marsh) that indicate a marine influence for the strata. High sulphur values in coal samples subjacent to the roof unit also indicate a marine to brackish input (i.e. source of SO_4^{-2}). Geochemical parameters indicate good source rock potential, with S_1 greater than 1.0 mg HC/g rock in offshore samples,

S₂ commonly greater than 5.0 mg HC/g rock (average-8.84 mg HC/g rock) and TOC averaging approximately 3.7% by weight. Hydrogen indices range from 150 to 500 mg HC/Corg and suggest terrestrially derived Type II to II/III kerogen. Sporinite is the most abundant liptinite maceral and lamalginite predominates locally. Numerous inertodetrinite and vitrodetrinite fragments support a terrestrial source for organic matter in this unit.

The Backpit roof and other similar units were probably deposited in an oxygenated to anaerobic open water bay or lake during periods of minimal clastic input.

2.3.4.3. Delta

Delta complexes consist of tabular, coarsening upward packages of sandstone and minor siltstone up to 4 m thick (Fig. 2.3d). Horizontally stratified bedsets (Plate 4b), up to 25 cm thick, contain individual planar beds from less than 1 mm to 1 cm thick. Plane beds with parting lineation are indicative of upper flow regime conditions. Ripple and ripple-drift cross-lamination, indicative of rapid deposition, are also common. Synsedimentary deformation features are locally present suggesting that the sediment surface was prone to liquefaction, as described for lacustrine delta deposits in the Westphalian Durham coalfield (Fielding, 1984).

Upper beds within the delta packages are commonly rooted and locally mudcracked (Plate 2c) indicative of shallowing upward and ultimately an emergent, vegetated platform. The thinness of these packages (generally less than 4 m) suggests that the lakes or bays were relatively shallow.

Deltas commonly occur above limestone/shale sequences (organic-rich lake/bay, Section 2.3.4.2.) and represent the progradation of clastics into the lake or bay. Prodelta and delta front mudstones/siltstones (organic-poor lake/bay)

commonly precede the delta package and are discussed in Section 2.3.4.1. Possible modern analogues for this assemblage include lacustrine and interdistributary bay deltas of the Atchafalaya Basin (Tye and Coleman, 1989).

2.3.5. Mire

Mires ("any freshwater wetland system in which peat accumulates": Moore, 1987) are represented by two types of deposits within the study interval. Extensive coals (traceable for more than 30 km along strike section) probably formed due to allogenic processes (Phalen seam, Backpit seam, unnamed seam, Figs. 2.1, 2.2). Inextensive coals (traceable for less than 5 km along strike; for example, the unnamed seam directly above the Backpit seam at New Waterford) probably formed locally on floodplains or delta tops as the result of such autogenic processes as differential compaction of underlying sediment, avulsion and delta switching.

The Backpit seam is one of the most continuous seams onshore in the SMF and can be traced for more than 45 km parallel to depositional strike without splits or fundamental petrographic change. It is a banded, high volatile B to A bituminous coal, with moderate to high ash and sulphur. The reader is referred to Chapter 3 for a detailed discussion of the Backpit mire development and paleoenvironmental assessment. The seam is thickest in the Sydney Mines and Glace Bay sub-basins, and seam interval correlation suggests that peat established first in slight topographic depressions and gradually spread across the depositional area. Peat may have accumulated for up to 15,000 years and was influenced by base-level fluctuations recorded in the upper seam section as a series of dulling upward lithotype trends, which ultimately led to the drowning of the peat. Moderate to high sulphur values, especially near the seam top and marsh foraminifera above

and below the seam indicate a coastal context for peat accumulation.

Bright lithotypes predominate (bright, bright banded, banded: Diessel, 1965), and vitrinite generally represents greater than 70 % by volume of each seam section. Thin dull layers (dull banded, dull, coaly shale) contain detrital macerals and minerals and suggest elevated groundwater levels. Some of these layers can be traced for tens of kilometres across the study area. Common fusain layers represent the charred remains of ancient fires.

2.4. SEDIMENTARY PATTERNS

2.4.1. Vertical Distribution

The three cyclothem studied contain slightly different patterns but each shows a similar vertical trend (Fig. 1.3). The cyclothem base is commonly underlain by the organic-rich lake/bay facies, directly overlying a coal seam. This marks the termination of peat accumulation and the establishment of a broad shallow lake or bay in which a fresh to brackish water fauna flourished in great abundance and low diversity (Chapter 4). The organic-rich facies is commonly overlain by stacked coarsening upward packages of organic-poor lake/bay (prodelta and delta front) to delta deposits. The delta sandstone beds are commonly rooted near the top, indicating the filling of the lake/bay and the establishment of vegetation on the emergent delta top. Delta deposits up to 4 m thick suggest shallow bodies of water. At some sites representing more distal environments, the delta facies is not present and fine-grained, organic-poor lake/bay deposits predominate. At other locations the bay-fill assemblage is completely or partially removed beneath a channel-base erosional surface (Plate 4c). These channel bodies probably represent distributary channels associated with the delta complex.

Red mudstones and/or calcareous paleosols (Plate 3)

commonly cap the channels and may have formed on well-drained interfluvial areas during a phase of channel incision, as documented for the younger Bonar Cyclothem (Gibling, 1992). Red soils are forming today in slightly raised deposits of the Mississippi delta region (Tye and Coleman, 1989), although these deposits are not regionally extensive as in the SMF. Thin tabular sandstone deposits abruptly interbedded with the red mudstones represent crevasse splays, and suggest that contemporaneous channels were a considerable distance away, and flood events were abrupt and flashy.

The well-drained assemblage is typically overlain by a poorly-drained assemblage that includes lacustrine deposits (limestone, mudstone and siltstone) and soils of the fine clastic grey sediment group. Some splay and sandstone channel deposits are present and rooted underclays with agglutinated "marsh" foraminifera (Thibaudeau and Medioli, 1986; Wightman *et al.*, 1992) typically cap this interval. A widespread mire became established on the resultant coastal plain, and an open bay or lake eventually replaced the mire, its deposits capping the cyclothem.

2.4.2. Lateral Distribution

Units traceable for 20 to more than 45 km parallel to depositional strike include mire and organic-rich lake/bay facies, well-drained floodplain soils (red mudstones) and calcareous paleosols (nodular carbonate) (Fig. 2.1). Other units (individual deltas and organic-poor lake/bay deposits, channel bodies, splay and poorly-drained floodplain assemblages) are more variable in areal extent.

The relative proportion of sediment groups and depositional facies within the PBI are illustrated in Figure 2.4a and 2.4b respectively. [Coarse clastic/(fine clastic + organic-rich)] ratios for each section are also indicated on Figure 2.4a. Channel sandstones are concentrated near



Figure 2.4. The distribution of a) sediment groups and b) depositional facies in the PBI. Numbers represent ratio of [(coarse clastic)/(fine clastic + organic-rich)] sediment groups.

the basin margins in the west and east, as well as at New Waterford (D), the region separating the Sydney Mines and Glace Bay sub-basins. The ratio of [(coarse clastic)/(fine clastic + organic-rich)] sediment groups is consistently high (> 2.0) in these regions.

Sections within the Sydney Mines sub-basin (SMS-91-29B, B, C and C-137) have low ratios (<1.5), indicating a predominance of the fine clastic sediment groups. The sub-basin also contains the highest proportion of lacustrine/bay-fill facies (> 20 %), and is relatively low in channel deposits (< 35 %). Wet conditions may have prevailed in the sub-basin, perhaps due to differential subsidence related to basement block movement.

The Glace Bay sub-basin (C136, E) contains a large proportion of coarse clastic groups, much of which consists of splay deposits, probably related to the nearby channel belt at New Waterford (D). Mire and organic-rich lake/bay facies form a relatively high proportion of this region and red strata are lacking.

Well-drained floodplain soils are limited to those sections near the faulted margins of the basin (SMS, B, J) in the PBI. Nodular carbonate units, typically associated with these red intervals, can be traced laterally, parallel to depositional strike for up to 20 km. The red intervals thicken upward and are more laterally extensive in Cyclothem 3 (Fig. 2.2). This may reflect a greater magnitude of base-level fluctuation upward, or a larger scale climatic cycle superimposed on several smaller cycles. Further work is necessary to evaluate these potential factors in the SMF.

2.5. CONTROLS ON CYCLOTHEM PATTERNS IN THE PBI

Using stratal proportionality, Gibling and Bird (submitted) estimated the average duration for SMF cyclothem at Bras d'Or (9 cyclothem) to be approximately 200 ka, assuming that the SMF comprised approximately 60 %

of the Westphalian D period (3 m.y., Hess and Lippolt, 1986). This agrees well with other workers' calculations, using the same time-scale (see Klein, 1990) but does not coincide closely with known orbital cycles. Cyclothem near the base of the SMF are much thinner than younger packages and may represent less time, if one assumes that thickness is proportional to time. Caution is suggested when using calculations such as these that include many assumptions.

The study interval comprises only a small portion of the lower SMF, however, inferences are made for the basin based on the patterns of depositional facies, as similar patterns occur throughout the SMF (Gibling and Bird, submitted). The lateral continuity of key units and systematic facies succession in the study interval suggests a regional control on the sedimentary distribution within these intervals. A coeval coal-bearing interval (Grant, 1992) and possibly individual seams (Hacquebard, 1986) are traceable in the Gulf of St. Lawrence, and suggest great areal extent for some of these cyclothem. The interplay of allogenic controls dominated by eustasy (controlled by climate), and influenced by sediment supply and tectonism (subsidence), coupled with more local autogenic processes, have influenced sedimentary patterns in the study interval. Autogenic processes have disrupted regional patterns and locally contributed to the poor development of cyclothem.

Vertical depositional facies patterns in the PBI are interpreted to reflect a shift in the depositional site from coastal to alluvial plain and are considered in terms of fluctuations in relative sea-level (RSL, Posamentier et al., 1988). A transgressive phase comprises poorly-drained floodplain soils, lacustrine deposits and widespread coal seams. Agglutinated foraminifera, ascribed to the "high marsh" environment, were extracted from underclay directly below the Backpit seam (Wightman et al., 1992), indicating proximity to a marine environment. At some point during

this transgression, sediment supply was cut off or completely by-passed the region, and conditions suitable for the accumulation and preservation of organic matter prevailed. The presence of foraminifera below the major coal seams suggests that major phases of peat accumulation represent local stillstands or minor regressions superimposed on the regional transgressive trend, as documented for the Holocene in Australia and Southeast Asia (Woodroffe *et al.*, 1985). Dulling upward cycles in the upper portion of the Backpit seam record transgressive pulses of short duration (1.2 ka: Chapter 3); eventually peat accumulation was unable to keep pace with relative sea-level rise and the mire was inundated. The resultant organic-rich limestone/shale roof unit probably accumulated during a highstand in sea-level and a transgressive lag at the base of the Backpit roof unit probably corresponds to the maximum flooding surface in sequence stratigraphic terminology (Galloway, 1989). Sediment influx remained at a minimum in the initial stages, and the bay supported biota that included sharks and foraminifera (see Chapter 4).

The highstand provided accommodation space for delta progradation into the bay. The bay continued to fill as relative sea-level rise moderated and channels locally cut into the bay-fill assemblage. Some channel deposits may represent delta-top distributary channels as suggested by Wanless *et al.* (1963) (see van Heerden and Roberts, 1988 for a modern analogue). Others, especially thick multistoried channel deposits (e.g. New Waterford-D), may represent regional channel incision and the establishment of a paleovalley (c.f. Gibling, 1992). Channel sandstones of this interval are under study for evolution of alluvial style during cyclothem development (P. Batson, M.Sc. thesis in progress, Dalhousie University).

A landward shift of the depositional site to a more proximal alluvial plain corresponds with lowering of

relative sea-level. At this level in the cyclothem, the sequence is dominated by autogenic alluvial processes of channel migration, switching and crevasse splay progradation. Well-drained floodplain soils (red) interbedded with thin sheet sand deposits are present near the faulted basin margins but periodically covered much of the depositional area. Calcareous paleosols may represent an extended period of non-deposition and soil-formation; some prominent units, such as those underlying the redbed units in Cyclothem 2 and 3, may reflect regional incision associated with relative sea-level lowering. Succeeding poorly-drained floodplain and extensive mire deposits represent a transgressive phase.

Systematic areal variations in thickness and sedimentary facies within the Sydney Mines and Glace Bay sub-basins during PBI deposition suggests a localised tectonic control superimposed upon, but not overwhelming, the regional controls. Local topography at any given time was relatively minor; major coals are traceable across the entire onshore area, with evidence in the Backpit seam of synchronous peat deposition over both sub-basins and adjoining or intervening areas. Tectonic activity probably was associated with differential subsidence of fault-bounded basement blocks, indicated from aeromagnetic surveys (Loncarevic *et al.*, 1989), which underlie much of the Sydney Basin (Gibling and Rust, 1990b).

2.6. SUMMARY

Well and poorly developed cyclothem (7 to 20 m thick) in the Phalen to Backpit Interval formed in response to both allogenic and autogenic processes dominated by eustasy. Major coal seams, red mudstone intervals, calcareous paleosol horizons and limestone/shale units are laterally extensive in the study area and probably reflect allogenic processes.

Depositional facies patterns occur in a somewhat predictable vertical succession from: 1)lake/bay-fill and distributary channels, 2)well-drained floodplain, 3)poorly drained floodplain to coastal plain and 4)extensive mire. This cyclothem pattern is interpreted as the result of a shift in the depositional site from a coastal environment to a more landward alluvial plain setting, back to a coastal environment, driven by fluctuations in relative sea-level.

Paleotopography influenced the distribution of sediment groups and depositional facies within the study area. Channel bodies (coarse clastic group) are proportionately more abundant near the basin margins and at New Waterford (D), whereas lake/bay-fill deposits, mires and vegetated floodplain deposits (fine clastic and organic-rich groups) are proportionately more abundant in the Sydney Mines and Glace Bay sub-basins. Differential movement over basement blocks may have caused increased subsidence in sub-basin areas resulting in generally wetter conditions.

3. THE BACKPIT SEAM: A RECORD OF PEAT ACCUMULATION AND TERMINATION IN A LATE WESTPHALIAN PALEOMIRE

3.1. INTRODUCTION

Cyclothems (Wanless and Weller, 1932), marked by basinwide coal seams, have been recognised and described in the Sydney Basin (Gibling and Bird, submitted; see Chapter 2). Coal seams are important members of Pennsylvanian cyclothems described from Europe (Ramsbottom, 1977; Leeder and Strudwick, 1987) and North America (Weller, 1930; 1964; Heckel, 1984). The extensive nature of many of these seams suggests allogenic (extrabasinal: Beerbower, 1964) control on their distribution.

Coal seams contain a detailed record of base-level fluctuations within a basin for an extended period. Investigation of variations in coal composition can reveal information on conditions and processes active during peat accumulation. Numerous authors (e.g. Hacquebard and Donaldson, 1969; Shibaoka and Smyth, 1975; Cameron, 1978; Marchioni, 1980; Hunt, 1982; Diessel, 1986; Kalkreuth and Leckie, 1989; Lamberson *et al.*, 1991) have used megascopic (lithotypes) and microscopic (microlithotype, maceral and mineral matter) analysis of coal to infer the environment of deposition and interpret the evolution of a paleomire.

The Backpit seam is one of the most continuous seams in the onshore portion of the Sydney Mines Formation (Figs. 1.2, 2.1). This study integrates the Backpit seam lithotype succession with detailed microscopic and physical coal quality analyses to characterize the Backpit mire environment. The term mire is applied here in the sense of Moore (1987) to describe "any freshwater wetland system in which peat accumulates". Investigations of vertical trends within a seam section and lateral variation between seam sections have enabled the evolution of the Backpit mire to be assessed and provided insight on relative sea-level variations in relation to cyclothem development.

3.2. THE BACKPIT SEAM

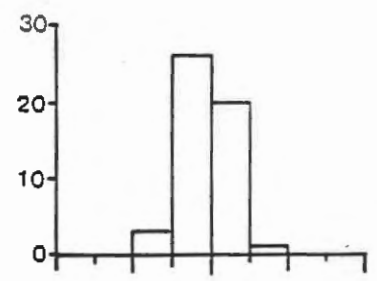
The Backpit seam (Plate 4a, b) is a banded, high volatile B to A bituminous coal, with moderate to high ash and sulphur content. The seam crops out in coastal sections and can be traced onshore Cape Breton Island for more than 45 km, parallel to depositional strike (Figs. 1.2, 2.1). It thins considerably (locally < 20 cm) in offshore wells and methane test holes drilled in mining districts within a 10 km radius of the coast. Little is known about the nature of the seam and other Sydney Basin strata beyond the mining limits. This study characterizes the Backpit seam and associated sedimentary units from coastal sections and a limited number of wells (represented by letters and symbols respectively, Fig. 1.2).

The mean vitrinite reflectance (random) of selected Backpit seam samples ranges from 0.69 to 0.76% and increases slightly from west to east (Fig. 3.1; Appendix A2.4.6, Tables A2.4a and A2.4b). Hacquebard and Donaldson (1970) documented a similar maturation trend for other Sydney Basin coal seams and attributed the trend to greater depth of burial in the east.

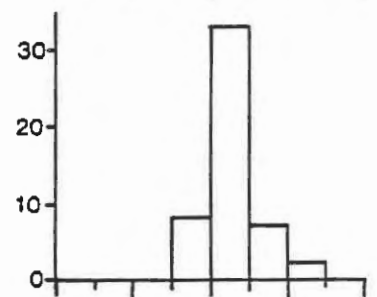
The Backpit seam in the study area ranges in thickness from about 0.6 m to 1.5 m and is thickest in the Sydney Mines and Glace Bay sub-basins (Fig. 3.2). This thickness variation may reflect a topographic influence on seam development. Hacquebard and Donaldson (1969) suggested that most Sydney Basin seams were initiated in the Glace Bay Syncline and then spread across topographic highs as the mire developed. In contrast to other Sydney Basin seams, the Backpit seam thins toward the faulted basin margins in the west and east but does not split, suggesting that the mire was removed or protected from active fluvial deposition. The Backpit seam contains several thin dull to coaly shale intervals that can be widely correlated (Fig 3.2). Hacquebard and Donaldson (1969) suggested that such

WEST

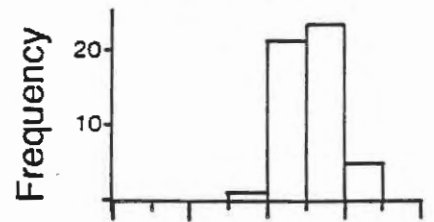
Sydney Mines
 Sample B-32
 Rrnd = 0.69 %



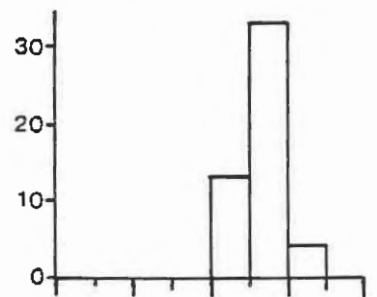
Victoria Mines
 Sample C-14.2
 Rrnd = 0.73 %



Glance Bay West
 Sample E-25
 Rrnd = 0.75 %



Glance Bay West
 Sample E-23
 Rrnd = 0.76 %



EAST

Donkin West
 Sample G-16
 Rrnd = 0.74 %

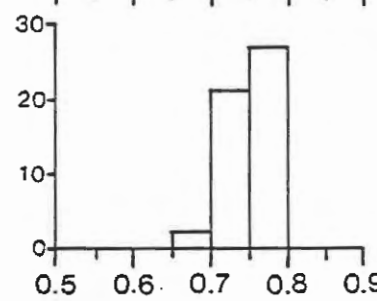


Figure 3.1. Frequency histograms generated from manual Ro analyses (random measurements). Fifty measurements were collected for each sample.

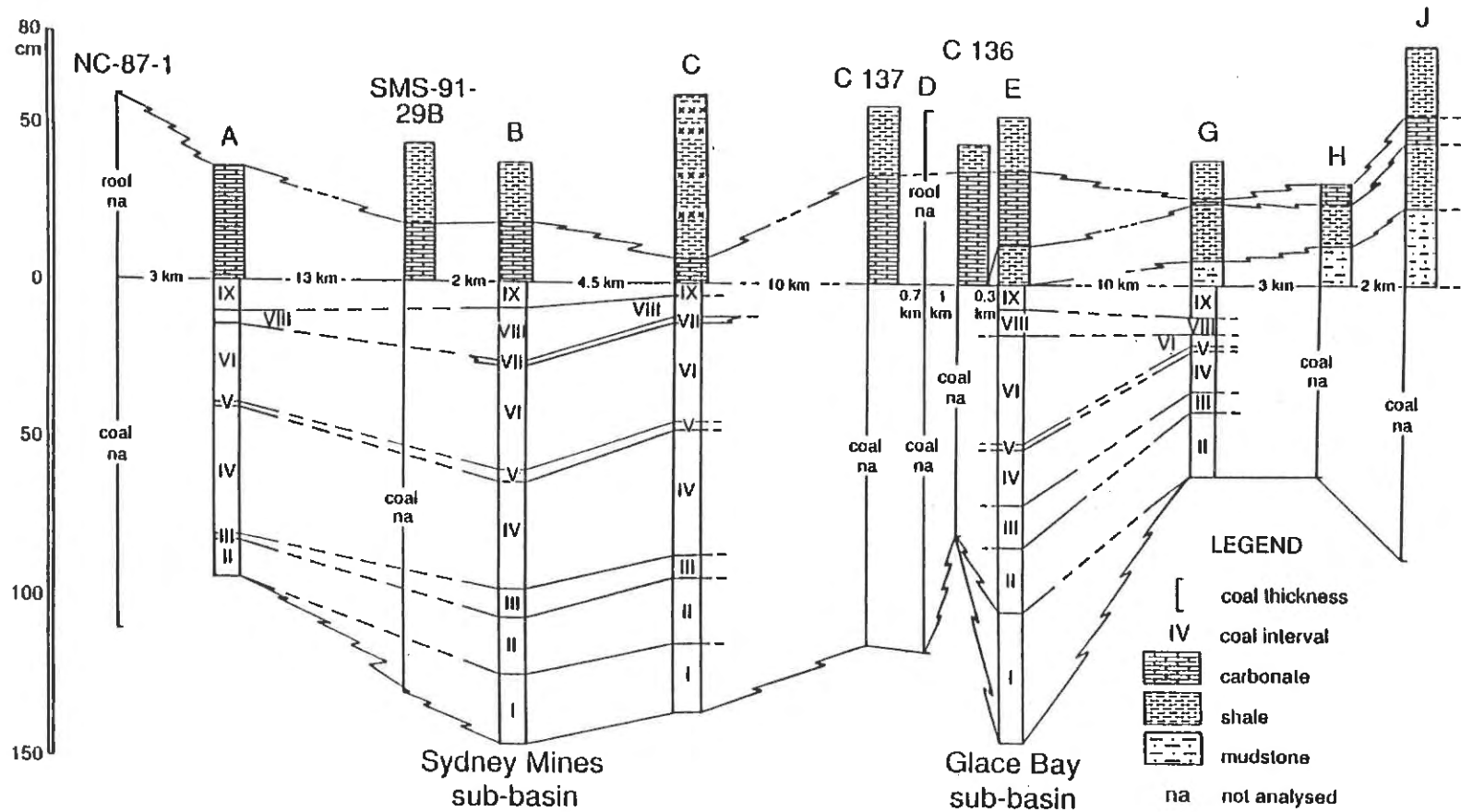


Figure 3.2. Distribution of the Backpit seam and Backpit roof unit, and lateral correlation of facies within the study interval. Datum is the top of the Backpit seam. Section locations from Figure 1.2.

intervals in the Sydney coals are time lines and divide the seams into natural depositional intervals. This interpretation assumes that these units are essentially isochronous and represent events of basinwide extent (allogenic).

In most locations, a well developed underclay with abundant root traces is present below the seam. This unit is generally a light grey, kaolinitic mudstone, void of primary sedimentary structures. Agglutinated foraminifera have been discovered above and below the seam (S. Thibaudeau, pers. comm., 1991; W. Wightman, pers. comm., 1991) indicating a paralic setting for the accumulation of the peat. Conditions were relatively stable for an extended period and peat accumulation kept pace with base-level rise. Eventually the mire drowned and an extensive organic-rich limestone to platy shale sequence was deposited (see Chapter 4).

3.3. SUMMARY OF METHODS

Two sample sets were collected to characterize the Backpit seam laterally and vertically within the basin (Appendix A2.1). At each of five coastal sections (A, B, C, E and G, Fig. 1.2) a series of channel samples representing specific seam intervals were collected. These samples were analysed for ash and sulphur following standard procedures (Appendix A2.2).

Oriented coal samples representing the total seam thickness were collected at each site for detailed lithotype analysis. Polished blocks were prepared perpendicular to bedding following the procedure outlined in Appendix A2.4.1. Lithotype logs were constructed for each section using a modified Australian classification scheme (Table 3.1) with a minimum band width of 5 mm (Diessel, 1965). Detailed maceral and microlithotype composition of the Glace Bay West section (E) was determined on polished blocks using a manual

Table 3.1. Lithotype classification scheme.

Lithotype (Diessel, 1965)	Description
Bright (BR)	subvitreous to vitreous lustre, or conchoidal fracture, <10 per cent dull
Bright Banded (BB)	Bright coal with some thin dull bands. 10-40 per cent dull
Banded (B)	Bright and dull coal bands in equal proportion. 40-60 per cent dull
Dull Banded (DB)	Dull coal with some thin bright bands. 10-40 per cent bright
Dull (D)	Matt lustre, uneven fracture. <10 per cent bright
Fibrous Coal (F) (fusain)	Satin lustre, friable.

Note: Minimum thickness for each lithotype is 0.5 cm with the exception of fusain layers (F), pyrite bands (PY) and coaly shales (CS).

Lithotype abbreviations (in brackets) used in tables and figures throughout text and Appendices.

point counting technique (Appendix A2.4.3). In addition, maceral group composition and vitrinite reflectance were determined microscopically using automated image analysis (IBAS-2 system, sections B, C and E; Appendix A2.4.2) or manual petrography (by grouping manual point counts, section E; Appendix A2.4.3).

3.4. RESULTS

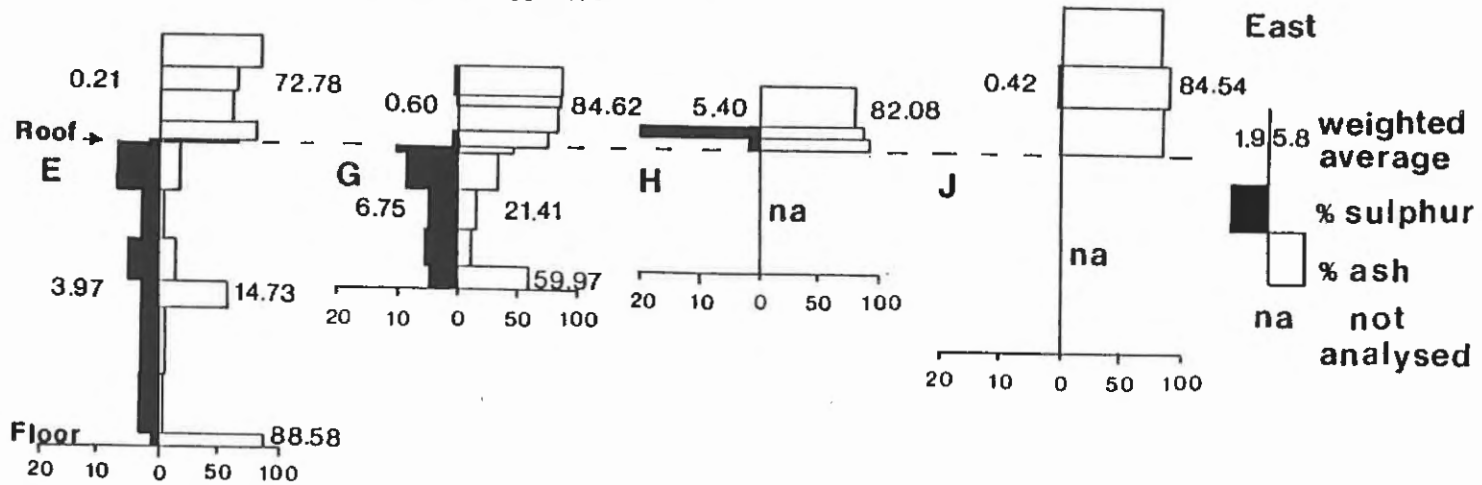
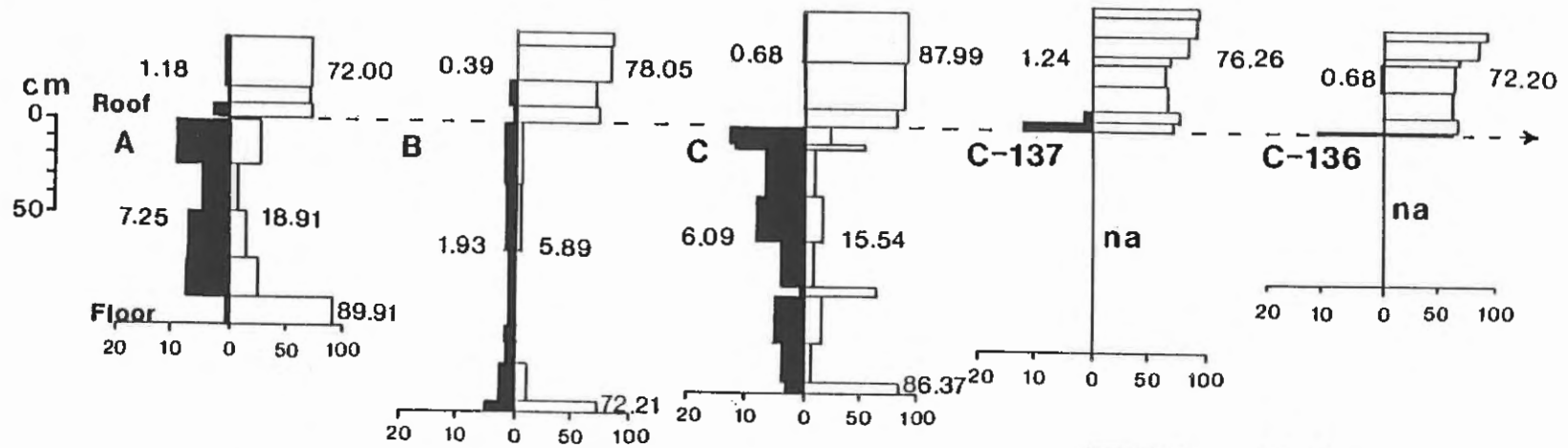
3.4.1. Mineral Matter: Occurrence and Distribution

The vertical and lateral distributions of ash and sulphur in the Backpit seam are illustrated in Figure 3.3 (Table A2.1a). Average ash and sulphur contents are slightly higher near the faulted basin margins (A - Bras d'Or and G - Donkin W). Both ash and sulphur typically increase upward within a seam section and exhibit highest values adjacent to the roof strata. The total seam average composition of $15.3 \pm 6\%$ ash and $5.2 \pm 2\%$ sulphur (Table A2.1c) compares well with reported Backpit coal quality (Haite, 1952). Hacquebard and Donaldson (1969) quote average values of 11.53% ash and 6.21% sulphur from the Backpit seam in the Sydney Mines mining district.

Other seams within the PBI include the unnamed seam that forms the upper unit of Cyclothem 1 as well as other less extensive seams (see Fig. 2.1 for stratigraphic position). These coals or coaly shales are generally high in ash and sulphur (Table A2.1b); ash content ranges from 5.81% to 41.27% (average 24.28%) and sulphur content ranges from 2.65% to 19.35% (average 8.58%). Localized organic-rich layers probably represent the remains of vegetation that accumulated on wet floodplains adjacent to active depositional systems.

A large portion of the sulphur in the Sydney Basin coals is pyritic (King, 1953; Hacquebard and Avery, 1982; Birk *et al.*, 1986). The Backpit seam contains abundant syngenetic and some epigenetic pyrite. Microscopically,

West



weighted average
 % sulphur
 % ash
 na not analysed

Figure 3.3. Sulphur and ash distribution in the Backpit seam and associated strata. Section locations from Figure 1.2.

these forms include framboids, euhedral to subhedral crystals, clusters, globules, veinlets, cell fillings and massive patches (as described in Pilgrim, 1983, p. 24-25). Pyrite is concentrated above the clay parting in the Glace Bay West seam section as well as near the top of the seam (Table A2.11d). Secondary sulphates and iron stains were noted locally on weathered cleat surfaces (Plate 4a).

Detrital clays constitute the major siliciclastic component observed in the Backpit coal matrix. Peats that yield economic coal seams are usually well removed from clastic input except for rare flooding events (McCabe, 1984). The Backpit seam records one such event in the lower to middle portion of the seam. This unit (Interval III, Fig. 3.2) can be traced for more than 45 km across the onshore portion of the basin and represents a major base-level rise. The layer varies from coaly shale to a dull banded lithotype and locally contains over 60% ash due to the influx of clastic sediment into the mire. Other minor sediment influxes are recorded in the numerous thin clay, inertodetrinite- and liptodetrinite-rich detrital layers recognised microscopically (Plate 5e). Microscopic examination revealed an increase in detrital clay minerals in the upper portion of the seam (Table A2.11d), corresponding with megascopic dulling upward trends.

3.4.2. Lithotypes

3.4.2.1. Character and Distribution

Stach et al. (1982, p. 171) defined 'coal lithotypes' as "the different macroscopically recognizable bands of coal seams". Lithotype logs (Fig.3.4) illustrate the vertical megascopic variability of the Backpit seam. The volume percent distribution of lithotypes for each section was calculated based on the aggregate thickness of each lithotype (Fig. 3.5). Total seam lithotype distributions are comparable across the basin suggesting that relatively

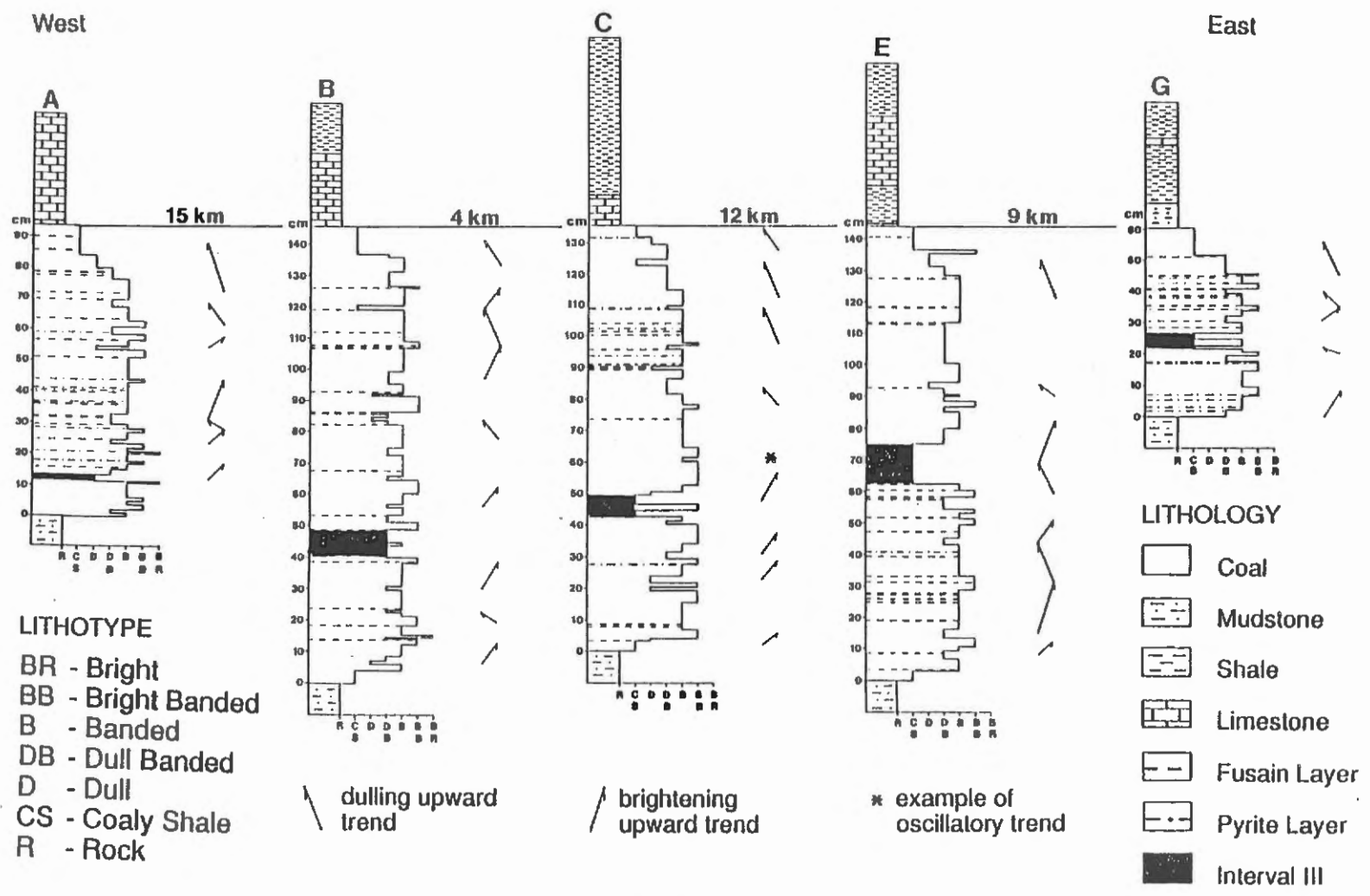


Figure 3.4. Lithotype logs for the Backpit seam: A-Bras d'Or; B-Sydney Mines; C-Victoria Mines; E-Glance Bay West; G-Donkin West. Top of seam is datum.

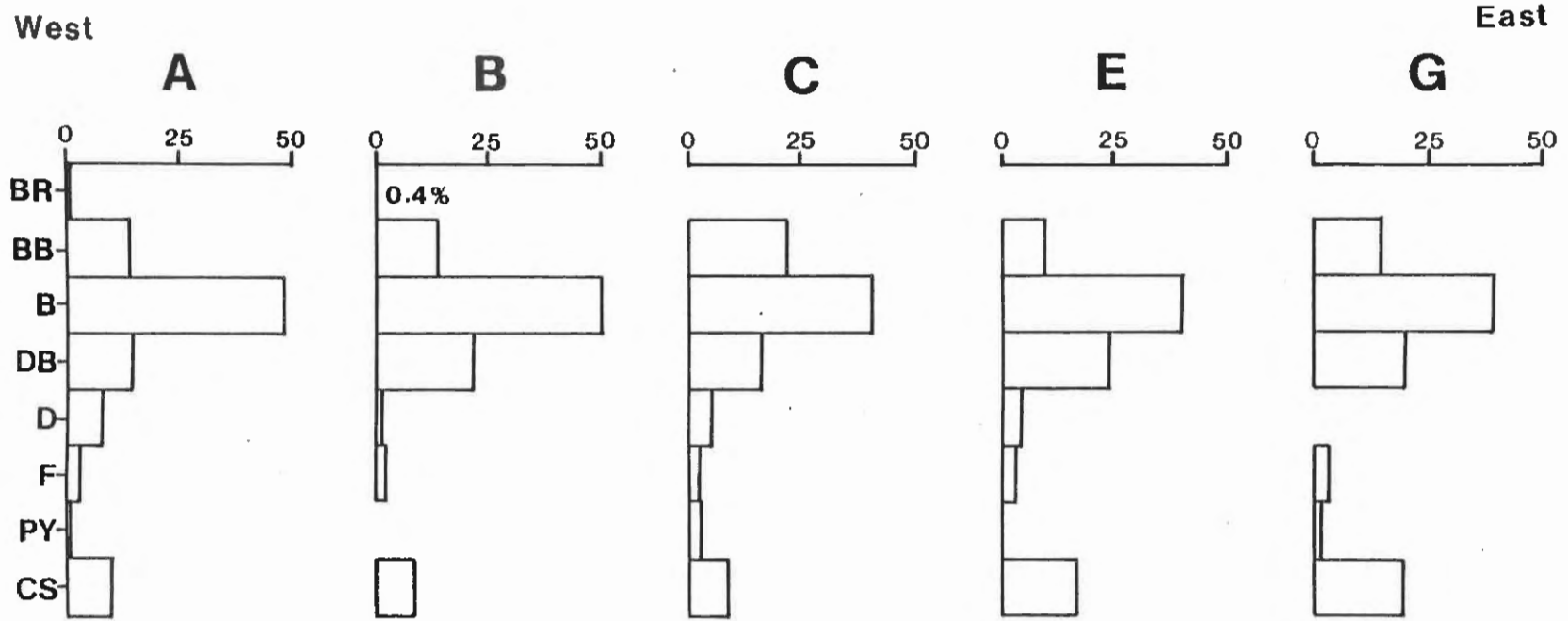


Figure 3.5. Distribution of lithotypes, pyrite and coaly shale in the Backpit seam (volume %).

similar conditions prevailed during the accumulation of the peat. Banded lithotypes comprise at least 40% of the total seam. Bright lithotypes are minor and were only recorded in the west (A-Bras d'Or and B-Sydney Mines). Coaly shales increase in proportion eastward. The Victoria Mines (C) seam section contains the greatest concentration of megascopic pyrite.

3.4.2.2. Fusain: A Distinctive Lithotype

Numerous fusain layers occur in all seam sections studied and can usually be traced laterally within outcrop limits. These layers are generally lenticular, thin (1 to 2 mm) and represent 3 to 4% of the total seam thickness. They are dull and fibrous in hand specimen and leave a sooty residue when handled. Bedding-plane surfaces reveal randomly oriented fusain patches (Plate 4d). Microscopically, these layers consist of well preserved, moderate to high reflecting cell wall structures (Plate 5f). The fusinite cell lumina are generally empty but can be filled or partially filled with pyrite, carbonates or clays. Some layers exhibit a typical "bogen" structure, the result of brittle fracture of the cell walls during compaction (Stach *et al.*, 1982). This suggests that the fusinite was in a brittle form prior to burial and coalification. These fusains exhibit characteristics of pyrofusain, the products of wildfires within a mire (Stach *et al.*, 1982; Scott, 1989).

Hacquebard and Donaldson (1969) also reported abundant fusain layers in the Backpit seam. Detailed microlithotype logs (courtesy of P. Hacquebard, 1991) reveal fusain distributions comparable to those observed in this study.

3.4.2.3. Lithotype Successions

Three patterns of lithotype succession were observed in the Backpit seam (Fig. 3.4): 1) brightening upward; 2)

dulling upward and 3) oscillatory. Brightening and dulling upward cycles are characterized by the increase/decrease in lithotype brightness in at least three consecutive lithotype intervals. Oscillatory patterns are characterized by alternating lithotypes and are especially common between banded and bright banded lithotypes. Fusain layers are often interbedded with other lithotypes or occur at the boundary between two lithotypes. These layers are not considered indicative of water level fluctuations within the Backpit mire (Scott and Jones, 1992), and are therefore ignored when establishing lithotype successions.

Brightening upward cycles are 10 cm thick on average (5 to 26 cm range). They are commonly abruptly punctuated by a dull to dull banded lithotype, or less commonly are succeeded by a gradual dulling upward cycle. Dulling upward cycles in the Backpit seam average 12 cm in thickness (2 to 22 cm range). They are succeeded by either a gradual brightening upward succession or brighter lithotypes. Brightening upward cycles predominate in the lower to middle portion, whereas dulling upward cycles predominate in the upper portion of the seam (Fig. 3.4). The Backpit mire terminated during a dulling upward cycle that culminated in the deposition of an organic-rich limestone/shale sequence.

3.4.3. Macerals and Microlithotypes

3.4.3.1. Introduction

Microscopically, coal is a heterogeneous substance that consists of organic components referred to as macerals (the organic equivalent of minerals in rocks) and a variety of inorganic minerals (Stach *et al.*, 1982; Bustin *et al.*, 1983). Macerals are divided into three main groups based on morphology and reflectance (in order of increasing reflectance): 1) liptinite, derived mainly from spores, resins, cuticles, algae; 2) vitrinite, predominantly woody material and tissues; and 3) inertinite, derived mainly from

charred or oxidised plant material. Each maceral group can be subdivided into specific macerals (Table 3.2).

Microlithotypes are natural associations of maceral groups with a minimum band width of 50 μm (Table 3.3). They are divided into four main groups: 1) monomaceralic (one maceral group represents at least 95%); 2) bimaceralic (two maceral groups, each represents greater than 5%); 3) trimaceralic (three maceral groups, each representing greater than 5%) and 4) carbominerite (mixture of macerals and minerals; represents 20 to 60% minerals for clays, carbonates and silicates; 5 to 20% for pyrite).

Numerous workers have shown a relationship between coal composition (macerals and microlithotypes) and lithotype (e.g. Diessel, 1965; Cameron, 1978; Marchioni, 1980). Vitrinite tends to increase at the expense of other constituents as the lithotype brightness increases. This study integrates the lithotype divisions of the Backpit seam with detailed coal compositional data collected using standard coal petrographic techniques and automated image analysis.

3.4.3.2. Automated Image Analysis

In the last twenty years various adaptations have been made to the standard petrographic microscope to automatically analyse the reflectance of coals and coal blends (e.g. England *et al.*, 1979; Riepe and Steller, 1984; Lee, 1985; Pratt, 1989). These systems generate a cumulative reflectance histogram from a single crushed grain mount sample, and the sample composition is determined from the histogram distribution. Other automated techniques have been developed to recognise and record vertical compositional variations of coal blocks and characterize lithotypes and/or microlithotypes (e.g. Chao *et al.*, 1982; Crelling, 1982; Davis *et al.*, 1983; Lamberson *et al.*, 1990). In this study, an IBAS-2 image analysis system is used to

Table 3.2. Detailed maceral/minerals included in manual counts.

GROUP MACERAL	MACERALS*
VITRINITE	Telinite (T) Telocollinite (TC) Desmocollinite (DC) Corpocollinite (CC) Gelocollinite (GC) Vitrodetrinite (VD)
LIPTINITE	Macrosporinite (Mg) Microsporinite (Ms) Tenuisporinite (T) Sporinite (Sp) Crassisporinite (C) Sporangium (Spg) Cutinite (Cu) Tenuicutinite (T) Crassicutinite (C) Resinite (Re) Bodies (B) Wisps (W) Exsudatinite (Ex) Alginite (Al) Telalginite (T) Lamalginite (L) Liptodetrinite (Ld)
LOW REF. INERTINITE	Semifusinite (SF) Semimacrinite (SM)
HIGH REF. INERTINITE	Empty Cells (E) Fusinite (F) Pyrofusinite (PF) Filled Cells (F) Bogen Structure (B) Degradofusinite (DF) Macrinite (Ma) Micrinite (Mi) Secretion Sclerotinite (Sc) Inertodetrinite (Id)
MINERAL MATTER	Clays (Cl) Carbonates (Ca) Quartz (Si) Pyrite (Py) Other (Oth)

* - as defined in Stach *et al.*, 1982.

() - abbreviations used in tables and figures

Table 3.3. Microlithotypes included in manual counts.

GROUP	MICRO-LITHOTYPE*	MACERAL/MINERAL ASSOCIATIONS
MONO	Vitrite	>95% V
	Liptite	>95% L
	Inertite	>95% I
BI	Clarite	>95% V+L
	Durite	>95% I+L
	Vitrinertite	>95% V+I
TRI	Duroclarite	V,L,I, where V>I+L
	Clarodurite	V,L,I, where I>V+L
	Vitrinertoliptite	V,L,I, where L>V+I
CARBO-MINERITE	Carbargilite	20-60% Ar
	Carbankerite	20-60% An
	Carbosilicite	20-60% Si
	Carbopyrite	5-20% Py
	Other	20-60% Oth
MINERAL MATTER	Argillite	>60% Ar
	Ankerite	>60% An
	Silicate	>60% Si
	Pyrite	>20% Py
	Other	>60% Oth

where: V - vitrinite
L - liptinite
I - inertinite
Ar - argillite
An - ankerite
Si - silicates
Py - iron pyrites (includes pyrite and marcasite)
Oth - other minerals

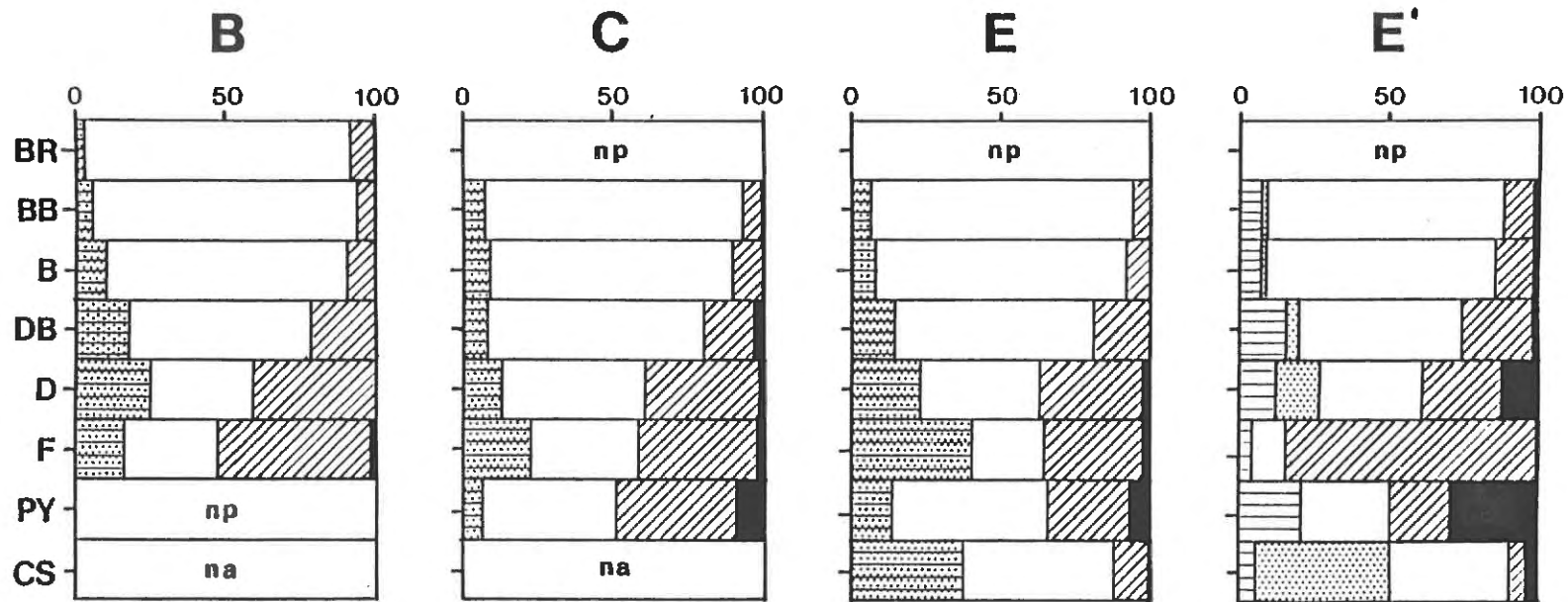
* - as defined in Stach *et al.*, 1982.

distinguish and record maceral groups within a microscopic image based on grey-level value. User-defined grey-level groups are "mapped" over the length of an oriented polished coal block and variation in organic composition is documented.

3.4.3.3 Group Maceral Composition

Three Backpit seam sections were analysed by the IBAS-2 image analysis system at 0.5 mm vertical and horizontal intervals and a continuous stacked-bar compositional profile was generated for each section (Appendix A2.4.2). Each megascopically recognised lithotype exhibited a characteristic stacked-bar profile signature (Fig. A2.3) and vertical variations in group maceral composition were calculated (Tables A2.5 to A2.10). A detailed maceral analysis (Table 3.2) was repeated on the Glace Bay West seam section at 1.0 mm vertical and horizontal intervals using manual petrographic methods (Appendix A2.4.3). These data were also grouped by lithotype (Tables A2.11 to A2.13).

The average maceral composition of bright verses dull lithotype groups is distinct (Fig. 3.6). Vitrinite is predominant in the bright to banded lithotypes and liptinite and inertinite increase gradually, at the expense of vitrinite, in the dull banded to dull lithotypes (data from Tables A2.6g, A2.8g, A2.10g and A2.13g). The brighter lithotypes (bright (BR), bright banded (BB) and banded (B)) generally contain greater than 75% vitrinite, low liptinite and inertinite (generally less than 10%) and very low pyrite (generally less than 1%). Vitrinite proportion decreases slightly from bright to banded lithotype groups. Dull banded (DB) lithotypes contain 55 to 70% vitrinite; liptinite and inertinite increase to approximately 15 to 20% and pyrite exhibits a slight increase. Vitrinite proportion in the dull (D) lithotypes drops to less than 50%. This is balanced by a substantial increase in inertinite and



Legend







-  Liptinite + Clays
 -  Liptinite Only
 -  Clays Only
 -  Vitrinite
 -  Inertinite
 -  Pyrite
- } E'

Figure 3.6. Average group maceral composition, by lithotype, for each Backpit seam section. Section locations from Figure 1.2. B, C, E - automated image analysis; E' - manual petrography. Lithotypes abbreviated as follows: BR-bright; BB-bright banded; B-banded; DB-dull banded; D-dull; F-fusain; PY-pyrite; CS-coaly shale; np-not present; na-not analysed.

liptinite.








Automated and manual microscopy results from the same samples (Fig. 3.6, E and E') suggest that the IBAS-2 automated system has difficulty with components such as pyrite and clay minerals. Pyrite is consistently under-represented, especially when it occurs in discrete layers (PY on Fig. 3.6). The grey-level of clays often overlap with liptinite values and it is difficult to distinguish between the two components using this method. Fusain layers also pose a problem due to the large volume of empty cells that are often misidentified by the IBAS system as liptinite. Although these problems are significant, it is relatively easy to recognise these layers when direct comparison is made with the polished coal block. A detailed discussion of the discrepancies between manual and automated petrographic data is found in Appendix A2.4.5.

To compare the IBAS-2 results and standard petrographic results, the following adjustments were made to the IBAS data:

1. The "liptinite group" is revised to include liptinite + other mineral matter (clays, carbonates, quartz).
2. Low- and high-reflecting inertinite are combined.
3. Pyrite content is considered in a relative sense (i.e. intervals with pyrite values $> 1\%$ are probably very high in pyrite).
4. Fusain layers are recognised by their distinctive IBAS composition (i.e. high inertinite and liptinite) as well as megascopic appearance. These layers are assumed to contain little or no liptinite.

The group maceral composition of the Backpit seam is variable and can change over a short vertical distance. This variability is reflected in the lithotype compositional profile of each seam section analysed (Figs. 3.7 and 3.8; data from Tables A2.5, A2.7, A2.9 and A2.12). Vitrinite is the main maceral group and seam average vitrinite proportion

LEGEND

	Liptinite + Clays	
	Liptinite Only	} E'
	Clays Only	
	Vitrinite	
	Total Inertinite	
	Fusain Layer	
	Pyrite Layer	
III	Coal Interval	
*	Seam Average (excluding coaly shale intervals)	

Legend for Figures 3.7 and 3.8.

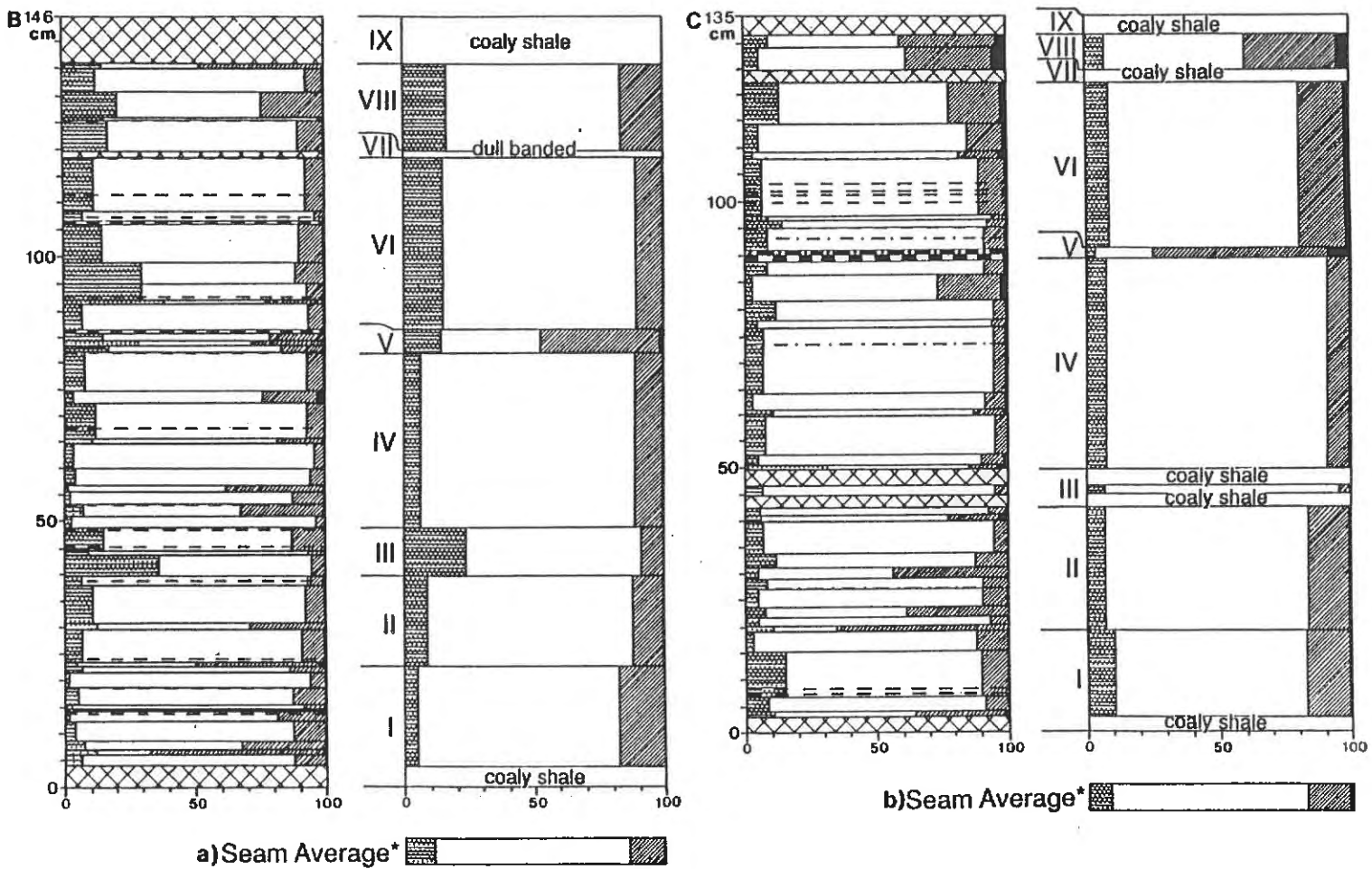


Figure 3.7. Group maceral composition profiles, by lithotype and seam interval for a) B-Sydney Mines (IBAS-2) and b) C-Victoria Mines (IBAS-2).

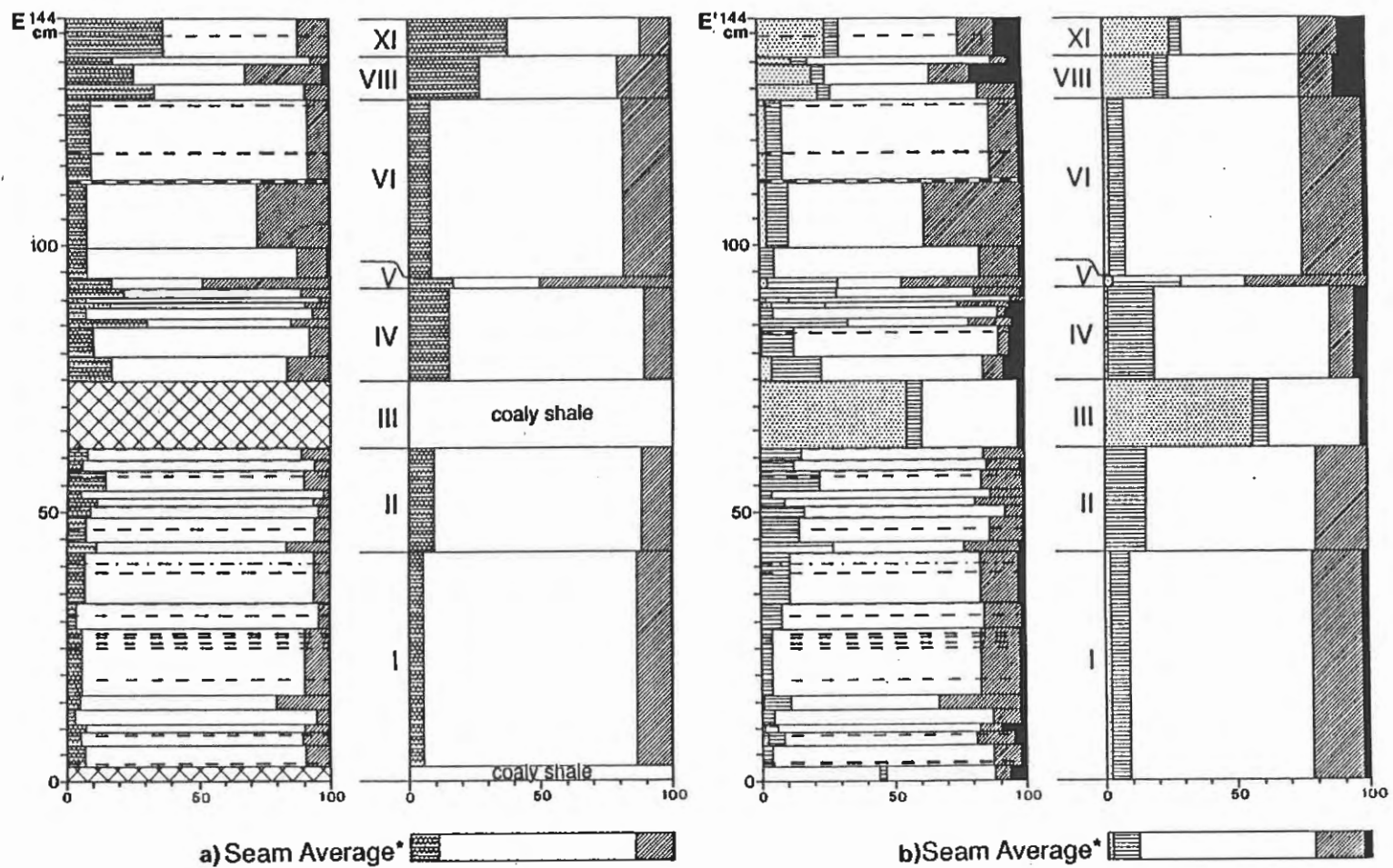


Figure 3.8. Group maceral composition profiles, by lithotype and seam interval for a) E-Glace Bay West (IBAS-2) and b) E'-Glace Bay West (Manual).

is generally greater than 70% (excluding coaly shale intervals). Brightening upward cycles show an upward decrease in liptinite + clays and/or inertinite and a concomitant increase in vitrinite. Dulling upward cycles exhibit the opposite trend. Slight compositional variations in maceral components are observed in the oscillatory sections.

3.4.3.4. Detailed Maceral Composition

A detailed manual petrographic analysis was conducted on the Glace Bay West seam section to identify specific maceral types and distributions and characterize coal facies (Section 3.4.4.3). Table 3.2 contains a list of the macerals considered in the point count analysis (as outlined in Appendix A2.4.3; data in Table A2.11).

Telocollinite (structured vitrinite, Plate 5a) and desmocollinite (unstructured vitrinite, Plate 5b, c) are the main vitrinite macerals in the seam section. Telocollinite content is higher in the lower portion of the seam and tends to be enriched in the bright banded and locally in banded lithotypes. This suggests relatively high water (excellent preservation of cell structures) and an abundance of arborescent vegetation (i.e. forest environment) in this portion of the seam. Desmocollinite provides a matrix for other macerals and is the most common vitrinite maceral in the upper portion of the seam. It forms from the gelification of attrital organic matter (densinite, attrinite) from a variety of sources (Diessel, 1986). Vitrodetrinite is present in the transitional interval at the base of the seam as well as in other coaly shales and some dull lithotypes and was probably transported prior to deposition. Corpocollinite occurs in minor amounts throughout the seam. These rounded to oval cell-fillings occur in situ or as detrital fragments within desmocollinite.

Sporinite (Plate 5) is the major liptinite component and includes miospores, megaspores and sporangia. Thin-walled miospores (tenuisporinite) are the most common type and occur in all lithotypes. Rare intact sporangia, with visible spores, occur in Intervals I and II (Fig. 3.8, below the parting). Liptodetrinite tends to be concentrated in the duller lithotypes and suggests degradation and transportation of liptinitic material; its association with inertinite fragments and clays confirms the detrital nature of these dull layers. Cutinite (leaf cuticle) occurs rarely in lithotypes above and below the parting (Interval III). Alginite is also rare.

Distinctive resinite bodies occur in certain layers in the Glace Bay West seam section. They are generally oval to flattened in shape and exhibit high relief, very low reflectance and high fluorescence; common oxidation rims suggest transport. The bodies are concentrated in dull layers above the coaly shale parting (Interval III). Some resinite bodies are vesicular and the cavities are filled with pyrite (Plate 5c, d). Hacquebard (1952) referred to these bodies as "squat bulky spores" and later reinterpreted them as "peculiar resin bodies" (Hacquebard and Donaldson, 1969). White (1914) described similar resin canals from Carboniferous and Permian plants.

Secretion sclerotia are commonly associated with fusain layers and probably represent a fusinitized equivalent of these resin bodies. They are usually ovoid in apparent shape and exhibit high relief and high reflectance. Draping of other macerals around these bodies (Plate 5b) suggests that they were in a fusinitized form prior to compaction. Lyons et al. (1982) and Thompson et al. (1982) attributed similar bodies in Appalachian Carboniferous coals to fusinitized resin rodlets and inferred that these bodies were once resin ducts from medullosan seed ferns. They suggested the term resino-sclerotinite to differentiate

these macerals from sclerotinite of fungal origin. Misra *et al.* (1990) suggested that resino-sclerotinite could provide a correlation tool for Indian Permian coals.

Fusinite is common in the Backpit seam typically as discrete layers (Section 3.4.2.2, Plate 5f). Inertodetrinite is common in the duller lithotypes and represents fragments of fusinite or other inert macerals that are too small to identify (Plate 5e). The curved and shard-like shape of these fragments suggest that they represent the brittle remains of charred cells, probably transported by wind and/or water and incorporated into the peat. Semifusinite is common in some layers and represents the partial or incomplete charring or oxidation of woody tissues. Cell structure is visible but cells are generally deformed or flattened in a non-brittle manner. Macrinite and semimacrinite occur as massive discrete bodies and show evidence of transport. They probably originated as humic colloids that were picked up by floods and oxidised before final burial (Diessel, 1982). Groundmass macrinite, caused by oxidation of the peat surface, was not observed in this study. Micrinite is common as lenses parallel to bedding and is often associated with liptinite macerals. It is a secondary maceral, and probably formed during coalification from the lipid components of various liptinite macerals (Stach *et al.*, 1982).

3.4.3.5. Microlithotype Composition

A total seam microlithotype analysis was also completed on the Glace Bay West seam section to characterize maceral associations (Table 3.3) and assess coal facies (Section 3.4.4.2). Average microlithotype composition for each lithotype (Fig. 3.9, Table A2.15) generally corresponds to lithotype brightness. Vitrinite-rich microlithotypes predominate and tend to decrease from bright to dull lithotypes. Inertinite- and liptinite-rich microlithotypes

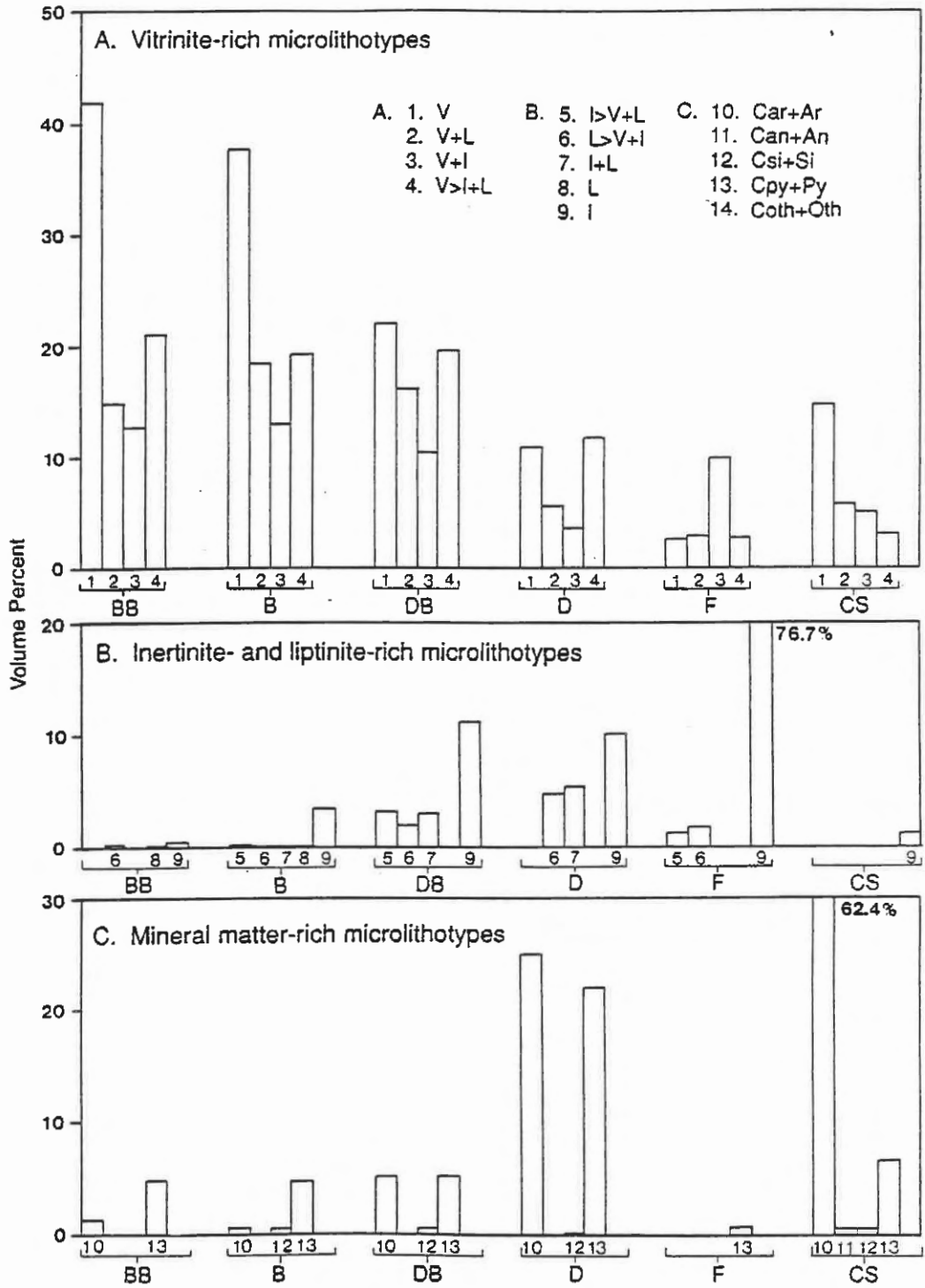


Figure 3.9. Average microlithotype composition for each lithotype, Glace Bay West seam section. Microlithotype abbreviations listed in Table 3.3.

are present in minor amounts in the bright banded, banded and coaly shale lithotypes. Their content increases in the dull banded and dull lithotypes. Fusain contains a large portion of inertite, as would be expected. Mineral matter-rich microlithotypes occur in minor amounts in the brighter lithotypes; a substantial increase in these components was observed in the dull to coaly shale lithotypes.

A ternary diagram (Fig. 3.10) illustrates the microlithotype compositional variations, by individual lithotype, for the Glace Bay West seam section. The bright banded and banded lithotypes overlap in range. They are low in durite + inertite and contain variable amounts of vitrite + clarite and intermediate microlithotypes. Dull banded to dull lithotypes tend to be higher in intermediates and durite + inertite.

3.4.4. Coal Facies Analysis

3.4.4.1. Seam Intervals

Variation in coal facies reflects changes in the depositional environment of the mire (Diessel, 1982; Strehlau, 1990). The Backpit seam was divided into nine intervals of peat accumulation (I to IX) based on the occurrence of clastic partings and distinctive dull layers (Figs. 3.2, 3.7 and 3.8). These duller intervals (III, V, VII, IX) exhibit lateral facies changes and can be traced across the onshore portion of the basin. Intervals I, II, IV, VI, and VIII vary in thickness and facies in the study area. Interval I is thickest in the Glace Bay West section, thins laterally and is absent near the basin margins at Bras d'Or and Donkin West, an observation that supports the diachronous spread of the Backpit mire from the Glace Bay sub-basin as postulated by Hacquebard and Donaldson (1969).

Interval III is a 13 cm thick coaly shale layer in the Glace Bay West seam section and thins into a dull to dull banded interval laterally. This change represents the

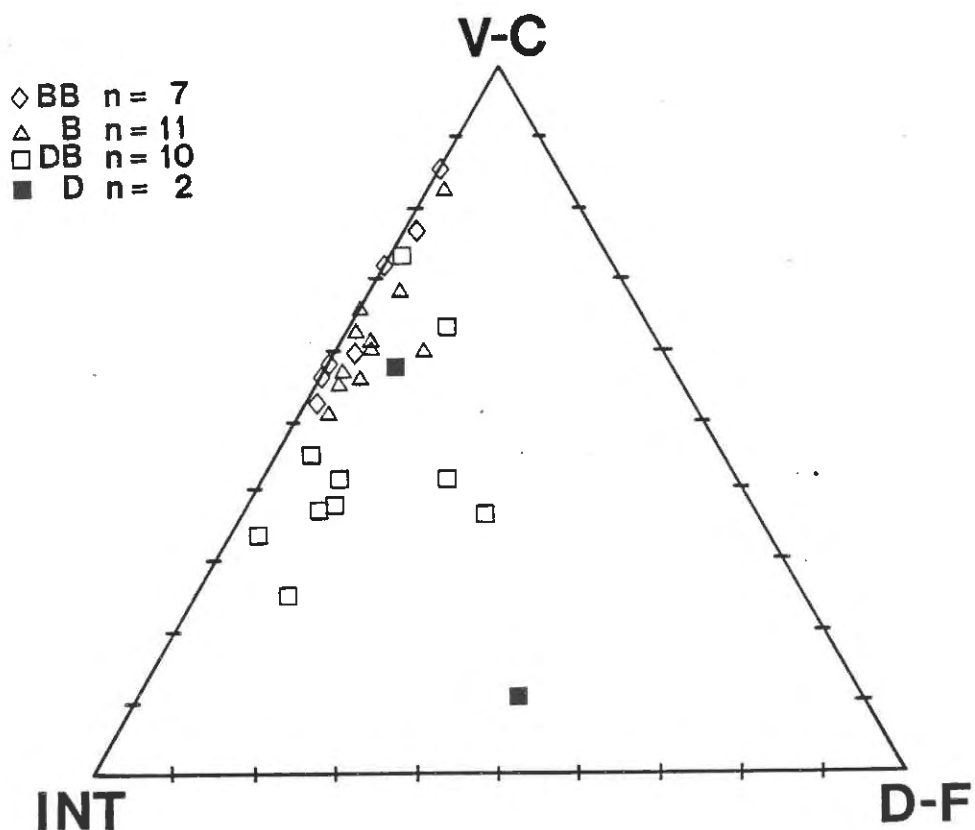


Figure 3.10. Microlithotype compositional variation, by lithotype, for the Glace Bay West section (mineral matter free). V-C = vitrite + clarite + liptite; D-F = durite + inertite; INT = intermediate microlithotypes, including vitrinertite, duroclarite, clarodurite and vitrinertoliptite.

transition from an open water environment in the Glace Bay sub-basin to a shallower limno-telmatic, possibly reed moor environment laterally. Interval VII, a shaley layer restricted to the Sydney Mines and Victoria Mines seam sections, probably represents localised flooding of the mire in the Sydney Mines sub-basin. A laterally extensive coaly shale (Interval IX) occurs at the top of the seam and provides evidence for a major base-level rise. A thin inertinite-rich interval (V) has tentatively been correlated across the basin. This interval is generally dull, contains abundant fusain and may represent a major fire horizon.

3.4.4.2. Microlithotype-derived Coal Facies

Hacquebard and Donaldson (1969) introduced a coal facies classification based on the microlithotype composition of coal intervals from seams in the Sydney Basin of Nova Scotia. Coal intervals were established based on the occurrence of clastic partings and distinctive dull layers. They integrated mire groundwater level as documented by Osvald (1937) with paleoenvironmental studies of Tertiary brown coals (Teichmüller, 1950; Teichmüller and Thompson, 1958) and proposed four main swamp environments:

1. Forest-terrestrial-moor (FtM) - terrestrial zone, above high water mark; abundant inertite and inertinite-rich vitrinertite.
2. Forest moor (FM) - telmatic to limno-telmatic zone; transitional between terrestrial and open moor environment; abundant vitrite, and vitrinite-rich clarite and vitrinertite.
3. Reed Moor (RM) - telmatic to limno-telmatic zone; transitional between terrestrial and open moor environment; abundant liptite, liptinite-rich clarite, duroclarite and vitrinertoliptite.
4. Open Moor (OM) - limnic zone; subaquatic; abundant clarodurite, liptinite-rich durite, carbominerite and

mineral matter.

Facies variations in the Glace Bay West section are here characterized using this classification scheme. The average microlithotype content of each lithotype and each seam interval was plotted on a four component facies diagram (Fig. 3.11, a and b respectively). Microlithotype groups (A, B, C and D, Fig. 3.11) were modified slightly to reflect the additional categories counted in this study.

The telmatic forest moor, the most prevalent environment in the Backpit seam, is represented primarily by bright banded to banded lithotypes. One bright banded lithotype plots anomalously in the limno-telmatic forest moor environment. It occurs near the top of the seam, contains abundant finely disseminated mineral matter and may represent a single drifted log. Dull to dull banded lithotypes plot in distinct fields in Figure 3.11a and represent either telmatic reed moor or limno-telmatic reed to forest moor environments. A small cluster of dull banded lithotypes plot in the telmatic forest moor region. These lithotypes are relatively rich in inertite and vitrinertite, thus accounting for their dull appearance. Open moor environments are represented by dull to coaly shale lithotypes. Fusain layers contain abundant inertite and plot in a cluster in the forest-terrestrial-moor environment (Fig. 3.11a). The reader is reminded of the problems associated with using fusain layers as environmental indicators and they are plotted on this diagram for consistency only.

According to this classification scheme (Fig 3.11b), accumulation of the Backpit peat began in a telmatic forest moor environment (Interval I). Three large-scale facies trends are apparent during the history of the seam. A "wetting" upward trend, from forest (I), to reed (II), to open moor (III) facies characterizes the lower portion of the seam at Glace Bay. This was followed by a "drying"

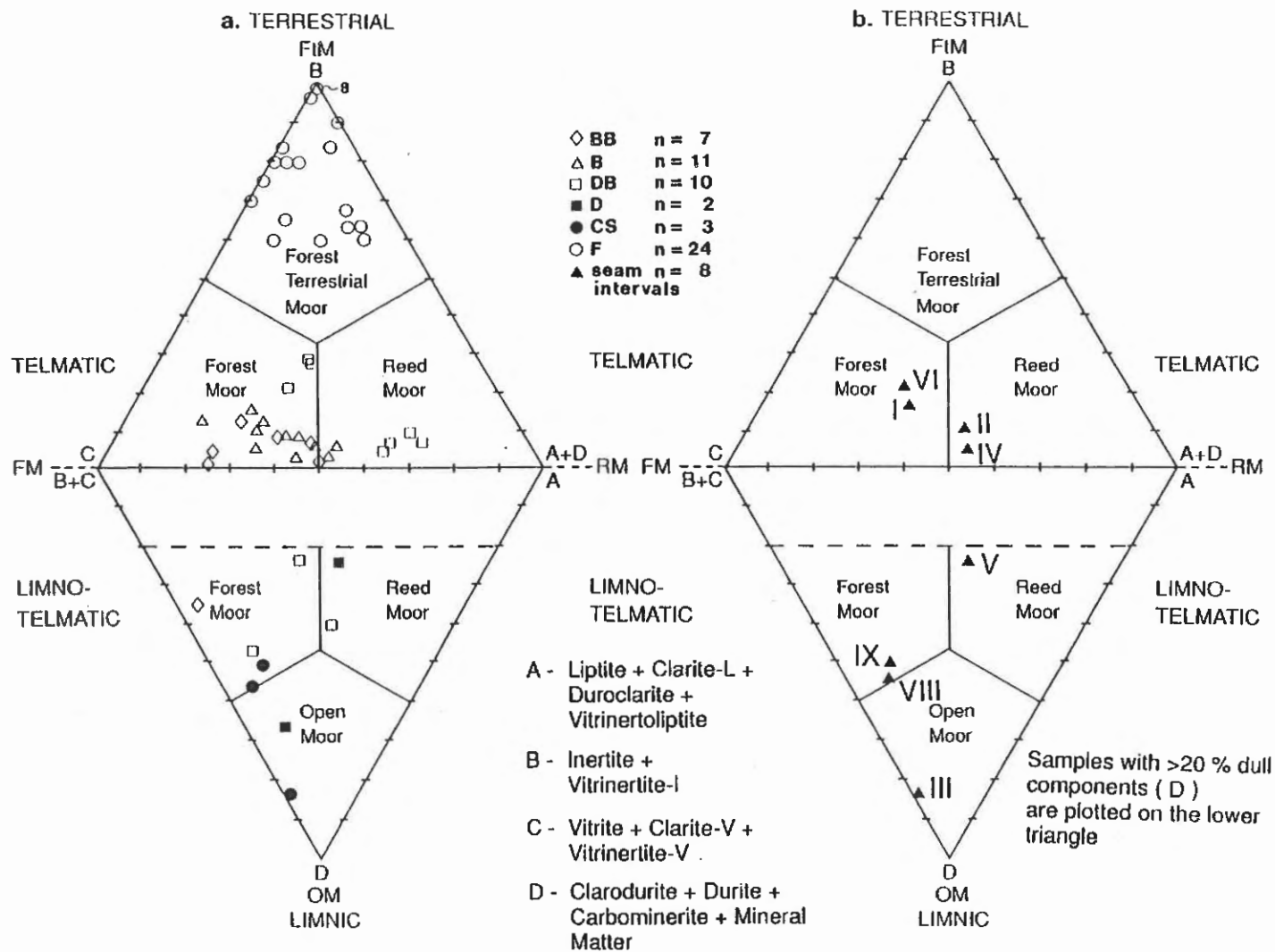


Figure 3.11. Microlithotype group composition of the Backpit seam, Glace Bay West; plotted on a modified facies diagram of Hacquebard and Donaldson (1969): a. lithotypes; b. seam intervals.

upward trend, from open moor (III), to reed (IV), to forest moor (VI) environments. An extensive fire event is recorded in Interval V. High spore content associated with inertinite suggests a water-lain origin for this interval in the Glace Bay sub-basin. A gradual rise in base-level in a forested setting is recorded from interval VI to IX (wetting upward trend). Interval VII is not present in the Glace Bay West section; deposition was probably limited to the Sydney Mines sub-basin. Eventually water level rose to a point where peat accumulation was no longer possible and a large embayment covered the Backpit mire (refer to Chapter 4).

3.4.4.3. Maceral-derived Coal Facies

Diessel (1982, 1986) devised a coal facies classification based on the ratios of what he considered to be environmentally diagnostic macerals:

1. Tissue Preservation Index (TPI) - compares the portion of those macerals in which tissue structure is preserved with those without structure; indicates the abundance of arborescent vegetation and/or the effects of oxidation.

$$TPI = \frac{\text{telinite} + \text{telocollinite} + \text{semifusinite} + \text{fusinite}}{\text{desmocollinite} + \text{macrinite} + \text{inertodetrinite}}$$

2. Gelification Index (GI) - compares partially and completely gelified macerals with those that are not gelified; indicates the degree of wetness within the mire.

$$GI = \frac{\text{vitrinite} + \text{macrinite}}{\text{semifusinite} + \text{fusinite} + \text{inertodetrinite}}$$

Diessel (1986) used this classification to characterize Permian Australian coal facies from a variety of established depositional settings, ranging from back barrier to piedmont plain. These coals plot in well defined compositional zones on Diessel's facies diagram and suggest environmental controls on average seam composition.

Most lithotypes in the Glace Bay West seam section have a high GI (>1.0) suggesting that relatively high water, low Eh conditions prevailed and enabled the preservation of large quantities of vitrinite (Fig. 3.12a). TPI values are mainly less than 1.0, and indicate that much of the vitrinite is unstructured desmocolinite. Anaerobic decomposition is postulated as the mechanism to account for the loss of cell structure without the production of large volumes of oxidised macerals.

Bright banded to banded lithotypes from Glace Bay West are concentrated in Diessel's marsh to fen environments with minor wet forest swamp contributions (Fig. 3.12a). Most of the dull to dull banded lithotypes are associated with a wetter limnic environment. Fusain layers have high TPI values and correspondingly low GI values and plot in the dry forest swamp environment in this classification scheme. As mentioned previously, fusain is not environmentally significant.

According to this facies interpretation (Fig. 3.12b), the Backpit mire began as a fen (Intervals I and II) in a limno-telmatic environment. Tissue Preservation Index decreased slightly from I to II suggesting a decrease in tissue preservation and a progression towards more limnic conditions. Interval III does not plot on this diagram due to negligible structured inertinite ($GI = \infty$), however, open water conditions existed with an influx of clastic sediments (limnic environment). The fen was re-established in interval IV and drier forest conditions are indicated for Interval V. The upper portion of the seam, intervals VI to IX plot in a limnic zone similar to Australian coals deposited in a transgressive back barrier environment (e.g. Greta, Melville and Wynn seams: Diessel, 1986). This supports a coastal setting for the Backpit seam.

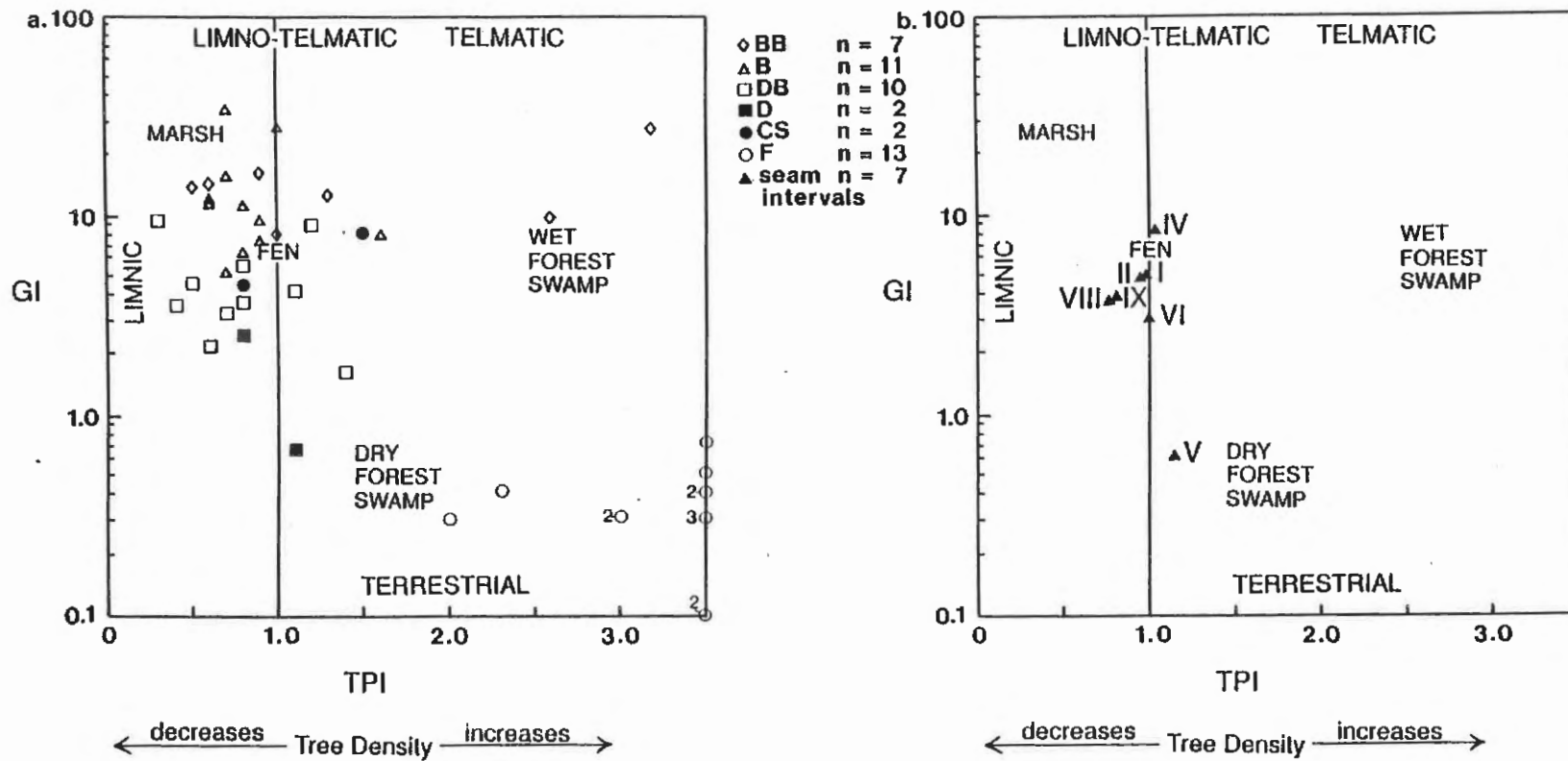


Figure 3.12. Facies characterization of the Backpit seam; Glace Bay West; plotted on a modified facies diagram of Diessel (1986): a. lithotypes; b. seam intervals.

3.5. DISCUSSION

3.5.1. Paleogeographic Setting

Paralic basins form in coastal areas and are influenced to some degree by relative sea-level fluctuation. Paralic peat-forming environments are variable and include (Bustin et al. 1983): 1) back-barrier; 2) delta (lower, middle and upper delta plains) and 3) coastal and interdelta plains.

Hacquebard et al. (1967) interpreted the Sydney Basin as a paralic basin based on the character and distribution of the coal seams. The Sydney Mines Formation consists of a series of vertically stacked, laterally extensive coal seams that usually terminate laterally by splitting. Relatively uniform seam thickness and variable vertical petrographic composition are characteristic. They postulated a floodplain environment for peat accumulation, distal from marine influence based on the absence of diagnostic marine units. The recent discovery of foraminifera above and below major seams in the basin, including the Backpit seam, confirms a paralic setting for these coals. Other fossils recovered from the Backpit roof unit suggest that brackish conditions prevailed (see Chapter 4). High sulphur values at the top of the Backpit seam may also be related to marine or brackish conditions as marine-influenced coals tend to be enriched in sulphur, especially adjacent to the roof strata (Williams and Keith, 1963; Gluskoter and Hopkins, 1970; Casagrande et al., 1977). Some sulphur may also have originated from dissolution of Windsor Group evaporites in the source area (Bell, 1928; Newman, 1934; Haites, 1951; Gibling et al., 1989).

This study proposes a broad, low-lying coastal plain, protected from clastic input, for the accumulation of the Backpit peat. A series of dulling upward trends in the upper portion of the seam indicate progressive drowning of the mire. This is consistent with peat accumulation during a relative sea-level rise (transgressive phase) as inferred

for many coal seams in the Carboniferous Ruhr coalfield (Stach et al., 1982). Coastal peats in southwestern Florida are presently undergoing transgression due to a rise in sea-level of approximately 3 m during the last 4000 years which has resulted in the deposition of marine and brackish water swamp sediments on slightly older freshwater swamp deposits (Scholl, 1969). At Snuggedy Swamp, South Carolina, freshwater peats were deposited on an essentially flat marsh surface, near remnant barrier islands (Pleistocene) (Staub and Cohen, 1979). In the past, these peats expanded laterally as peat accumulation was greater than sea-level rise. Recent sea-level rise and sediment influx however, have been faster than peat accumulation, so that in many locations salt marsh and lagoon deposits overlie these peats (Gayes et al., in press).

3.5.2. Backpit Mire Evolution

A coal seam contains a detailed record of basinal variations over an extended period. The Backpit seam varies in thickness in the study area in response to paleo-topography (0.6 to 1.5 m). The seam thickens in the Sydney Mines and Glace Bay sub-basins possibly due to the differential subsidence of a series of north-east trending pre-Carboniferous basement blocks as suggested by Gibling et al. (1987) and Gibling and Rust (1990b).

McCabe (1984) reported peat accumulation rates of 0.1 to 2.3 mm/year for recent mires. Estimates of peat:bituminous coal compaction ratios range from 1.4:1 to 30:1, with a median value of 7:1 (Ryer and Langer, 1980). Assuming a peat accumulation rate of 1 mm/year and a peat:coal compaction ratio of 10:1 (McCabe, 1984; Styan and Bustin, 1984; Gibling and Bird, submitted), the Backpit mire would have existed for approximately 6000 to 15000 years (i.e. 1 cm coal/100 years). This method provides at best a broad estimate as to the time period for peat accumulation

without substantial clastic intervention. Brightening and dulling upward lithotype successions within the seam vary considerably in thickness; average thickness values (10 and 12 cm) represent approximately 1000 and 1200 years, respectively, using this method.

Backpit lithotypes vary considerably both vertically within the seam and laterally across the study area. A major cause of lithotype variation within a mire is the water level, which can influence both the type of plant community and the degradation of maceral precursors (Diessel, 1982; Marchioni and Kalkreuth, 1991). Tasch (1960) suggested that subsidence was the driving force controlling groundwater level in the mire. He suggested that the progression from bright (vitrain) to dull (durain) lithotypes resulted from an increase in subsidence rate and a corresponding increase in groundwater level in the mire. Carbonaceous shale required the highest water level. Tasch considered fusain layers to form during low subsidence periods, under very shallow water to emergent conditions. Fusain layers in this study are interpreted as the remnants of ancient fires and are not considered indicative of groundwater level within the mire as discussed in Section 3.5.3. Other factors that might affect the groundwater level include topography of the mire surface, catastrophic flood events, peat accumulation and degradation rate and differential compaction of underlying sediment.

Two distinct dull coal lithotypes were recognised by later workers (Stach, 1955; Smith, 1962; 1968; Marchioni, 1980; Neavel, 1981; Diessel, 1982), representing extremes of water level in a mire:

1. a "wet" dull lithotype, indicative of high water levels; contains evidence of transported organic matter and detrital minerals; characterized by abundant inertodetrinite, sporinite, possibly alginite, and detrital minerals (Diessel, 1982).

2. a "dry" dull lithotype, indicative of very shallow water to subaerial exposure; contains evidence of oxidation of vegetation; characterized by structured inertinite and groundmass macrinite (Diessel, 1982).

Dull lithotypes in the Backpit seam were formed in a wet environment due to the presence of abundant detrital clays, inertodetrinite and liptodetrinite. Brightening upward cycles probably represent relatively stable periods during which the mire gradually built up and progressed from very wet (dull to coaly shale) to moderately wet (banded, bright banded) conditions. Peat accumulation thus exceeded base-level rise. These stable periods were too short for the mire surface to build substantially above the water table, as there is no evidence for subaerial exposure of the mire (e.g. "dry" dull layers of Diessel, 1982). These brightening upward cycles are commonly abruptly punctuated by a dull to dull banded layer, probably induced by local flooding. Some of these flooding events can be traced for up to 45 km and may be allogenic in origin.

Dulling upward cycles in the Backpit seam probably represent gradual rises in base-level such that moderately wet (banded to bright banded) evolved to high water conditions (dull to coaly shale). Base-level rise exceeded peat accumulation in this situation. Compaction of underlying peat and sediments may have been a factor in the drowning. Dull lithotypes and coaly shales are locally succeeded by brighter lithotypes. Esterle and Ferm (1986) suggested that this pattern recorded the response of vegetation to the increase in available nutrients due to the influx of water. Shibaoka and Smyth (1975) attributed it to the ability of arborescent vegetation to establish in relatively deep water.

Oscillatory patterns in the Backpit seam are characterized by alternating lithotypes and probably represent minor to major fluctuations in the groundwater

level of the mire. These fluctuations are common, especially between the banded and bright banded lithotypes.

The Backpit seam may represent a proximal to distal transition within the mire, from a position tens of kilometres away from the coast (lower portion) to a position close to the coast (mid to upper portion). The lower portion of the Backpit seam accumulated during a relatively stable period in the mire's history, characterized by a predominance of brightening upward cycles. Minor transgressive pulses penetrated far into the mire, abruptly punctuating these brightening upward cycles. The mid- to upper portion of the seam is characterized by a predominance of dulling upward cycles representing periodic drowning of the mire. Transgressive episodes combined with compaction of the underlying peat dominated, resulting in less stable conditions. Peat accumulation was eventually halted by the drowning of the mire. An extensive organic-rich limestone to shale unit caps the mineral-rich top of the coal seam and represents deposition in a broad shallow lake or embayment. Faunal evidence indicates that a fresh to brackish water assemblage of sharks, fish, ostracods, foraminifera and bivalves inhabited this body of water (see Chapter 4).

3.5.3. Fusain: A Fire Origin

The presence of fusain in coals has been used to indicate a dry forested terrestrial environment, dominated by oxidation processes (Hacquebard and Donaldson, 1969; Diessel, 1982; 1986). Some earlier workers (e.g. White, 1933; Stopes, 1935; Marshall, 1954; Schopf, 1975) suggested that the formation of fusain was limited to biochemical and/or oxidation processes (degradofusinite of Stach et al., 1982). However, numerous studies (e.g. Austen et al., 1966; Cope and Chaloner, 1980, 1985; Scott, 1989) support a fire origin for fusain layers in ancient mires. Lightning strikes are the most probable source of ignition although

volcanic activity, meteorite fall, spontaneous combustion and sparks caused by rock falls have all been invoked as potential sources (Cope and Chaloner, 1980; Scott, 1989).

Fires have been well documented in present day mires, often due to drought conditions. Cypert (1972) described five major fire events in the Okefenokee Swamp in 1954 and 1955. A major fire in East Kalimantan, Borneo in 1982 to 1983 destroyed a large tropical forest (up to 37,000 km²), including peat-forming areas (Johnson, 1984). Other workers (e.g. Komarek, 1972; Cohen and Spackman, 1980; and Cohen et al., 1987) attributed fusain layers to the spread of crown (tree top) fires through a water-logged swamp environment where the charred material would fall into the water below and be incorporated in the peat.

This study indicates that much of the fusain in the Backpit seam is pyrofusain, the product of charring during wildfires within the mire. Wildfire has occurred regularly from at least the Late Devonian onward (Cope and Chaloner, 1985). Such wildfires represent a geological event (Scott, 1989) and could potentially occur in any environment, thus limiting the use of fusain as a sensitive paleoenvironmental indicator (Calder et al., 1991). The allochthonous nature of many of these fusain-rich layers also supports this conclusion. Bedding-plane exposures of the Backpit seam indicate that the fusain layers are composed of randomly oriented patches, suggesting that they drifted to the depositional site (Plate 4d). Since evidence for desiccation of the peat is lacking in the Backpit mire (e.g. layers of massive macrinite), crown fires are envisioned as the most probable mechanism for the production of fusain layers. The abundance of fine-grained inertodetrinite shards in some layers supports transport by wind and/or water.

3.5.4. Ombrotrophic Versus Rheotrophic Mires

The geometry of a peat deposit is a product of the hydrologic system within the mire, as well as climate and tectonics. Modern peats are classified as: 1) ombrotrophic (rain-fed, commonly domed) or 2) rheotrophic (rain- and flow-fed, commonly planar) (Moore, 1987). Rheotrophic mires are generally slightly acidic, rich in plant nutrients (eutrophic) and have a high diversity of plant types (Teichmüller and Teichmüller, 1982). Their surfaces rarely build above the water table, and are prone to floods which carry detrital sediment. In contrast, a domed ombrotrophic mire produces a mineral-poor peat because the mire surface is above flood levels. Mineral matter is attributed to inherent vegetal constituents and air borne particulates. Domed mires are generally highly acidic due to limited circulation (Esterle et al., 1989), a condition unsuitable for bacterial growth and therefore limiting pyrite precipitation. Many ions remain in solution under acidic conditions and are removed from the system, thus contributing to the low ash content. The size and diversity of vegetation decreases upward, probably in response to a progressively decreasing nutrient supply (Moore, 1987). Numerous authors (Flores, 1981; Ethridge et al., 1981; Esterle and Ferm, 1986; Warwick and Stanton, 1988) have used domed tropical peats as modern analogues for ancient low-ash coals that exhibit dulling upward trends. These trends were attributed to stunted vegetation (reduction in vitrinite maceral precursor) and increased oxidation of the upper levels of the mire. However, Esterle et al. (1989) studied a domed peat in Sarawak, Malaysia that would result in a consistently bright, low ash coal. Although the vegetation was stunted in the upper levels of the mire, acidic conditions inhibited the decay of organic matter, and high humidity and rainfall maintained saturated anoxic conditions in the peat, thus preserving bright lithotype precursors.

Calder et al. (1991) discussed criteria for recognizing ombrotrophic tendencies in an ancient mire: 1) an upward decrease in ash content; 2) an upward increase in structured vitrinite (telinite + telocollinite) and 3) evidence of floral succession as indicated by an increased abundance of herbaceous over arborescent vegetation. Although palynological data was not obtained in this study, the first two points do not characterize trends within the Backpit seam.

Rheotrophic conditions probably prevailed during the history of the Backpit mire as suggested by the high ash content and the occurrence of a clay-rich parting near the centre. High detrital clay content in the upper portion of the seam accounts for the megascopic dulling upward trend and precludes the development of the mire above the water table. Hoffmann (1933, in Teichmüller, 1989, p. 60) described similar dulling upward facies trends from the Carboniferous Ruhr Coalfield where a progression from vitrinite-rich to liptinite-rich macerals and clays was interpreted as a development from drier (forests) to wetter (marshes, open-water) environments. Significant concentrations of pyrite throughout the Backpit seam suggest that sulphate and ferrous enriched groundwater circulated freely within the mire and that the pH was high enough to permit the activity of sulphate-reducing bacteria.

Cecil et al. (1985) suggested that most late Pennsylvanian mires in the Appalachian region developed a planar geometry due to the switch to a "seasonal tropical" climate. Rainfall was no longer consistent enough throughout the year to support mire growth above the water table. Evidence that suggests a seasonal climate in the Sydney Mines Formation and slightly older Waddens Cove Formation includes gilgai structures in paleosols, deep desiccation cracks, and upright trees and in situ rhizoconcretions in channel bodies (Gibling and Rust, 1990a;

Gibling and Bird, submitted).

3.5.5. Significance of Vertical Coal Facies

Microlithotype- (Hacquebard and Donaldson, 1969) and maceral-derived (Diessel, 1986) coal facies analyses (Section 3.4.4) are based on the assumption that variations in coal facies represent changes in the depositional environment of the mire. These facies variations are dependent on changes in groundwater level, vegetation type, peat accumulation rates and degree of organic decomposition in the mire.

The bright banded to banded lithotypes in the Backpit seam contain abundant vitrinite and plot in Hacquebard and Donaldson's forest-moor environment. Since unstructured desmocollinite predominates (low TPI), these lithotypes plot in marsh to fen environments with minor wet forest swamp contributions on Diessel's diagram. This may not represent a conflict in environmental setting between the two facies classifications if low TPI values are interpreted to be the result of anaerobic microbial attack in a wet forest environment. This would account for an abundance of vitrinite (forest environment) and subsequent loss of vitrinite structure (biochemical gelification).

Dull banded to dull lithotypes commonly plot in limno-telmatic to limnic (reed-moor) environments in both facies diagrams. Fusain layers are indicative of oxidation in both schemes and plot in the terrestrial-forest-moor (Hacquebard and Donaldson) or the dry forest swamp environment (Diessel). As suggested in Section 3.5.3, fusain in the Backpit seam originated from mire fires and the use of this component to interpret environmental setting is dubious.

Despite the differences in environmental interpretation, both facies classifications indicate a predominantly wetting upward trend for the Backpit mire. This is consistent with a mire developed during a

transgressive phase, on a low-lying coastal plain.

3.6. SUMMARY

The Backpit seam is a banded bituminous coal that contains moderate to high amounts of mineral matter in the form of detrital clays and syngenetic pyrite. It extends for more than 45 km parallel to depositional strike. Thickness variation reflects paleotopography probably due to differential subsidence of underlying pre-Carboniferous fault blocks. Fusain layers in the seam probably represent ancient wildfires. The seam records a transgressive phase within the Phalen-Backpit Interval and lithotype successions reflect variations in groundwater level throughout the history of the mire. The seam dunks near the top in response to an influx of detrital clays, and eventually terminates by the drowning of the mire.

A coastal setting is inferred for the Backpit mire for the following reasons:

1. Agglutinated foraminifera are present in associated strata (Thibaudeau and Medioli, 1986; Thibaudeau et al., 1987; Wightman et al., 1992).
2. The mire was removed or protected from active fluvial interaction. Clastic input was the result of basinwide base-level rises (open moor facies of Hacquebard and Donaldson, 1969), probably related to sea-level rise. Peat accumulation was terminated in this manner.
3. The seam contains abundant sulphur in the form of pyrite, especially in the uppermost layers. This suggests a marine influence.
4. Vertical coal facies trends suggest a progressively wetting upward environment of peat accumulation, typical of recent mires in a transgressive setting.
5. The Backpit mire is elongated parallel to depositional strike and thins considerably downdip, consistent with deposition along a coastline.

The Backpit mire probably accumulated under "rheotrophic" conditions. Evidence to support this interpretation includes:

1. High proportion of detrital mineral matter, especially near the top of the seam, precludes a domed geometry above groundwater influence.
2. There is no evidence for "dry" dull intervals, characteristic of mire desiccation. The dull to dull banded lithotypes contain abundant detrital macerals (inertodetrinite, liptodetrinite) and/or minerals, indicative of subaquatic deposition.
3. High pyrite content in this coal suggests moderate pH conditions were present in the peat, suitable for the activity of sulphate-reducing bacteria. Raised bogs are generally highly acidic and are not conducive to the precipitation of pyrite.
4. A high proportion of vitrinite and vitrinite-rich lithotypes and microlithotypes suggest that the mire was nutrient-rich and able to support arborescent vegetation.

Lithotypes in the Backpit seam are petrographically distinct and are useful for seam correlation. Three types of lithotype successions were documented for the Backpit seam, representing variations in the groundwater level:

1. Brightening upward cycles - stable conditions during which peat gradually built up the surface of the mire; net base-level fall.
2. Dulling upward cycle - pulses of subsidence and/or sea-level rise during which peat accumulation could not keep pace; net base-level rise.
3. Oscillatory cycles - fluctuations in the groundwater level.

Brightening upward cycles predominate in the lower portion of the seam whereas dulling upward cycles characterize the upper seam section. This reflects the

transition from forest moor to open moor environments (based on Hacquebard and Donaldson's (1969) facies scheme) or from fen to limnic (transgressive back barrier) environments (based on Diessel's (1986) facies scheme). This trend documents the shift of the mire closer to the coastline.

4. THE BACKPIT ROOF UNIT: A ZONE OF MAXIMUM TRANSGRESSION WITHIN A CYCLOTHEM PACKAGE

4.1. INTRODUCTION

Thin, extensive marine bands are rare but prominent features of European Carboniferous successions (Edwards and Stubblefield, 1948; Calver, 1968a, b; Rippon, 1984) and contain open marine assemblages of brachiopods, cephalopods, conodonts, foraminifera, crinoids, trilobites and/or corals. These units indicate periodic marine incursions within the sedimentary sequence, probably related to glacioeustasy (Leeder, 1988).

Similar organic-rich marine shale units have been described from the Carboniferous in the mid-continental region of the United States (Eagar, 1960; Zangerl and Richardson, 1963; Heckel, 1977, 1984). Schenk (1967) interpreted phosphatic black shale as the bathymetrically deepest unit within a cyclothem transgression in this region. Heckel (1984) agreed with this interpretation and attributed their formation to glacioeustatic fluctuations associated with pene-contemporaneous Gondwanan glaciation in the southern hemisphere.

Thin, organic-rich "nonmarine" limestone and shale units are also characteristic of the Euramerican cyclothem package and are often associated with coal seams (Trueman, 1946; Eagar, 1961; Fielding, 1984; Haszeldine, 1984). These units commonly contain a fossil assemblage including bivalves, ostracods, serpulids, sharks and/or other fish with a broad salinity range. Many paleontologists working in the Carboniferous have used "nonmarine" as a broad environmental term that "embraces several distinct habitats ranging from brackish water contact with the sea, through lagoons, rivers, lakes and water courses to freshwater swamps" (Calver, 1968b, p. 148). The inclusion of brackish environments within the scope of nonmarine deposits has led to much confusion, especially when comparing ancient

environments with regions such as the Mississippi delta that include freshwater to open marine environments (Scott et al., 1991). The term "marginal marine" is used in this study to denote previously described "nonmarine" units that have a proven marine connection.

Open marine intervals have not been documented in the Upper Carboniferous strata of the Maritimes Basin although Duff and Walton (1973) argued for a marine connection at Joggins, based on inferences from bivalve paleoecology. The discovery of agglutinated foraminifera (Thibaudeau and Medioli, 1986; Thibaudeau et al., 1987; Wightman et al., 1992) and the identification of cyclothem patterns in the Sydney Mines Formation (Gibling and Bird, submitted) indicate a marine influence for the basin.

Thin, extensive, organic-rich limestones and shales were recognised in the Sydney Basin by early geologists from the ca. 400 m stratigraphic interval between the Emery and Lloyd Cove seams (Brown, 1850; Dawson, 1868; Robb, 1876; Hyde, 1913). Bird (1987) was able to trace several limestone/shale units along depositional strike for tens of kilometres on the western side of the basin. Masson and Rust (1990) considered these units to be lacustrine equivalents of marine bands. Gibling and Kalkreuth (1991) studied the petrology of a suite of samples collected from several such units in the Maritime sub-basins, including the Sydney Basin. Although these units appeared megascopically similar, a wide range in petrographic composition was reported.

Other workers conducted specific studies on the type and distribution of fossils in these units, including bivalves, gastropods, ostracods, foraminifera, serpulids, sharks and other fish (Sternberg, 1941; Copeland, 1957; Baird, 1958; Masson and Rust, 1984; Vasey, 1983; Thibaudeau and Medioli, 1986; Thibaudeau et al., 1987; Wightman et al., 1992). Algal stromatolites were reported from specific

intervals by Masson and Rust (1983) and Vasey and Zodrow (1983).

This study documents the facies, biota and organic content of the most continuous such unit in the Sydney Mines Formation - the Backpit roof unit (BRU). It lies directly above the Backpit seam and represents the flooding of the Backpit mire due to relative sea-level rise.

4.2. THE BACKPIT ROOF UNIT

The BRU (Plates 6 and 7) is a medium grey to black, 30 to 75 cm thick limestone/shale unit in a stratigraphic interval dated from spores as Westphalian D (Dolby, 1988). The dark colour is attributed to finely disseminated organic matter, with total organic carbon (TOC) content up to 20% by weight. The unit is compact, resistant to weathering and forms an excellent stratigraphic marker (Plate 4a), traceable for more than 45 km parallel to depositional strike. It is rich in ostracods and bivalves, compressed shells of which impart a crenulated appearance to some beds. A light to medium grey mudstone separates the BRU from the underlying coal in the eastern part of the basin (Fig. 4.1).

The organic-rich BRU interval is typically succeeded by a coarsening upward bay-fill sequence. The unit is cut into, but not completely eroded, by a distributary channel at several coastal locations (E-Glace Bay West; G-Donkin West) and in drill core (SMS-91-29B) (Figs. 2.1 and 4.1).

4.3. SUMMARY OF METHODS

Two sample sets were collected to characterize the BRU, as outlined in Appendix A3.1. Bulk channel samples representing specific vertical roof intervals were collected from seven coastal sections (A, B, C, E, G, H and J; Fig.1.2) and splits were pulverized for ash and sulphur determinations (Appendix A3.2) and Rock-Eval pyrolysis (Appendix A3.4).

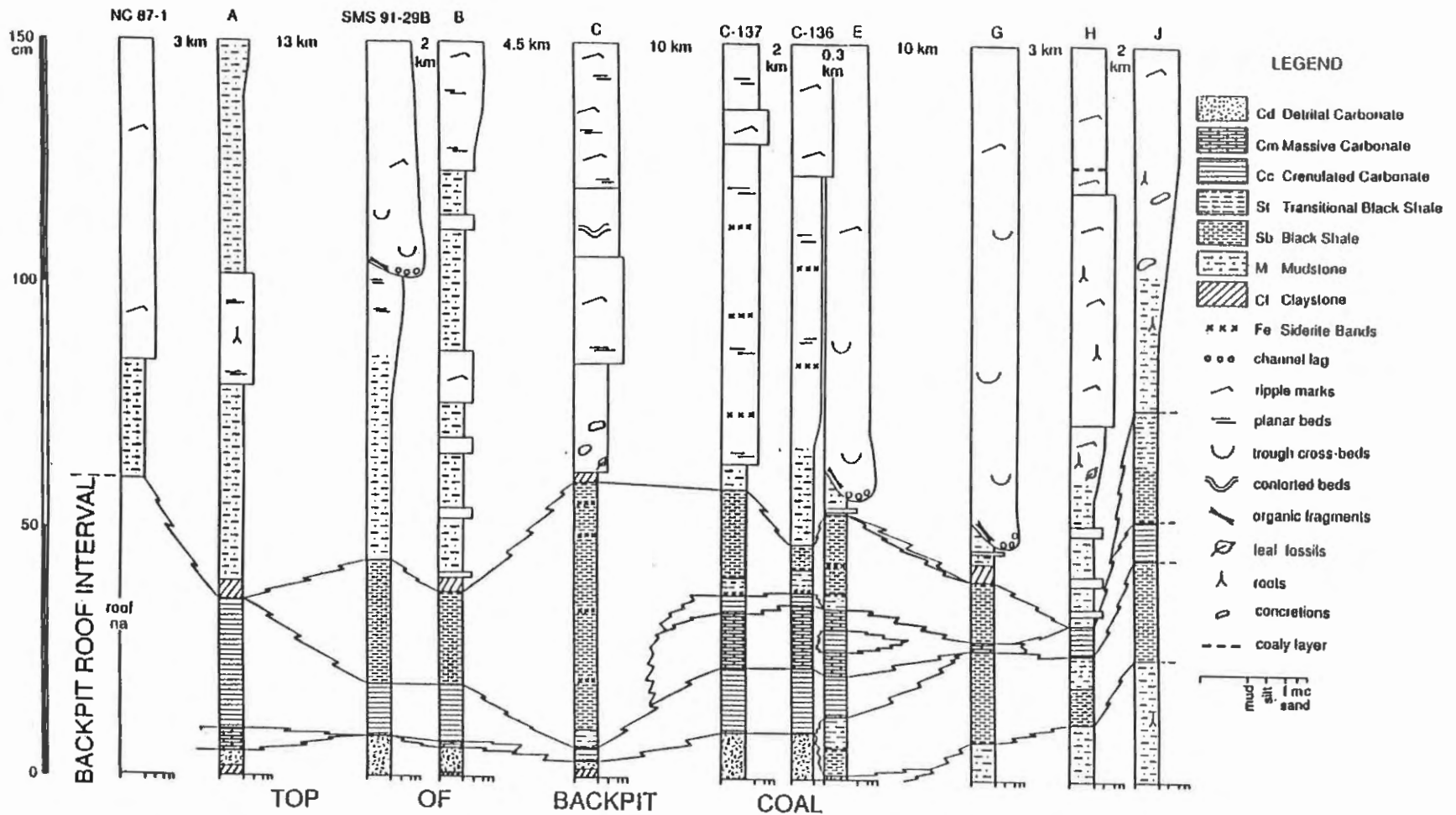


Figure 4.1. Vertical and lateral distribution of facies in the Backpit roof unit (BRU), from a section roughly parallel to depositional strike. Location outlined on Figure 1.2.

Point counts were made on grain-mount pellets from each sample interval in the Sydney Mines (B) and Glace Bay West (E) roof sections (Appendix A3.3.2). Table 3.2 lists macerals and minerals considered in the analysis. Fossils were concentrated from these samples (approximately 2 kg) using dilute acetic acid and examined by W. Parkins, Brock University, as outlined in Appendix A3.5. Foraminiferal assemblages were examined from the BRU, Backpit underclay and other lithologies in the Sydney Mines Formation by W. Wightman, Dalhousie University.

Oriented roof samples from coastal and core sections were slabbed for detailed facies analysis. Mineral, fossil and matrix content were estimated from thin sections of core (C-136, C-137; Plates 6 and 7) using the logarithmically weighted abundance groups (Appendix A3.3.1, Tables A3.1 and A3.2).

4.4. RESULTS

4.4.1. Megascopic Facies

4.4.1.1. Description

Major lithofacies of the BRU were identified in the field and eight distinct facies were later distinguished using slabbed samples (Table 4.1). Figure 4.1 illustrates their vertical and lateral distribution in the study area. Facies typically occur only once in a given profile, but locally alternate in thin beds.

A soft kaolinite-rich clay band, 1 to 3 cm thick, bounds the BRU at most coastal sections (Fig. 4.1). Such bands were not observed in the cores and probably represent weathered clay produced at the interface of competent and less competent rock units.

Mudstone (M) forms the basal layer in the eastern portion of the study area and thickens southeastward. At Donkin West (G) this bed is slightly calcareous and contains ostracods and organic debris. Farther southeastward, at

Table 4.1. Backpit Roof Unit (BRU) facies description.

LITHOFACIES	FOSSIL GROUPS	THICKNESS RANGE/ ORGANIC CONTENT	INFERRED SETTING
Mudstone (M) light-medium grey; locally calcareous	± ostracods; ± roots	0 - 25 cm detrital organic debris	mudflat or shoreline
Carbonate			
detrital (Cd) medium-dark grey; commonly includes shell hash; slump or dewatering structures	shark; other fish; foraminifera; ostracods; bivalves; serpulids	0 - 7.3 cm detrital organic debris; coaly rip- up clasts	transgressive shell lag
massive (Cm) medium-dark grey; fine-grained; competent	ostracods; fish; foraminifera; ± bivalves and sharks	0 - 14.4 cm organic-rich wisps	oxygenated open water
crenulated (Cc) alternate layers of organic-rich mud (black) and shell- rich carbonate (white- light grey); carbonate predominates	bivalves ± fish and ostracods	0 - 26.2 cm thin organic-rich mud layers; spores common	oxygenated water column; dysaerobic bottom; flotant (?)

Table 4.1 (con't). Backpit Roof Unit (BRU) facies description.

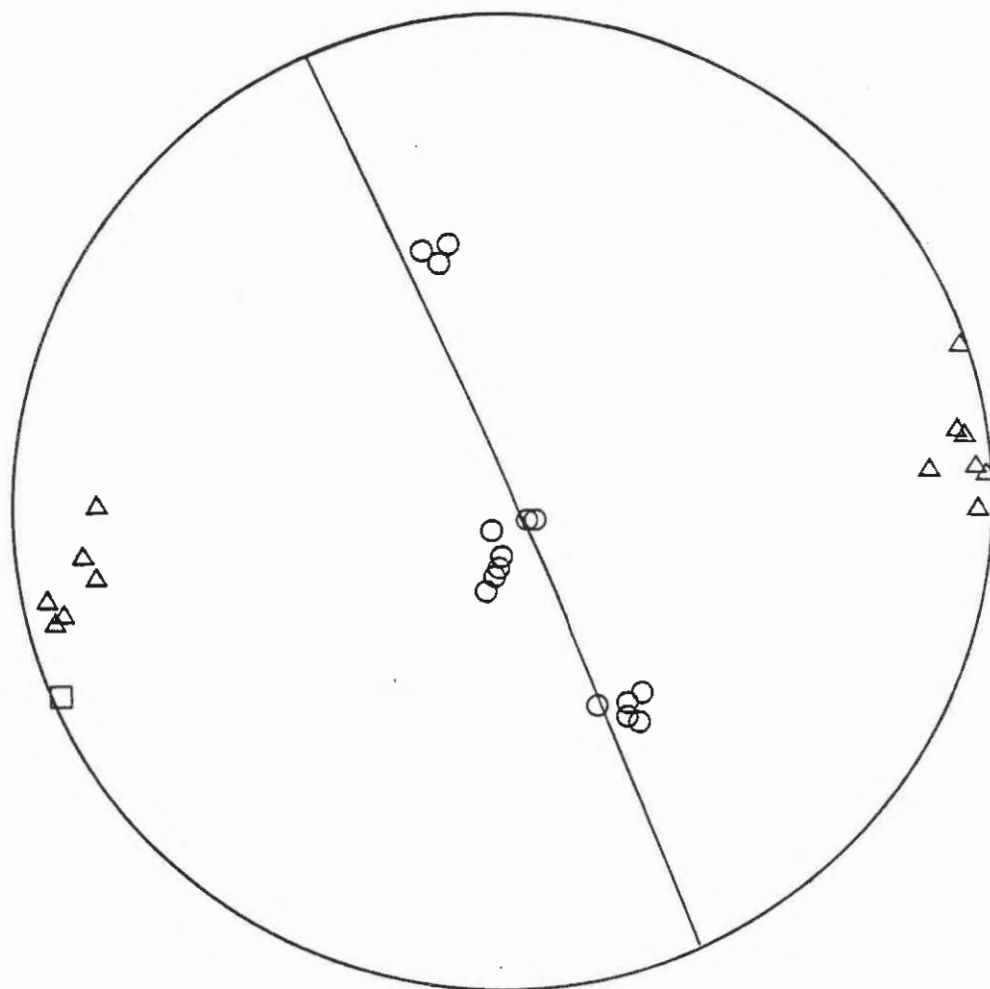
LITHOFACIES	FOSSIL GROUPS	THICKNESS RANGE/ ORGANIC CONTENT	INFERRED SETTING
Shale			
transitional (St) dark grey-black; organic-rich; fissile, with shell layers	minor bivalves, ostracods and fish	0 - 11.3 cm organic-rich mud (gyttja); spores common	transitional between Cc and Sb
black (Sb) dark grey-black; organic-rich; fissile	sparse bivalves and fish near base	0 - 47.0 cm undisturbed organic mud; spores and plant fossils	restricted circulation; anaerobic bottom water
Siderite (Fe) prominent light- bluish grey bands or nodules; orange-brown weathered surface; competent	not analysed	0.5 - 2 cm not analysed	reducing conditions; alkaline environment
Mudstone/Siltstone (MZ) thin siltstones (light grey, planar laminated, rippled) interbedded with thicker, planar laminated medium grey mudstone beds	plant fragments; branchiopods	0 - 2 m detrital organic debris	coarsening upward pro- delta and delta

Longbeach (J), mudstone is bioturbated and contains abundant organic debris and carbonaceous root traces.

Detrital carbonate (Cd, Plate 9a) occurs at the base of each succession in the mid- to western portion of the study area. Bedding is weakly developed and the interval commonly resembles a shell hash. Massive carbonate (Cm, Plate 9b) is present in minor amounts in all but three sections (C-Victoria Mines; H-Donkin East and J-Longbeach) and is well developed in the Glace Bay sub-basin. It is compact and contains organic wisps and clays. Crenulated carbonate (Cc) consists of alternating thick laminae of organic-rich mudstone and crenulated bivalve-rich shells (Plates 8a and 9c). The carbonate portion is greater than fifty percent. Beds are thickest in the western portion of the basin (A-Bras d'Or) and locally occur interbedded with massive carbonate (Cm) elsewhere (e.g. E-Glace Bay West). A stereonet plot of shell crenulation lineations measured on bedding plane surfaces shows that the lineations sub-parallel the east-northeast trending fold axis in the study area (Fig 4.2) and suggests that they reflect post-depositional deformation related to folding.

Shale facies (St, Sb) consist primarily of organic-rich fissile black shale with a significant amount of shelly material in facies St (Plate 9d). Sparse bivalves, ostracods and rare Lepidodendron branches and other plant fossils were observed on bedding planes of Sb. This facies attains its greatest aggregate thickness at Victoria Mines (C) where it contains numerous resistant siderite bands (Fe) parallel to bedding. These bands are commonly associated with the shale facies and the overlying mudstone/siltstone facies (MZ) at other locations. A single siderite band can be correlated between offshore cores (C-136 and C-137, Plates 6 and 7), 1.8 km apart.

The BRU is commonly capped by a coarsening upward package of interbedded mudstone and siltstone (MZ) of



EQUAL AREA PROJECTION	SYMBOL
Bedding n = 15	○
Crenulation Lineation n = 13	△
Pole to great circle (avg. fold axis of study area)	□

Figure 4.2. Stereonet plot of poles to bedding and crenulation lineations for the study area.

variable thickness. The siltstone beds are light to medium grey, with planar and ripple cross-lamination, and show abrupt lower and upper contacts with mudstone beds. Siltstone beds range in thickness from 1 to 25 cm and tend to increase in thickness upward. The interbedded mudstone is medium grey, up to 50 cm thick, with planar lamination and no visible rooting. Carbonized plant fossils are common and Leaia impressions were noted on some bedding surfaces at Sydney Mines (B) and in offshore core (C-136, C-137). This package is eroded by a distributary channel at several coastal sections and core sites (Fig. 4.1, Plate 4c). At other locations the package coarsens upward into well developed deltaic sheet sandstones with parting lamination, ripples and localized slump structures (Plate 4b).

4.4.1.2. Vertical Facies Trends

Contrasted vertical facies trends typify the east to southeastern and mid- to western portions of the study area, with a transitional trend at Glace Bay West (Fig. 4.3).

The main difference between these trends occurs near the base of the BRU. In the east, mudstone (M) lies directly above the coal followed abruptly by organic-rich shale (Sb, St) and then carbonates (Cm, Cc). In the west, detrital carbonate (Cd) succeeds the coal, followed directly by other carbonate-rich facies (Cm and/or Cc). In both regions, an upper shale facies (St, Sb) is followed by an interbedded mudstone/siltstone package (MZ). Correlation of beds across the basin is difficult; however, the top of the Backpit seam, which is petrographically similar at all sampled locations (Chapter 3), is presumed to be an isochronous, or only mildly diachronous surface.

At Glace Bay West, a thin (1 cm) Cd unit rests upon the coal (as in the west), followed by black shale (Sb and St) (as in the east). Succeeding facies include interbedded Cc and Cm, St and Sb and finally the MZ facies, as described

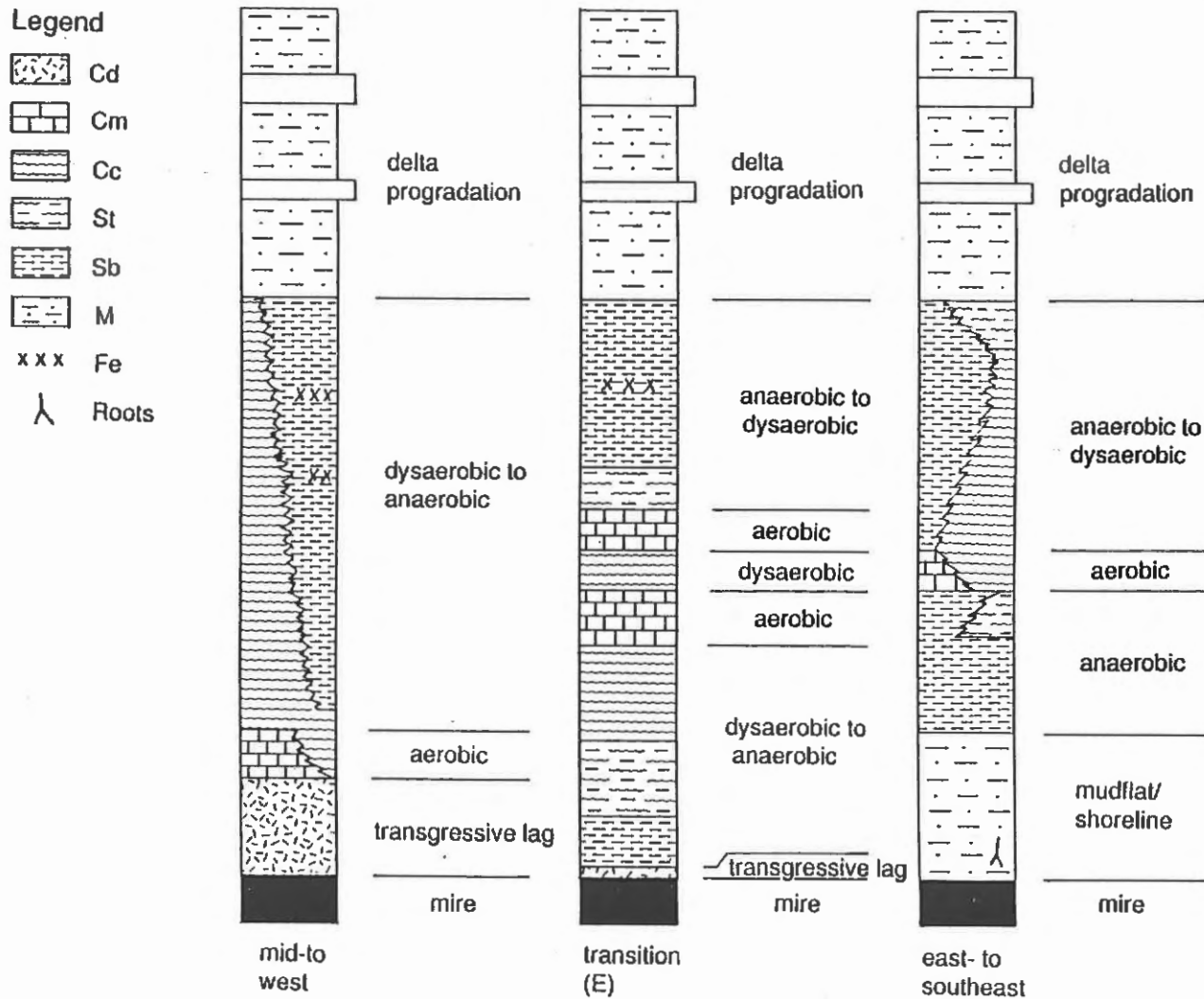


Figure 4.3. Summary of vertical facies trends for the BRU. Facies described in Table 4.1.

for both facies trends.

4.4.2. Mineral Matter

4.4.2.1. Ash and Sulphur

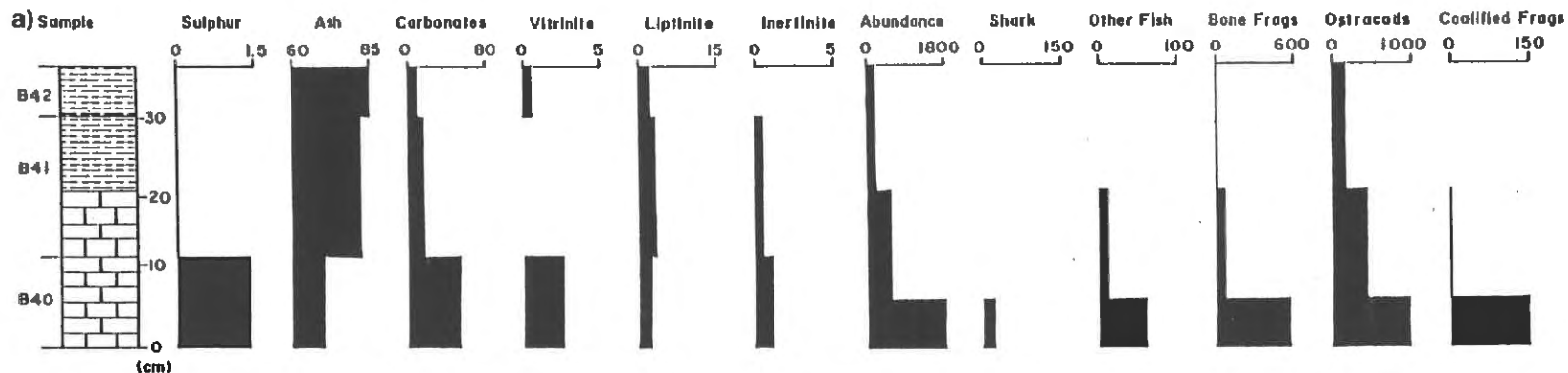
The ash and sulphur content of the BRU is illustrated in Figures 3.3, 4.4a and b. Table A2.1a contains the analytical data for these figures. Ash content is inversely proportional to volume percent carbonate (determined from point counts under reflected light microscopy) and tends to increase upward. Ash values are generally greater than 60% and range as high as 92% by weight. Sulphur is generally low (< 1.0% by weight) but forms up to 11.9% of samples adjacent to the coal seam (Fig. 3.2). The anomalously high sulphur value from a Donkin West (H) roof sample (25.0% S) may be due to a concentration of nodular pyrite.

4.4.2.2. Minerals

The mineral matter composition of the BRU varies depending on the facies analysed. Observations described here are based on reflected light (Figs. 4.4a and b; Tables A3.3 to A3.6) and transmitted light (Figs. 4.5a and b; Tables A3.1 and A3.2) microscopy from selected samples.

Bioclastic material comprises a major portion of the BRU and will be discussed in detail in Section 4.4.4. The predominant bioclastic components include ostracods and bivalves; minor components include phosphatic fragments of vertebrate bones, teeth, spines and scales.

Calcite is present as micrite and sparite. Micrite is uncommon to abundant and predominates in the massive carbonate facies (Cm). It provides a fine-grained matrix for other minerals and fossil remains and also coats some fossil fragments, possibly along borings. Peloids, probably fecal, occur as small oval aggregates (< 50 μm apparent diameter) of clays and/or carbonates within the micritic intervals. Large, light brown coprolites (up to 3 cm long)



Values given in weight % (sulphur and ash) and volume % (others)

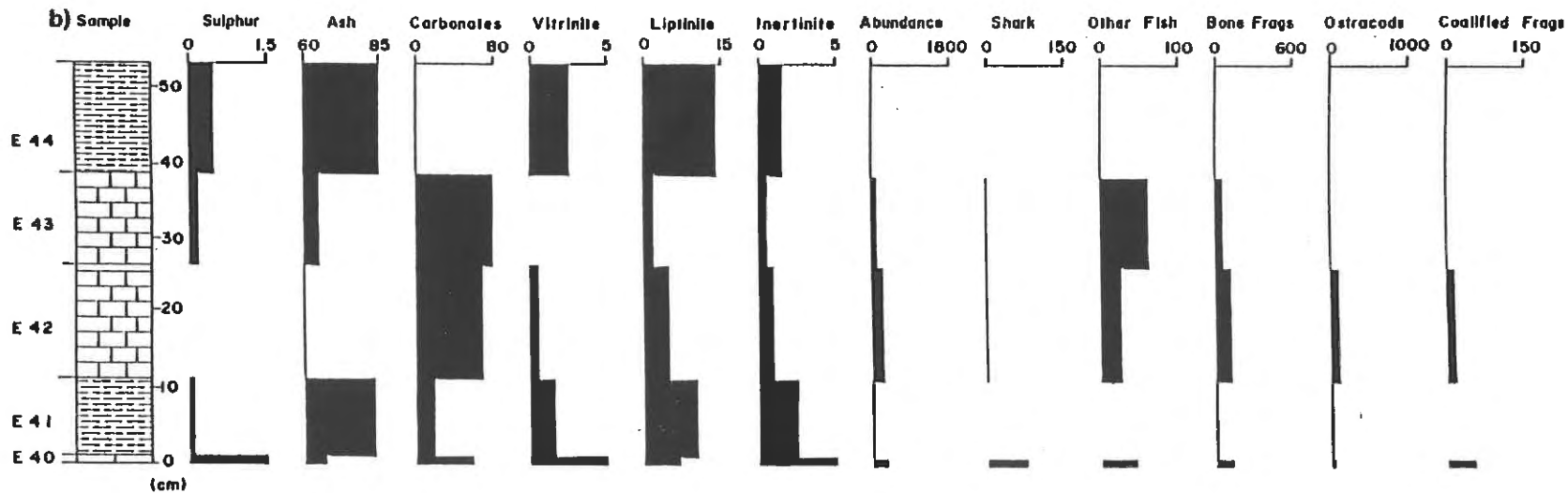


Figure 4.4. BRU mineral, organic matter and fossil trends for a) Sydney Mines (B) and b) Glace Bay West (E). Values given in weight % ash, sulphur; volume % carbonates, vitrinite, liptinite, inertinite; abundance of fossil groups per 1 kg sample.

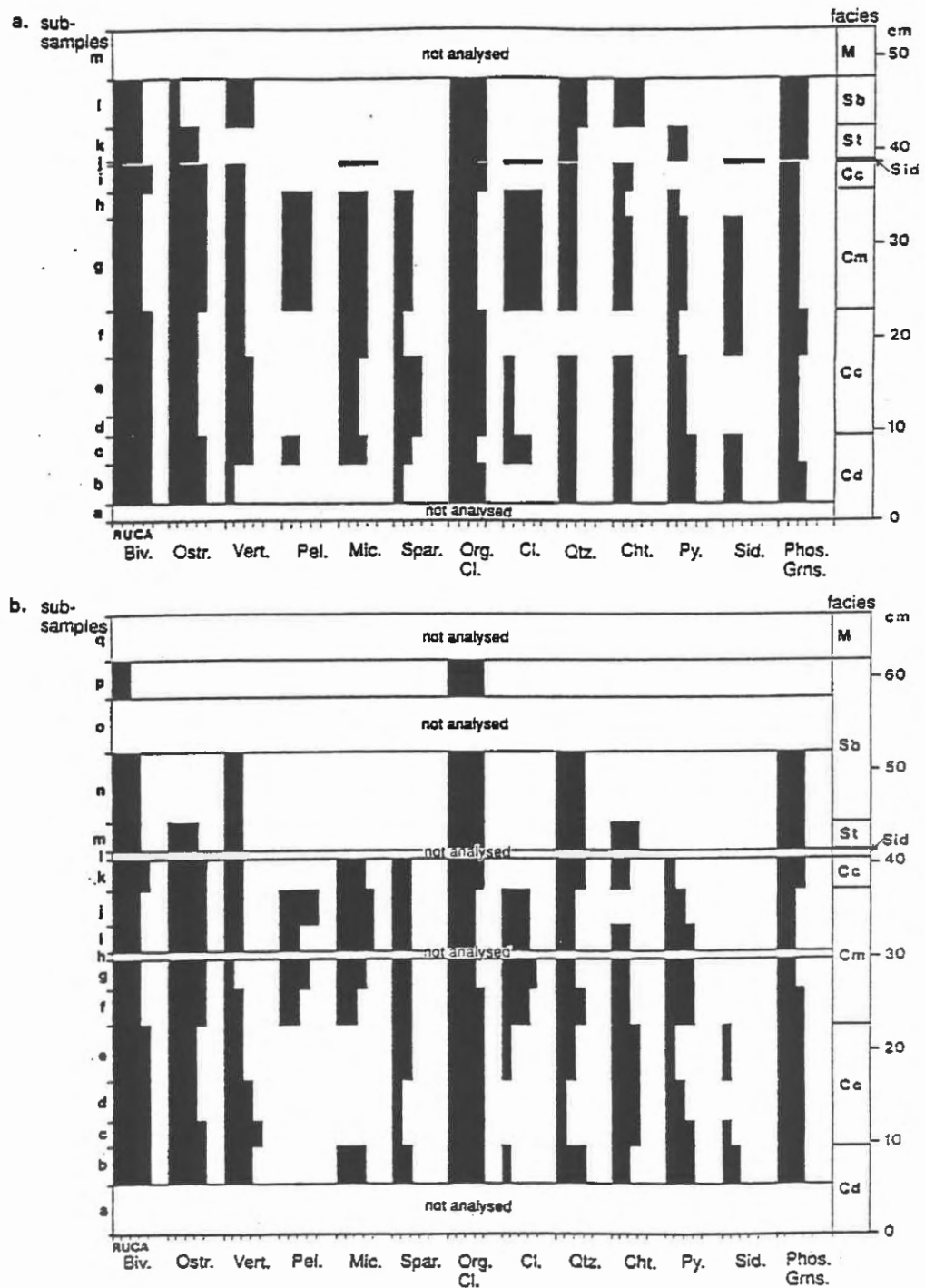


Figure 4.5. Thin-section abundance estimates from the BRU - a) C-136; b) C-137. R-rare, found with intensive searching; U-uncommon, found with searching; C-common, present in many fields of view; A-abundant, present in all fields of view. Biv.-bivalves; Ostr.-ostracods; Vert.-vertebrate fragments; Pel.-pellets; Mic.-micrite; Spar.-sparite; Org. Cl.-organic-rich clay; Cl.-clay; Qtz.-quartz; Cht.-chert; Py.-pyrite; Sid.-siderite; Phos. Grns.-phosphatic grains.

were observed on bedding surfaces at some coastal outcrops. The contrasting colour and coiled internal structure of similar bodies from above the Phalen seam (observed in polished cross-sections, J. Paul, pers. comm., 1990) is typical of shark excrement (Zangerl and Richardson, 1963).

Sparite cement is rare to common in the carbonate-rich facies. Interlocking crystals (10-20 μm) occur in void spaces such as spine, shell and bone interiors (Plate 9a). Patches of sparry calcite also occur within micritic and peloidal layers.

Clay minerals are rare to abundant in the Cd and Cm facies; mineral identification was not attempted but kaolinite, illite and minor chlorite were identified from similar organic-rich carbonate intervals from Glace Bay West and Victoria Mines sections (Gibling and Kalkreuth, 1991). Clay minerals are commonly intimately mixed with degraded organic matter to form an opaque to slightly translucent structureless mud or gyttja ("an organic mud deposited under oxygen-deficient conditions, the result of excess organic substances in stagnant water": Krejci-Graf (1963) cited in Stach *et al.*, 1982, p. 292). This organic-rich mudstone occurs in layers from several microns to greater than 500 μm thick in the crenulated carbonate facies and provides a matrix for bivalve-rich layers (Plate 9d). It forms a major portion of the shale facies (St, Sb).

Phosphate nodules (collophane) are common to uncommon in most facies examined. They are pale to dark orange-brown, rounded, somewhat elongate bodies (up to 200 μm in apparent length) with a granular to smooth internal texture. They may represent reworked vertebrate fragments or reprecipitated phosphate.

Detrital grains (quartz, chert, siderite and rare muscovite) are finely dispersed, or form minor lenses or layers in most facies. Quartz grains are generally silt-sized (< 50 μm apparent diameter), subangular to subrounded

monocrystalline grains. Polycrystalline quartz and sand-sized quartz grains (up to 200 μm in apparent diameter) are rare.

Chert (cryptocrystalline silica) is generally uncommon to common in most facies. It occurs rarely as silt-sized detrital grains (< 50 μm apparent diameter) and more commonly filling shell and bone cavities. Chert also replaces or partially replaces shell walls.

Rounded siderite-rich grains up to 2 mm in apparent diameter are rare to uncommon in the lower portion of the roof succession. They probably represent reworked sideritic concretions, common in associated strata.

Pyrite is common to rare in the roof sections examined (0-11.3% by volume, Table A3.3 and A3.5) and tends to be concentrated in the detrital carbonate facies (Cd) adjacent to the coal. This distribution agrees well with total sulphur analyses. Pyrite usually occurs as 1-10 μm euhedral to subhedral crystals, either finely disseminated throughout the rock matrix or as rare clusters of tiny crystals (framboids) up to 50 μm in apparent diameter (Plate 9a). Pyrite crystals also occur within compressed spore cavities, suggesting crystal growth prior to compaction of the sediment. It also forms the lower layer of some geopetal fillings, supporting early syngenetic emplacement (sparry calcite and/or chert form later phases). Pyrite coats the outer surfaces of shells and penetrates into them, possibly along borings. Partial to complete shell replacement by pyrite is common in some layers, especially near the base of the roof (Plate 9a).

4.4.3. Organic Matter

4.4.3.1. Organic Components

The organic matter content of two roof sections (B-Sydney Mines and E-Glace Bay West) was quantified microscopically by point counting under reflected light

following the procedure outlined in Appendix A3.3.2. White light was supplemented with fluorescent light illumination to assist in distinguishing hydrogen-rich liptinite macerals from fine-grained clays and carbonates. Results are found in Tables A3.3 and A3.5; Table A3.4 and A3.6 include results calculated on a mineral-matter-free basis. Figures 4.4a and b illustrate vertical trends of the main maceral groups including vitrinite, liptinite and inertinite. These trends correlate well with pyrolysis data (Section 4.4.3.2).

Amorphous liptinitic material is intimately associated with fine-grained mineral detritus, and hence this material was difficult to quantify. Microscopically identifiable organic matter in the Glace Bay West section (E) ranges from 2.5 to 17.0% by volume. Carbonate-rich facies (samples E-42, E-43) are lower in organic matter than shale facies (Sb, St) which tend to be liptinite-rich. Microscopically identifiable organic matter in the Sydney Mines section (B) is considerably lower, ranging from 3.0 to 6.0% by volume, and decreases upward, corresponding with an increase in ash content (Fig. 4.4a).

The predominant maceral group in most samples is liptinite (2-14.5% by volume), usually embedded in an organic-rich mudstone matrix. Thin-walled tenuisporinite is the most common liptinite maceral (0.5-6.0% by volume), followed by finely disseminated liptodetrinite (nil to 4.0% by volume). Cutinite (leaf remains) and crassisporinite (thick-walled spores) occur locally. The Glace Bay West roof section contains a significant proportion of lamalginitite (nil to 4.5% by volume) in layers parallel to bedding.

The vitrinite group is also present in some samples (nil to 5.0% by volume), especially those just above the coal seam. Vitrodetrinite predominates (nil to 2.5% by volume), with telocollinite present in the lowermost sample at Glace Bay West (2.7% by volume).

The inertinite group is also most abundant just above the coal seam. Inertodetrinite fragments are the most common maceral type encountered (nil to 5.7% by volume), with minor semifusinite, fusinite, macrinite, micrinite and rare secretion sclerotia.

4.4.3.2. Source Rock Character

Organic quantity, quality and maturity level of the BRU was determined using Rock-Eval pyrolysis (Appendix A3.4, Table A3.9 to A3.11). Tables A3.7 and A3.8 outline the parameters determined. Results are summarized in Figures 4.6 and 4.7.

Hydrocarbon quantities were measured directly by the Rock-Eval instrument as S_1 (free hydrocarbons) and S_2 (hydrocarbons released from kerogen upon pyrolysis). Carbon dioxide quantities were measured as S_3 and values range from 0.07 to 2.23 mg CO_2 /g rock (avg-0.64 mg CO_2 /g rock). The Petroleum Potential (PP) represents the sum of S_1 and S_2 and ranges from 0.18 to 44.70 mg HC/g rock (avg-9.31 mg HC/g rock). S_1 values range from 0.02 to 6.01 mg HC/g rock (avg-0.46 mg HC/g rock). S_1 values obtained from coastal sections are consistently low (<1.0 mg HC/g rock) whereas offshore the S_1 contents are generally greater than 1.0 mg HC/g rock. S_2 values range from 0.13 to 40.47 mg HC/g rock (avg-8.84 mg HC/g rock) and are generally greater than 5.0 mg HC/g rock. Total organic carbon content (TOC) of these samples range from 0.41 to 19.98% (by weight) and most samples contain greater than 1.0% organic carbon (avg-3.67% TOC). S_1 , S_2 and TOC values indicate good to very good source rock potential (Fig. 4.6) and there is a good correspondence between values. Vertical trends vary locally and generally correlate with abundance of liptinite identified microscopically (Figs. 4.4a and b).

T_{max} values provide an estimate of the maturity of the sediments and range from 434 °C to 450 °C. This corresponds

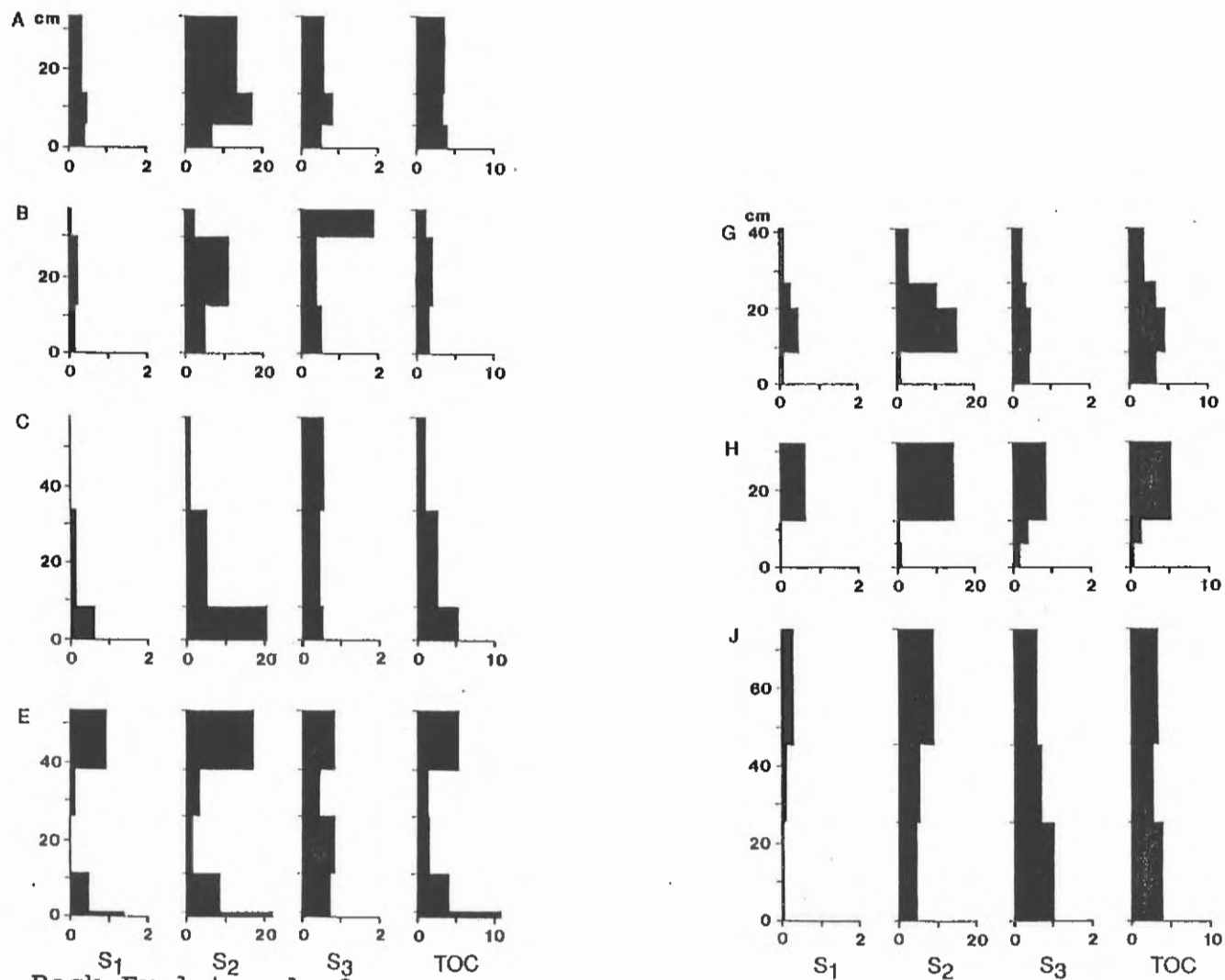


Figure 4.6. Rock-Eval trends for coastal sections: A-Bras d'Or; B-Sydney Mines; C-Victoria Mines; E-Glace Bay West; H-Donkin East; G-Donkin West and J-Longbeach. Section locations on Figure 1.2. S₁ and S₂ in mg HC/g rock; S₃ in mg CO₂/g rock TOC in weight %.

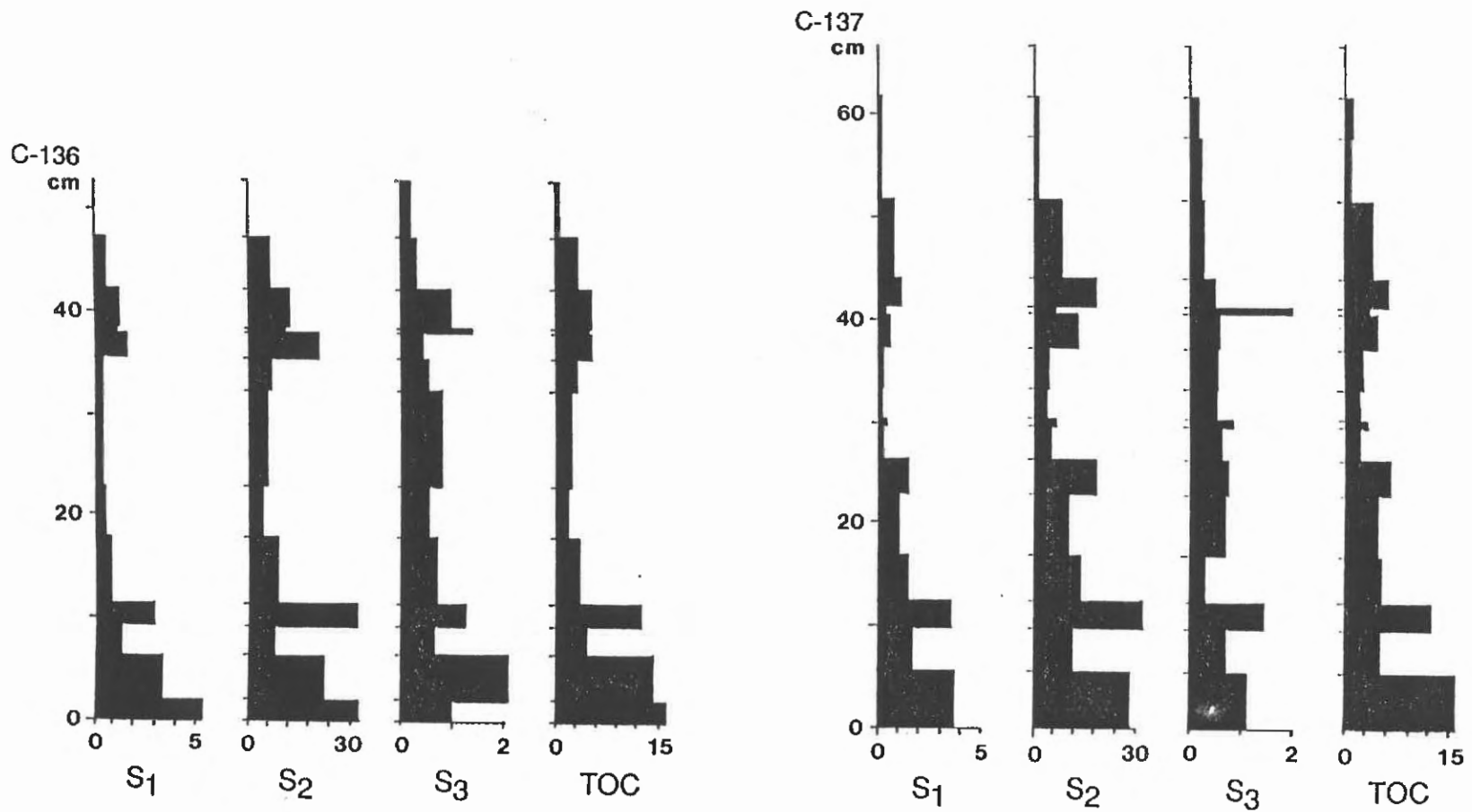


Figure 4.7. Rock-Eval trends for offshore core: C-136 and C-137. Core locations on Figure 1.2. S₁ and S₂ in mg HC/g rock; S₃ in mg CO₂/g rock and TOC in weight %.

with the top of the oil window, as defined by Peters (1986). Tmax exhibits a slight increase in the offshore samples, consistent with an increase in vitrinite reflectance values down dip for coal seams in the basin (Hacquebard and Donaldson, 1970). A few anomalously high Tmax values ($> 500^{\circ}\text{C}$) may be due to oxidized organic matter or the adsorption of pyrolytic organic compounds onto the mineral matrix (Espitalié *et al.*, 1980).

Calculated Production Indices ($\text{PI} = S_1 / (S_1 + S_2)$) also provide a measure of the maturity of the sediments (Peters, 1986). Onshore PI values tend to be low (< 0.1) suggesting immaturity. Offshore values are higher (generally close to or > 0.1) suggesting greater maturity. Lower PI values in outcrop samples may be due to loss of S_1 hydrocarbons (free hydrocarbons) during weathering, in which case PI values are questionable.

For each coastal site, the Hydrogen and Oxygen Indices (HI and OI, respectively) are plotted by sample (Espitalié *et al.*, 1977) to provide information on variations in organic matter types (Fig. 4.8). Trend lines for the three main kerogen types (Type I-algal, Type II-herbaceous, and Type III-woody) are included in these diagrams. Average values for each roof succession are indicated on each plot and summarized on Figure 4.8 (BRU AVG). Most samples plot in an area indicative of Type II to Type II/III kerogen with low to intermediate hydrogen indices in the range of 150 to 500 mg HC/g Corg. Weighted average values per section cluster around 200 mg HC/g Corg, with the exception of the Bras d'Or section (A-avg: 354 mg HC/g Corg). Oxygen Indices are generally less than 50 mg CO_2 /g Corg.

Vertical HI trends are variable in the coastal sections (Fig. 4.6) and include increasing, then decreasing upward (A,B); decreasing upward (C,G); decreasing, then increasing upward (E,H) and increasing upward trends (J). Offshore holes (C-136, C-137) reveal three to four decreasing upward

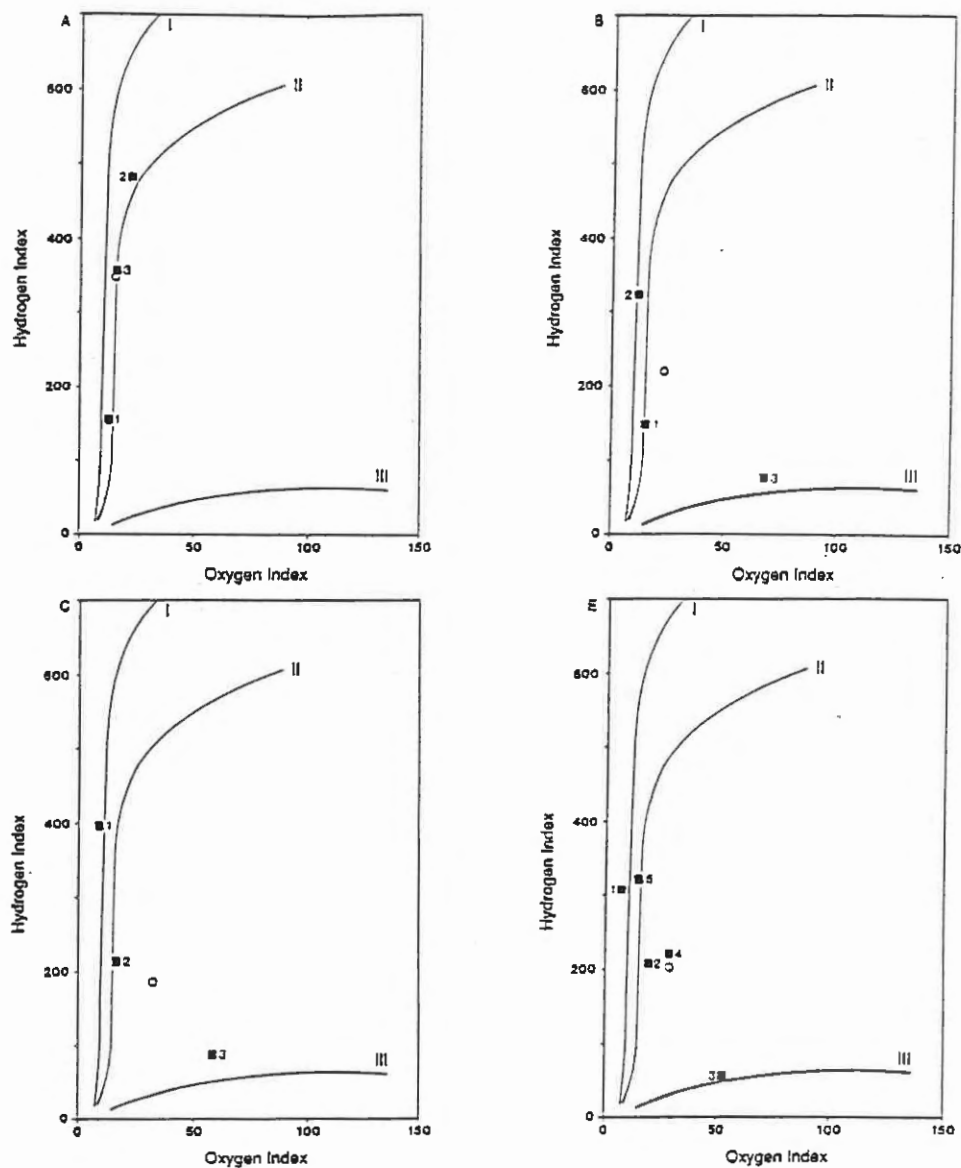


Figure 4.8. Hydrogen Index - Oxygen Index (HI-OI) plots for: A-Bras d'Or; B-Sydney Mines; C-Victoria Mines; E-Glace Bay West; cores C-136, C-137; G-Donkin West; H-Donkin East; J-Longbeach and BRU Avg-average per section studied (O). Numbers represent sample intervals in ascending order, from the base of the roof (1) to the top (n).

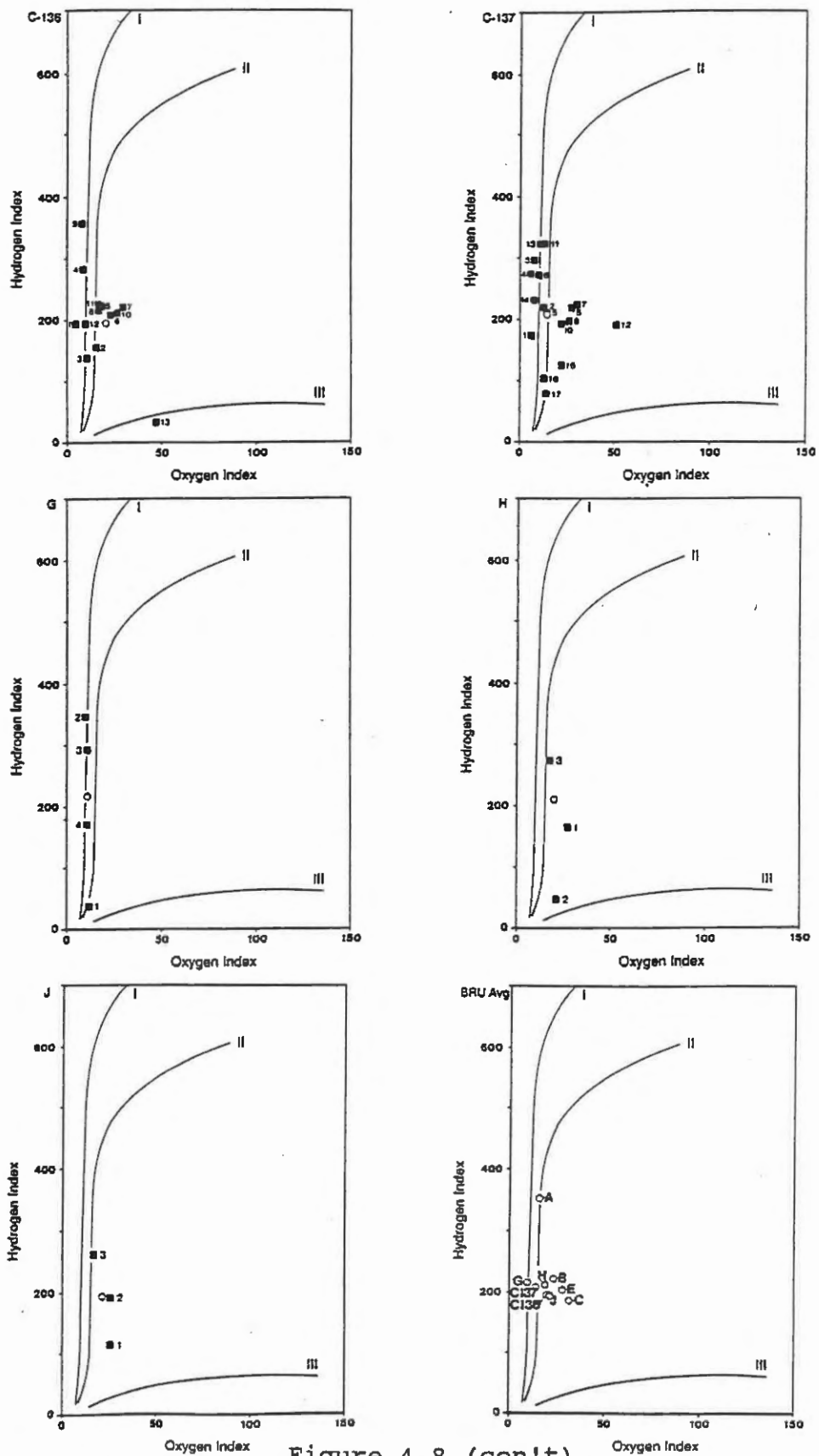


Figure 4.8 (con't)

organic cycles (Figs. 4.7 and 4.8). This variability reflects variations in organic type and quantity and is probably related to the facies trends described in Section 4.4.1.2. Oxidation of organic matter as well as increased maturity are two additional mechanisms that can account for a decrease in the hydrogen content of a sample, thus lowering HI values. Maturity fluctuations at individual sampling sites, however, can be ruled out due to the close proximity of sample intervals.

4.4.4. Fossil Content

The distribution of fossil groups identified in thin sections from the offshore cores (C-136 and C-137) are illustrated in Figure 4.5a, b (Tables A3.1 and A3.2). Bivalve and ostracod shells are the most common constituents; they tend to occur in distinct beds but locally occur together.

Fossils were also isolated from 1 to 2 kg bulk samples representing specific vertical intervals at two coastal locations (B-Sydney Mines and E-Glace Bay West) following the procedure outlined in Appendix A3.5. Fossil identifications were made by W. Parkins, Brock University. Results are summarized in Tables 4.2 and 4.3, by total numbers and percent of sample, based on a 1 kg sample. Fossils recovered were grouped into the following categories: 1) ostracods, 2) annelids, 3) shark, 4) other fish, 5) bone fragments and 6) coalified fragments. Bivalves were common to abundant in most samples but were destroyed during sample processing and could not be quantified. Organic-rich shales (B-202, E-41 and E-42) were difficult to break down and results may not accurately represent all biota present in the interval. The vertical distribution of fossil groups and total abundance per sample are illustrated in Figures 4.4a and b.

Table 4.2. Fossil distribution in the BRU - Sydney Mines section (recalculated based on a 1 Kg sample).

Picked fossils	JW-90-8200		JW-90-8201		JW-90-8202	
	n=	%	n=	%	n=	%
1. Ostracods:	987	53.5	455	83.0	183	97.9
a. <i>Carbonita inflata</i>	113	6.1	267	48.7	108	57.8
b. <i>G. scalpellus</i>	746	40.5	87	15.9	10	5.3
c. <i>G. fabulina</i>						
d. <i>Gandona salteriana</i>	128	6.9	101	18.4	65	34.8
2. Annelids:						
<i>Spirorbis</i> sp.:	17	0.9	9	1.6	3	1.6
3. Shark:	43	2.2				
a. Hybodontoides teeth	2	0.1				
b. Xenacanthidae teeth	3	0.2				
c. Xenacanthidae mucous membrane denticles or fragments						
d. elasmobranch dermal denticles	38	2.1				
4. Other Fish:	60	3.3	10	1.8		
a. fish scale - Paleoniscoidea	10	0.5				
b. fish scale fragments - Paleoniscoidea			3	0.5		
c. lepidotrichia - Paleoniscoidea	10	0.5				
d. denticles - possibly Coelolepida						
e. unidentified scale fragments	2	0.1				
f. fish spine	2	0.1				
g. pterygoid plate - Dipnoi			1	0.2		
h. socketed teeth						
i. unidentified teeth or denticles	35	1.9	3	0.5		
j. bone fragments with fused teeth (probably Paleoniscoidea)	1	0.1	3	0.5		
5. Bone Fragments:	582	31.6	71	13.0	1	0.5
6. Coalified Fragments:	155	8.4	3	0.5		
a. megaspore	10	0.5				
b. plant fragments						
c. wood	7	0.4	2	0.4		
d. rootlets	138	7.5	1	0.2		
Total counts, percent	1844	100	548	100	187	100

Table 4.3. Fossil distribution in the BRU, Glace Bay West section (recalculated based on 1 Kg samples).

Picked fossils	JW-90-E40		JW-90-E41		JW-90-E42		JW-90-E43		JW-90-E44	
	n=	%	n=	%	n=	%	n=	%	n=	%
1. Ostracods:	25	7.9	24	92.3	101	59.4	2	1.5	6	50.0
a. <u>Carbonita inflata</u>	12	3.8	10	38.5	60	35.3	1	0.7	2	16.7
b. <u>C. scalpellus</u>	3	0.9	6	23.1	11	6.5				
c. <u>C. fabulina</u>	1	0.3								
d. <u>Cardona salteriana</u>	9	2.8	8	30.8	30	17.6	1	0.7	4	33.3
2. Annelids:										
<u>Spirorbis</u> sp.:	1	0.3	1	3.8	1	0.6			1	8.3
3. Shark:	77	23.9			3	1.8	1	0.7		
a. Hybodontoida teeth										
b. Xenacanthidae teeth	2	0.6			1	0.6				
c. Xenacanthidae mucous membrane denticles or fragments	4	1.3					1	0.7		
d. elasmobranch dermal denticles	70	22.0			2	1.2				
4. Other Fish:	43	13.2			30	17.6	63	47.0	1	8.3
a. fish scale - Palaeoniscoidea	1	0.3			6	3.5	29	21.6		
b. fish scale fragments - Palaeoniscoidea							12	9.0		
c. lepidotrichia - Palaeoniscoidea										
d. denticles - possible Coelolepid?	4	1.3			1	0.6				
e. unidentified scale fragments	15	4.7			13	7.6	19	14.2		
f. fish spine	1	0.3								
g. pterygoid plate - Dipnoi										
h. socketed teeth	7	2.2			4	2.4	1	0.7		
i. unidentified teeth or denticles	12	3.8			2	1.2	1	0.7	1	8.3
j. bone fragments with fused teeth (probably Palaeoniscoidea)	2	0.6			4	2.4	1	0.7		
5. Bone Fragments:	121	38.1	1	3.8	124	72.9	65	48.5	2	16.7
6. Coalified Fragments:	51	16.0			13	7.6	5	3.7	2	16.7
a. megaspore	1	0.3			5	2.9	4	3.0		
b. plant fragments	1	0.3								
c. wood	12	3.8					1	0.7	2	16.7
d. rootlets	37	11.6			8	4.7				
Total counts; percent	318	100	26	100	170	100	134	100	12	100

Foraminifera: Agglutinated foraminifera assigned to the genera Ammobaculites, Ammotium, Milliammina, Reophax and Trochammina were recovered from coal-bearing strata in the Sydney Mines Formation (Wightman et al., 1992). An assemblage dominated by coiled forms (Trochammina) is present in the underclay below the Backpit seam whereas strata directly above the seam contain predominantly uncoiled forms (Ammobaculites, Ammotium, Reophax) (W. Wightman, pers. comm., 1992). A single calcareous open marine (?) species has tentatively been identified from the Cm facies, Glace Bay West (W. Wightman, pers. comm., 1992).

Bivalves: The most abundant bivalve in these samples is Anthraconauta phillipsii (Williamson) (Plate 8b). Other, less common bivalves include Anthraconauta cf. A. phillipsii and Anthraconaia cf. A. arenacea. These elongate shells are concentrated in layers parallel to bedding and are common throughout the BRU. They form a major component of the Cc facies (Plate 9c). Shell walls exhibit a prismatic to laminar structure in thin section and are rarely fragmented. Most valves are articulated and adult forms predominate and constitute a life assemblage (W. Parkins, pers. comm., 1991).

Ostracods: Ostracods Carbonita inflata, C. scalpellus, C. fabulina and Candona salteriana are common to abundant in most intervals. Their shells are visible on bedding planes of many unprocessed samples. In thin section they are thin-walled and commonly disarticulated, although shells with geopetal fillings are present (Plate 9a). The most common mode of preservation observed in the processed residue is internal molds consisting of calcite, chert or organic-rich mudstone. Shells replaced by pyrite occasionally survived the isolation procedure.

Ostracods are abundant in the Sydney Mines section (B) and occur predominantly in the carbonate facies (Cd, Cm and Cc). Their abundance decreases upward, corresponding with

an increase in ash content. Carbonita scalpellus is concentrated in the basal sample and is significantly less abundant in higher samples. Candona salteriana also decreases upward. Carbonita inflata is most common in the Cc facies (B-201).

Ostracods Carbonita inflata, C. scalpellus and Candona salteriana are also concentrated in the carbonate facies (sample E-42) at the Glace Bay West section (E). Vertical trends are less obvious in this roof section as far fewer ostracods were recovered. Intervals above this contain very few ostracods.

Other Arthropods: Leaia sp. (branchiopods) were observed on the bedding planes of some units in the field but none were recovered from the processed samples. They tend to be concentrated in slightly coarser medium grey mudstone beds above the black shale facies.

Annelids: Calcareous annelid tubes (Spirorbis sp.) were recovered principally from Sydney Mines (B) samples. They were rarely observed attached to the posterior margin of bivalve shells. In the fossil residue these tubes were preserved as coiled internal molds of calcite. These molds, when intact, were flattened on one side, suggesting an encrusting mode of life.

Sharks: Fossils attributed to sharks include xenacanthid and hybodontoid teeth, xenacanthid mucous membrane denticles and elasmobranch dermal denticles. Figure 4.9 outlines the classification of sharks and other fish fossils identified in this study. Isolated shark remains are virtually restricted to the detrital carbonate facies (Cd) at the base of the roof strata in both coastal sections studied (Figs. 4.4a and b).

Elasmobranch dermal denticles (Plate 9d) are the most common fossil type recovered but are not diagnostic of any particular group of sharks. Xenacanthid mucous membrane denticles are limited to the Glace Bay West section (E).

They have many cusps which are reclined and gently curved towards the edge of the denticle. Rare xenacanthid teeth consist of a thick base, prominent apical button and a pair of large lateral cusps with a smaller cuspule between them. These are typical features of dipodus teeth, diagnostic of xenacanthid sharks. They are well preserved but lateral cusps are often broken. One tooth was identified as belonging to Orthacanthus sp.. Rare hybodontoid teeth have a cladont morphology, with a large central cusp and a varying number of smaller lateral cusps. These teeth were well preserved and limited to the basal sample, Sydney Mines section (B).

Other Fish: Fish fossils include scales, denticles, spines, jaw plate, teeth and bone fragments. Fish fossils generally decrease in abundance upward in the Sydney Mines section and tend to be concentrated in carbonate-rich facies in both sections. Few if any fish remains were recovered from the organic-rich black shales (St and Sb). This may be due to their resistance to chemical breakdown during sample processing as vertebrate fragments were observed in thin sections from the base of these facies (Plate 9d).

Most fish remains are of palaeoniscoids (Fig. 4.9) and include scales and scale fragments, some of which retain the diagnostic socket and peg articulation (Lambe, 1916). Most of the scales differ only in size and may belong to the same unidentified taxon. Bone fragments with fused teeth probably belong to palaeoniscoids as do lepidotrichia (fin scales) recovered from the Sydney Mines section (B) only.

Socketed teeth occur in the Glace Bay West section (E) and may belong either to crossopterygians (lobe-finned fish) or to amphibians. Other teeth recovered were unidentifiable. Fish spines are rare and may be attributed either to acanthodians (primitive bony fish) or elasmobranchs. Small dermal denticles were recovered that strongly resemble those of thelodonts (jawless coelolepid).

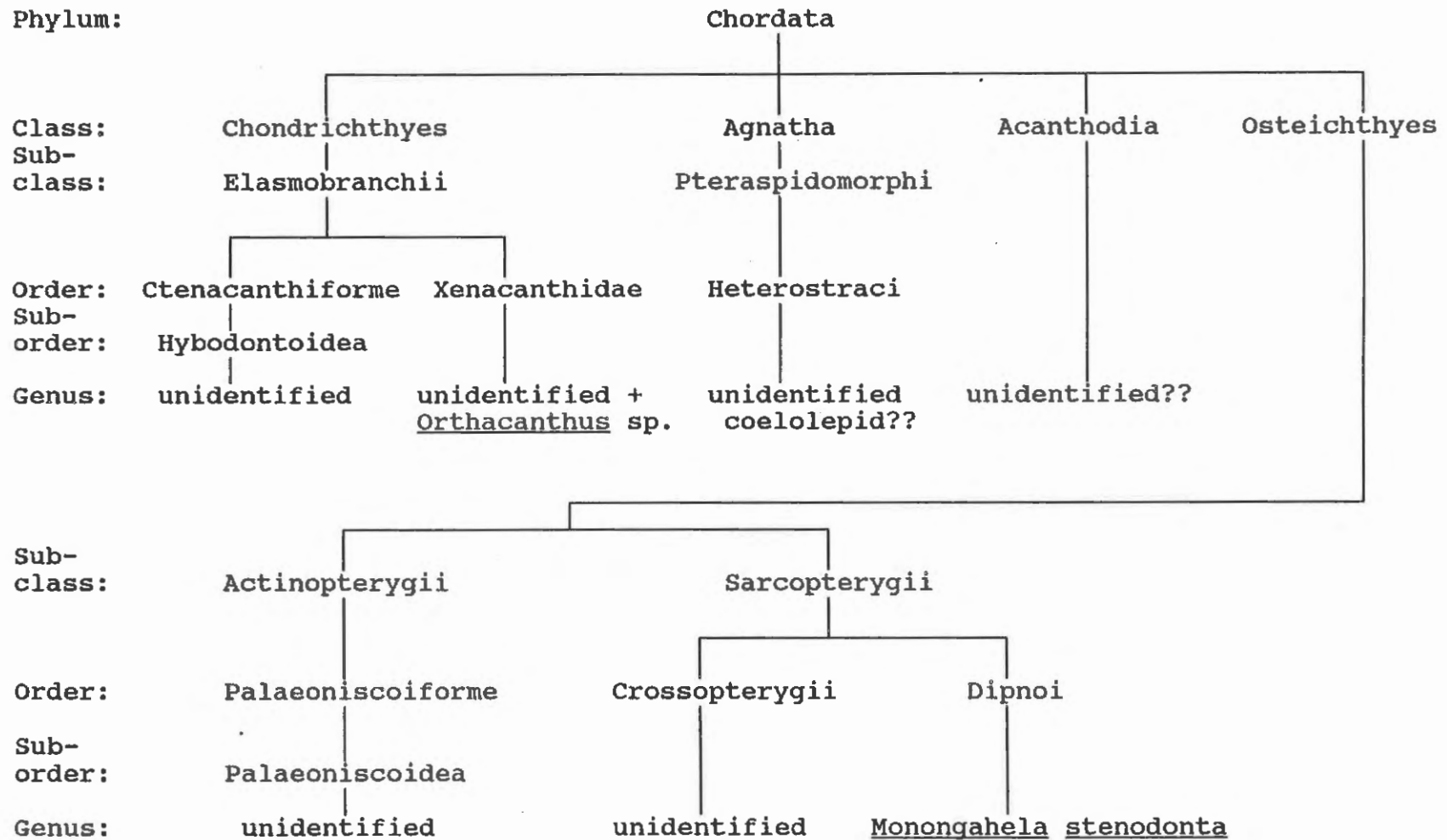


Figure 4.9. Classification of isolated fish fossils from the BRU. Classification scheme from Carroll (1988).

These fish, however, are not known to occur beyond the Devonian period (Romer, 1945). These denticles could, less certainly, belong to acanthodian fish.

A pterygoid plate (jaw bone) recovered from the Sydney Mines section (B-201) was identified as Monongahela stenodonta, a lungfish (Dipnoi). The plate shows rows of flattened cusps along the axis of several ridges.

Bone Fragments: Bone fragments, broken and too small for identification, are common to abundant in samples near the base of the roof strata. They may have been fractured during compaction or by predators. The vertical distribution of these bones is comparable with that of identifiable fish fossils.

Coalified Fragments: Coalified fragments recovered include rootlets, wood and plant fragments and megaspores. Outer ornamentation on the megaspores was not preserved, suggesting transport. The number of coalified fragments isolated by this process tends to decrease upward in both sections, in disagreement with the microscopic organic matter trends. This may be due to the incomplete breakdown of the organic-rich shale samples.

4.5. DISCUSSION

4.5.1. Environmental Significance of Fossils

The BRU contains a restricted fossil assemblage comparable to many "nonmarine" intervals of the British Carboniferous coal measures (Eager and Rayner, 1952; Rippon, 1984). The presence of agglutinated foraminifera, geometry of major seams and cyclothem patterns of strata, however, indicate a marine connection for the basin. The significance of fossils recovered from the BRU is summarized below. Table A3.13 lists fossil fauna described in the literature from the Morien Group.

Foraminifera: Agglutinated foraminifera were identified from underclay units directly below the Backpit

seam (S. Thibaudeau, pers. comm., 1991; W. Wightman, pers. comm., 1991). These marginal marine organisms are predominantly high marsh varieties (coiled forms), capable of tolerating a wide range in salinity. This discovery establishes a depositional setting close to a marine influence for the Backpit mire. Recent investigation of the Backpit roof by W. Wightman, Dalhousie University, has identified agglutinated foraminifera (dominated by straight forms-lower marsh) as well as a calcareous specimen that may be open marine. Additional work is under way to document these foraminifera, the discovery of which confirms a marine connection for the roof strata. Scott *et al.* (1991) documented a transition from marginal marine to open marine foraminifera in the modern-day Mississippi Delta. The restricted nature of the associated BRU fauna suggests that a distal barrier may have permitted fresh to brackish water conditions to prevail for extended periods. Penland *et al.* (1988) found that during Gulf Coast transgression, sand barriers and shoals developed offshore from drowned coastal sands, leading to extensive brackish bays landward.

Bivalves: The bivalve fauna in the Backpit roof strata is abundant but of low diversity: predominantly Anthraconauta sp. with minor Anthraconaia sp.. Anthraconauta ranges from mid Westphalian C to Westphalian D whereas Anthraconaia is present throughout the Westphalian (Calver, 1968b).

Many studies have been completed on the British bivalve faunas (e.g. Trueman and Weir, 1946; Eagar, 1952, 1960; Weir, 1960). Hind (1899) suggested that these shells occupied a fresh to brackish environment and he recognized marine bands as "discrete horizons carrying a fully marine fauna". Eagar (1961) and Calver (1968b) suggested that Anthraconauta inhabited predominantly freshwater niches but were tolerant of slightly brackish conditions. The salinity range for Anthraconaia was broader, including fresh to

brackish conditions.

Most valves are articulated, suggesting very quiet (low energy) depositional conditions and lack of significant predation or scavenging. Articulated valves also suggest either slow decay, probably under anaerobic to dysaerobic conditions or a high sedimentation rate (Zangerl and Richardson, 1963). The former is favoured in this environment due to the high organic and low detrital content of the BRU. The abundance of bivalves suggests that they were tolerant of oxygen-deficient bottom conditions. Rosenberg (1977) documented diverse benthic communities in an estuary in Sweden with O_2 levels around 1 ml/l. Between 0.5 and 0.1 ml O_2 /l, a low diversity highly stressed, suspension feeding (non-burrowing) epifauna can still survive above the sediment water interface (Demaison and Moore, 1980). The occurrence of Spirorbis sp. attached to the posterior end of some bivalves suggests that the bivalves were not active burrowers.

Alternatively, these bivalves may have adopted a pelagic mode of life, attached by byssal threads to floating vegetation in a manner similar to that discussed by Ramsbottom (1978) for Naiadites. As the bivalve died or became too heavy, it would come to rest on the mud substrate. This floating vegetation (flotant of Russell, 1942) would provide a continuous "rain" of finely disseminated organic matter; the decomposition of which would increase oxygen consumption and contribute to anoxia. This scenario could explain the co-existence of organic-rich mud and bivalve shells (Cc facies).

Annelids: As previously mentioned Spirorbis sp. frequently lived attached to floating plants or to bivalves, in what may have been a commensal relationship (Trueman, 1942). All living Spirorbis species are marine, and freshwater polychaetes are rare. This may suggest marine to brackish conditions during accumulation of the BRU although

as pointed out by Trueman (1946), Spirorbis is rarely found attached to marine organisms in true Carboniferous marine bands. Alternatively, these calcareous tubes may represent vermiform gastropods as suggested by Burchette and Riding (1977) and Weedon (1990).

Ostracods: The main ostracod identified in this study is Carbonita sp. (C. inflata, C. scalpellus and C. fabulina), with minor Candona salteriana. These organisms molt many times in their life cycle, thus accounting for the numerous disarticulated valves observed in some layers. All species are present in most carbonate-rich facies, suggesting either that the sampling intervals may have been too large to define distinct populations or that all species co-existed. Carbonita scalpellus probably favoured open water conditions and exhibits a significant decrease in abundance upward in the Sydney Mines roof section, which may correspond with a decrease in water depth (W. Parkins, pers. comm., 1991). These organisms can occupy fresh to slightly brackish environments (Bless and Pollard, 1972). No exclusively marine ostracods were identified in this study.

Sharks and Other Fish: Rare xenacanthid and hybodontoid teeth, as well as numerous elasmobranch dermal denticles, are concentrated at the base of the BRU. Xenacanthid sharks belong to a specialized group of elasmobranchs that lived almost exclusively in freshwater (Carroll, 1988). Hybodontoid sharks, however, evolved separately and are thought to be the ancestors of modern day sharks. The occurrence of both forms may indicate variation in water salinity.

The presence of shark remains suggests that oxygenated, open water conditions prevailed during the deposition of the carbonate-rich facies. These fish were predators of smaller fish and bivalves (Moy-Thomas, 1971).

Other fish fossils recovered include common Osteichthyes (ray-finned palaeoniscoids) and rare Dipnoi

(lungfish), plus questionable remains of Acanthodia (primitive bony), Crossopterygii (lobe-finned) and Agnatha (jawless coelolepid ?) fish.

Palaeoniscoids are a diversified group of fish that occur in freshwater and marine environments (Carroll, 1988). Although identification to genus level was not possible with the fossils recovered from this study, Robb (1876) identified Gyrolepir sp., Amblypterus sp. and Palaeoniscus sp. from similar lithologies in the Sydney Basin. Vasey (1983, 1984) also identified palaeoniscoid fish including Rhadinichthys sp. and Elonichthys sp. from intervals above coal seams in the Sydney Mines Formation. These genera were interpreted as freshwater by both authors.

The occurrence of rare lungfish (Monongahela stenodonta) in an interval near the top of the carbonate facies at Sydney Mines suggests that water levels were dropping and the ability to breathe above water was an asset. Masson and Rust (1984) described the same species of lungfish isolated from a limestone unit at New Waterford and Sternberg (1941) described Ctenodus murchisoni from a Glace Bay limestone/shale unit. Other fossil fish identified in the literature from the Morien Group are summarized in Table A3.13.

4.5.2. Interpretation of Facies

The eight facies described from the Backpit roof represent abrupt to gradational changes in the environment of deposition. The environment of each facies (Table 4.1) is interpreted below, based on detailed analysis of the lithology, organic matter, inorganic mineral and fossil content.

M facies: Mudstone is present directly above the coal in the eastern portion of the basin. Abundant roots at the Longbeach section (J) and disrupted bedding and ostracods elsewhere suggests a mudflat or shoreline environment.

Cd facies: Detrital carbonate is present at the base of the BUR in the mid- to western portion of the basin and onlaps the M facies in the east. The facies consists primarily of carbonate minerals and bioclasts, with minor to abundant organic matter. Many of the shells are disarticulated and were probably transported. This interval probably represents a transgressive shell lag, with reworking of bioclasts. It contains the highest concentration of shark remains, suggesting oxygenated, open water conditions. High sulphur content in this facies and the subjacent coal suggests brackish to marine waters; numerous authors (Williams and Keith, 1963; Gluskoter and Hopkins, 1970; Casagrande et al., 1977) have associated high sulphur values in upper parts of peat and coal with marine inundation. The absence of marine fossils, however, has led some workers in the Sydney Basin to suggest that the high sulphur coals reflect the influence of sulphate-rich surface and/or basinal waters draining the underlying Windsor Group evaporites (Bell, 1928; Newman, 1934; Haites, 1951). Both mechanisms are possible and would be difficult to distinguish in the ancient record.

Cm facies: Massive carbonate is best developed in the Glace Bay sub-basin, with thin intervals in most other sections. It consists predominantly of bioclastic fragments and localized pellets in a fine-grained micritic matrix. The setting favoured ostracods over bivalves. Rare open marine foraminifera, abundant fish and traces of shark remains suggest oxygenated, open water conditions with a marine connection. Sediment supply remained limited to fine-grained clays and wind-blown quartz grains.

Cc facies: Crenulated carbonate is present in most sections and consists of layers of bivalve shells embedded in a matrix of organic-rich mud (gyttja). Most of the shells are adult forms of Anthraconauta phillipsii and they represent a life assemblage indicative of calm conditions.

Abundant finely disseminated, unstructured organic debris is preserved, suggesting that reducing and oxygen-deficient bottom conditions prevailed, capable of supporting bivalve communities (Demaison and Moore, 1980). Vertebrate fragments suggest that the surface waters remained oxygenated and able to support pelagic life forms. Roots were not observed and plants (flotant) may have covered the surface of the water during the deposition of the Cc facies. Under ordinary conditions, the depositional environment under a flotant is extremely quiet and undisturbed (Zangerl and Richardson, 1963). Reworking of nearby peats may also have contributed to the organic mud.

St and Sb facies: Transitional shale (St) and black shale (Sb) facies are present near the top of most organic-rich roof sections. The St facies is transitional between the Cc and Sb facies, and contains significant to minor amounts of shelly layers. The Sb facies consists predominantly of undisturbed, dark grey to black organic-rich shale with sparse shell horizons. Fish and bivalves occur at the base and decrease upward indicating a decline in conditions favourable for these life forms. Transported organic matter such as sporinite and liptodetrinite are more common in these facies, and plant fossils observed on bedding planes suggest an encroachment of vegetation into the area. Clastic input remained limited; organic matter was allochthonous to hypautochthonous. Anaerobic bottom conditions may have developed, possibly as water-level dropped, as suggested by Moore (1929), Weller (1957) and Zangerl and Richardson (1963) for black shales associated with coal seams in the Pennsylvanian mid-continent of the United States.

Alternatively, the black shale facies may represent the deepest interval in the cyclothem as proposed by Schenk (1967) and Heckel (1977, 1984) for black shale units in the Pennsylvanian mid-continent of the United States. These

"core" shales contain conodonts and phosphatic nodules and are often sandwiched between two marine shale and limestone units, considered by Schenk to be transgressive (lower) and regressive (upper) intervals. Upwelling of low oxygen, nutrient-rich ocean waters in depths of up to 200 m were invoked to cause planktonic blooms in the surface waters, from which the organic matter settled back into the incoming bottom layer, depleting it of remaining oxygen and enriching it in phosphorus. This accounted for the fine-suspended detritus, organic matter and phosphorus, the major constituents of the black shale facies in mid-continent of the United States.

Weller (1957) recognised two environmentally distinct black shale types; those associated with coals and those associated with fossiliferous marine grey shales and limestones. The BRU more closely resembles the former shale type and a relatively shallow, restricted environment is favoured in this study. Sedimentological evidence to support this interpretation can be found in strata above the Backpit seam at the New Waterford section (D). Here a coarsening upward deltaic package, approximately 6 m thick, overlies the BRU, followed by a thin coal seam (rider?) (Fig. 2.1). If the BRU shale was deposited in 200 m of water then much thicker deltaic deposits would be expected before localized peat accumulation could continue. A much shallower body of water (<20 m) is therefore proposed for the BRU shale.

Fe facies: Laterally extensive siderite bands and nodules are associated with the Sb and/or MZ facies in the upper portion of the BRU. Similar nodules have been described from intertidal marsh (Pye et al., 1990) and interdistributary bays (Ho and Coleman, 1969).

Reducing conditions (low Eh) and an alkaline environment (pH > 7) are necessary for the precipitation of siderite (Krumbein and Garrels, 1952). Other factors that

control the distribution of siderite include the availability of reactive organic matter and the levels of sulphate and ferrous iron in the water column (Curtis, 1987). Upon decay, organic matter produces carbon dioxide, which dissolves in water to form bicarbonate ions which can react with ferrous iron to precipitate siderite. Low SO_4^{-2} values and consequently low H_2S are required for the precipitation of siderite; otherwise the available iron will react with H_2S to form pyrrhotite (FeS) or pyrite (FeS_2).

MZ facies: The interbedded mudstone/siltstone facies occurs directly above the organic-rich intervals in most of the roof sections studied. It is very thin to absent in sections where a channel cuts into the BRU (Fig. 4.1). This facies represents a coarsening upward prodelta to deltaic succession and marks the return of clastic sedimentation to the region.

4.5.3. Depositional Setting

The Backpit mire accumulated on a low-lying coastal plain (Chapter 3). The upper portion of the seam shows evidence for drowning, including a series of dulling upward trends, due to an increase in detrital clay input. Relative sea-level rise eventually terminated peat accumulation and formed a bay - the maximum transgression within the cyclothem package. Water depth in this bay is difficult to ascertain but relatively shallow depths are favoured. Facies and fossil distribution indicate variations in the oxygen content of the water column and bottom sediments. Oxygenated conditions prevailed during the initial transgressive phase when the bay supported sharks, other fish, foraminifera, bivalves, ostracods and serpulids (Cd and Cm facies), indicative of fresh to brackish-marine conditions. This stratigraphic position corresponds to a marine zone recognized by Zangerl and Richardson (1963) at the base of two fossiliferous black shales (Middle

Pennsylvanian) from Indiana. The absence of typical open marine fossils (e.g. brachiopods, conodonts, cephalopods, corals etc.) in the BRU suggests that the bay was partially isolated from the ocean.

Restricted environments (Cc, St facies), with a high abundance and low diversity of fauna, followed. Dysaerobic, reducing bottom sediments preserved relatively undisturbed organic-rich mud, whereas the water column remained oxygenated and supported fish. Conditions in the bay gradually deteriorated and the water became inhospitable, even for the hardy bivalve communities. Vegetation (flotant) may have taken over the bay and anoxic conditions persisted (Sb facies).

The scarcity of terrigenous sediment input for the BRU suggests that there was a landward shift in the locus of sedimentation, as would be expected during a marine transgression. Sediments could also have by-passed this region. Detrital silt-sized grains were probably wind-blown. The bay was eventually filled by a coarsening upward sequence attributed to a prograding bayhead delta (MZ facies). These deposits were cut into by distributary channels at some locations.

In the east, the BRU initially occupied a more landward paleogeographic position. Here a shoreline or mudflat environment (M facies) is present directly above the coal and subsequent organic-rich intervals include restricted facies (Sb, St and Cc) with rare open-water facies (Cm).

4.5.4. Source Rock Potential

The BRU is marginally mature onshore based on Tmax data. Vitrinite reflectance values from the associated Backpit coal provide a comparable yet slightly higher maturity index (0.69 to 0.76% R_{rnd}; Section 3.2). Hacquebard and Donaldson (1970) noted that vitrinite reflectance of coal increases as the seams are traced

downdip in the offshore region. Higher maturity levels offshore are favourable for the production of oil and/or gas from these organic-rich lithologies.

The unit has good to very good hydrocarbon generative potential. Average TOC content is approximately 3.7% by weight. Offshore, free and in situ hydrocarbons (S_1 and S_2) are generally greater than 1.0 and 5.0 mg HC/g rock, respectively. The organic type is herbaceous to woody (Type II and Type II/III) indicating an oil- to gas-prone source rock. Much of the identifiable organic matter is terrestrially derived (e.g. sporinite, vitrinite and inertinite), except at Glace Bay West where lamalginite was identified. Floating plants and reworked peat material may have provided a significant proportion of the finely disseminated organic matter typical of the Cc, St and Sb facies.

The BRU is continuous for more than 45 km parallel to depositional strike. The thinness of the interval (30-75 cm), however, limits the quantity of oil and gas that could have been generated. This limestone/shale unit is one of many similar units in the Sydney Mines Formation and their combined thickness is considerable locally; Gibling and Kalkreuth (1991) estimated 5% of the total stratigraphic column in places.

4.6. SUMMARY

The BRU is a thin (30-75 cm) resistant, laterally continuous limestone/shale sequence directly above the Backpit seam. It comprises up to eight facies, the associations of which represent an overall shallowing upward, bay-fill succession. The bay progressed from oxygenated conditions with a diversity of fauna directly above the coal to a more restricted environment with dysaerobic bottom waters, to an inhospitable, probably anoxic environment. The bay was eventually filled by a

coarsening upward sequence of prodelta and deltaic sediments.

The initial limited siliciclastic input permitted the accumulation of large amounts of bioclastic material and organic matter. The discovery of foraminifera above and below the Backpit seam indicates a paralic setting for the mire. The BRU fossil assemblage is considered marginal marine, with many taxa capable of tolerating fresh to brackish conditions. The restricted nature these fossils suggests that a barrier hindered the development of open marine conditions. High sulphur values in basal roof and upper coal samples support a brackish inundation of the mire.

Maceral analyses show that the interval contains predominantly terrestrially derived organic matter (sporinite, vitrinite and inertinite) with lamalginite at the Glace Bay West section. Type II to Type II/III kerogen predominates, indicating an oil- to gas-prone source rock. Rock-Eval parameters, including TOC, S₁ and S₂ indicate good to very good hydrocarbon generative potential. The thinness of the BRU, however, limits its economic significance.

5. ECONOMIC SIGNIFICANCE OF THE PHALEN-BACKPIT INTERVAL

5.1. INTRODUCTION

This study, although limited in stratigraphic extent, provides data on the Backpit seam and associated organic-rich lithologies as an energy resource, and proposes a predictive depositional facies model that may prove useful to mine geologists when assessing roof conditions in underground mines. The implications of these contributions are briefly outlined in this chapter.

5.2. ENERGY RESOURCE

The Backpit seam, one of eight high volatile B to A, bituminous coal seams within the SMF, is the most continuous seam in the onshore portion of the basin. The seam attains maximum known thickness onshore (1.5 m) and thins to 20 cm within 10 km of the coastline (D. MacNeil, pers. comm., 1991). It was mined in the Sydney Mines and Bras d'Or districts in the mid 19th to early 20th centuries (Haïtes, 1952), but inferior quality (avg. ash-15.3%; avg. sulphur-5.2%) and considerable thinning of the seam offshore, render it uneconomic from a present-day mining perspective.

A significant potential resource yet to be fully exploited is the extraction of coal-bed methane from the Backpit and other seams in the SMF. The rank of the Backpit coal onshore is approximately V7 ($R_o = 0.69-0.76\%$) and like other seams in the basin, rank increases downdip in the offshore region (Hacquebard and Donaldson, 1970). Vitrinite reflectance values from mine sites in the Glace Bay region are generally close to or slightly higher than 1.0% (White and Birk, 1989), well within the "oil window" (Peters, 1986). Thus, maturity ranges favourable for the production of methane gas exist basinward. This, coupled with the association of extensive organic-rich limestone/shale roof lithologies, with good to very good hydrocarbon generative potential (Chapter 4), provide a promising field for future

investigation. These rocks contain oil- to gas-prone type II to II/III organic matter (avg TOC-3.67%), predominantly in the form of sporinite.

Methane production within a working mine, however, can create potentially hazardous conditions and the recognition and mapping of such distinctive organic-rich lithologies should be included in routine underground mapping by mine geologists.

5.3. ASSOCIATED FACIES

An understanding of the paleoenvironment of the mire and associated strata are important from a mining perspective. The seams included in the study interval (Phalen, unnamed, Backpit) all terminated by drowning and typically have an organic-rich lake/bay deposit directly above the coal, followed by a muddy coarsening upward lake/bay-fill to delta package. Organic-rich limestones and shales deposited in the lakes/bays are very cohesive and provide a relatively stable roof. Distributary channels locally cut into this package and can affect coal thickness and quality in the submarine workings (White and Birk, 1989). The sandstone roof also poses a potential sparking hazard (Forgeron *et al.*, 1986). The recognition of delta facies commonly associated with these distributary channels may help geologists predict the channel position in advance and reduce costly shut-downs.

The onshore distribution of these channel belts tends to show clustering or stacking in specific regions through time, including the faulted margin areas and New Waterford (D), bordering the Sydney Mines and Glace Bay sub-basins. This suggests a channel distribution possibly controlled by differential subsidence of underlying basement blocks. The areas of increased subsidence (sub-basins) typically contain a larger proportion of floodplain and lacustrine/bay-fill deposits, suggesting wetter conditions. This observation

may be extended to the offshore mining districts.

The floor rock commonly observed in the study area is a highly rooted kaolinite-rich underclay, which is firm and generally poses no major mining problems. Rarely, a channel sandstone deposit was observed directly below a coal seam in the coastal sections. The prediction of this occurrence in a mine would be very difficult, however, especially with the limited exposure of the floor rocks.

5.4. SUMMARY

The Backpit seam is not economic from a mining perspective, however, the occurrence of stacked coal seams and associated organic-rich lithologies within the oil-window make the Sydney Basin a potential coal-bed methane exploration target and further investigation is warranted.

Detailed mapping of depositional facies may provide a useful tool for predicting the distribution of distributary channels, although the mine geologist is limited by the exposure. Recognition of depositional facies patterns at outcrop scale may provide the missing link required to make these interpretations.

6. CONCLUSIONS

The coal-bearing SMF (Westphalian D to Stephanian) within the Sydney Coalfield, Nova Scotia, contains eleven cyclothems onshore, bounded by extensive coal seams. Up to three cyclothems near the base of the SMF provide a data base for study of the distribution and significance of organic and inorganic facies in coal-bearing strata. The following points summarize the main conclusions of this thesis:

1. The relatively uncomplicated PBI contains a well- and a poorly-developed cyclothem (7 to 20 m thick) that show a systematic vertical facies succession: 1)lake/bay-fill and distributary channel (including organic-rich limestone/shale, mudstone, siltstone and sandstone), 2)well-drained floodplain (including red/grey mudstone, nodular carbonate, siltstone, sandstone) 3)poorly-drained floodplain (\pm channel deposits) to coastal plain (including grey mudstone, limestone, thin coal, sandstone) and 4)extensive mire (including coal and coaly shale). This cyclothem facies succession is interpreted as the result of a shift in the depositional site from a coastal environment to a more landward alluvial plain setting, back to a coastal environment, driven by fluctuations in relative sea-level.
2. Four depositional facies are laterally extensive and can be traced for more than 20 km parallel to depositional strike: 1)extensive mires (coal), 2)organic-rich roof units (limestone/shale) 3)calcareous paleosols (nodular carbonate) and 4)well-drained floodplain soils (red to red/grey mottled mudstone).
3. The lateral continuity of key units and systematic facies successions in the study interval suggests regional control over their formation. The interplay of allogenic

controls, dominated by eustasy (controlled by climate) and influenced by sediment supply and tectonism (subsidence), coupled with more local autogenic processes, have determined sedimentary patterns. Autogenic processes such as channel avulsion, crevasse splay progradation, delta switching and differential compaction of underlying sediment, have locally affected these patterns. Detailed mapping of these facies patterns and facies associations has practical applications as a predictive tool in mining.

4. Areal distribution of stratigraphic thickness and depositional facies is influenced by paleotopography, possibly due to differential subsidence of fault-bounded basement blocks. Lacustrine/bay-fill and floodplain deposits are more abundant in the Sydney Mines and Glace Bay sub-basins, whereas channel sandstone deposits are more abundant in intervening regions near the basin margins and at New Waterford.

5. The Backpit seam (top of Cyclothem 2) is a high volatile B to A bituminous coal ($R_o=0.69-0.76\%$ onshore), with moderate to high ash (avg- $15.3 \pm 6\%$) and sulphur (avg- $5.2 \pm 2\%$) that ranges from 0.6 to 1.5 m thick in the study interval. Banded lithotypes constitute a major portion of the seam; vitrinite macerals and vitrinite-rich microlithotypes predominate. Thin (2-13 cm thick) dull to coaly shale intervals are correlated across the onshore basin for more than 45 km and represent regional intervals of elevated base-level. Distinct fusain layers are common and represent the remains of ancient wildfires.

6. The Backpit peat accumulated in a relatively planar rheotrophic mire based on the following petrographic evidence:

a. the seam contains a high proportion of detrital mineral

matter, especially near the top.

- b. "dry" dull intervals characteristic of mire desiccation are absent; dull to coaly shale lithotypes contain abundant detrital macerals and/or minerals indicative of subaquatic deposition.
- c. high pyrite content in the coal suggests moderate pH conditions suitable for the activity of sulphate-reducing bacteria; domed mires are typically acidic and low in sulphur.
- d. a high proportion of vitrinite and vitrinite-rich microlithotypes in the seam suggest arborescent vegetation predominated.

7. Assemblages of agglutinated foraminifera found above and below the seam (W. Wightman, pers. comm., 1992) indicate a coastal or paralic setting for the mire, however, the presence of fresh to brackish water fauna in associated roof strata (bivalves, ostracods, sharks, other fish and serpulids) and the paucity of typical open marine fauna, suggests marginal or restricted marine conditions.

8. Additional data to support a coastal setting for the Backpit mire include:

- a. the elongate form of the mire, parallel to depositional strike.
- b. total sulphur is high in the seam, especially near the roof. The distribution of microscopic pyrite supports this trend.
- c. the seam preserves no evidence of fluvial interaction (i.e. major seam splits) and clastic input was the result of regional base-level rises, probably related to relative sea-level rise (e.g. seam interval III).
- d. vertical coal facies trends suggest a progressively wetting upward environment of peat accumulation in the upper portion of the seam typical of recent mires in a

transgressive setting.

9. The Backpit roof unit (BRU) is a thin limestone/shale unit deposited in a laterally extensive embayment during maximum flooding of the Backpit mire, when clastic input was minimal. The embayment progressed from oxygenated conditions, supporting a diversity of fauna directly above the peat, to a more restricted environment with dysaerobic to anaerobic bottom waters. This relatively shallow body of water was eventually filled in by a coarsening upward sequence of prodelta, delta front and delta deposits.

10. The BRU is one of numerous organic-rich limestone/shale units within the SMF that show good to very good source rock potential. Organic matter in the BRU is predominantly terrestrially-derived type II to II/III kerogen and TOC content averages approximately 3.7 % by weight. The occurrence of these units associated with stacked coal seams within the 'oil window' make the basin a potential target for coal-bed methane exploration.

PLATE 1

- 1a. Incised channel cutting through floodplain soils and splays; Bras d'Or section (A). Metre stick for scale.
- 1b. Pebbly channel lag at the base of a channel, Longbeach section (J); abundant quartz pebbles and lithic fragments. Hammer head is 18 cm long.
- 1c. View of large-scale trough cross-beds looking down axis in the direction of paleoflow (80° E); channel directly above the Backpit seam, Glace Bay West (E). Metre stick for scale.
- 1d. Planar cross bed sets in a channel sandstone from Sydney Mines (B); note the erosive contacts between sets. Hammer is 33 cm long.

PLATE 1



PLATE 2

- 2a. Primary current lineations on multiple bed surfaces from a sandstone channel, Longbeach (J). Lineations oriented north-south. Hammer head is 18 cm wide.
- 2b. Sinuous crested ripples on an exposed bedding plane in the upper portion of a sandstone channel deposit, Victoria Mines (C). Paleowind to the north. Markings on hammer handle are 3 cm long.
- 2c. Mudcracks in a coarsening upward interbedded sandstone/siltstone deltaic (?) package, Donkin East (H). May represent an emerged delta top. Lens cover is 7 cm in diameter.
- 2d. Well developed siderite bands and nodules in a fine-grained sandy lacustrine deposit, Glace Bay West (E). There is no evidence for root activity in this unit. Markings on metre stick are 10 cm long.

PLATE 2

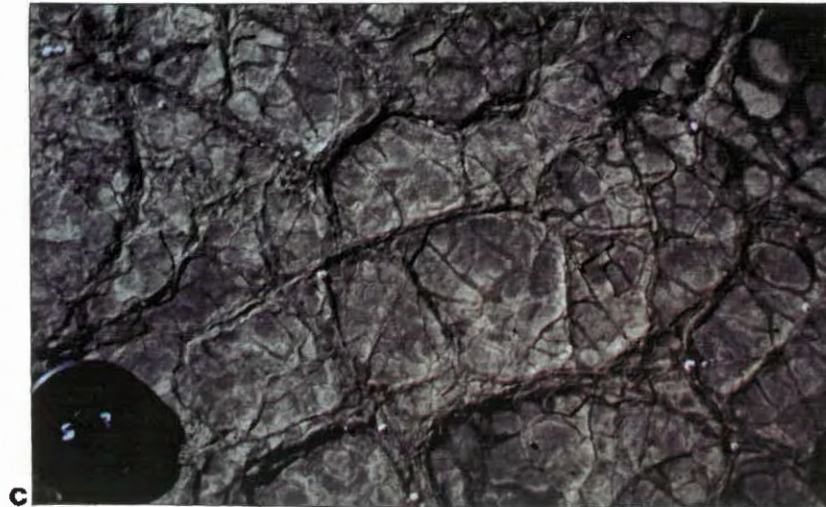


PLATE 3

- 3a. Mottled red-green/grey soil horizon, Donkin East (H). Note the whitish calcareous rhizoconcretions (Rh). Metre stick for scale.
- 3b. "Duricrusted" calcareous paleosol horizon forms a resistant wave cut platform, Glace Bay West (E). The unit contains abundant calcareous root concretions.
- 3c. Cross-section view of a similar paleosol horizon, Donkin East (H). Roots extend downward into underlying rippled channel top. Hammer is 33 cm long.
- 3d. Photomicrograph of rootlets from a calcareous paleosol, Bras d'Or (A). Rootlet is filled with spary calcite and surrounded by ankerite (?); matrix is also impregnated with calcite.

PLATE 3

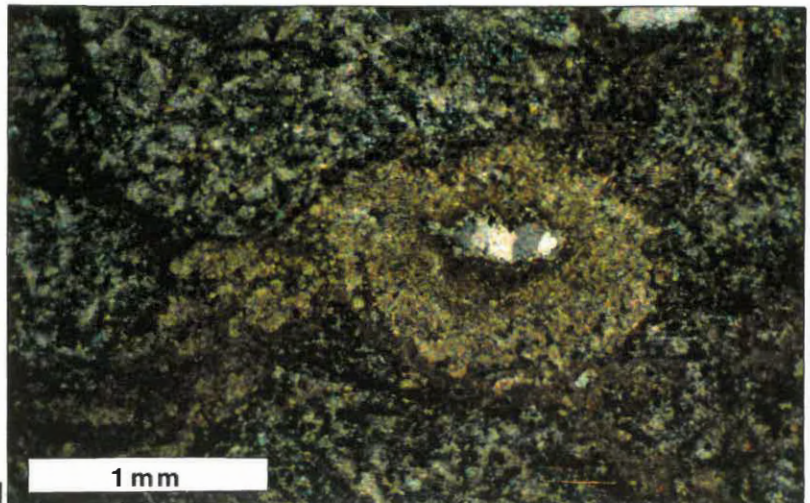


PLATE 4

- 4a. The Backpit seam (BP) in cliffs at Bras d'Or (A). The seam is approximately 1 m thick at this location. Note the sulphate and iron stains on the weathered seam face. The Backpit roof unit (BRU) is resistant to weathering and protrudes from the cliff.
- 4b. The Backpit seam (BP) in a moderately dipping outcrop at Victoria Mines (section C). The Backpit roof unit (BRU) is succeeded by a coarsening upward, planar bedded deltaic package (D) that locally exhibits slumped bedding. Metre stick for scale.
- 4c. An erosive channel base that abruptly cuts into the Backpit roof unit (BRU) at Glace Bay West (E). This channel did not erode down to the coal in the area examined. The coal/roof contact is near the base of the photo. Metre stick for scale.
- 4d. Plan view of a bedding plane surface of the Backpit seam (BP) illustrating randomly oriented fusain (Fu) patches. Pencil is 18 cm long.

PLATE 4

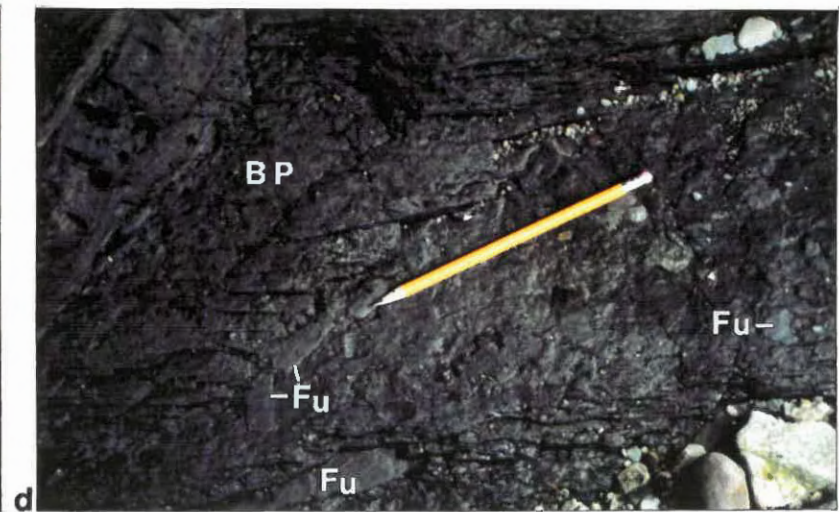
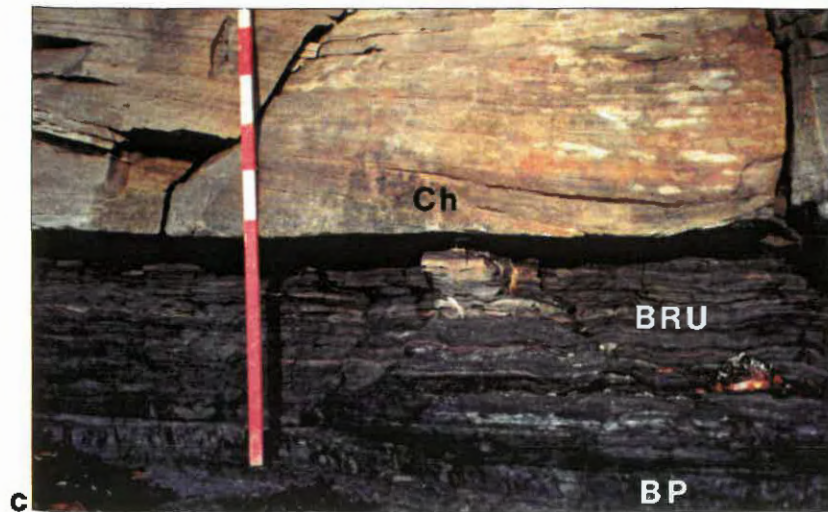
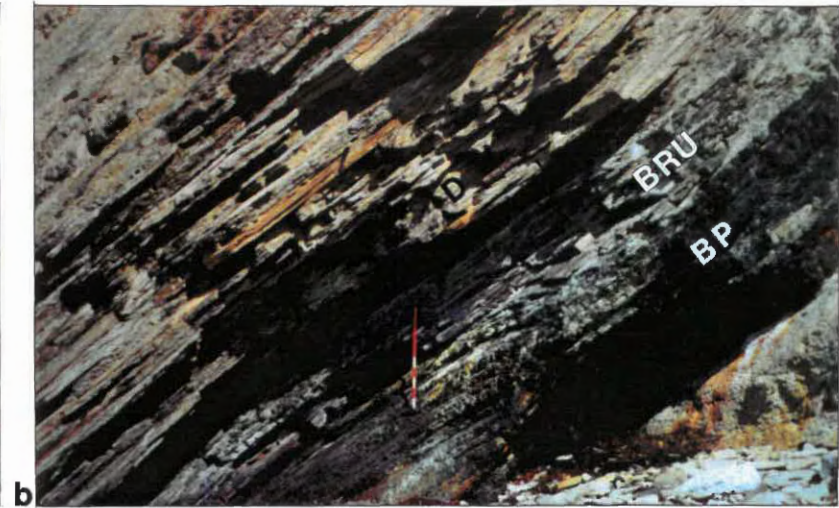


PLATE 5

Photomicrographs taken from polished blocks of the Backpit seam section, Glace Bay West (E), using a reflected light microscope and white light. Fluorescent light was used for photomicrograph 5d. Scale bar for all photomicrographs is in the upper right corner of 5a.

- 5a. Abrupt contact between spore-rich clarite and vitrite. TC-telocollinite; DC-desmocollinite; CSp-crassispornite; TSp-tenuisporinite; Id-inertodetrinite.
- 5b. Secretion sclerotinite (Sc) in a desmocollinite (DC) matrix. Numerous draped tenuisporites (TSp) suggest that the body was inert (resistant) prior to compaction. Py-pyrite grain; Id-inertodetrinite.
- 5c. Slightly flattened resin body (Re) with pyrite-filled central vesicles. Numerous spores (TSp), liptodetrinite (Ld), and inertodetrinite (Id) surround the body in a desmocollinite matrix (DC).
- 5d. Same view as 5c under fluorescent light. Note the highly fluorescing resin body (Re) compared with the weaker fluorescing sporinite (TSp).
- 5e. Carbargilite with abundant fine-grained detrital clays (Cl), inertodetrinite (Id), spores (TSp), semimacrinite (SM), and finely disseminated pyrite crystals (Py) in a desmocollinite matrix (DC).
- 5f. Highly reflecting pyrofusain (Fu) with well preserved cell wall structure. Note the "bogen" texture in the lower right corner of the photomicrograph. Cell lumens are empty.

PLATE 5

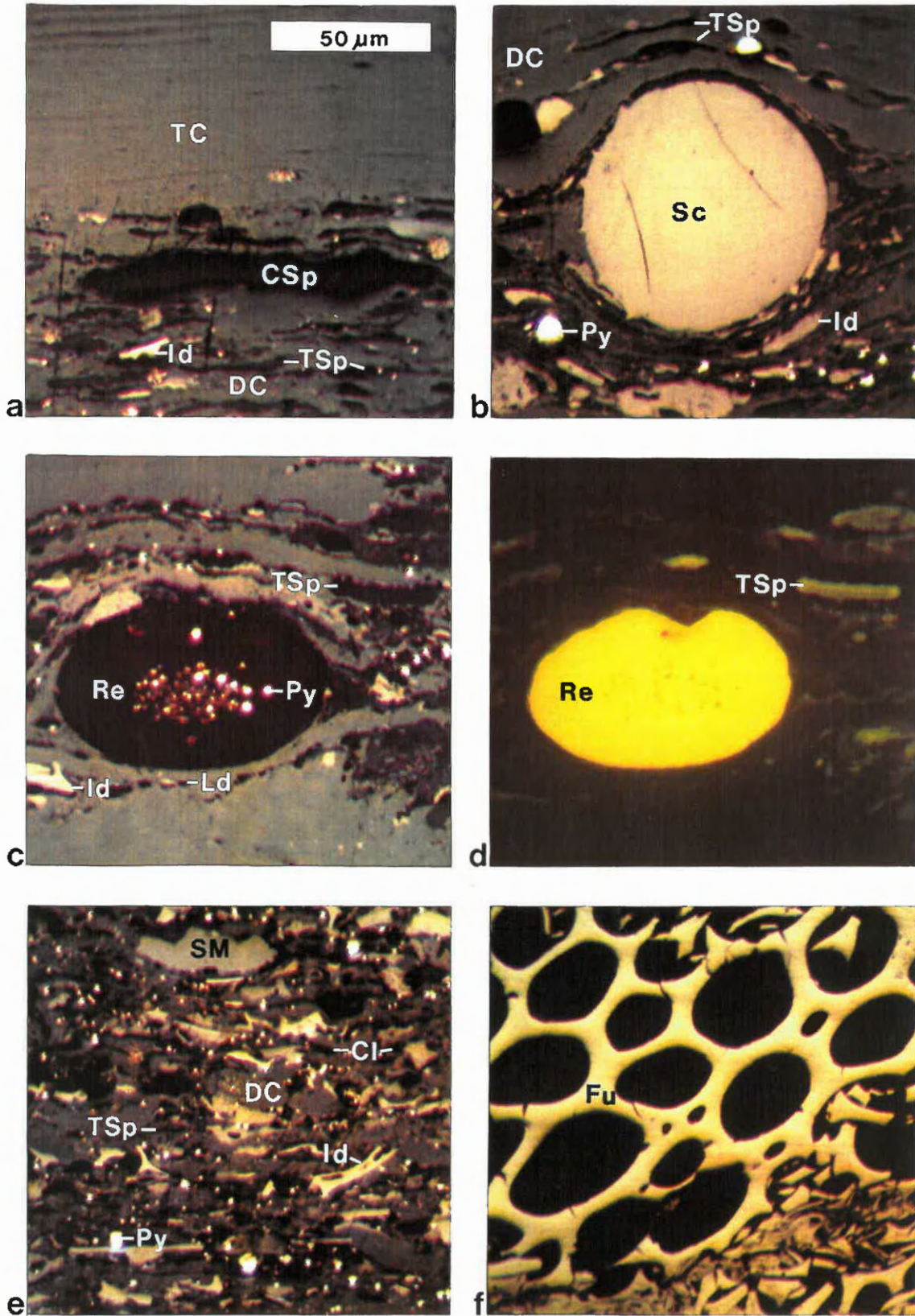
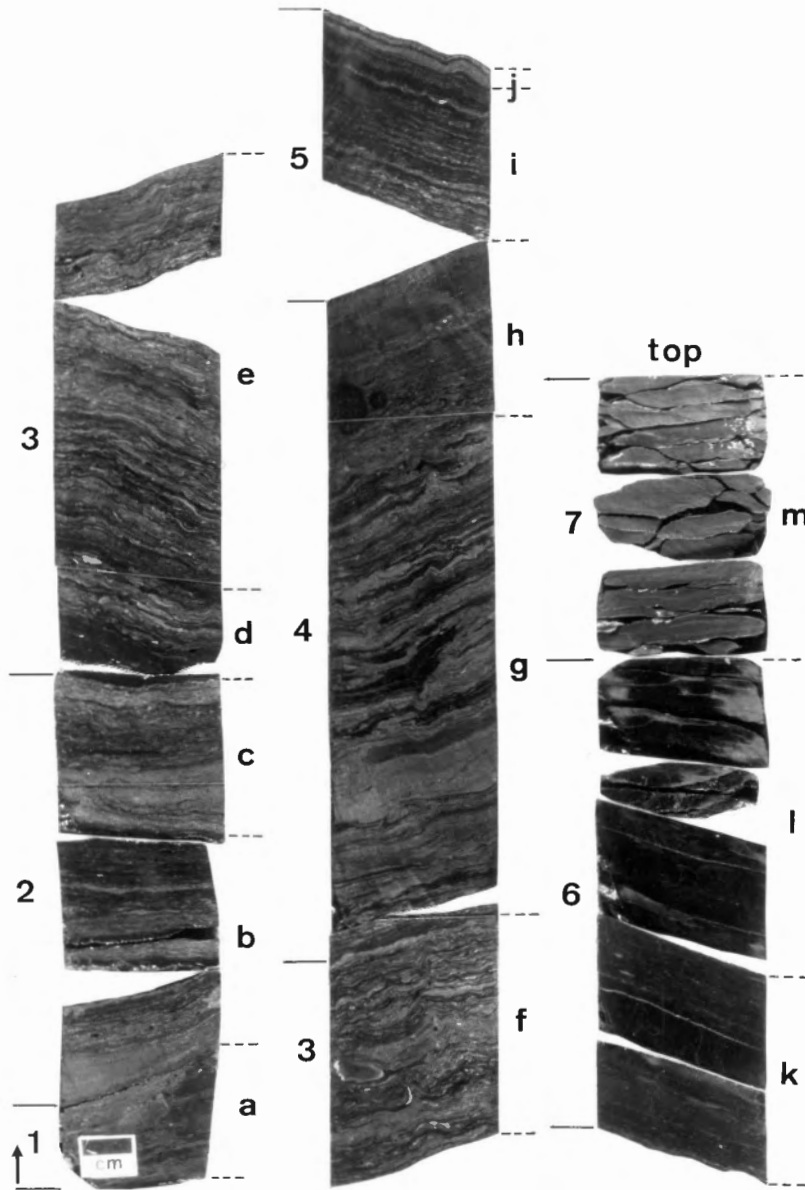
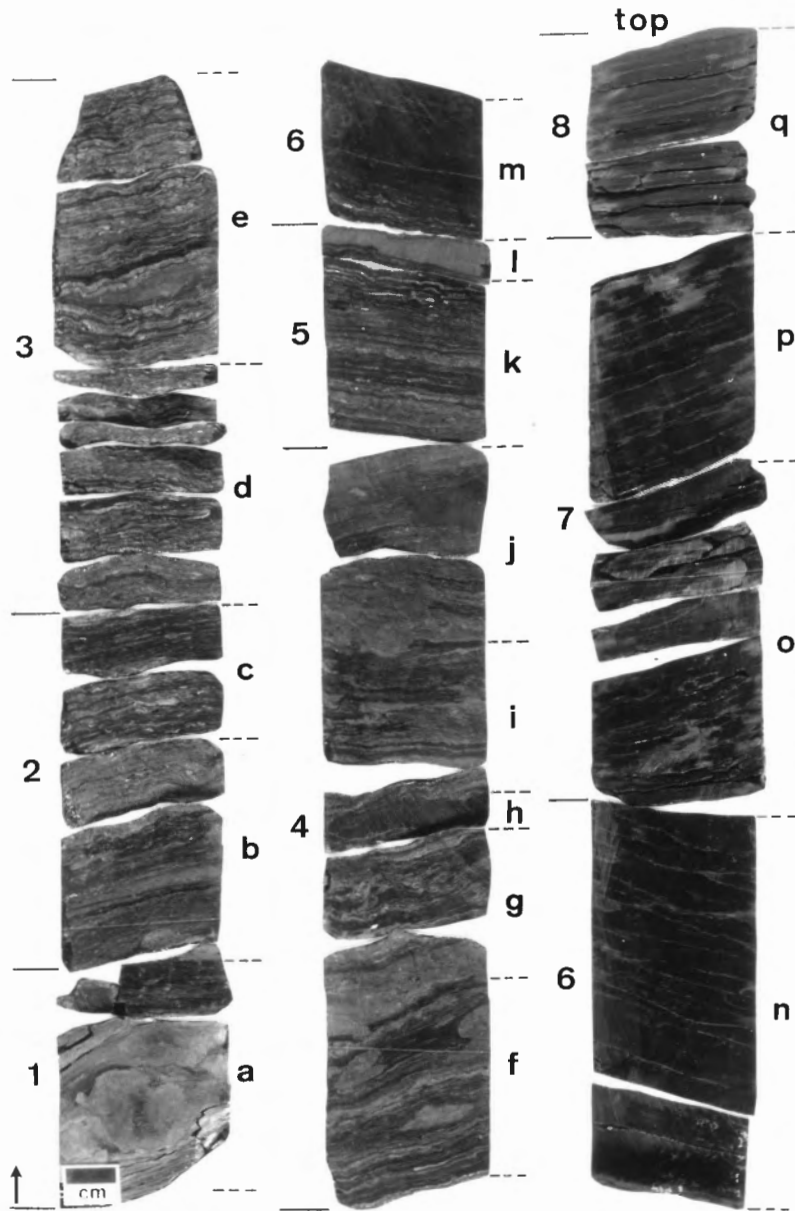


PLATE 6



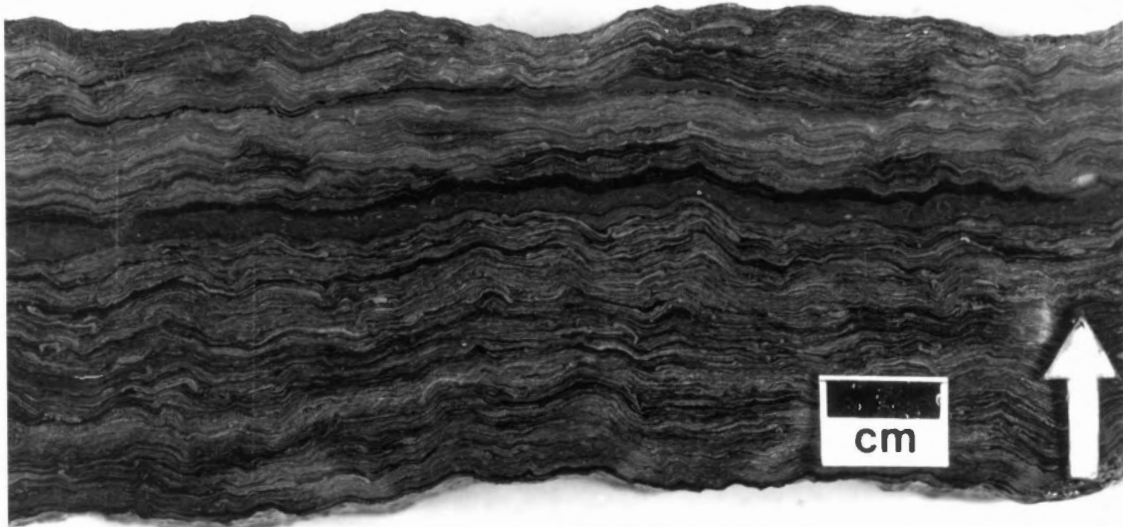
Slabbed section of BRU from offshore core C-136. Numbers represent sampling intervals for ash and sulphur; letters represent sampling intervals for Rock-Eval pyrolysis. Note: the siderite band (j) correlates with (l), Plate 7.

PLATE 7



Slabbed section of BRU from offshore core C-137. Numbers represent sampling intervals for ash and sulphur; letters represent sampling intervals for Rock-Eval pyrolysis. Note: the siderite band (l) correlates with (j). Plate 6.

PLATE 8



a



b

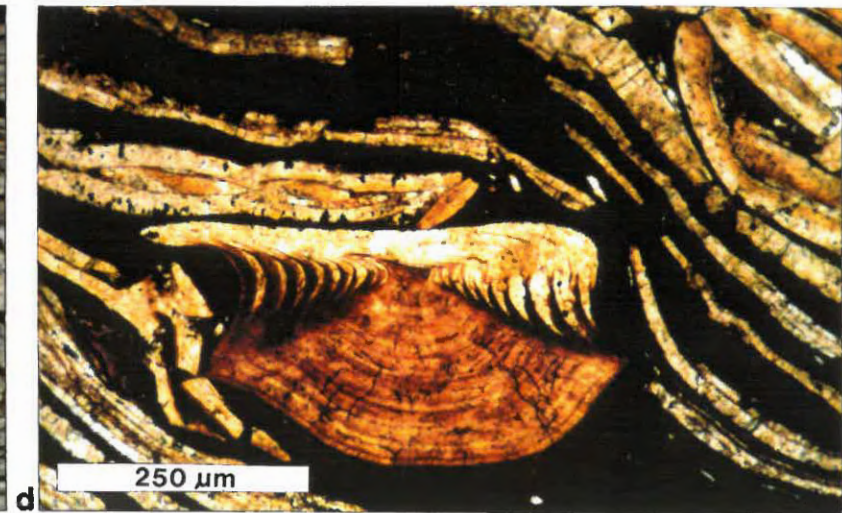
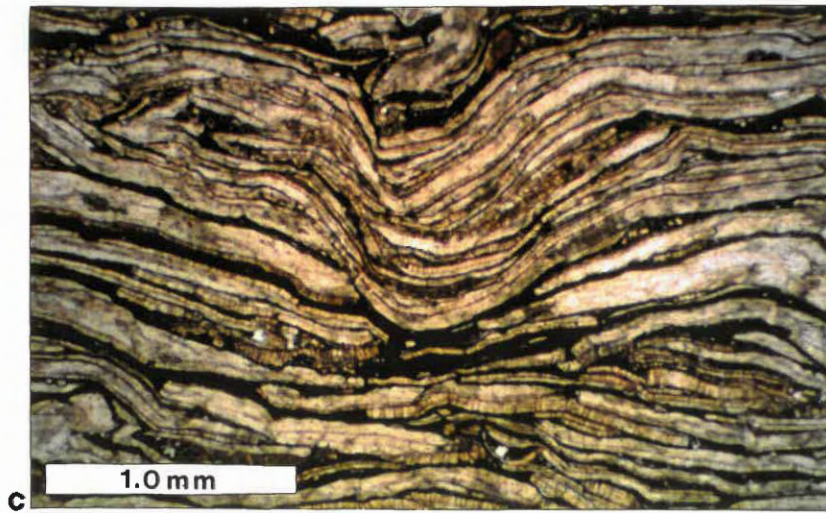
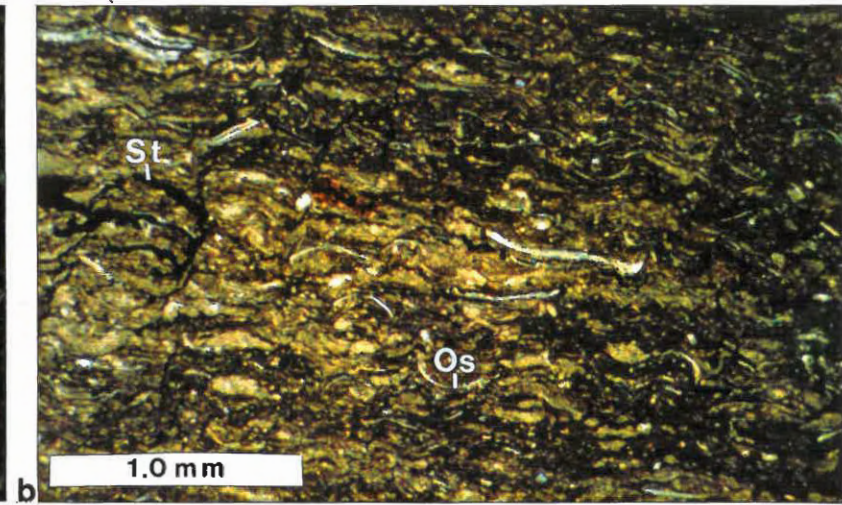
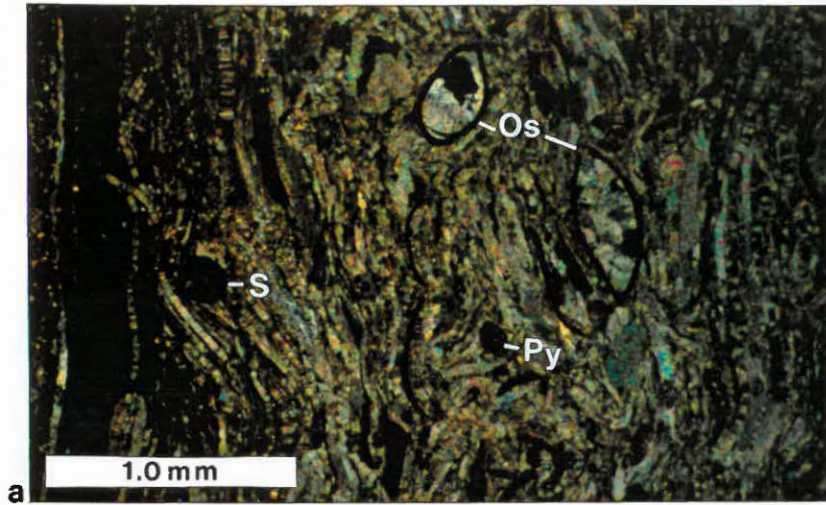
- a. Slab of crenulated carbonate facies (Cc) from the BRU, with abundant bivalve shell layers in an organic-rich matrix (A-Bras d'Or section).
- b. Bedding plane surface of BRU with Anthraconauta phillipsii impression, long axis - 2 cm. Specimen painted with enamel for contrast.

PLATE 9

Photomicrographs taken from thin sections of the Backpit roof unit (BRU), cut perpendicular to bedding.

- 9a. Detrital carbonate facies (Cd) near the base of core C-136. Note articulated ostracods (Os) filled with sparry calcite, shell walls replaced by pyrite; phosphatic spine ? (S); and pyrite framboid (Py). Cross-polarized light.
- 9b. Massive carbonate facies (Cm) in core C-136 with numerous disarticulated ostracod valves (Os) in a micritic matrix with abundant organic wisps. Note stylolites (St). Plane-polarized light.
- 9c. Crenulated carbonate facies (Cc) in core C-137 consisting predominately of bivalve shells. Plane-polarized light.
- 9d. Transitional shale facies (St) in core C-136 with elasmobranch dermal denticle and bivalve fragments in an organic-rich matrix (black). Plane-polarized light.

PLATE 9



APPENDIX 1

Sedimentology -
Field Measurements and Core Description

A1. Contents

Page

A1.1. Data Collection	153
-----------------------------	-----

List of Figures

Figure A1.1. Location map of the coastal and core sections outlining four expanded areas in Figure A1.2.	154
Figure A1.2. Detailed maps of measured sections:	
a. Bras d'Or and core NC-87-1.	155
b. Sydney Mines, Victoria Mines and core SMS-91-29B.	155
c. New Waterford, Glace Bay West and cores C-136 and C-137.	156
d. Donkin West, Donkin East and Longbeach.	156

List of Tables

Table A1.1. Field/core checklist.	157
--	-----

A1.1. Data Collection

Eight coastal sections were measured in detail from the top of the Phalen seam or organic-rich roof unit to a short distance above the Backpit roof unit. At some locations, field measurements were extended upward to the lower leaf of the Bouthillier seam (Fig. 2.1, enclosure). Three cores were also measured: SMS-92-29B, drilled near Big Pond by the Nova Scotia Department of Natural Resources and two cores drilled into the roof of the Phalen Mine, by the Cape Breton Development Corporation. A fourth core from New Campbellton (NC-87-1), logged by Mr. Don MacNeil, NSDNR, was included in the compilation. The measured sections extend across the onshore and nearshore portion of the basin, parallel to depositional strike, for more than 45 km, as outlined in Figures A1.1 and A1.2.

Each section was divided into sedimentary units and the characteristics of each unit was recorded as outlined in Table A1.1. Special attention was paid to documenting lateral facies changes and unit contacts at outcrop scale. Cores preserved the sedimentary features of the fine units including mudstone and underclay that are generally rubbly and nondescript at outcrop locations. Each unit was tested with HCl acid, including the matrix and any nodules present. Sedimentary logs were drawn at 1:100 scale (Fig 2.1, enclosure). Samples were collected from typical lithologies and slabbed for further study. Organic-rich lithofacies, including coals and limestone/shale units were sampled in detail and sample collection and processing is described in Appendix 2 and 3, respectively.

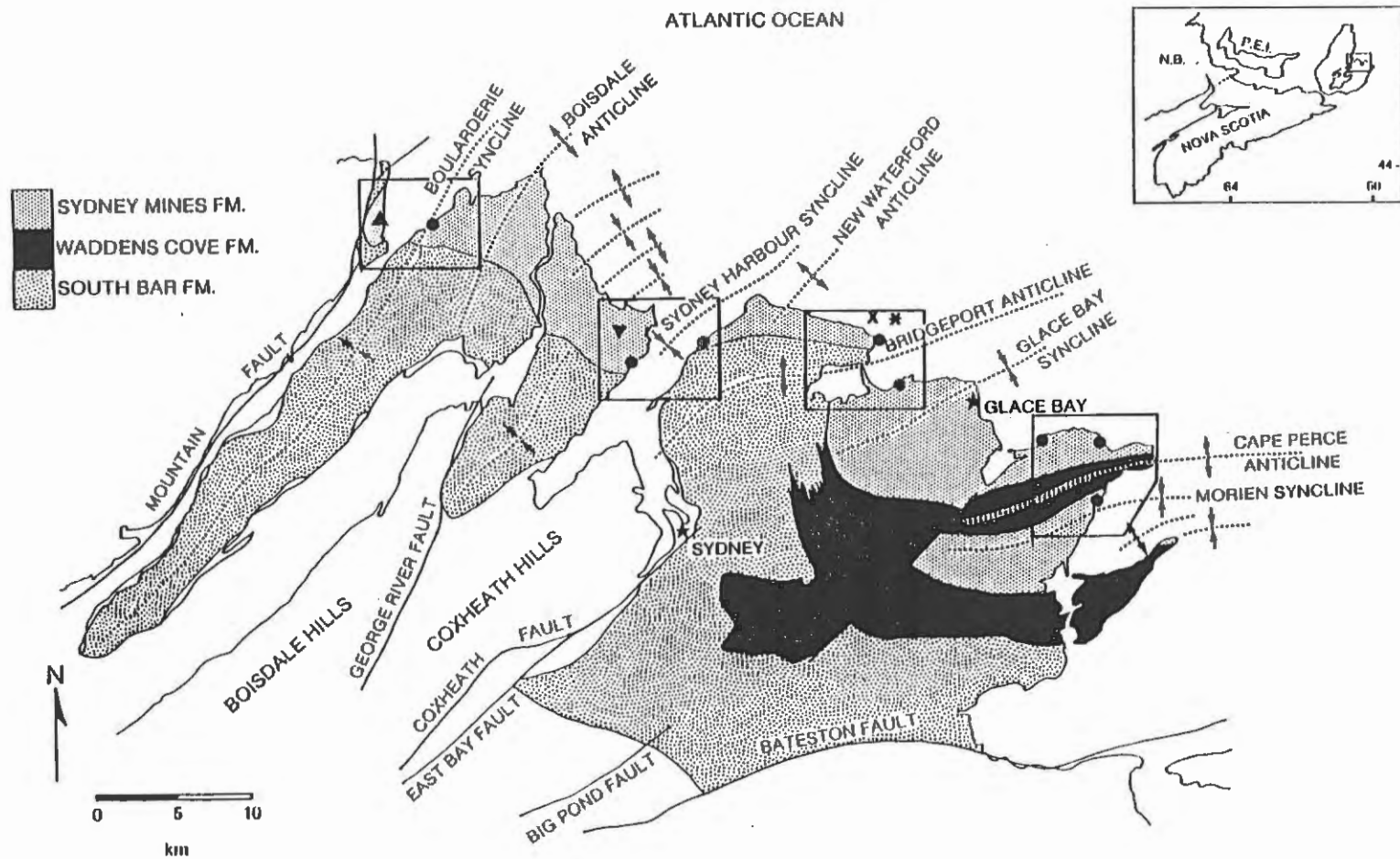


Figure A1.1. Location map of the coastal and core sections outlining four expanded areas in Figure A1.2.

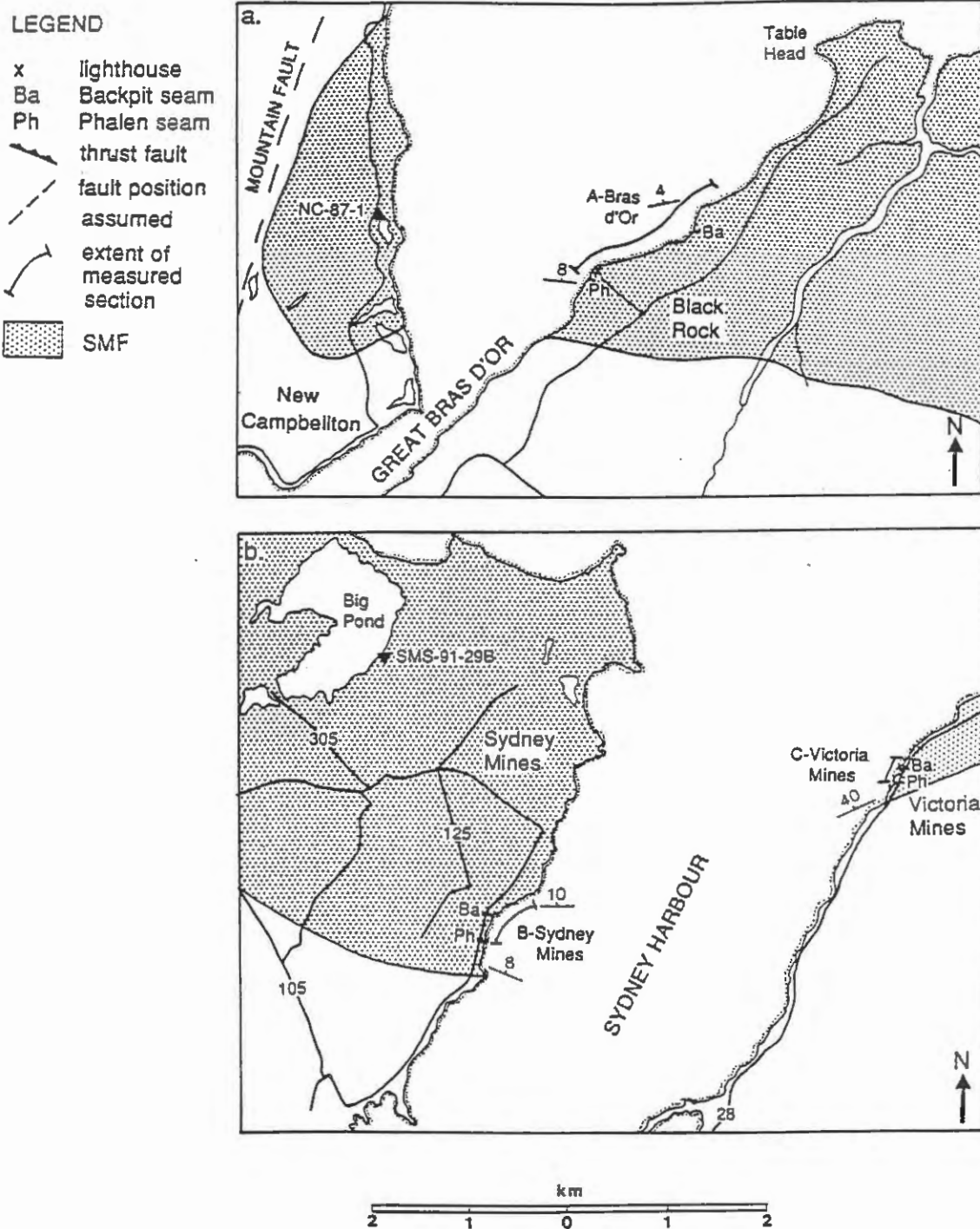


Figure A1.2. Detailed map of measured sections: a. Bras d'Or and core NC-87-1, b. Sydney Mines, Victoria Mines and core SMS-91-29B, c. New Waterford, Glace Bay West and cores C-136 and C-137 and d. Donkin West, Donkin East and Longbeach.

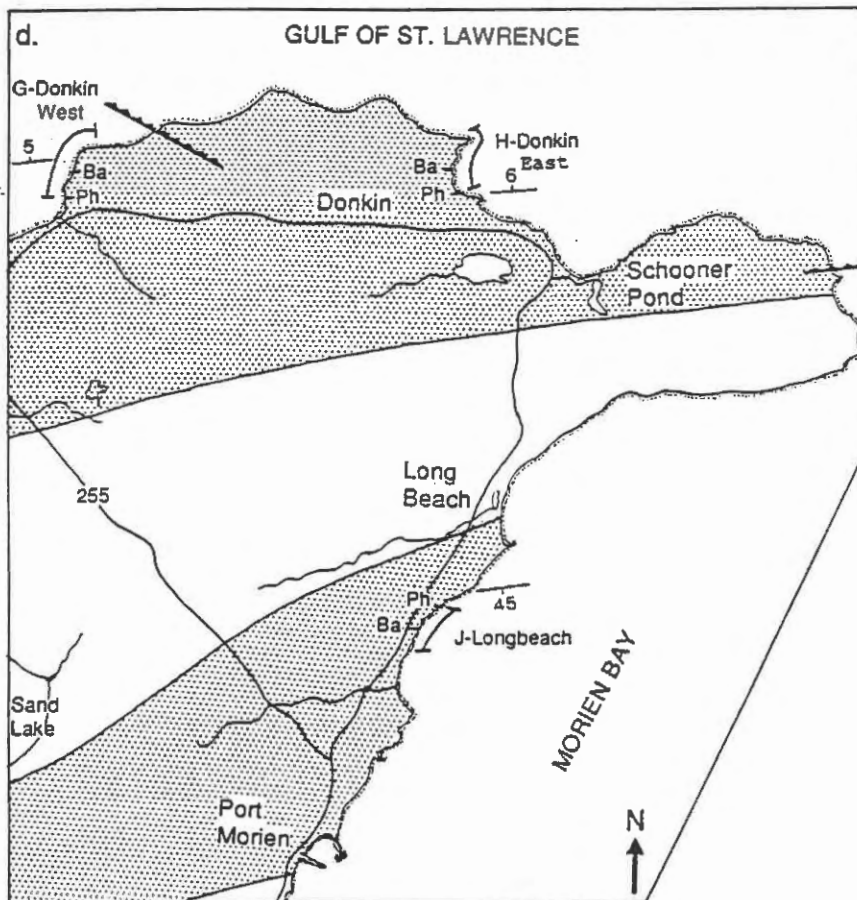
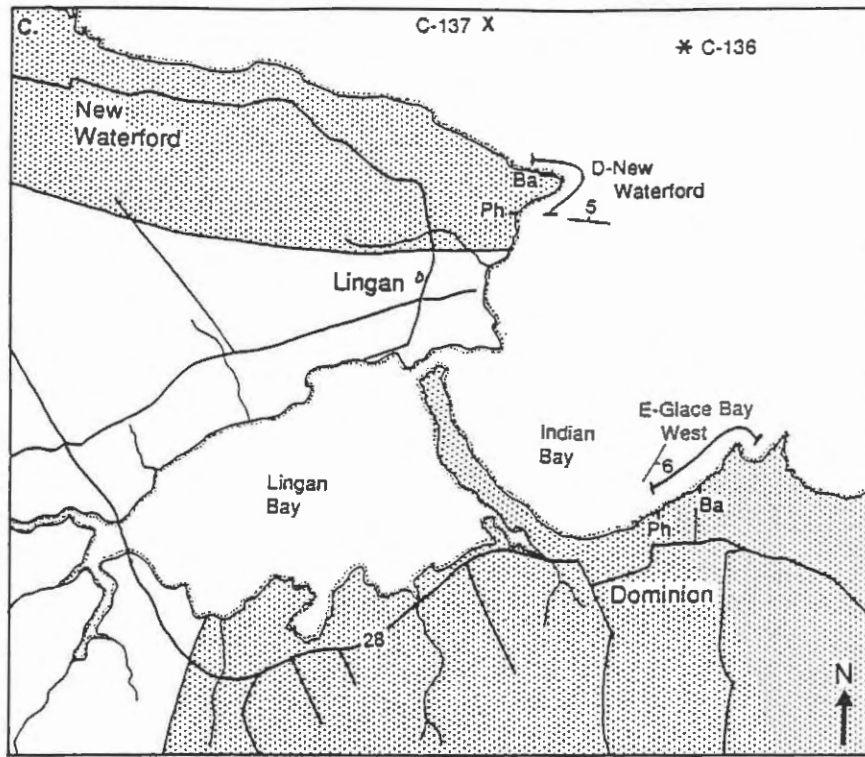


Figure A1.2. (con't)

Table A1.1. Field/core checklist.

Section: _____ Unit No: _____ Date: _____

Sample No: _____ Photo No: _____

Thickness: _____ Base: _____ Top: _____

Lithology: _____

Basal Contact: _____ Strike/Dip: _____

Grain Size: _____ Sorting: _____ Matrix: _____

Colour-fresh: _____ -weathered: _____

Bed Thickness/Style:

Sedimentary Structures:

Paleocurrent: _____

Concretions: _____

Organic Content: _____

Calcareous-matrix: _____ -concretions: _____

Depositional Environment?

APPENDIX 2

Backpit Coal -
Sample Collection and Analysis

A2. Contents	Page
A2.1. Coal Sample Collection	162
A2.2. Coal Quality Assessment	162
A2.3. Lithotype Characterization	164
A2.4. Microscopy	
A2.4.1. Sample Preparation	165
A2.4.2. Image Analysis - Automated Microscopy.....	165
A2.4.3. Manual Microscopy	166
A2.4.4. Coal Composition - Data Manipulation	170
A2.4.5. Comparison of Automated and Manual Microscopy	172
A2.4.6. Vitrinite Reflectance Measurements	175

List of Figures

Figure A2.1. Flow chart for coal sample analyses.	163
Figure A2.2. Petrographic analysis of coal blocks; a) IBAS-2; b) manual microscopy.	167
Figure A2.3. Stacked bar profile produced from IBAS data.	168
Figure A2.4. Petrographic analysis of coal pellets; a) IBAS-2; b) manual microscopy.	169

List of Tables

Table A2.1. Ash and sulphur analysis.	
1a. Backpit seam, roof and floor rocks	177
1b. Minor coal seams	179
1c. Summary of average data	180
Table A2.2. Duplicate ash and sulphur analyses.	180
Table A2.3. Grey-level regions established for automated image analysis of each seam section	181
Table A2.4. Vitrinite reflectance measurements for selected samples.	
4a. Manual vitrinite reflectance measurements (random)	181
4b. Mean vitrinite reflectance values using manual and IBAS automatic measuring techniques	182

Table A2.5. Group maceral composition of lithotypes, Sydney Mines seam section (B); compiled from IBAS image analysis data.	185
Table A2.6. Compositional summary of lithotypes, Sydney Mines seam section - compiled from IBAS image analysis data.	
6a. bright	187
6b. bright banded	187
6c. banded	188
6d. dull banded	188
6e. dull	189
6f. fusain	189
6g. weighted average of all lithotypes	190
6h. seam intervals	190
Table A2.7. Group maceral composition of lithotypes, Victoria Mines seam section (C); compiled from IBAS image analysis data.	192
Table A2.8. Compositional summary of lithotypes, Victoria Mines seam section - compiled from IBAS image analysis data.	
8a. bright banded	194
8b. banded	194
8c. dull banded	195
8d. dull	195
8e. fusain	196
8f. coaly shale, pyrite	196
8g. weighted average of all lithotypes	197
8h. seam intervals	197
Table A2.9. Group maceral composition of lithotypes, Glance Bay W seam section (E); compiled from IBAS image analysis data.	199
Table A2.10. Compositional summary of lithotypes, Glance Bay W seam section - compiled from IBAS image analysis data.	
10a. bright banded	201
10b. banded	201
10c. dull banded	202
10d. dull	202
10e. fusain	203
10f. coaly shale, pyrite	203
10g. weighted average of all lithotypes	204
10h. seam intervals	204

Table A2.11. Detailed maceral analysis, Glace Bay W seam section (E'); compiled from manual data.	
11a. vitrinite group	207
11b. liptinite group	209
11c. inertinite group	211
11d. mineral matter	213
Table A2.12. Group maceral composition of lithotypes, Glace Bay W seam section (E'); compiled from manual data.	215
Table A2.13. Compositional summary of lithotypes, Glace Bay W seam section - compiled from manual data.	
13a. bright banded	217
13b. banded	217
13c. dull banded	218
13d. dull	218
13e. fusain	219
13f. coaly shale, pyrite	219
13g. weighted average of all lithotypes	220
13h. seam intervals	220
Table A2.14. Summary of lithotype composition for each seam section.	221
Table A2.15. Microlithotype composition of lithotypes, Glace Bay W seam section - compiled from manual data.	
15a. mono, bi, tri microlithotypes	224
15b. carbominerite, mineral matter	226
Table A2.16. Microlithotype summary of lithotypes, Glace Bay W seam section - compiled from manual data.	
16a. bright banded	228
16b. banded	229
16c. dull banded	230
16d. dull	231
16e. fusain	232
16f. coaly shale, pyrite	234
16g. weighted average of all lithotypes	235

A2.1. Coal Sample Collection

Coal samples were collected from the Backpit seam at five coastal locations (Fig. 1.2 in text), as follows:

- A. Bras d'Or
- B. Sydney Mines
- C. Victoria Mines
- E. Glace Bay West
- G. Donkin West

The Backpit seam was fully exposed at most sites, however the base of the seam required excavation in the Sydney Mines and Glace Bay West sections. Wherever possible, consecutive oriented samples were collected, representing the total thickness of the seam. The friable nature of the coal and the abundance of fusain lenses made it impossible to extract intact samples from some seam intervals and unoriented samples (i.e. channel samples - chipped pieces of coal, collected to represent a specified interval in the seam) were collected in their place. Detailed study, including manual and automated microscopy was completed on these samples as outlined in '1', Figure A2.1. In addition, the seam was divided into larger "bulk" intervals from 2 to 33 cm thick. Shaley partings were logged as separate intervals. Channel samples were collected from each of these divisions for more routine coal quality tests as outlined in '2', Figure A2.1.

Whole seam channel samples were collected from minor coal seams located between the Backpit and Phalen seams. These seam samples were also analysed as in 'B', Figure A2.1.

A2.2. Coal Quality Assessment

Variation in coal quality of the Backpit seam was determined from the analysis of bulk channel samples for ash and sulphur ('2' in Fig. A2.1). Roof and floor rocks were also analysed for comparison. In addition to outcrop

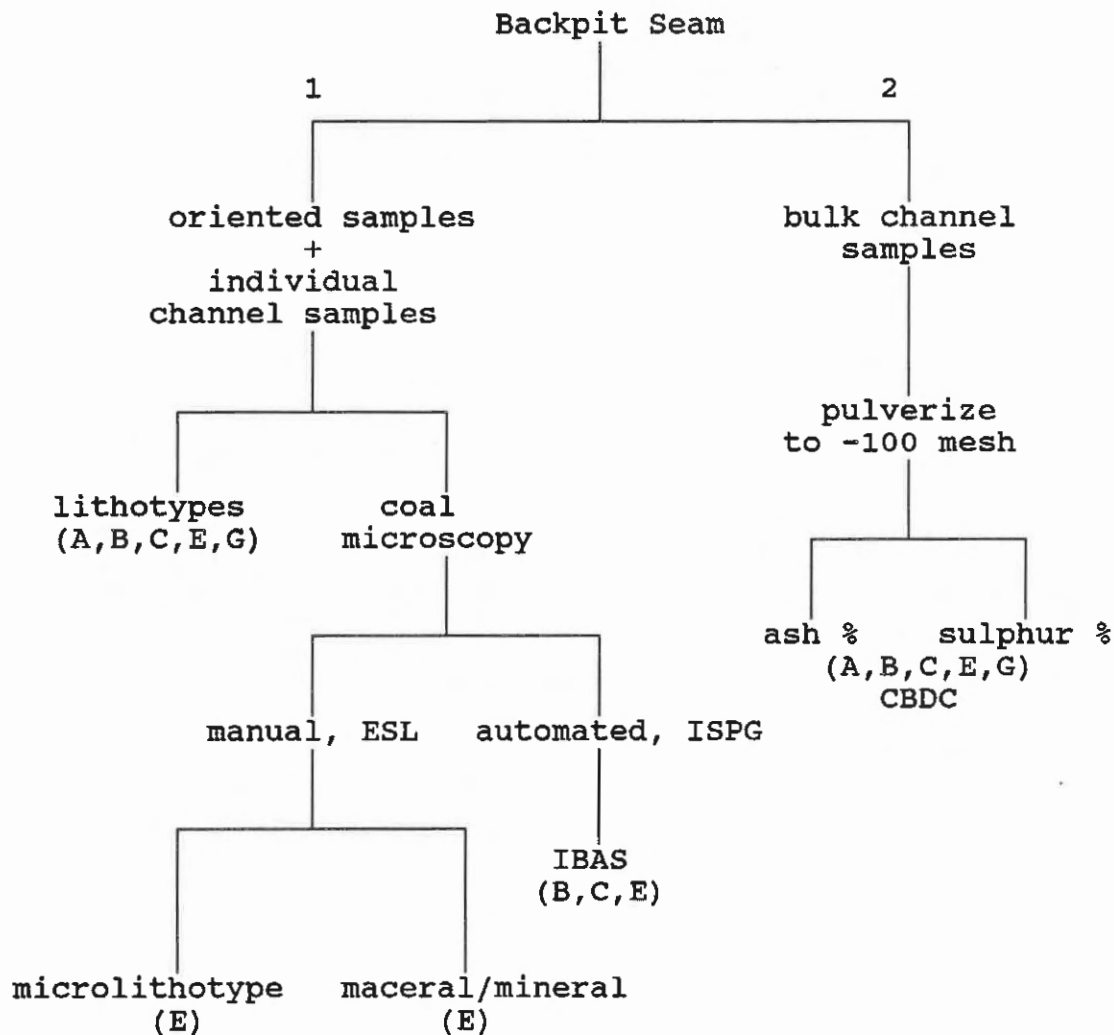


Figure A2.1. Flow chart for coal sample analysis. A-Bras d'Or; B-Sydney Mines; C-Victoria Mines; E-Glace Bay W; G-Donkin W; ESL-Environmental Services Laboratory; ISPG-Institute of Sedimentary and Petroleum Geology; CBDC-Cape Breton Development Corporation.

samples, splits were analysed from the roof section in two Cape Breton Development Corporation (CBDC) cores (C136, C137, Plates 6 and 7). Minor seams were also analysed. Results for the Backpit seam and associated strata from each sample location are found in Table A2.1a and A2.1b summarised in Table A2.1c and Figure 3.3 in the text.

The bulk samples were pulverized to -100 mesh (-15 μm) and submitted to the Coal Laboratory, Cape Breton Development Corporation, Sydney, Nova Scotia, for ash and sulphur analyses. Ash analyses were completed using a Leco - Mac 400 analyser. One gram of sample was heated to a temperature of 750 $^{\circ}\text{C}$ for 4 hours. The percent ash in the sample was calculated as: $[100 - ((\text{residual sample weight} / \text{original sample weight}) * 100)]$. Sulphur analyses were completed using a Leco SC-32 sulphur analyser. One-quarter of a gram of sample was burned in a furnace for 3 minutes at a temperature of 2300 $^{\circ}\text{C}$. The amount of SO_2 gas given off upon combustion was automatically detected and reported by way of a digital read-out. The Coal Laboratory routinely runs standard samples to check the calibration of their instruments. In addition to this check, several unknown duplicates were dispersed among the sample batch and the results are reported in Table A2.2. These analyses were highly reproducible (within 5 %) for both analytical techniques, across a wide range of values.

A2.3. Lithotype Characterization

Lithotype profiles of five coal seam sections were constructed using a modified Australian classification scheme (e.g. Diessel, 1965; Bustin *et al.*, 1983). Macroscopic layers in the coal were classified according to the categories in Table 3.1 (in text). A minimum thickness of 0.5 cm was used to define a lithotype. Exceptions to this minimum thickness were made for fusain bands, pyrite bands and carbonaceous shales due to their environmental

significance.

Vertical profiles were compiled to illustrate the megascopic variations within each seam (Fig. 3.4 in text). These seam divisions established the framework for averaging detailed microscopic data (discussed in Section A2.4.4). Major lithotype intervals were identified, often separated by carbonaceous shales or fusain rich layers.

A2.4. Microscopy

A2.4.1. Sample Preparation

A series of polished blocks were prepared (total = 124) from available oriented coal samples. The samples were split wherever possible to retain a reference sample. The samples were cut perpendicular to bedding, supported in cardboard boxes and embedded in Epofix slow curing epoxy. The sample was trimmed to remove excess cardboard and polished by hand, using three grinding stages and two polishing stages.

Standard coal petrographic pellets were prepared from channel samples collected from friable intervals. A split of each of these samples was crushed to -20 mesh (- 850 μm) in stages to minimize the fines. The sample was placed in a 2.5 cm mould, mixed with epoxy and left to cure overnight. The resultant pellet was then polished using a Buehler automet polisher. This procedure resulted in a fine polished surface suitable for reflected light microscopy.

A2.4.2. Image Analysis - Automated Microscopy

Automated image analysis of polished blocks and pellets was completed at the Institute of Sedimentary and Petroleum Geology (ISPG), Calgary, Alberta. Three seam sections (Sydney Mines, Victoria Mines and Glace Bay West) were analysed using a Zeiss IBAS-2 image analysis system linked with a Bausch television camera and a Zeiss universal microscope. The microscope was calibrated before and after

each analysis with glass standards of known reflectance.

For each seam section, grey-level regions were established from a reflectance histogram measured from one sample in the centre of the seam. The histogram was produced following the procedure outlined in Pratt (1989) for grain mount pellets. Grey-level ranges for the following maceral groups were determined: 1) liptinite, 2) vitrinite, 3) low reflecting inertinite and 4) high reflecting inertinite. Pyrite was also determined (see Table A2.3). An automated stage enabled the analysis of a large number of fields perpendicular to bedding as illustrated in Figure A2.2. Each field represented 0.19 mm^2 and contained a matrix of 512 by 512 pixels. Each pixel was measured for its grey-level value on a scale from 0 (black) to 255 (white), and the data stored in the corresponding grey-level region. The stage automatically moved 0.5 mm laterally (parallel to bedding) and the collection process was repeated. The data measured from four fields in the lateral traverse were combined to obtain an overall composition for that 0.5 mm interval. The stage then moved 0.5 mm vertically and the lateral traverse was repeated in the opposite direction (Fig. A2.2). This procedure automatically continued up the height of the block and resulted in the compilation of a group maceral plot of the block, displayed as a stacked bar profile (Fig. A2.3).

Grain mount pellets were analysed by the IBAS-2 system by a slightly different method. A 12 by 12 grid was set up with a stepping distance of 0.5 mm in both the X and Y directions (Fig. A2.4). A cumulative reflectance histogram was compiled from all fields and grey-level groups calculated, as described in Pratt (1989).

A2.4.3. Manual Microscopy

Manual petrographic analysis of one total seam section (Glance Bay West) was completed for comparison with the

Coal Block

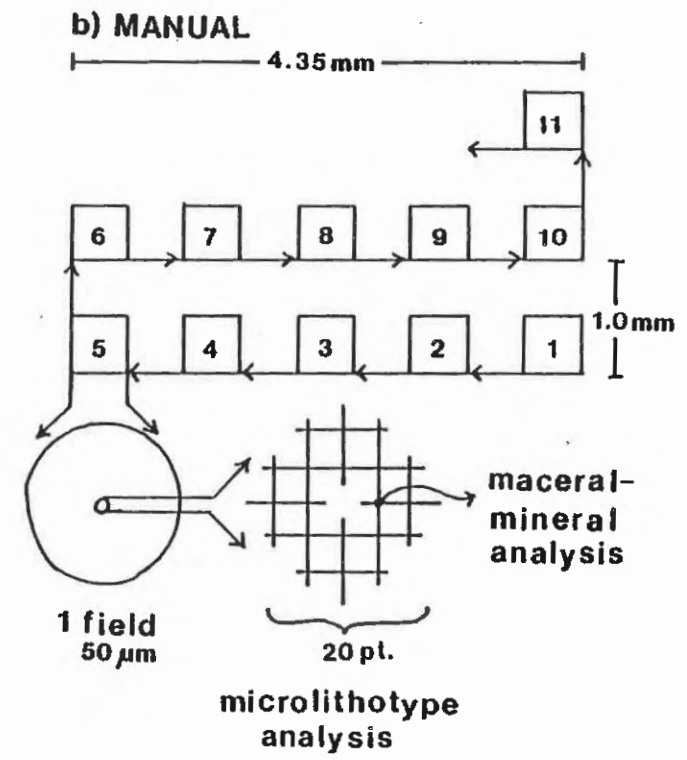
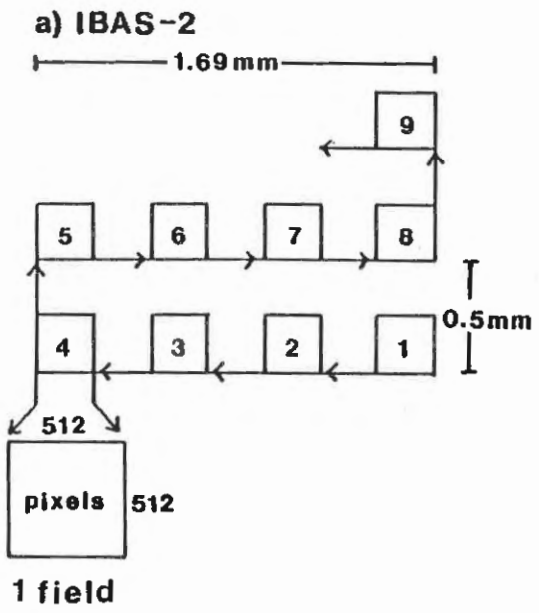
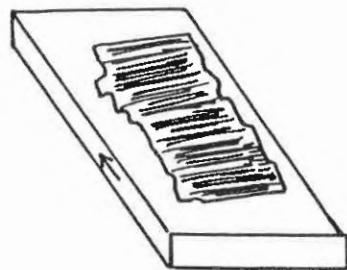


Figure A2.2. Petrographic analysis of coal blocks: a) IBAS-2; b) manual microscopy.

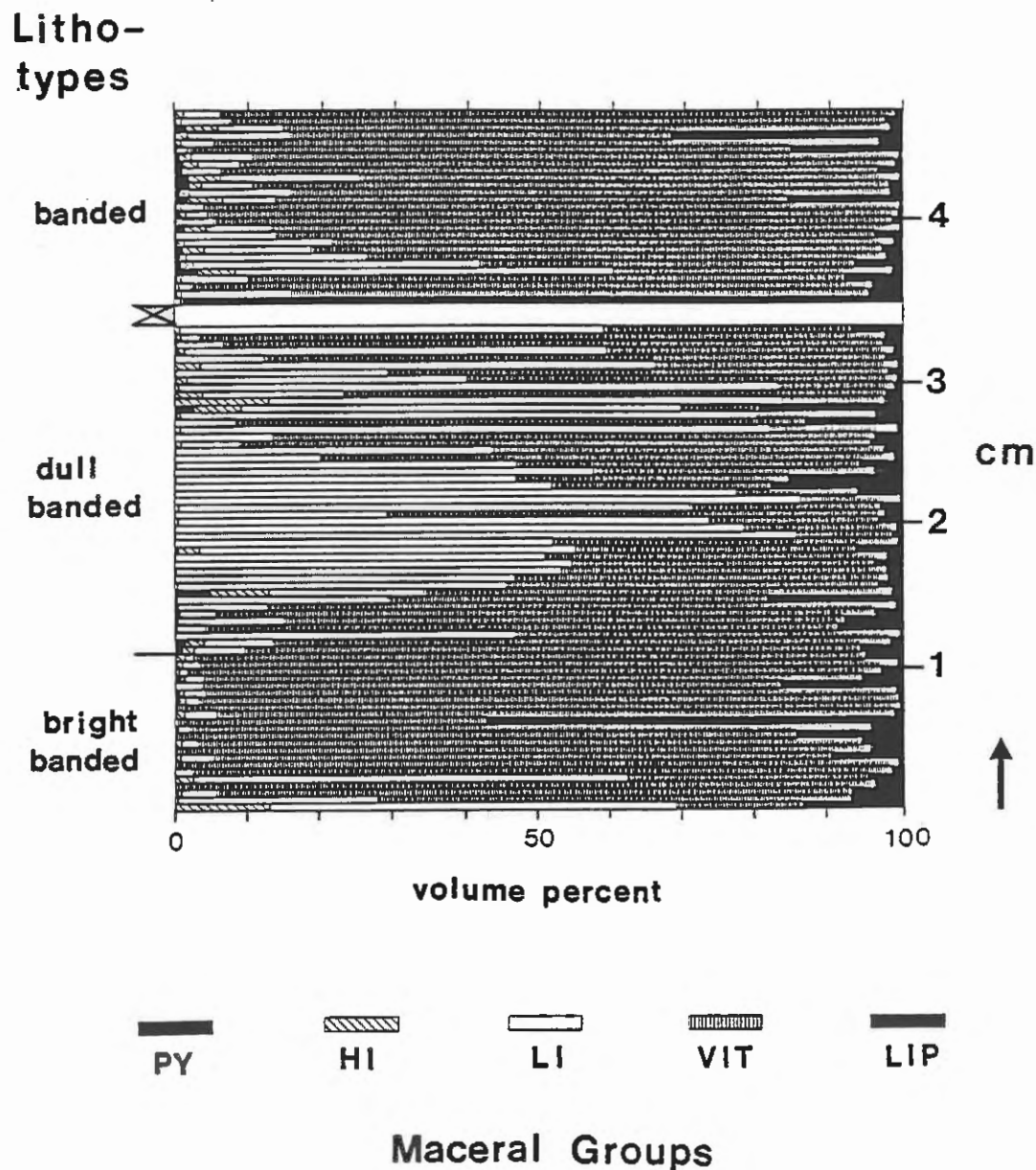


Figure A2.3. Stacked-bar profile produced from IBAS-2 data. PY - pyrite; HI - high reflecting inertinite; LI - low reflecting inertinite; VIT - vitrinite; LIP - liptinite.

Coal Pellet

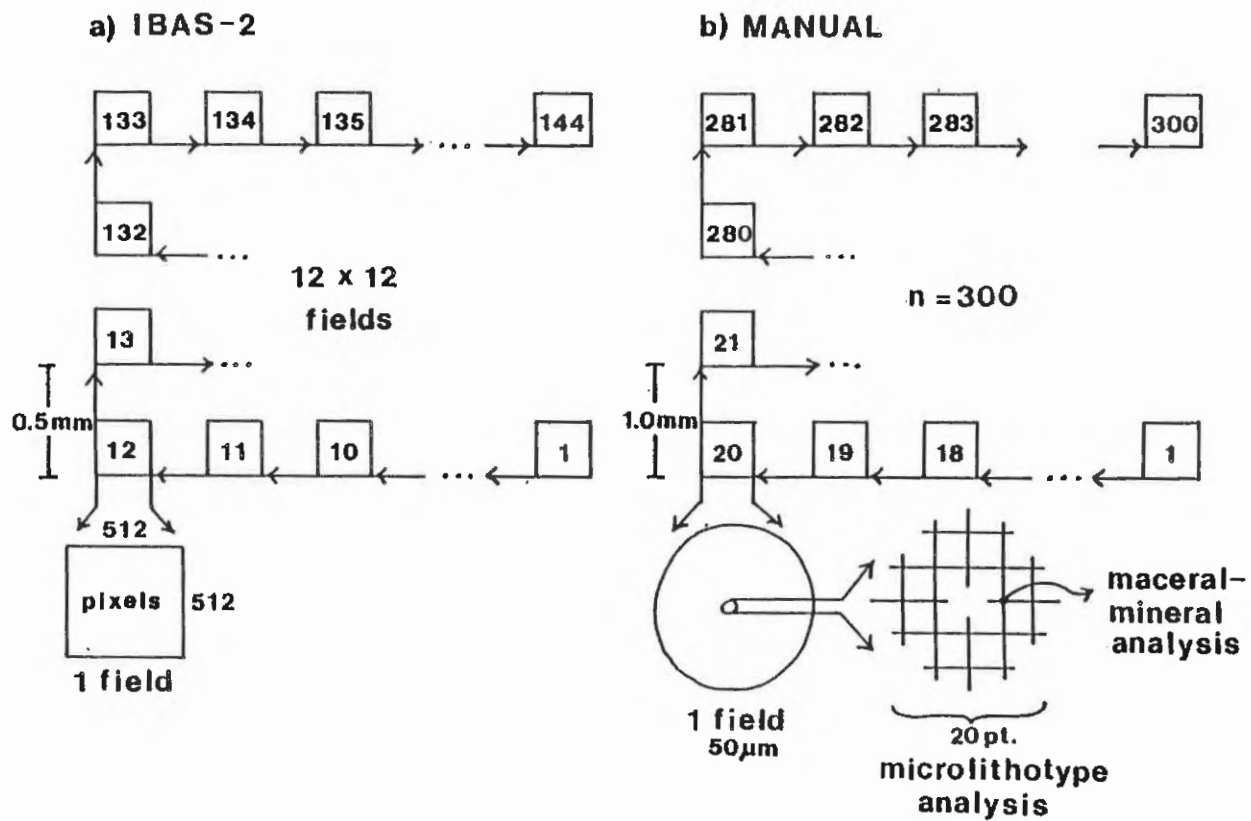
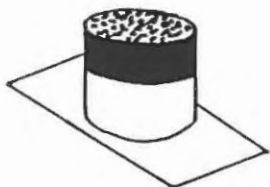


Figure A2.4. Petrographic analysis of coal pellets: a) IBAS-2; b) manual microscopy.

automated image analysis technique. The analyses were completed in the Environmental Services Laboratory (ESL), Sydney, Nova Scotia, using a Zeiss universal petrographic microscope. A combined maceral/microlithotype analysis was designed to obtain the maximum information on variations in seam composition. Both white and fluorescent light microscopy were used to identify the maceral. Kotter's twenty point graticule (see Stach *et al.*, 1982) was placed in the ocular for the microlithotype analysis (Fig. A2.2). One intersection in the grid was selected to simultaneously count the maceral composition in the same field of view.

The blocks were transected at 1 mm intervals, perpendicular to bedding as outlined in Figure A2.2. Each transect consisted of five fields at 1 mm spacing, parallel to bedding. For each field, a record was made of the microlithotype (based on twenty graticule intersections, see Table 3.3, in text) and the maceral or mineral (based on one graticule intersection, see Table 3.2, in text). Thus the block was scanned in a similar zig-zag fashion as the image analysis technique, although far fewer counts were collected.

Three hundred points were counted from pellets, when coal blocks were not available, as illustrated in Figure A2.4. Counts were recorded for both microlithotypes and maceral/minerals as described above.

A2.4.4. Coal Composition - Data Manipulation

The IBAS and manual microscopic techniques generated a large volume of coal compositional data for each seam section at 0.5 mm and 1.0 mm vertical increments, respectively. In order to reduce the volume of data and assist in interpretation, average values were calculated for previously defined lithotype groups, based on the megascopic appearance of the coal (see Section A2.3). Distinctive layers such as fusain bands, pyrite layers and carbonaceous

shales were averaged separately. Several such bands commonly occurred within a lithotype. In this case, the distinctive band was removed from the data set temporarily, the average composition of the lithotype calculated, and then the band reinserted in its proper position within the interval.

IBAS data were available in ASCII format and files were imported into a Lotus 123 database program for manipulation. The average group maceral composition of each lithotype is recorded in stratigraphic sequence (from top to base) in Tables A2.5, A2.7 and A2.9 for Sydney Mines, Victoria Mines and Glace Bay W seam sections, respectively (see Figs. 3.7 and 3.8, in text). Tables A2.6, A2.8 and A2.10 contain compositional summaries and weighted average composition, by lithotype, for each seam section (Fig. 3.6 in text).

The IBAS data required editing in places due to the nature of the individual coal block. Rare cracks in the block resulted in very low pixel counts, therefore data from either side of the crack was averaged to produce an estimated value for the cracked interval. Any epoxy filled intervals (e.g. empty spaces between coal blocks) were eliminated from the data set completely.

Manual counts provided both maceral and microlithotype data for the Glace Bay West seam section only. Data were entered into Lotus 123 database worksheets by hand. A very detailed maceral composition was determined for this seam as outlined in Table 3.2 (in text). To compare this data directly to the IBAS image analysis data set, analogous maceral groups were established as reported in Table A2.12 (Fig. 3.8, in text). Table A2.13 contains compositional summaries and weighted average composition for each lithotype (see E', Fig. 3.6, text). Lithotype compositions from all sections studied, including both automated and manual techniques, are reported in Table A2.14 for comparison. Microlithotype data was treated in a similar

manner; data for each lithotype interval was averaged and results are reported in Tables A2.15 and A2.16.

A2.4.5. Comparison of Automated and Manual Microscopy

The Glace Bay West seam section was analysed by automated as well as manual petrographic techniques. The data compare well when examining general compositional trends (Fig. 3.6, text) but several discrepancies are apparent when examining the two data sets:

1. Fusain layers contain erroneously high liptinite concentrations in the IBAS-2 data set.
2. IBAS-2 pyrite tends to be under represented.
3. The IBAS system has difficulty distinguishing liptinite from clays.
4. Vitrinite is consistently higher in the IBAS-2 data set.
5. IBAS-2 low inertinite is over-estimated; high inertinite is under-estimated; total inertinite is comparable to or slightly lower than manual total inertinite.

Fusain consists of carbonized cell walls, often with empty cell cavities (see Plate 5f). These cells can also be filled or partially filled with clays, carbonate or pyrite. This morphology created a problem for the IBAS-2 system as the grey-level of much of these empty cells overlapped with the liptinite grey-level region. Hence, "liptinite free" fusain layers were considered by the IBAS-2 system to have an erroneously high (often greater than 30%) liptinite content (Fig. 3.6, text). Attempts were made to adjust the lower grey-level boundary for liptinite, to eliminate the cavities. This successfully eliminated the cell cavities but also eliminated a large portion of "real" liptinite from the analysis.

Another problem was recognised in the distribution of pyrite and the composition of pyrite layers. Pyrite is very

common in the Backpit seam (average sulphur = 5.20 %), but the IBAS-2 data does not reflect this. Pyrite content of most lithotypes is less than 1 %. Megascopic pyrite layers exhibit higher IBAS-2 pyrite concentrations than other lithotypes but in true compositional terms, the pyrite content tends to be under represented. The inertinite group is high in these layers, however, suggesting that at least some of the pyrite falls within the inertinite grey-level region. The morphology and relief of pyrite grains may account for this discrepancy. Pyrite grains are generally poorly polished and have edges and halo effects that exhibit grey-level values in the inertinite range.

The inability of the IBAS-2 system to distinguish clays from liptinite is also recognised as a major problem. The Backpit seam contains several major episodes of high water "open moor" conditions; one near the centre and another at the top of the seam, representing the gradual drowning of the mire. The IBAS-2 system classifies this detrital clay as liptinite because its reflectance value lies within the liptinite grey-level region.

Consistently higher vitrinite compositions and correspondingly lower amounts of other maceral groups in the IBAS-2 data when compared to manual data may be explained by the difference in the volume of data points for each method of analysis. The IBAS-2 system measures over 260,000 data points from each field of view (Fig. A2.2) whereas the manual technique records one point at the intersection of the cross-hairs. Since vitrinite is the main maceral in this coal and provides a matrix for other macerals, higher values would be expected using the IBAS-2 technique. The compositional data is proportional and therefore lower inertinite and/or liptinite contents would be inevitable in the IBAS data to compensate for higher vitrinite contents. Also, the manual counting technique includes mineral matter, whereas the IBAS-2 system attempts to eliminate this group

(although unsuccessfully). Another factor which may account for lower liptinite values in the IBAS-2 technique are the presence of large resin bodies that have very low grey-level values (i.e. dark under reflected light, see Plate 5c). These bodies occur in layers and may actually be eliminated from the counting process due to their grey-level intensity. Manually, these bodies are very distinct and would be noted in the counting process. Liptodetrinite and some clays also exhibit low grey-levels and may be eliminated from the automated counting procedure.

In the manual technique, inertinite macerals were identified by morphology as well as reflectance as suggested in the ICCP Handbook (1961). This led to discrepancies in the proportions of inertinite attributed to low and high reflecting IBAS groups. Thus although the IBAS-2 data represents inertinite macerals in a specific grey-level range (see Table A2.3), these ranges do not correspond directly to semi-inertinite and inertinite, respectively. Combining these two maceral groups into a "total inertinite" group provides less misleading compositional data.

In order to compare the IBAS-2 results directly with standard petrography, the following adjustments were made:

1. The liptinite group is revised to include liptinite + other mineral matter (i.e. clays, carbonates, quartz).
2. Low and high reflecting inertinite are combined into one group - total inertinite.
3. Pyrite content is considered in a relative sense (i.e. intervals with pyrite values $>1\%$ are probably very high in pyrite).
4. Fusain layers are recognised by their distinctive IBAS composition (i.e. high inertinite and liptinite) as well as megascopic appearance. These layers are assumed to contain little or no liptinite.

A2.4.6. Vitrinite Reflectance Measurements (Ro)

Reflectance histograms, generated to establish grey-level regions in the IBAS image analysis procedure (see Section A2.4.2), were used to estimate the vitrinite reflectance of the sample. As mentioned previously, one sample from the centre of each of three seams was analysed in this manner. The Ro value at the maximum "vitrinite" peak on the histogram was selected to approximate the mean Ro of the sample.

To investigate the accuracy of this technique compared with conventional coal petrographic methods, vitrinite reflectance histograms were generated manually from the same samples, as illustrated in Figure 3.1 (in text). Table A2.4a lists raw data collected for this purpose. Fifty vitrinite reflectance readings were measured using the random reflectance technique described in Bustin et al. (1983). Results of the mean reflectance from both methods are very similar as outlined in Table A2.4b.

Appendix 2

Data Tables:

Ash, sulphur, vitrinite reflectance

Table A2.1a. Ash and sulphur data for the Backpit seam, roof and floor rocks.

Section	No.	Thickness (cm)		Ash %		Sulphur %	
		Ply	Total	Total	Wtd Avg	Total	Wtd Avg
A. BRAS D'OR							
Roof	A45	20		72.11		0.96	
Roof	A44	8		71.38		0.56	
Roof	A43	6	34	72.44	72.00	2.74	1.18
Coal	A19	25		27.10		9.63	
Coal	A20	24		7.45		4.38	
Coal	A21	25		15.50		7.28	
Coal	A22	20	94	26.71	18.91	7.66	7.25
Floor	A17	15	15	89.91	89.91	0.73	0.73
B. SYDNEY MINES							
Roof	B42	7		86.13		0.01	
Roof	B41	18		82.79		0.02	
Roof	B40	12		70.19		1.46	
Coaly Shale	B5	9	46	72.77	78.05	0.86	0.39
Coal	B100	33		6.62		2.12	
Coal	B101	33		6.06		2.04	
Coal	B102	33		3.25		1.34	
Coal	B4	8		2.60		1.93	
Coal	B3	10		3.06		1.84	
Coal	B2	20	137	11.66	5.89	2.49	1.93
Floor	B1a	3		68.44		7.92	
Floor	B1b	2	5	77.86	72.21	0.70	5.03
C. VICTORIA MINES							
Roof	C43	24		90.53		0.78	
Roof	C42	25		87.63		0.62	
Roof	C41	8	57	81.49	87.99	0.59	0.68
Coal	C1	11		21.44		12.60	
Coaly Shale	C30	2		55.96		12.30	
Coal	C2	25		9.42		6.51	
Coal	C3	25		18.38		8.07	
Coal	C4	25		10.35		4.05	
Coaly Shale	C14	4		64.48		1.74	
Coal	C5	23		17.10		4.89	
Coal	C6	20	135	7.26	15.54	3.70	6.09
Floor	C35	5	5	86.37	86.37	2.53	2.53

Table A2.1a. Ash and sulphur data for the Backpit seam, roof and floor rocks (con't).

Section	No.	Thickness (cm)		Ash %		Sulphur %	
		Ply	Total	Total Wtd Avg	Total Wtd Avg	Total Wtd Avg	Total Wtd Avg
E. GLACE BAY W							
Roof	E44	15		84.85		0.44	
Roof	E43	12		64.28		0.17	
Roof	E42	15		60.78		0.00	
Roof	E41	10		83.39		0.09	
Roof	E40	1	53	67.46	72.78	1.47	0.21
Coal	E12	26		18.90		7.17	
Coal	E13	22		7.88		2.68	
Coal	E14	21		14.77		5.65	
Coaly Shale	E15	13		58.39		2.62	
Coal	E16	32		7.02		2.57	
Coal	E17	30	144	5.41	14.73	3.05	3.97
Floor	E2	5	5	88.58	88.58	1.29	1.29
G. DONKIN W							
Roof	G41	14		89.10		0.82	
Roof	G42	6.5		88.32		0.26	
Roof	G43	12		83.49		0.21	
Roof	G44	8	40.5	75.48	84.62	1.07	0.60
Coaly Shale	G5	3		47.42		10.60	
Coal	G4	19		31.20		8.62	
Coal	G3	19		17.97		5.21	
Coal	G2	19	60	10.95	21.41	5.82	6.75
Floor	G1	10	10	59.97	59.97	5.52	5.52
H. DONKIN E							
Roof	H55	20		77.03		0.60	
Roof	H54	6		89.79		25.00	
Roof	H53	6	32	91.18	82.08	1.81	5.40
J. LONGBEACH							
Roof	J57	30		80.90		0.17	
Roof	J56	20		88.21		0.80	
Roof	J58	25	75	85.98	84.54	0.42	0.42

Table A2.1a. Ash and sulphur data for the Backpit roof unit,
Cape Breton Development Corporation (CBDC) cores (con't).

Section	No.	Thickness (cm)		Ash %		Sulphur %		
		Ply	Total	Total Wtd Avg	Total Wtd Avg	Total Wtd Avg	Total Wtd Avg	
C-136	Roof	.7	5.3	92.14	0.00			
	Roof	.6	9.2	86.22	0.09			
	Roof	.5	3.0	69.25	0.00			
	Roof	.4	12.5	65.52	0.65			
	Roof	.3	13.6	64.98	0.17			
	Roof	.2	7.3	67.98	0.35			
	Roof	.1	2.0	52.9	65.41	72.20	11.00	0.68
C-137	Roof	.8	5.0	91.47	0.00			
	Roof	.7	10.0	90.28	0.06			
	Roof	.6	10.6	85.90	0.20			
	Roof	.5	4.1	67.41	0.04			
	Roof	.4	14.6	64.40	0.00			
	Roof	.3	10.5	68.95	0.46			
	Roof	.2	6.7	75.53	1.50			
	Roof	.1	5.5	67.0	71.40	76.26	11.90	1.24

Table A2.1b. Ash and sulphur data for minor coal seams
in each section.

Section	No.	Thickness	Ash wt%	Sulphur wt%
A - Bras d'Or	A54	15	10.76	5.87
	A60	2	41.27	4.86
B - Sydney Mines	B58	18	22.73	8.74
	B68	40	5.81	2.65
C - Victoria Mines	C62	6	27.92	19.35
	C64	20	37.20	9.98
Total Average:			24.28	8.58

Table A2.1c. Average ash and sulphur data (weighted by thickness)
for the Backpit seam.

Coastal Section/ Core	Ash (wtd avg, %)			Sulphur (wtd avg %)		
	Roof	Coal	Floor	Roof	Coal	Floor
A - Bras d'Or	72.00	18.91	89.91	1.18	7.25	0.73
B - Sydney Mines	78.05	5.89	72.21	0.39	1.93	5.03
C - Victoria Mines	87.99	15.54	86.37	0.68	6.09	2.53
E - Glace Bay W	72.78	14.73	88.58	0.21	3.97	1.29
G - Donkin W	84.62	21.41	59.97	0.60	6.75	5.52
H - Donkin E	82.08	na	na	5.40	na	na
J - Longbeach	84.54	na	na	0.42	na	na
CBDC - C136	72.20	na	na	0.68	na	na
CBDC - C137	76.26	na	na	1.24	na	na
Backpit average:	78.95	15.30	79.41	1.20	5.20	3.02
Standard Deviation	6.07	5.90	12.97	1.61	2.21	2.17

na - not analysed

Table A2.2. Duplicate ash and sulphur analyses.

No.	WT. %			WT. %		
	ASH	AVG	STD	SULPHUR	AVG	STD
C43	90.61	90.53	0.12	0.79	0.78	0.01
	90.44			0.77		
C62	27.80	27.92	0.16	19.30	19.35	0.07
	28.03			19.40		
C5	17.17	17.10	0.11	5.20	5.05	0.22
	17.02			4.89		
B101	5.91	6.06	0.21	2.11	2.04	0.11
	6.20			1.96		
E17	5.38	5.41	0.04	2.95	3.05	0.13
	5.43			3.14		

Table A2.3. Grey-level regions established for automated image analysis of each seam section.

Maceral Group	B-Sydney Mines	C-Victoria Mines	E-Glace Bay W.
Liptinite	40 - 60	40 - 63	40 - 65
Vitrinite	61 - 87	64 - 91	66 - 93
Low Reflecting Inertinite	88 - 166	92 - 166	94 - 166
High Reflecting Inertinite	167 - 245	167 - 245	167 - 245
Pyrite	> 245	> 245	> 245

Table A2.4a. Manual vitrinite reflectance measurements (random) for selected samples.

Sydney Mines		Victoria Mines		Glace Bay W				Donkin W	
B32		C14.2		E25		E23		G16	
0.63	0.69	0.68	0.72	0.68	0.76	0.70	0.77	0.67	0.75
0.64	0.69	0.68	0.72	0.70	0.76	0.70	0.77	0.69	0.75
0.64	0.69	0.68	0.72	0.71	0.76	0.72	0.77	0.70	0.75
0.65	0.69	0.69	0.72	0.71	0.76	0.73	0.77	0.70	0.75
0.65	0.70	0.69	0.73	0.71	0.76	0.73	0.77	0.71	0.75
0.65	0.70	0.69	0.73	0.72	0.76	0.73	0.77	0.72	0.75
0.66	0.70	0.69	0.73	0.72	0.76	0.73	0.77	0.72	0.75
0.66	0.70	0.69	0.73	0.72	0.78	0.73	0.78	0.72	0.75
0.66	0.70	0.70	0.73	0.72	0.78	0.74	0.78	0.72	0.76
0.66	0.70	0.70	0.73	0.72	0.78	0.74	0.78	0.72	0.76
0.66	0.70	0.70	0.73	0.73	0.78	0.74	0.78	0.72	0.76
0.67	0.71	0.70	0.74	0.73	0.78	0.74	0.78	0.72	0.76
0.67	0.71	0.70	0.74	0.73	0.78	0.74	0.78	0.73	0.76
0.67	0.71	0.70	0.74	0.73	0.78	0.75	0.78	0.73	0.76
0.67	0.71	0.71	0.74	0.74	0.78	0.75	0.78	0.73	0.76
0.67	0.71	0.71	0.74	0.74	0.78	0.75	0.78	0.73	0.76
0.67	0.72	0.71	0.76	0.74	0.79	0.75	0.78	0.74	0.76
0.67	0.72	0.71	0.76	0.74	0.79	0.75	0.78	0.74	0.76
0.68	0.72	0.71	0.76	0.74	0.79	0.76	0.79	0.74	0.76
0.68	0.72	0.71	0.77	0.74	0.79	0.76	0.79	0.74	0.77
0.68	0.72	0.71	0.77	0.74	0.80	0.76	0.79	0.74	0.77
0.68	0.72	0.72	0.79	0.74	0.80	0.76	0.80	0.74	0.77
0.68	0.73	0.72	0.79	0.75	0.80	0.76	0.80	0.74	0.77
0.68	0.74	0.72	0.81	0.75	0.81	0.76	0.80	0.75	0.78
0.68	0.75	0.72	0.84	0.75	0.81	0.77	0.81	0.75	0.78
Avg:	0.69	0.73		0.75		0.76		0.74	
Std:	0.03	0.03		0.03		0.03		0.02	

Table A2.4b. Mean vitrinite reflectance values for selected samples using manual and IBAS automatic measuring techniques.

No.	MANUAL		IBAS
	Ro rnd	std	Ro rnd
B32	0.69	0.03	0.69
C14.2	0.73	0.03	0.72
E25	0.75	0.03	0.71
E23	0.76	0.03	0.80
G16	0.74	0.02	na

na - not analysed

IBAS petrographic data for:

a) Sydney Mines seam section

Abbreviations used in the following Tables:

LITHOTYPES AND LAYERS:

BR - Bright Coal
BB - Bright Banded Coal
B - Banded Coal
DB - Dull Banded Coal
D - Dull Coal
CS - Coaly Shale
PY - Pyrite Layers
F - Fusain

OTHERS:

Wtd Avg - weighted average

mmf - mineral matter free

na - not analysed

Table A2.5. Group maceral composition of lithotypes, Sydney Mines seam section (B); compiled from IBAS image analysis data.

LITHO- TYPE	mm	VITRINITE	LIPTINITE	LOW INERTINITE	HIGH INERTINITE	(TOTAL INERTINITE)	PYRITE	
THRESHOLDS:		61 - 87	40 - 60	88 - 166	167 - 245	88 - 245	> 245	
CS	90.0	na	na	na	na	na	na	
DB	11.0	37.10	15.47	43.61	3.82	(47.44)	0.00	
B	45.5	80.54	12.49	5.68	0.79	(6.47)	0.50	
DB	46.5	54.47	21.54	22.67	1.21	(23.89)	0.10	
BB	5.5	80.82	16.94	2.07	0.14	(2.21)	0.02	
F	1.0	28.81	68.51	2.22	0.45	(2.67)	0.02	
B	54.0	71.38	17.85	8.73	1.61	(10.34)	0.43	
DB	15.0	na	na	na	na	na	na	
F	2.5	19.92	16.38	36.46	20.99	(57.45)	6.25	
B	F	66.5	80.86	11.63	6.85	0.47	(7.31)	0.20
		1.0	66.71	22.15	11.10	0.05	(11.15)	0.00
BB	F	31.0	80.86	11.63	6.85	0.47	(7.31)	0.20
		12.0	88.45	7.63	3.18	0.45	(3.63)	0.28
BB	F	1.0	45.28	13.87	34.08	6.73	(40.80)	0.05
		6.5	88.45	7.63	3.18	0.45	(3.63)	0.28
F	4.0	28.85	16.94	51.62	2.59	(54.21)	0.00	
B	73.0	74.74	15.30	7.66	1.43	(9.09)	0.87	
DB	41.0	58.42	30.08	10.48	0.59	(11.06)	0.44	
B	F	23.5	63.23	30.01	5.23	0.99	(6.22)	0.54
		1.5	32.79	10.39	56.79	0.03	(56.81)	0.00
B	F	6.5	63.23	30.01	5.23	0.99	(6.22)	0.54
		5.0	38.29	38.65	20.36	2.53	(22.89)	0.18
BB	52.0	85.91	7.60	4.96	0.97	(5.93)	0.57	
F	11.0	27.52	13.73	44.07	13.22	(57.29)	1.47	
DB	6.5	63.96	15.15	20.60	0.28	(20.88)	0.01	
D	12.5	43.37	28.68	25.39	2.39	(27.78)	0.17	
DB	11.0	66.83	16.67	15.35	1.05	(16.40)	0.10	
F	3.5	29.51	21.72	29.94	16.50	(46.44)	2.33	
B	70.5	85.01	8.14	5.32	0.90	(6.22)	0.63	
DB	25.5	72.92	3.36	14.68	5.83	(20.51)	3.21	
B	F	49.5	81.04	11.92	5.75	0.94	(6.69)	0.35
		1.0	25.96	21.04	48.89	3.85	(52.74)	0.27
B	F	17.0	81.04	11.92	5.75	0.94	(6.69)	0.35
		10.5	71.52	10.53	16.15	1.07	(17.22)	0.73
BB	43.5	92.26	3.88	3.24	0.47	(3.71)	0.15	
B	33.0	89.89	4.29	4.87	0.75	(5.61)	0.20	
DB	11.0	60.86	1.46	34.37	2.44	(36.81)	0.88	
B	26.5	85.05	2.33	10.71	1.22	(11.93)	0.69	
F	1.5	28.64	15.80	41.63	12.31	(53.94)	1.62	
DB	20.0	59.95	7.75	17.84	13.88	(31.72)	0.57	
BB	21.5	92.95	3.29	3.37	0.27	(3.64)	0.12	
F	1.0	33.38	25.43	32.64	6.56	(39.20)	1.99	

Table A2.5. Group maceral composition of lithotypes, Sydney Mines seam section (B); compiled from IBAS image analysis data (con't).

LITHO- TYPE	mm	VITRINITE	LIPTINITE	LOW INERTINITE	HIGH INERTINITE	(TOTAL INERTINITE)	PYRITE
THRESHOLDS:		61 - 87	40 - 60	88 - 166	167 - 245	88 - 245	> 245
DB	F	5.0	72.59	15.16	10.94	1.17 (12.10)	0.14
	F	1.0	18.58	24.75	51.16	5.46 (56.62)	0.06
	F	28.0	72.59	15.16	10.94	1.17 (12.10)	0.14
	F	1.0	50.69	2.59	34.35	12.08 (46.42)	0.31
B		6.5	72.59	15.16	10.94	1.17 (12.10)	0.14
	B	8.5	84.67	9.50	5.71	0.11 (5.81)	0.02
DB		38.0	58.43	36.81	4.23	0.36 (4.60)	0.17
	F	10.5	86.01	6.94	5.95	0.85 (6.80)	0.26
BB	F	1.0	42.80	37.19	16.08	3.83 (19.91)	0.11
	F	6.0	86.01	6.94	5.95	0.85 (6.80)	0.26
B		72.0	81.62	10.71	5.40	1.48 (6.88)	0.79
	DB	11.0	58.99	12.47	28.22	0.21 (28.43)	0.10
B	F	59.0	83.73	7.09	7.44	1.00 (8.44)	0.73
	F	1.0	33.97	7.04	57.80	1.07 (58.87)	0.12
DB		7.5	83.73	7.09	7.44	1.00 (8.44)	0.73
	DB	6.0	46.21	4.22	40.01	5.76 (45.77)	3.79
B		14.0	79.46	6.93	11.94	1.04 (12.98)	0.63
	BB	29.0	92.07	2.13	4.89	0.58 (5.47)	0.33
F		1.0	29.94	3.53	33.12	22.16 (55.28)	11.27
	B	28.0	82.79	4.78	10.80	1.13 (11.93)	0.50
BR		6.5	89.72	2.94	6.60	0.47 (7.08)	0.26
	DB	9.0	76.68	3.93	17.48	1.37 (18.85)	0.55
F		1.0	41.23	4.22	45.25	9.07 (54.32)	0.23
	F	3.0	80.13	2.26	16.50	0.92 (17.42)	0.19
BB	F	1.0	14.32	5.73	57.48	18.11 (75.58)	4.38
	F	10.5	80.13	2.26	16.50	0.92 (17.42)	0.19
B		37.0	83.68	4.18	10.13	1.34 (11.47)	0.67
	DB	15.0	60.14	7.76	29.08	2.03 (31.11)	0.99
D		9.5	20.73	12.16	63.58	2.24 (65.82)	1.29
	B	21.0	81.73	6.33	11.21	0.51 (11.72)	0.22
CS	40.0	na	na	na	na	na	na
*Wtd avg:		74.31	11.62	9.74	3.72	(13.46)	0.61

Total thickness of the seam section (including CS) - 1459.5 mm or 1.46 m

Thickness of analysed intervals - 1314.5 mm or 1.31 m

na- not analysed

* - Weighted average based on analysed intervals (excluding CS). The composition of fusain layers was adjusted in the calculation to estimate true composition (i.e. inertinite + pyrite).

Table A2.6a. Compositional summary of bright (BR) lithotypes, Sydney Mines seam section - compiled from IBAS image analysis data.

LITHO- TYPE	mm	VITRINITE	LIPTINITE	LOW INERTINITE	HIGH INERTINITE	(TOTAL INERTINITE)	PYRITE
BR	6.5	89.72	2.94	6.60	0.47	(7.08)	0.26

Table A2.6b. Compositional summary of bright banded (BB) lithotypes, Sydney Mines seam section - compiled from IBAS image analysis data.

LITHO- TYPE	mm	VITRINITE	LIPTINITE	LOW INERTINITE	HIGH INERTINITE	(TOTAL INERTINITE)	PYRITE
BB	5.5	80.82	16.94	2.07	0.14	(2.21)	0.02
BB	18.5	88.45	7.63	3.18	0.45	(3.63)	0.28
BB	52.0	85.91	7.60	4.96	0.97	(5.93)	0.57
BB	43.5	92.26	3.88	3.24	0.47	(3.71)	0.15
BB	21.5	92.95	3.29	3.37	0.27	(3.64)	0.12
BB	16.5	86.01	6.94	5.95	0.85	(6.80)	0.26
BB	29.0	92.07	2.13	4.89	0.58	(5.47)	0.33
BB	13.5	80.13	2.26	16.50	0.92	(17.42)	0.19
Wtd Avg	200.0	88.65	5.38	5.02	0.64	(5.67)	0.30
(mmf)		88.92	5.40	5.04	0.65	(5.68)	

mmf - calculated on a mineral matter free basis

Table A2.6c. Compositional summary of banded (B) lithotypes, Sydney Mines seam section - compiled from IBAS image analysis data.

LITHO- TYPE	mm	VITRINITE	LIPTINITE	LOW INERTINITE	HIGH INERTINITE	(TOTAL INERTINITE)	PYRITE
B	45.5	80.54	12.49	5.68	0.79	(6.47)	0.50
B	54.0	71.38	17.85	8.73	1.61	(10.34)	0.43
B	97.5	80.86	11.63	6.85	0.47	(7.31)	0.20
B	73.0	74.74	15.30	7.66	1.43	(9.09)	0.87
B	30.0	63.23	30.01	5.23	0.99	(6.22)	0.54
B	70.5	85.01	8.14	5.32	0.90	(6.22)	0.63
B	66.5	81.04	11.92	5.75	0.94	(6.69)	0.35
B	33.0	89.89	4.29	4.87	0.75	(5.61)	0.20
B	26.5	85.05	2.33	10.71	1.22	(11.93)	0.69
B	8.5	84.67	9.50	5.71	0.11	(5.81)	0.02
B	72.0	81.62	10.71	5.40	1.48	(6.88)	0.79
B	66.5	83.73	7.09	7.44	1.00	(8.44)	0.73
B	14.0	79.46	6.93	11.94	1.04	(12.98)	0.63
B	28.0	82.79	4.78	10.80	1.13	(11.93)	0.50
B	37.0	83.68	4.18	10.13	1.34	(11.47)	0.67
B	21.0	81.73	6.33	11.21	0.51	(11.72)	0.22
Wtd Avg	743.5	80.38	10.89	7.16	1.03	(8.19)	0.53
(mmf)		80.82	10.95	7.20	1.03	(8.24)	

Table A2.6d. Compositional summary of dull banded (DB) lithotypes, Sydney Mines seam section - compiled from IBAS image analysis data.

LITHO- TYPE	mm	VITRINITE	LIPTINITE	LOW INERTINITE	HIGH INERTINITE	(TOTAL INERTINITE)	PYRITE
DB	11.0	37.10	15.47	43.61	3.82	(47.44)	0.00
DB	46.5	54.47	21.54	22.67	1.21	(23.89)	0.10
DB	15.0	na	na	na	na	na	na
DB	41.0	58.42	30.08	10.48	0.59	(11.06)	0.44
DB	6.5	63.96	15.15	20.60	0.28	(20.88)	0.01
DB	11.0	66.83	16.67	15.35	1.05	(16.40)	0.10
DB	25.5	72.92	3.36	14.68	5.83	(20.51)	3.21
DB	10.5	71.52	10.53	16.15	1.07	(17.22)	0.73
DB	11.0	60.86	1.46	34.37	2.44	(36.81)	0.88
DB	20.0	59.95	7.75	17.84	13.88	(31.72)	0.57
DB	39.5	72.59	15.16	10.94	1.17	(12.10)	0.14
DB	38.0	58.43	36.81	4.23	0.36	(4.60)	0.17
DB	11.0	58.99	12.47	28.22	0.21	(28.43)	0.10
DB	6.0	46.21	4.22	40.01	5.76	(45.77)	3.79
DB	9.0	76.68	3.93	17.48	1.37	(18.85)	0.55
DB	15.0	60.14	7.76	29.08	2.03	(31.11)	0.99
Wtd Avg	316.5	61.60	17.80	17.52	2.45	(19.97)	0.63
(mmf)		61.99	17.91	17.63	2.47	(20.10)	

na - not analysed

mmf - calculated on a mineral matter free basis

Table A2.6e. Compositional summary of dull (D) lithotypes, Sydney Mines seam section
- compiled from IBAS image analysis data.

LITHO- TYPE	mm	VITRINITE	LIPTINITE	LOW INERTINITE	HIGH INERTINITE	(TOTAL INERTINITE)	PYRITE
D	5.0	38.29	38.65	20.36	2.53	(22.89)	0.18
D	12.5	43.37	28.68	25.39	2.39	(27.78)	0.17
D	9.5	20.73	12.16	63.58	2.24	(65.82)	1.29
Wtd Avg	27.0	34.46	24.71	37.90	2.36	(40.26)	0.57
(mmf)		34.26	24.57	37.68	2.35	(40.03)	

Table A2.6f. Compositional summary of fusain (F) layers, Sydney Mines seam section
- compiled from IBAS image analysis data.

LITHO- TYPE	mm	VITRINITE	LIPTINITE	LOW INERTINITE	HIGH INERTINITE	(TOTAL INERTINITE)	PYRITE
F	1.0	28.81	68.51	2.22	0.45	(2.67)	0.02
F	2.5	19.92	16.38	36.46	20.99	(57.45)	6.25
F	1.0	66.71	22.15	11.10	0.05	(11.15)	0.00
F	1.0	45.28	13.87	34.08	6.73	(40.80)	0.05
F	4.0	28.85	16.94	51.62	2.59	(54.21)	0.00
F	1.5	32.79	10.39	56.79	0.03	(56.81)	0.00
F	11.0	27.52	13.73	44.07	13.22	(57.29)	1.47
F	3.5	29.51	21.72	29.94	16.50	(46.44)	2.33
F	1.0	25.96	21.04	48.89	3.85	(52.74)	0.27
F	1.5	28.64	15.80	41.63	12.31	(53.94)	1.62
F	1.0	33.38	25.43	32.64	6.56	(39.20)	1.99
F	1.0	18.58	24.75	51.16	5.46	(56.62)	0.06
F	1.0	50.69	2.59	34.35	12.08	(46.42)	0.31
F	1.0	42.80	37.19	16.08	3.83	(19.91)	0.11
F	1.0	33.97	7.04	57.80	1.07	(58.87)	0.12
F	1.0	29.94	3.53	33.12	22.16	(55.28)	11.27
F	1.0	41.23	4.22	45.25	9.07	(54.32)	0.23
F	1.0	14.32	5.73	57.48	18.11	(75.58)	4.38
Wtd Avg	36.0	30.41	16.97	40.53	10.39	(50.91)	1.70
(mmf)		30.94	17.27	41.23	10.56	(51.79)	

mmf - calculated on a mineral matter free basis

Table A2.6g. Weighted average composition for all lithotypes; Sydney Mines seam section - compiled from IBAS image analysis data.

LITHO- TYPE	mm	n=	Vol %		VITRINITE	LIPTINITE	LOW INERTINITE	HIGH INERTINITE	(TOTAL INERTINITE)	PYRITE
			1	2						
BR	6.5	1	0.4	0.5	89.72	2.94	6.60	0.47	(7.08)	0.26
BB	200.0	8	13.8	15.0	88.65	5.38	5.02	0.64	(5.67)	0.30
B	743.5	16	51.3	55.9	80.38	10.89	7.16	1.03	(8.19)	0.53
DB	316.5	16	21.8	23.8	61.60	17.80	17.52	2.45	(19.97)	0.63
D	27.0	3	1.9	2.0	34.36	24.71	37.90	2.36	(40.26)	0.57
F	36.0	18	2.5	2.7	30.41	16.97	40.53	10.39	(50.91)	1.70
CS	120.0	2	8.3		na	na	na	na	(na)	na

1. Volume % of lithotype in seam (including CS) - 1449.5 mm

2. Volume % of lithotype in seam (excluding CS) - 1329.5 mm

na - not analysed

Table A2.6h. Group maceral composition of seam intervals, Sydney Mines seam section (B); compiled from IBAS image analysis data.

SEAM INTERVAL	mm	VITRINITE	LIPTINITE	LOW INERTINITE	HIGH INERTINITE	(TOTAL INERTINITE)	PYRITE
IX	90.0	na	na	na	na	(na)	na
VIII	163.5	66.69	17.11	13.92	1.97	(15.89)	0.31
VII	15.0	na	na	na	na	(na)	na
VI	327.0	73.17	15.64	6.82	3.82	(10.64)	0.54
V	44.5	38.04	14.39	13.94	31.93	(45.87)	1.70
IV	331.0	81.85	6.58	8.14	2.77	(10.91)	0.66
III	89.0	66.4	23.94	8.53	0.95	(9.48)	0.16
II	174.0	79.25	8.73	8.81	2.43	(11.24)	0.77
I	225.5	77.45	4.84	14.47	2.58	(17.05)	0.66

IBAS petrographic data for:

b) Victoria Mines seam section

Table A2.7. Group maceral composition of lithotypes, Victoria Mines seam section (C); compiled from IBAS image analysis data.

LITHO- TYPE	mm	VITRINITE	LIPTINITE	LOW INERTINITE	HIGH INERTINITE	(TOTAL INERTINITE)	PYRITE		
THRESHOLDS:		64 - 91	40 - 63	92 - 166	167 - 245	92 - 245	> 245		
CS	35.0	na	na	na	na	na	na		
PY	5.0	26.42	16.23	22.98	22.97	(45.95)	11.39		
D	18.5	50.44	8.87	26.96	9.79	(36.74)	3.95		
DB	47.0	56.29	5.10	22.42	10.92	(33.34)	5.27		
CS	20.0	na	na	na	na	na	na		
DB	79.0	64.33	13.36	16.00	4.29	(20.28)	2.02		
B	50.0	81.14	5.62	8.71	3.07	(11.77)	1.47		
DB	9.5	78.86	2.78	9.85	5.52	(15.37)	2.99		
PY	7.5	45.94	3.58	21.92	19.32	(41.25)	9.24		
B	F	40.0	81.59	7.39	7.89	2.11	(9.99)	1.03	
		2.5	25.19	47.12	24.30	3.37	(27.66)	0.03	
		15.0	81.59	7.39	7.89	2.11	(9.99)	1.03	
		PY	3.0	19.91	9.96	26.38	30.21	(56.59)	13.54
		3.0	81.59	7.39	7.89	2.11	(9.99)	1.03	
		F	5.0	25.23	7.27	63.54	2.67	(66.21)	1.29
		9.5	81.59	7.39	7.89	2.11	(9.99)	1.03	
		F	4.0	43.87	11.60	35.62	7.42	(43.04)	1.49
		22.0	81.59	7.39	7.89	2.11	(9.99)	1.03	
		BB	8.0	85.11	8.70	2.97	2.09	(5.06)	1.12
DB	13.0	77.62	14.36	5.18	1.93	(7.11)	0.90		
F	2.5	27.56	40.34	16.48	11.52	(28.00)	4.10		
B	PY	14.5	82.35	8.37	5.97	2.13	(8.10)	1.18	
		7.5	48.22	1.94	23.73	15.90	(39.63)	10.22	
		18.5	82.35	8.37	5.97	2.13	(8.10)	1.18	
		6.5	49.37	10.37	21.01	13.06	(34.07)	6.20	
		14.5	42.06	24.30	27.07	3.93	(31.00)	2.64	
29.0	82.35	8.37	5.97	2.13	(8.10)	1.18			
DB	45.0	68.91	3.65	17.97	6.76	(24.73)	2.71		
B	36.5	82.70	11.80	2.68	1.76	(4.44)	1.06		
BB	12.5	89.72	4.53	2.78	1.85	(4.64)	1.10		
B	PY	34.0	87.13	7.32	3.27	1.36	(4.63)	0.92	
		1.5	49.94	4.48	11.24	21.73	(32.97)	12.61	
		87.0	87.13	7.32	3.27	1.36	(4.63)	0.92	
BB	33.5	88.21	3.11	4.09	2.80	(6.90)	1.78		
B	12.0	75.80	10.83	7.21	4.19	(11.40)	1.98		
BB	72.5	86.89	8.62	3.26	0.93	(4.18)	0.30		
B	22.0	84.02	5.66	6.43	2.20	(8.63)	1.68		
D	8.5	54.52	30.98	7.76	3.69	(11.44)	3.06		

Table A2.7. Group maceral composition of lithotypes, Victoria Mines seam section (C); compiled from IBAS image analysis data (con't).

LITHO- TYPE	mm	VITRINITE	LIPTINITE	LOW INERTINITE	HIGH INERTINITE	(TOTAL INERTINITE)	PYRITE	
THRESHOLDS:		64 - 91	40 - 63	92 - 166	167 - 245	92 - 245	> 245	
CS	30.0	na	na	na	na	na	na	
BB	20.0	88.87	7.04	3.12	0.55	(3.67)	0.42	
CS	20.0	na	na	na	na	na	na	
B	14.5	86.89	5.70	5.19	1.28	(6.47)	0.94	
DB	11.5	70.81	6.53	15.38	3.69	(19.07)	3.59	
BB	61.0	86.78	7.55	4.16	0.93	(5.09)	0.58	
B	25.5	75.89	11.99	9.92	1.49	(11.41)	0.71	
DB	23.0	51.56	4.73	42.28	1.13	(43.41)	0.30	
BB	14.0	82.06	8.62	8.18	0.95	(9.13)	0.19	
PY	4.0	53.27	7.20	22.47	11.44	(33.91)	5.62	
B	35.0	85.24	4.95	7.11	1.86	(8.97)	0.85	
D	21.5	54.03	7.50	36.94	1.28	(38.22)	0.26	
BB	15.0	88.36	4.73	5.71	0.79	(6.50)	0.41	
D	10.5	24.10	10.30	64.24	1.28	(65.52)	0.07	
BB	39.5	83.84	3.47	10.80	1.37	(12.17)	0.51	
B	67.0	74.11	15.43	8.71	1.14	(9.85)	0.61	
	F	2.5	43.51	5.82	34.92	11.69	(46.61)	4.06
	F	8.0	74.11	15.43	8.71	1.14	(9.85)	0.61
	F	1.5	28.88	14.85	48.46	5.61	(54.07)	2.20
	7.5	74.11	15.43	8.71	1.14	(9.85)	0.61	
BB	27.0	82.45	8.92	5.65	1.72	(7.37)	1.26	
D	8.5	52.70	11.61	26.76	6.32	(33.08)	2.62	
F	1.0	20.82	66.56	8.92	2.19	(11.11)	1.52	
CS	30.0	na	na	na	na	na	na	
*Wtd avg:		74.39	8.05	10.29	5.55	(15.84)	1.72	

Total thickness of the seam section (including CS) - 1352.5 mm or 1.35 m

Thickness of analysed intervals - 1217.5 mm or 1.22 m

na - not analysed

* - Weighted average based on analysed intervals (excluding CS). The composition of fusain layers was adjusted in the calculation to estimate true composition (i.e. inertinite + pyrite).

Table A2.8a. Compositional summary of bright banded (BB) lithotypes, Victoria Mines seam section - compiled from IBAS image analysis data.

LITHO- TYPE	mm	VITRINITE	LIPTINITE	LOW INERTINITE	HIGH INERTINITE	(TOTAL INERTINITE)	PYRITE
BB	8.0	85.11	8.70	2.97	2.09	(5.06)	1.12
BB	12.5	89.72	4.53	2.78	1.85	(4.64)	1.10
BB	33.5	88.21	3.11	4.09	2.80	(6.90)	1.78
BB	72.5	86.89	8.62	3.26	0.93	(4.18)	0.30
BB	20.0	88.87	7.04	3.12	0.55	(3.67)	0.42
BB	61.0	86.78	7.55	4.16	0.93	(5.09)	0.58
BB	14.0	82.06	8.62	8.18	0.95	(9.13)	0.19
BB	15.0	88.36	4.73	5.71	0.79	(6.50)	0.41
BB	39.5	83.84	3.47	10.80	1.37	(12.17)	0.51
BB	27.0	82.45	8.92	5.65	1.72	(7.37)	1.26
Wtd Avg (mmf)	303.0	86.27	6.69	5.04	1.30	(6.34)	0.70
		86.87	6.74	5.08	1.31	(6.39)	

Table A2.8b. Compositional summary of banded (B) lithotypes, Victoria Mines seam section - compiled from IBAS image analysis data.

LITHO- TYPE	mm	VITRINITE	LIPTINITE	LOW INERTINITE	HIGH INERTINITE	(TOTAL INERTINITE)	PYRITE
B	50.0	81.14	5.62	8.71	3.07	(11.77)	1.47
B	89.5	81.59	7.39	7.89	2.11	(9.99)	1.03
B	62.0	82.35	8.37	5.97	2.13	(8.10)	1.18
B	36.5	82.70	11.80	2.68	1.76	(4.44)	1.06
B	121.0	87.13	7.32	3.27	1.36	(4.63)	0.92
B	12.0	75.80	10.83	7.21	4.19	(11.40)	1.98
B	22.0	84.02	5.66	6.43	2.20	(8.63)	1.68
B	14.5	86.89	5.70	5.19	1.28	(6.47)	0.94
B	25.5	75.89	11.99	9.92	1.49	(11.41)	0.71
B	35.0	85.24	4.95	7.11	1.86	(8.97)	0.85
B	82.5	74.11	15.43	8.71	1.14	(9.85)	0.61
Wtd Avg (mmf)	550.5	81.88	8.84	6.41	1.85	(8.26)	1.02
		82.72	8.93	6.48	1.87	(8.35)	

mmf - calculated on a mineral matter free basis

Table A2.8c. Compositional summary of dull banded (DB) lithotypes, Victoria Mines seam section - compiled from IBAS image analysis data.

LITHO- TYPE	mm	VITRINITE	LIPTINITE	LOW INERTINITE	HIGH INERTINITE	(TOTAL INERTINITE)	PYRITE
DB	47.0	56.29	5.10	22.42	10.92	(33.34)	5.27
DB	79.0	64.33	13.36	16.00	4.29	(20.28)	2.02
DB	9.5	78.86	2.78	9.85	5.52	(15.37)	2.99
DB	13.0	77.62	14.36	5.18	1.93	(7.11)	0.90
DB	45.0	68.91	3.65	17.97	6.76	(24.73)	2.71
DB	11.5	70.81	6.53	15.38	3.69	(19.07)	3.59
DB	23.0	51.56	4.73	42.28	1.13	(43.41)	0.30
Wtd Avg	228.0	63.98	8.14	19.46	5.71	(25.17)	2.71
(mmf)		65.76	8.37	20.00	5.87	(25.87)	

Table A2.8d. Compositional summary of dull (D) lithotypes, Victoria Mines seam section - compiled from IBAS image analysis data.

LITHO- TYPE	mm	VITRINITE	LIPTINITE	LOW INERTINITE	HIGH INERTINITE	(TOTAL INERTINITE)	PYRITE
D	18.5	50.44	8.87	26.96	9.79	(36.74)	3.95
D	8.5	54.52	30.98	7.76	3.69	(11.44)	3.06
D	21.5	54.03	7.50	36.94	1.28	(38.22)	0.26
D	10.5	24.10	10.30	64.24	1.28	(65.52)	0.07
D	8.5	52.70	11.61	26.76	6.32	(33.08)	2.62
Wtd Avg	67.5	48.29	11.78	33.49	4.55	(38.04)	1.89
(mmf)		49.22	12.01	34.14	4.64	(38.77)	

mmf - calculated on a mineral matter free basis

Table A2.8e. Compositional summary of fusain (F) layers, Victoria Mines seam section - compiled from IBAS image analysis data.

LITHO- TYPE	mm	VITRINITE	LIPTINITE	LOW INERTINITE	HIGH INERTINITE	(TOTAL INERTINITE)	PYRITE
F	2.5	25.19	47.12	24.30	3.37	(27.66)	0.03
F	5.0	25.23	7.27	63.54	2.67	(66.21)	1.29
F	4.0	43.87	11.60	35.62	7.42	(43.04)	1.49
F	2.5	27.56	40.34	16.48	11.52	(28.00)	4.10
F	14.5	42.06	24.30	27.07	3.93	(31.00)	2.64
F	2.5	43.51	5.82	34.92	11.69	(46.61)	4.06
F	1.5	28.88	14.85	48.46	5.61	(54.07)	2.20
F	1.0	20.82	66.56	8.92	2.19	(11.11)	1.52
Wtd Avg	33.5	36.31	22.60	33.54	5.28	(38.82)	2.27
(mmf)		37.15	23.13	34.32	5.41	(39.72)	

Table A2.8f. Compositional summary of coaly shales (CS) and pyrite (PY) layers, Victoria Mines seam section - compiled from IBAS image analysis data.

LITHO- TYPE	mm	VITRINITE	LIPTINITE	LOW INERTINITE	HIGH INERTINITE	(TOTAL INERTINITE)	PYRITE
CS	35.0						
CS	20.0			Coaly shales not analysed by IBAS			
CS	50.0						
CS	30.0						

	135.0						
PY	5.0	26.42	16.23	22.98	22.97	(45.95)	11.39
PY	7.5	45.94	3.58	21.92	19.32	(41.25)	9.24
PY	3.0	19.91	9.96	26.38	30.21	(56.59)	13.54
PY	7.5	48.22	1.94	23.73	15.90	(39.63)	10.22
PY	6.5	49.37	10.37	21.01	13.06	(34.07)	6.20
PY	1.5	49.94	4.48	11.24	21.73	(32.97)	12.61
PY	4.0	53.27	7.20	22.47	11.44	(33.91)	5.62
Wtd Avg	35.0	43.05	7.30	22.28	18.08	(40.36)	9.29
(mmf)		47.46	8.05	24.56	19.93	(44.49)	

mmf - calculated on a mineral matter free basis

Table A2.8g. Weighted average composition for all lithotypes; Victoria Mines seam section - compiled from IBAS image analysis data.

LITHO- TYPE	mm	n=	Vol % 1	Vol % 2	VITRINITE	LIPTINITE	LOW INERTINITE	HIGH INERTINITE	(TOTAL INERTINITE)	PYRITE
BB	303.0	10	22.4	24.9	86.27	6.69	5.04	1.30	(6.34)	0.70
B	550.5	11	40.7	45.2	81.88	8.84	6.41	1.85	(8.26)	1.02
DB	228.0	7	16.9	18.7	63.98	8.14	19.46	5.71	(25.17)	2.71
D	67.5	6	5.0	5.5	48.29	11.78	33.49	4.55	(38.04)	1.89
F	33.5	8	2.5	2.8	36.31	22.60	33.54	5.28	(38.82)	2.27
PY	35.0	7	2.6	2.9	43.05	7.30	22.28	18.08	(40.36)	9.29
CS	135.0	4	10.0		na	na	na	na	(na)	na

1. Volume % of lithotype in seam (including CS) - 1352.5 mm

2. Volume % of lithotype in seam (excluding CS) - 1217.5 mm

na - not analysed

Table A2.8h. Group maceral composition of seam intervals, Victoria Mines seam section (C); compiled from IBAS image analysis data.

SEAM INTERVAL	mm	VITRINITE	LIPTINITE	LOW INERTINITE	HIGH INERTINITE	(TOTAL INERTINITE)	PYRITE
IX	35.0	na	na	na	na	(na)	na
VIII	70.5	52.64	6.88	23.65	11.48	(35.13)	5.36
VII	20.0	na	na	na	na	na	na
VI	314.0	71.22	8.37	10.22	8.06	(18.28)	2.14
V	21.0	15.28	3.21	6.50	66.18	(72.68)	8.82
IV	394.0	83.05	7.70	5.57	2.39	(7.96)	1.29
III	70.0	na	na	na	na	na	na
II	210.0	76.17	7.22	14.18	1.59	(15.77)	0.84
I	218.0	72.76	10.26	12.16	3.91	(16.07)	0.91

IBAS petrographic data for:

c) Glace Bay W seam section

Table A2.9. Group maceral composition of lithotypes, Glace Bay W seam section (E); compiled from IBAS image analysis data.

LITHO- TYPE	mm	VITRINITE	LIPTINITE	LOW INERTINITE	HIGH INERTINITE	(TOTAL INERTINITE)	PYRITE
THRESHOLDS:		66 - 93	40 - 65	94 - 166	167 - 245	94 - 245	> 245
CS	F	31.5	50.64	37.31	8.08	(10.83)	1.21
		1.0	14.22	45.39	27.67	(39.47)	0.93
	BB	41.5	50.64	37.31	8.08	(10.83)	1.21
	D	11.0	75.08	18.16	4.21	(6.24)	0.52
	DB	42.5	42.50	25.82	21.74	(28.82)	2.86
B	DB	27.0	57.06	33.25	6.80	(9.00)	0.68
		11.0	82.03	9.43	5.99	(7.75)	0.80
	F	1.5	12.06	25.14	18.49	(51.33)	11.48
		90.0	82.03	9.43	5.99	(7.75)	0.80
	F	3.0	13.37	73.60	9.49	(12.79)	0.25
		47.0	82.03	9.43	5.99	(7.75)	0.80
	F	7.0	12.92	78.30	7.07	(8.50)	0.28
	DB	120.0	64.78	7.45	22.80	(26.70)	1.06
	B	60.0	80.23	7.49	7.65	(10.46)	1.81
	D	19.5	34.52	17.03	32.52	(48.23)	0.23
	F	1.0	36.73	55.62	7.51	(7.65)	0.01
	DB	18.0	66.84	21.63	9.64	(11.15)	0.37
B	7.5	88.77	7.31	2.58	(3.53)	0.39	
DB	17.0	73.65	16.59	7.14	(9.19)	0.57	
BB	14.5	86.44	6.44	4.99	(6.49)	0.63	
DB	16.0	51.95	32.78	12.53	(14.55)	0.71	
B	52.5	81.41	9.74	5.68	(7.88)	0.97	
DB	49.0	66.20	16.66	13.67	(16.02)	1.13	
CS	130.0	na	na	na	na	na	na
F	1.0	53.66	25.95	20.40	0.00	(20.40)	0.00
B	17.5	81.20	7.56	9.60	1.43	(11.03)	0.21
F	1.0	45.27	42.51	10.27	1.87	(12.14)	0.08
BB	18.0	86.90	7.04	5.30	0.63	(5.93)	0.13
F	1.5	18.16	44.50	23.22	11.16	(34.38)	2.96
DB		7.0	75.31	14.37	7.77	(9.97)	0.37
	F	1.5	14.92	29.86	37.90	(54.36)	0.87
		29.0	75.31	14.37	7.77	(9.97)	0.37
BB	13.0	91.13	5.73	2.36	0.53	(2.89)	0.26
B	13.5	82.23	11.03	5.31	0.94	(6.25)	0.49
F	3.0	27.01	12.78	34.41	24.87	(59.28)	0.94
BB	18.0	86.80	8.90	3.72	0.44	(4.16)	0.14
B		22.0	86.84	7.05	5.12	(5.87)	0.25
	F	1.0	41.26	6.94	33.52	(50.26)	1.55
		22.5	86.84	7.05	5.12	(5.87)	0.25

Table A2.9. Group maceral composition of lithotypes, Glace Bay W seam section (E); compiled from IBAS image analysis data (con't).

LITHO- TYPE	mm	VITRINITE	LIPTINITE	LOW INERTINITE	HIGH INERTINITE	(TOTAL INERTINITE)	PYRITE	
THRESHOLDS:		66 - 93	40 - 65	94 - 166	167 - 245	94 - 245	> 245	
DB	22.0	72.43	11.48	14.40	1.39	(15.79)	0.30	
B	PY	21.0	86.38	6.97	5.54	0.75	(6.29)	0.36
		2.5	53.26	13.52	16.70	10.40	(27.10)	6.11
B	F	13.0	86.38	6.97	5.54	0.75	(6.29)	0.36
		2.0	35.15	45.30	16.01	3.48	(19.49)	0.06
B	F	60.5	86.38	6.97	5.54	0.75	(6.29)	0.36
		0.5	64.12	11.53	19.14	4.28	(23.42)	0.92
BB	F	18.5	92.25	2.93	4.41	0.31	(4.72)	0.09
		1.0	21.03	8.01	68.86	2.11	(70.97)	0.01
B	F	24.0	92.25	2.93	4.41	0.31	(4.72)	0.09
		7.0	84.60	5.45	8.71	0.94	(9.65)	0.29
B	F	2.5	46.81	8.32	32.72	10.49	(43.21)	1.67
		4.0	84.60	5.45	8.71	0.94	(9.65)	0.29
B	F	2.0	16.63	11.66	31.69	32.63	(64.32)	7.40
		10.0	84.60	5.45	8.71	0.94	(9.65)	0.29
B	F	2.5	14.06	20.67	27.52	29.75	(57.27)	8.00
		9.5	84.60	5.45	8.71	0.94	(9.65)	0.29
B	F	2.5	14.37	23.97	30.02	28.72	(58.74)	2.91
		56.5	84.60	5.45	8.71	0.94	(9.65)	0.29
B	F	3.5	18.60	39.30	35.31	5.02	(40.33)	1.76
		26.0	84.60	5.45	8.71	0.94	(9.65)	0.29
DB	27.0	74.51	4.70	19.45	0.95	(20.40)	0.38	
BB	26.0	91.06	2.91	4.32	1.05	(5.37)	0.67	
B	17.0	83.10	6.84	6.89	2.06	(8.95)	1.12	
DB	F	8.0	83.91	4.91	8.82	1.56	(10.38)	0.79
		1.0	45.39	37.67	14.71	2.16	(16.87)	0.08
B	F	13.5	83.91	4.91	8.82	1.56	(10.38)	0.79
		32.0	83.58	6.31	8.26	1.27	(9.53)	0.59
B	F	4.5	39.17	51.57	5.57	2.38	(7.95)	1.31
		3.0	83.58	6.31	8.26	1.27	(9.53)	0.59
CS	30.0	na	na	na	na	na	na	
*Wtd Avg:		74.28	10.18	9.69	5.54	(15.23)	0.87	

Total thickness of the seam section - 1441.5 mm or 1.44 m

Thickness of analysed intervals - 1281.0 mm or 1.28 m

na - not analysed

* - Weighted average based on analysed intervals (excluding CS). The composition of fusain layers was adjusted in the calculation to estimate true composition (inertinite + pyrite).

Table A2.10a. Compositional summary of bright banded (BB) lithotypes, Glace Bay W seam section - compiled from IBAS image analysis data.

LITHO- TYPE	mm	VITRINITE	LIPTINITE	LOW INERTINITE	HIGH INERTINITE	(TOTAL INERTINITE)	PYRITE
BB	11.0	75.08	18.16	4.21	2.03	(6.24)	0.52
BB	14.5	86.44	6.44	4.99	1.50	(6.49)	0.63
BB	18.0	86.90	7.04	5.30	0.63	(5.93)	0.13
BB	13.0	91.13	5.73	2.36	0.53	(2.89)	0.26
BB	18.0	86.80	8.90	3.72	0.44	(4.16)	0.14
BB	42.5	92.25	2.93	4.41	0.31	(4.72)	0.09
BB	26.0	91.06	2.91	4.32	1.05	(5.37)	0.67
Wtd Avg	143.0	88.66	5.98	4.28	0.77	(5.05)	0.31
(mmf)		88.94	6.00	4.29	0.78	(5.07)	

Table A2.10b. Compositional summary of banded (B) lithotypes, Glace Bay W seam section - compiled from IBAS image analysis data.

LITHO- TYPE	mm	VITRINITE	LIPTINITE	LOW INERTINITE	HIGH INERTINITE	(TOTAL INERTINITE)	PYRITE
B	148.0	82.03	9.43	5.99	1.76	(7.75)	0.80
B	60.0	80.23	7.49	7.65	2.81	(10.46)	1.81
B	7.5	88.77	7.31	2.58	0.95	(3.53)	0.39
B	52.5	81.41	9.74	5.68	2.20	(7.88)	0.97
B	17.5	81.20	7.56	9.60	1.43	(11.03)	0.21
B	13.5	82.23	11.03	5.31	0.94	(6.25)	0.49
B	44.5	86.84	7.05	5.12	0.75	(5.87)	0.25
B	94.5	86.38	6.97	5.54	0.75	(6.29)	0.36
B	113.0	84.60	5.45	8.71	0.94	(9.65)	0.29
B	17.0	83.10	6.84	6.89	2.06	(8.95)	1.12
B	35.0	83.58	6.31	8.26	1.27	(9.53)	0.59
Wtd Avg	603.0	83.50	7.66	6.71	1.46	(8.17)	0.68
(mmf)		84.07	7.71	6.75	1.47	(8.22)	

mmf - calculated on a mineral matter free basis

Table A2.10c. Compositional summary of dull banded (DB) lithotypes, Glace Bay W seam section - compiled from IBAS image analysis data.

LITHO- TYPE	mm	VITRINITE	LIPTINITE	LOW INERTINITE	HIGH INERTINITE	(TOTAL INERTINITE)	PYRITE
DB	27.0	57.06	33.25	6.80	2.20	(9.00)	0.68
DB	120.0	64.78	7.45	22.80	3.90	(26.70)	1.06
DB	18.0	66.84	21.63	9.64	1.51	(11.15)	0.37
DB	17.0	73.65	16.59	7.14	2.05	(9.19)	0.57
DB	16.0	51.95	32.78	12.53	2.02	(14.55)	0.71
DB	49.0	66.20	16.66	13.67	2.35	(16.02)	1.13
DB	36.0	75.31	14.37	7.77	2.20	(9.97)	0.37
DB	22.0	72.43	11.48	14.40	1.39	(15.79)	0.30
DB	27.0	74.51	4.70	19.45	0.95	(20.40)	0.38
DB	21.5	83.91	4.91	8.82	1.56	(10.38)	0.79
Wtd Avg	353.5	67.79	13.60	15.26	2.56	(17.83)	0.78
(mmf)		68.33	13.70	15.39	2.58	(17.97)	

Table A2.10d. Compositional summary of dull (D) lithotypes, Glace Bay W seam section - compiled from IBAS image analysis data.

LITHO- TYPE	mm	VITRINITE	LIPTINITE	LOW INERTINITE	HIGH INERTINITE	(TOTAL INERTINITE)	PYRITE
D	42.5	42.50	25.82	21.74	7.08	(28.82)	2.86
D	19.5	34.52	17.03	32.52	15.71	(48.23)	0.23
Wtd Avg	62.0	39.99	23.06	25.13	9.79	(34.92)	2.03
(mmf)		40.82	23.53	25.65	10.00	(35.65)	

mmf - calculated on a mineral matter free basis

Table A2.10e. Compositional summary of fusain (F) layers, Glace Bay W seam section - compiled from IBAS image analysis data.

LITHO- TYPE	mm	VITRINITE	LIPTINITE	LOW INERTINITE	HIGH INERTINITE	(TOTAL INERTINITE)	PYRITE
F	1.0	14.22	45.39	27.67	11.80	(39.47)	0.93
F	1.5	12.06	25.14	18.49	32.84	(51.33)	11.48
F	3.0	13.37	73.60	9.49	3.30	(12.79)	0.25
F	7.0	12.92	78.30	7.07	1.43	(8.50)	0.28
F	1.0	36.73	55.62	7.51	0.14	(7.65)	0.01
F	1.0	53.66	25.95	20.40	0.00	(20.40)	0.00
F	1.0	45.27	42.51	10.27	1.87	(12.14)	0.08
F	1.5	18.16	44.50	23.22	11.16	(34.38)	2.96
F	1.5	14.92	29.86	37.90	16.46	(54.36)	0.87
F	3.0	27.01	12.78	34.41	24.87	(59.28)	0.94
F	1.0	41.26	6.94	33.52	16.74	(50.26)	1.55
F	2.0	35.15	45.30	16.01	3.48	(19.49)	0.06
F	0.5	64.12	11.53	19.14	4.28	(23.42)	0.92
F	1.0	21.03	8.01	68.86	2.11	(70.97)	0.01
F	2.5	46.81	8.32	32.72	10.49	(43.21)	1.67
F	2.0	16.63	11.66	31.69	32.63	(64.32)	7.40
F	2.5	14.06	20.67	27.52	29.75	(57.27)	8.00
F	2.5	14.37	23.97	30.02	28.72	(58.74)	2.91
F	3.5	18.60	39.30	35.31	5.02	(40.33)	1.76
F	1.0	45.39	37.67	14.71	2.16	(16.87)	0.08
F	4.5	39.17	51.57	5.57	2.38	(7.95)	1.31
Wtd Avg	44.5	24.76	40.46	21.64	11.13	(32.76)	2.02
(mmf)		25.27	41.29	22.08	11.35	(33.43)	

Table A2.10f. Compositional summary of coaly shales (CS) and pyrite (PY) layers, Glace Bay W seam section - compiled from IBAS image analysis data.

LITHO- TYPE	mm	VITRINITE	LIPTINITE	LOW INERTINITE	HIGH INERTINITE	(TOTAL INERTINITE)	PYRITE
CS	73.0	50.64	37.31	8.08	2.75	(10.83)	1.21
CS	130.0						
CS	30.0						

	233.0						
PY	2.5	53.26	13.52	16.70	10.40	(27.10)	6.11

mmf - calculated on a mineral matter free basis

Table A2.10g. Weighted average composition for all lithotypes; Glace Bay W seam section - compiled from IBAS image analysis data.

LITHO- TYPE	mm	n=	Vol % 1	Vol % 2	VITRINITE	LIPTINITE	LOW INERTINITE	HIGH INERTINITE	(TOTAL INERTINITE)	PYRITE
BB	143.0	7	9.9	11.8	88.66	5.98	4.28	0.77	(5.05)	0.31
B	603.0	11	41.8	49.9	83.50	7.66	6.71	1.46	(8.17)	0.68
DB	353.5	10	24.5	29.3	67.79	13.60	15.26	2.56	(17.83)	0.78
D	62.0	2	4.3	5.1	39.99	23.06	25.13	9.79	(34.92)	2.03
F	44.5	21	3.1	3.7	24.76	40.46	21.64	11.13	(32.76)	2.02
PY	2.5	1	0.2	0.2	53.26	13.52	16.70	10.40	(27.10)	6.11
CS	233.0	2	16.2		na	na	na	na	na	na

1. Volume % of lithotype in seam (including CS) - 1441.5 mm

2. Volume % of lithotype in seam (excluding CS) - 1208.5 mm

na - total lithotype interval not analysed

Table A2.10h. Group maceral composition of seam intervals, Glace Bay W seam section (E); compiled from IBAS image analysis data.

SEAM INTERVAL	mm	VITRINITE	LIPTINITE	LOW INERTINITE	HIGH INERTINITE	(TOTAL INERTINITE)	PYRITE
IX	74.0	49.56	36.81	7.97	4.00	(11.97)	1.26
VIII	80.5	49.20	24.25	18.14	6.04	(24.18)	2.38
(VII)	not present						
VI	339.5	72.84	8.01	12.02	5.96	(17.98)	1.11
V	20.5	32.84	16.20	30.93	19.82	(50.75)	0.22
IV	174.5	72.91	15.31	8.91	2.03	(10.94)	0.84
III	130.0	na	na	na	na	na	na
II	191.5	78.39	9.01	6.56	5.67	(12.23)	0.37
I	431.0	80.54	5.18	7.41	6.11	(13.52)	0.76

Manual petrographic data for:

Glance Bay W seam section

Summary of IBAS and Manual data

Abbreviations used in following Tables:

VITRINITE:	LIPTINITE:	INERTINITE:	MINERAL MATTER:
T - Telinite	Mg - Macrosporinite	SF - Semifusinite	Cl - Clays
TC - Telocollinite	Sp - Sporangium	SM - Semimacrinite	Ca - Carbonates
DC - Desmocollinite	Ms - Miosporinite	PF - Pyrofusinite	Qt - Quartz
CC - Corpocollinite	C - Crassisporinite	E - empty cells	Py - Pyrite
GC - Gelocollinite	T - Tenuisporinite	F - filled cells	Oth- Other Minerals
VD - Vitrodetrinite	Cu - Cutinite	B - bogen structure	
	C - Crassicutinite	DF - Degradofusinite	
	T - Tenuicutinite	Ma - Macrinite	
	Ex - Exsudatinite	Mi - Micrinite	
	Re - Resinite	Sc - Secretion Sclerotinite	
	B - Bodies	Id - Inertodetrinite	
	W - wisps		
	Al - Alginite		
	T - Telalginite		
	L - Lamalginite		
	Ld - Liptodetrinite		

Table A2.11a. Detailed maceral analysis, vitrinite group -
Glance Bay W seam section (E'); compiled from
manual data.

LITHO- TYPE	mm	VITRINITE (Volume %)						
		T	TC	DC	CC	GC	VD	
CS	F	30	---	18.8	25.9	0.3	---	---
	F	1	---	---	---	---	---	---
	BB	40	---	18.8	25.9	0.3	---	---
	D	13	---	40.0	26.7	3.3	---	---
	DB	44	---	19.0	19.0	---	---	1.0
B	DB	26	---	13.9	37.7	3.3	---	0.8
	F	11	---	31.4	42.8	3.2	---	0.4
	F	1	---	---	---	---	---	---
	F	90	---	31.4	42.8	3.2	---	0.4
	F	3	---	---	20.0	---	---	---
	F	49	---	31.4	42.8	3.2	---	0.4
	F	5	---	---	---	---	---	---
	DB	120	---	17.0	28.0	2.0	---	4.0
	B	60	---	23.3	51.0	2.0	---	0.3
	D	20	---	5.5	17.6	---	---	1.1
	DB	16	---	17.3	30.7	1.3	---	2.7
	B	9	---	36.4	47.7	---	---	---
	DB	18	---	8.0	38.6	3.4	---	---
	BB	15	14.3	48.6	18.6	2.9	---	---
	DB	15	---	18.9	25.7	1.4	---	---
B	F	13	---	37.3	38.7	1.1	---	---
	F	1	---	20.0	20.0	---	---	---
	DB	42	---	37.3	38.7	1.1	---	---
	DB	52	0.8	32.3	25.1	3.2	---	---
	CS	130	---	17.1	2.3	0.3	---	15.1
	F	1	---	---	20.0	---	---	---
	B	17	---	28.0	37.8	2.4	---	---
	F	2	---	---	25.0	---	---	---
	BB	17	---	23.5	43.5	5.9	---	---
	F	5	---	---	4.8	---	---	---
DB	F	5	---	25.4	30.6	3.5	---	1.2
	F	2	---	---	25.0	---	---	---
	BB	30	---	25.4	30.6	3.5	---	1.2
	BB	13	---	57.8	23.4	1.6	---	---
	B	14	---	25.7	41.4	4.3	---	---
	F	2	---	10.0	---	---	---	---
	BB	19	---	32.6	40.2	3.3	---	---
B	F	21	---	23.7	43.7	4.2	---	---
	F	1	---	---	20.0	---	---	---
		23	---	23.7	43.7	4.2	---	---

Table A2.11a. Detailed maceral analysis, vitrinite group -
Glance Bay W seam section (E'); compiled from
manual data (con't).

LITHO- TYPE	mm	VITRINITE (Volume %)						Total
		T	TC	DC	CC	GC	VD	
DB	21	---	20.0	26.7	2.9	---	---	
F	1	---	---	20.0	---	---	---	
B	PY	22	---	33.2	38.2	0.6	---	---
		2	---	---	30.0	---	---	---
	14	---	33.2	38.2	0.6	---	---	
	F	1	---	---	---	---	---	---
BB	F	61	---	33.2	38.2	0.6	---	---
		1	---	---	---	---	---	---
	19	---	38.0	37.1	0.9	---	---	
	1	---	---	---	---	---	---	
B	F	24	---	38.0	37.1	0.9	---	---
		7	0.2	35.7	41.0	1.5	---	---
	2	---	---	22.2	---	---	---	
	4	0.2	35.7	41.0	1.5	---	---	
	2	---	---	---	---	---	---	
	10	0.2	35.7	41.0	1.5	---	---	
	3	---	---	27.3	---	---	---	
	9	0.2	35.7	41.0	1.5	---	---	
	3	---	---	---	---	---	---	
	57	0.2	35.7	41.0	1.5	---	---	
DB	F	3	---	---	---	---	---	---
		3	0.2	35.7	41.0	1.5	---	---
	1	---	---	---	---	---	---	
	22	0.2	35.7	41.0	1.5	---	---	
DB	27	---	9.0	42.1	3.8	---	---	
BB	26	---	25.4	51.6	6.3	---	---	
B	18	---	31.5	44.9	---	---	---	
DB	F	7	---	14.1	57.6	1.0	---	---
		1	---	---	20.0	---	---	---
B	F	13	---	14.1	57.6	1.0	---	---
		31	---	49.7	33.9	---	---	---
	1	---	---	---	---	---	---	
	3	---	49.7	33.9	---	---	---	
B	F	3	---	20.0	10.0	---	---	---
		4	---	49.7	33.9	---	---	---
CS	30	---	21.3	16.7	0.7	---	2.7	Total
Wtd avg:	1.	0.2	25.7	32.0	1.8	---	2.0	61.7
	2.	0.2	27.0	35.8	2.1	---	0.6	65.8

1. Weighted average including CS

2. Weighted average excluding CS

Table A2.11b. Detailed maceral analysis, liptinite group - Glace Bay W seam section (E');
compiled from manual data (con't).

LITHO- TYPE	mm	LIPTINITE (Volume %)												
		Mg	Sp	Ms		Cu		Ex	Re		AL		Ld	
				C	T	C	T		B	W	T	L		
DB	21	---	---	---	18.1	---	---	---	---	---	---	1.0	8.6	
F	1	---	---	---	---	---	---	---	---	---	---	---	---	
B	PY	22	0.2	0.2	0.2	7.3	---	---	0.4	0.4	0.4	---	---	2.5
		2	---	---	---	20.0	---	---	---	---	---	---	---	---
B	F	14	0.2	0.2	0.2	7.3	---	---	0.4	0.4	0.4	---	---	2.5
		1	---	---	---	---	---	---	---	---	---	---	---	---
B	F	61	0.2	0.2	0.2	7.3	---	---	0.4	0.4	0.4	---	---	2.5
		1	---	---	---	---	---	---	---	---	---	---	---	---
BB	F	19	0.9	---	0.5	3.3	---	---	---	---	---	---	---	3.3
		1	---	---	---	---	---	---	---	---	---	---	---	---
B	F	24	0.9	---	0.5	3.3	---	---	---	---	---	---	---	3.3
		7	---	0.2	---	2.5	---	---	---	---	0.2	---	---	1.3
B	F	2	---	---	---	11.1	---	---	---	---	---	---	---	---
		4	---	0.2	---	2.5	---	---	---	---	0.2	---	---	1.3
B	F	2	---	---	---	---	---	---	---	---	---	---	---	---
		10	---	0.2	---	2.5	---	---	---	---	0.2	---	---	1.3
B	F	3	---	---	---	---	---	---	---	---	---	---	---	18.2
		9	---	0.2	---	2.5	---	---	---	---	0.2	---	---	1.3
B	F	3	---	---	---	---	---	---	---	---	---	---	---	---
		57	---	0.2	---	2.5	---	---	---	---	0.2	---	---	1.3
B	F	3	---	---	---	---	---	---	---	---	---	---	---	---
		3	---	0.2	---	2.5	---	---	---	---	0.2	---	---	1.3
B	F	1	---	---	---	---	---	---	---	---	---	---	---	---
		22	---	0.2	---	2.5	---	---	---	---	0.2	---	---	1.3
DB	27	---	---	---	4.5	---	---	---	---	---	---	---	6.8	
BB	26	---	1.6	---	2.4	---	---	---	---	---	---	---	0.8	
B	18	---	---	---	4.5	---	---	---	---	---	---	---	1.1	
DB	F	7	---	1.0	---	1.0	---	---	---	---	1.0	---	---	3.0
		1	---	---	---	---	---	---	---	---	20.0	---	---	---
B	F	13	---	1.0	---	1.0	---	---	---	---	1.0	---	---	3.0
		31	---	---	---	1.1	---	0.5	---	---	1.6	---	---	1.1
B	F	1	---	---	---	---	---	---	---	---	---	---	---	---
		3	---	---	---	1.1	---	0.5	---	---	1.6	---	---	1.1
B	F	3	---	---	---	---	---	---	---	---	---	---	---	---
		4	---	---	---	1.1	---	0.5	---	---	1.6	---	---	1.1
CS	30	---	0.7	---	1.3	0.7	---	---	---	---	---	---	---	
Wtd avg:	1.	0.1	0.2	0.3	4.8	0.1	0.1	---	0.2	0.1	---	---	3.5	
	2.	0.1	0.2	0.4	5.3	0.1	0.1	---	0.3	0.2	---	---	3.6	

Total Liptinite

1. Weighted average including CS intervals
2. Weighted average excluding CS intervals

Wtd avg: 1. 9.5
2. 10.3

Table A2.11c. Detailed maceral analysis, inertinite group - Glace Bay W seam section (E'); compiled from manual data.

LITHO- TYPE	mm	INERTINITE (Volume %)										
		SF	SM	PF		DF	Ma	Mi	Sc	Id		
				E	F	B						
CS	F	30	3.4	---	0.3	---	1.2	---	0.3	3.1	0.3	4.9
	F	1	---	---	---	---	100	---	---	---	---	---
	F	40	3.4	---	0.3	---	1.2	---	0.3	3.1	0.3	4.9
	BB	13	---	---	---	---	---	---	---	1.7	---	5.0
	D	44	1.5	---	1.5	---	2.0	0.5	0.5	0.5	---	9.3
B	DB	26	---	0.8	---	---	6.6	---	---	1.6	---	4.9
	F	11	0.8	0.1	1.2	---	1.8	0.1	0.7	3.9	---	2.4
	F	1	---	---	---	---	100	---	---	---	---	---
	F	90	0.8	0.1	1.2	---	1.8	0.1	0.7	3.9	---	2.4
	F	3	---	---	---	---	70.0	---	---	10.0	---	---
	F	49	0.8	0.1	1.2	---	1.8	0.1	0.7	3.9	---	2.4
	F	5	---	---	---	---	90.0	---	---	---	---	---
	DB	120	9.0	4.7	6.0	0.7	12.3	1.0	0.7	---	---	3.3
	B	60	3.0	---	1.0	0.3	8.7	---	---	2.0	---	1.0
	D	20	3.3	1.1	4.4	---	22.0	---	2.2	1.1	1.1	11.0
	DB	16	5.3	---	1.3	---	1.3	1.3	---	4.0	---	4.0
	B	9	---	---	---	---	---	---	---	2.3	---	2.3
	DB	18	4.5	2.3	---	---	2.3	1.1	---	3.4	---	5.7
	BB	15	---	---	---	---	1.4	---	---	---	---	1.4
	DB	15	5.4	1.4	---	---	---	---	---	1.4	---	8.1
B	F	13	1.5	---	0.7	---	0.4	---	---	1.5	0.4	---
	F	1	---	---	---	---	60.0	---	---	---	---	---
	F	42	1.5	---	0.7	---	0.4	---	---	1.5	0.4	---
	DB	52	2.4	---	---	---	---	---	---	2.0	---	4.0
	CS	130	---	---	---	---	---	---	---	---	---	---
	F	1	---	---	---	---	40.0	---	---	---	---	20.0
	B	17	1.2	---	---	---	4.9	---	---	6.1	---	3.7
	F	2	---	---	25.0	---	37.5	---	---	---	---	---
	BB	17	1.2	---	---	---	3.5	---	---	8.2	---	---
	F	5	---	---	14.3	---	71.4	---	---	---	---	4.8
DB	F	5	2.9	---	---	0.6	1.2	---	---	5.2	0.6	5.2
	F	2	---	---	---	12.5	37.5	---	---	---	12.5	12.5
	F	30	2.9	---	---	0.6	1.2	---	---	5.2	0.6	5.2
	BB	13	4.7	1.6	---	---	1.6	---	---	3.1	---	1.6
	B	14	1.4	---	1.4	---	---	---	1.4	11.4	---	2.9
	F	2	---	---	---	---	60.0	---	---	---	---	30.0
	BB	19	3.3	---	---	---	---	---	---	2.2	---	1.1
B	F	21	2.3	---	0.9	---	1.4	---	0.5	6.5	---	0.9
	F	1	---	---	---	---	60.0	---	---	---	20.0	---
	F	23	2.3	---	0.9	---	1.4	---	0.5	6.5	---	0.9

Table A2.11c. Detailed maceral analysis, inertinite group - Glace Bay W seam section (E'); compiled from manual data (con't).

LITHO- TYPE	mm	INERTINITE (Volume %)										Total	
		SF	SM	E	PF F	B	DF	Ma	Mi	Sc	Id		
DB	21	10.5	1.9	---	---	---	---	---	---	7.6	---	1.0	
F	1	---	---	---	---	60.0	---	---	---	---	---	20.0	
	22	2.9	---	---	---	1.3	---	0.4	6.3	0.4	---	2.9	
PY	2	---	---	---	---	---	---	---	10.0	---	---	10.0	
B	14	2.9	---	---	---	1.3	---	0.4	6.3	0.4	---	2.9	
F	1	---	---	---	---	100	---	---	---	---	---	---	
	61	2.9	---	---	---	1.3	---	0.4	6.3	0.4	---	2.9	
F	1	---	---	---	---	100	---	---	---	---	---	---	
	19	3.3	---	---	---	---	---	0.5	5.6	---	---	5.2	
BB	1	---	---	---	---	---	100	---	---	---	---	---	
	24	3.3	---	---	---	---	---	0.5	5.6	---	---	5.2	
	7	4.9	---	0.2	---	0.9	0.4	0.2	5.3	---	---	3.4	
F	2	66.7	---	---	---	---	---	---	---	---	---	---	
	4	4.9	---	0.2	---	0.9	0.4	0.2	5.3	---	---	3.4	
F	2	10.0	---	---	---	80.0	---	---	---	10.0	---	---	
	10	4.9	---	0.2	---	0.9	0.4	0.2	5.3	---	---	3.4	
F	3	---	---	---	---	54.5	---	---	---	---	---	---	
B	9	4.9	---	0.2	---	0.9	0.4	0.2	5.3	---	---	3.4	
F	3	---	---	---	---	100	---	---	---	---	---	---	
	57	4.9	---	0.2	---	0.9	0.4	0.2	5.3	---	---	3.4	
F	3	16.7	---	---	16.7	66.7	---	---	---	---	---	---	
	3	4.9	---	0.2	---	0.9	0.4	0.2	5.3	---	---	3.4	
F	1	---	---	---	100	---	---	---	---	---	---	---	
	22	4.9	---	0.2	---	0.9	0.4	0.2	5.3	---	---	3.4	
DB	27	15.8	3.0	---	---	---	---	2.3	3.8	---	---	6.8	
BB	26	1.6	---	---	---	---	---	---	4.8	---	---	4.0	
B	18	2.2	---	---	---	---	---	---	3.4	---	---	2.2	
	7	1.0	---	1.0	---	1.0	1.0	---	7.1	---	---	3.0	
DB	1	---	---	---	---	60.0	---	---	---	---	---	---	
	13	1.0	---	1.0	---	1.0	1.0	---	7.1	---	---	3.0	
	31	6.0	---	0.5	---	0.5	1.1	---	0.5	---	---	1.6	
F	1	---	---	100	---	---	---	---	---	---	---	---	
B	3	6.0	---	0.5	---	0.5	1.1	---	0.5	---	---	1.6	
F	3	---	---	---	70.0	---	---	---	---	---	---	---	
	4	6.0	---	0.5	---	0.5	1.1	---	0.5	---	---	1.6	
CS	30	2.7	---	0.7	---	0.7	0.0	---	0.7	0.7	0.7	0.7	Total
Wtd avg:	1.	3.3	0.6	1.0	0.3	4.2	0.3	0.3	3.1	0.1	3.0	16.2	
	2.	3.7	0.7	1.2	0.4	5.2	0.4	0.3	3.5	0.1	3.3	18.8	

1. Weighted average including CS

2. Weighted average excluding CS

Table A2.11d. Detailed mineral matter analysis -
 Glace Bay West seam section (E');
 compiled from manual data.

LITHO- TYPE	mm	MINERAL MATTER (Volume %)					
		Cl	Ca	Qt	Oth	Py	
CS	F	30	21.9	1.5	2.5	---	10.8
		1	---	---	---	---	---
	BB	40	21.9	1.5	2.5	---	10.8
		13	11.7	---	1.7	---	5.0
		D	44	18.1	---	2.0	---
DB	26	20.5	---	1.6	---	2.5	
B	F	11	2.1	---	1.0	0.1	1.8
		1	---	---	---	---	---
	F	90	2.1	---	1.0	0.1	1.8
		3	---	---	---	---	---
		49	2.1	---	1.0	0.1	1.8
	F	5	---	---	---	---	10.0
	DB	120	2.0	---	0.7	---	0.3
	B	60	0.3	---	---	---	1.3
	D	20	3.3	---	---	---	---
	DB	16	---	---	---	---	1.3
	B	9	2.3	---	---	---	---
	DB	18	5.7	---	---	---	5.7
	BB	15	---	---	---	---	7.1
	DB	15	---	---	---	---	4.1
	B	F	13	0.4	---	0.4	---
1			---	---	0.0	---	---
DB		42	0.4	---	0.4	---	5.2
		52	4.4	---	---	---	7.2
		CS	130	53.4	---	---	2.3
DB	F	1	---	---	---	---	
	B	17	---	---	---	---	
	F	2	---	---	---	---	
	BB	17	---	---	---	1.2	
	F	5	---	---	---	---	
	F	5	---	---	---	---	0.6
		2	---	---	---	---	---
	BB	30	---	---	---	---	0.6
		13	---	---	---	---	---
		B	14	---	---	---	---
F		2	---	---	---	---	
BB		19	---	---	---	---	
B	F	21	---	---	---	0.5	
		1	---	---	---	---	
		23	---	---	---	0.5	

Table A2.11d. Detailed mineral matter analysis -
 Glace Bay West seam section (E');
 compiled from manual data (con't).

LITHO- TYPE	mm	MINERAL MATTER (Volume %)					
		Cl	Ca	Qt	Oth	Py	
DB	21	---	---	---	---	1.9	
F	1	---	---	---	---	---	
B	PY	22	---	---	---	2.1	
		2	---	---	---	30.0	
B	F	14	---	---	---	2.1	
		1	---	---	---	---	
BB	F	61	---	---	---	2.1	
		1	---	---	---	---	
BB	F	19	---	---	0.5	0.9	
		1	---	---	---	---	
B	F	24	---	---	0.5	0.9	
		7	---	---	0.6	1.5	
B	F	2	---	---	---	---	
		4	---	---	0.6	1.5	
B	F	2	---	---	---	---	
		10	---	---	0.6	1.5	
B	F	3	---	---	---	---	
		9	---	---	0.6	1.5	
B	F	3	---	---	---	---	
		57	---	---	0.6	1.5	
B	F	3	---	---	---	---	
		3	---	---	0.6	1.5	
B	F	1	---	---	---	---	
		22	---	---	0.6	1.5	
DB	27	---	---	---	---	1.5	
BB	26	---	---	---	---	1.6	
B	18	---	---	1.1	---	9.0	
DB	F	7	---	---	3.0	4.0	
		1	---	---	---	---	
B	F	13	---	---	3.0	4.0	
		31	---	---	---	1.6	
B	F	1	---	---	---	---	
		3	---	---	---	1.6	
B	F	3	---	---	---	---	
		4	---	---	---	1.6	
CS	30	44.7	---	---	---	5.3	Total

Wtd avg: 1. 8.6 0.1 0.5 0.2 3.1 12.5
 2. 2.1 --- 0.5 --- 2.7 5.3

1. Weighted average including CS

2. Weighted average excluding CS

Table A2.12. Group maceral composition of lithotypes, Glace Bay W seam section (E');
compiled from manual data.

LITHO- TYPE	mm	VITRINITE	LIPTINITE	LOW INERTINITE	HIGH INERTINITE	(TOTAL INERTINITE	OTHER MIN. MAT.	PYRITE	
CS	F	30	45.1	4.6	3.4	10.2	(13.6)	25.9	10.8
	F	1	0.0	0.0	0.0	100.0	(100.0)	0.0	0.0
		40	45.1	4.6	3.4	10.2	(13.6)	25.9	10.8
	BB	13	70.0	5.0	0.0	6.7	(6.7)	13.3	5.0
	D	44	39.0	5.4	1.5	14.1	(15.6)	20.0	20.0
B	DB	26	55.7	5.7	0.8	13.1	(13.9)	22.1	2.5
		11	77.8	6.1	1.0	10.1	(11.1)	3.2	1.8
	F	1	0.0	0.0	0.0	100.0	(100.0)	0.0	0.0
	F	90	77.8	6.1	1.0	10.1	(11.1)	3.2	1.8
	F	3	20.0	0.0	0.0	80.0	(80.0)	0.0	0.0
		49	77.8	6.1	1.0	10.1	(11.1)	3.2	1.8
	F	5	0.0	0.0	0.0	90.0	(90.0)	0.0	10.0
	DB	120	51.0	8.3	13.7	24.0	(37.7)	2.7	0.3
	B	60	76.7	5.7	3.0	13.0	(16.0)	0.3	1.3
	D	20	24.2	26.4	4.4	41.8	(46.2)	3.3	0.0
	DB	16	52.0	29.3	5.3	12.0	(17.3)	0.0	1.3
	B	9	84.1	9.1	0.0	4.5	(4.5)	2.3	0.0
	DB	18	50.0	19.3	6.8	12.5	(19.3)	5.7	5.7
	BB	15	84.3	5.7	0.0	2.9	(2.9)	0.0	7.1
	DB	15	45.9	33.8	6.8	9.5	(16.2)	0.0	4.1
B		13	77.1	12.5	1.5	3.0	(4.4)	0.7	5.2
	F	1	40.0	0.0	0.0	60.0	(60.0)	0.0	0.0
		42	77.1	12.5	1.5	3.0	(4.4)	0.7	5.2
	DB	52	61.4	18.7	2.4	6.0	(8.4)	4.4	7.2
	CS	130	34.8	6.9	0.0	0.0	(0.0)	55.7	2.6
DB	F	1	20.0	20.0	0.0	60.0	(60.0)	0.0	0.0
	B	17	68.3	15.9	1.2	14.6	(15.9)	0.0	0.0
	F	2	25.0	12.5	0.0	62.5	(62.5)	0.0	0.0
	BB	17	72.9	12.9	1.2	11.8	(12.9)	0.0	1.2
	F	5	4.8	4.8	0.0	90.5	(90.5)	0.0	0.0
		5	60.7	23.1	2.9	12.8	(15.7)	0.0	0.6
	F	2	25.0	0.0	0.0	75.0	(75.0)	0.0	0.0
		30	60.7	23.1	2.9	12.8	(15.7)	0.0	0.6
	BB	13	82.8	4.7	6.3	6.3	(12.5)	0.0	0.0
	B	14	71.4	10.0	1.4	17.1	(18.6)	0.0	0.0
B	F	2	10.0	0.0	0.0	90.0	(90.0)	0.0	0.0
	BB	19	76.1	17.4	3.3	3.3	(6.5)	0.0	0.0
		21	71.6	15.3	2.3	10.2	(12.6)	0.0	0.5
	F	1	20.0	0.0	0.0	80.0	(80.0)	0.0	0.0
		23	71.6	15.3	2.3	10.2	(12.6)	0.0	0.5

Table A2.12. Group maceral composition of lithotypes, Glace Bay W seam section (E');
compiled from manual data (con't).

LITHO- TYPE	mm	VITRINITE	LIPTINITE	LOW INERTINITE	HIGH INERTINITE	(TOTAL INERTINITE)	OTHER MIN. MAT.	PYRITE	
DB	21	49.5	27.6	12.4	8.6	(21.0)	0.0	1.9	
F	1	20.0	0.0	0.0	80.0	(80.0)	0.0	0.0	
PY	22	72.0	11.7	2.9	11.3	(14.2)	0.0	2.1	
	2	30.0	20.0	0.0	20.0	(20.0)	0.0	30.0	
B	14	72.0	11.7	2.9	11.3	(14.2)	0.0	2.1	
	F	1	0.0	0.0	0.0	100.0	(100.0)	0.0	0.0
F	61	72.0	11.7	2.9	11.3	(14.2)	0.0	2.1	
	1	0.0	0.0	0.0	100.0	(100.0)	0.0	0.0	
BB	19	76.1	8.0	3.3	11.3	(14.6)	0.5	0.9	
	F	1	0.0	0.0	0.0	100.0	(100.0)	0.0	0.0
F	24	76.1	8.0	3.3	11.3	(14.6)	0.5	0.9	
	7	78.4	4.2	4.9	10.4	(15.4)	0.6	1.5	
F	2	22.2	11.1	66.7	0.0	(66.7)	0.0	0.0	
	4	78.4	4.2	4.9	10.4	(15.4)	0.6	1.5	
F	2	0.0	0.0	10.0	90.0	(100.0)	0.0	0.0	
	10	78.4	4.2	4.9	10.4	(15.4)	0.6	1.5	
B	F	3	27.3	18.2	0.0	54.5	(54.5)	0.0	0.0
	F	9	78.4	4.2	4.9	10.4	(15.4)	0.6	1.5
F	3	0.0	0.0	0.0	100.0	(100.0)	0.0	0.0	
	57	78.4	4.2	4.9	10.4	(15.4)	0.6	1.5	
F	3	0.0	0.0	16.7	83.3	(100.0)	0.0	0.0	
	3	78.4	4.2	4.9	10.4	(15.4)	0.6	1.5	
F	1	0.0	0.0	0.0	100.0	(100.0)	0.0	0.0	
	22	78.4	4.2	4.9	10.4	(15.4)	0.6	1.5	
DB	27	54.9	11.3	18.8	12.8	(31.6)	0.8	1.5	
BB	26	83.3	4.8	1.6	8.7	(10.3)	0.0	1.6	
B	18	76.4	5.6	2.2	5.6	(7.9)	1.1	9.0	
DB	7	72.7	6.1	1.0	13.1	(14.1)	3.0	4.0	
	F	1	20.0	20.0	0.0	60.0	(40.0)	0.0	0.0
F	13	72.7	6.1	1.0	13.1	(14.1)	3.0	4.0	
	31	83.6	4.4	6.0	4.4	(10.4)	0.0	1.6	
B	F	1	0.0	0.0	0.0	100.0	(100.0)	0.0	0.0
	F	3	83.6	4.4	6.0	4.4	(10.4)	0.0	1.6
F	3	30.0	0.0	0.0	70.0	(70.0)	0.0	0.0	
	4	83.6	4.4	6.0	4.4	(10.4)	0.0	1.6	
CS	30	41.3	2.7	2.7	3.3	(6.0)	44.7	5.3	
Wtd avg:	1.	61.7	9.5	3.9	12.3	(16.2)	9.4	3.1	
	2.	65.8	10.3	4.4	14.4	(18.8)	2.6	2.7	
	3.	69.5	10.7	4.6	15.2	(19.9)			

1. Weighted average including CS

2. Weighted average excluding CS

3. Weighted average, mineral matter free (mmf), excluding CS

Table A2.13a. Compositional summary of bright banded (BB) lithotypes, Glace Bay W seam section - compiled from manual data.

LITHO- TYPE	mm	VITRINITE	LIPTINITE	LOW INERTINITE	HIGH INERTINITE	(TOTAL INERTINITE	OTHER MIN. MAT.	PYRITE
BB	13	70.0	5.0	0.0	6.7	(6.7)	13.3	5.0
BB	15	84.3	5.7	0.0	2.9	(2.9)	0.0	7.1
BB	17	72.9	12.9	1.2	11.8	(12.9)	0.0	1.2
BB	13	82.8	4.7	6.3	6.3	(12.5)	0.0	0.0
BB	19	76.1	17.4	3.3	3.3	(6.5)	0.0	0.0
BB	43	76.1	8.0	3.3	11.3	(14.6)	0.5	0.9
BB	26	83.3	4.8	1.6	8.7	(10.3)	0.0	1.6
Wtd Avg	146	77.9	8.4	2.4	8.1	(10.5)	1.3	1.9
(mmf)		80.5	8.7	2.4	8.4	(10.8)		

Table A2.13b. Compositional summary of banded (B) lithotypes, Glace Bay W seam section - compiled from manual data.

LITHO- TYPE	mm	VITRINITE	LIPTINITE	LOW INERTINITE	HIGH INERTINITE	(TOTAL INERTINITE	OTHER MIN. MAT.	PYRITE
B	150	77.8	6.1	1.0	10.1	(11.1)	3.2	1.8
B	60	76.7	5.7	3.0	13.0	(16.0)	0.3	1.3
B	9	84.1	9.1	0.0	4.5	(4.5)	2.3	0.0
B	55	77.1	12.5	1.5	3.0	(4.4)	0.7	5.2
B	17	68.3	15.9	1.2	14.6	(15.9)	0.0	0.0
B	14	71.4	10.0	1.4	17.1	(18.6)	0.0	0.0
B	44	71.6	15.3	2.3	10.2	(12.6)	0.0	0.5
B	97	72.0	11.7	2.9	11.3	(14.2)	0.0	2.1
B	112	78.4	4.2	4.9	10.4	(15.4)	0.6	1.5
B	18	76.4	5.6	2.2	5.6	(7.9)	1.1	9.0
B	38	83.6	4.4	6.0	4.4	(10.4)	0.0	1.6
Wtd Avg	614	76.4	8.1	2.7	9.7	(12.4)	1.0	2.0
(mmf)		78.8	8.4	2.8	10.0	(12.8)		

mmf - calculated on a mineral matter free basis

Table A2.13c. Compositional summary of dull banded (DB) lithotypes, Glace Bay W seam section - compiled from manual data.

LITHO- TYPE	mm	VITRINITE	LIPTINITE	LOW INERTINITE	HIGH INERTINITE	(TOTAL INERTINITE)	OTHER MIN. MAT.	PYRITE
DB	26	55.7	5.7	0.8	13.1	(13.9)	22.1	2.5
DB	120	51.0	8.3	13.7	24.0	(37.7)	2.7	0.3
DB	16	52.0	29.3	5.3	12.0	(17.3)	0.0	1.3
DB	18	50.0	19.3	6.8	12.5	(19.3)	5.7	5.7
DB	15	45.9	33.8	6.8	9.5	(16.2)	0.0	4.1
DB	52	61.4	18.7	2.4	6.0	(8.4)	4.4	7.2
DB	35	60.7	23.1	2.9	12.8	(15.7)	0.0	0.6
DB	21	49.5	27.6	12.4	8.6	(21.0)	0.0	1.9
DB	27	54.9	11.3	18.8	12.8	(31.6)	0.8	1.5
DB	20	72.7	6.1	1.0	13.1	(14.1)	3.0	4.0
Wtd Avg	350	55.1	15.0	8.5	15.2	(23.7)	3.7	2.4
(mmf)		58.7	16.0	9.1	16.2	(25.3)		

Table A2.13d. Compositional summary of dull (D) lithotypes, Glace Bay W seam section - compiled from manual data.

LITHO- TYPE	mm	VITRINITE	LIPTINITE	LOW INERTINITE	HIGH INERTINITE	(TOTAL INERTINITE)	OTHER MIN. MAT.	PYRITE
D	44	39.0	5.4	1.5	14.1	(15.6)	20.0	20.0
D	20	24.2	26.4	4.4	41.8	(46.2)	3.3	0.0
Wtd Avg	64	34.4	11.9	2.4	22.8	(25.2)	14.8	13.8
(mmf)		48.1	16.7	3.3	31.9	(35.2)		

mmf - calculated on a mineral matter free basis

Table A2.13e. Compositional summary of fusain (F) layers, Glace Bay W seam section - compiled from manual data.

LITHO- TYPE	mm	VITRINITE	LIPTINITE	LOW INERTINITE	HIGH INERTINITE	(TOTAL INERTINITE)	OTHER MIN. MAT.	PYRITE
F	1	0.0	0.0	0.0	100.0	(100.0)	0.0	0.0
F	1	0.0	0.0	0.0	100.0	(100.0)	0.0	0.0
F	3	20.0	0.0	0.0	80.0	(80.0)	0.0	0.0
F	5	0.0	0.0	0.0	90.0	(90.0)	0.0	10.0
F	1	40.0	0.0	0.0	60.0	(60.0)	0.0	0.0
F	1	20.0	20.0	0.0	60.0	(60.0)	0.0	0.0
F	2	25.0	12.5	0.0	62.5	(62.5)	0.0	0.0
F	5	4.8	4.8	0.0	90.5	(90.5)	0.0	0.0
F	2	25.0	0.0	0.0	75.0	(75.0)	0.0	0.0
F	2	10.0	0.0	0.0	90.0	(90.0)	0.0	0.0
F	1	20.0	0.0	0.0	80.0	(80.0)	0.0	0.0
F	1	20.0	0.0	0.0	80.0	(80.0)	0.0	0.0
F	1	0.0	0.0	0.0	100.0	(100.0)	0.0	0.0
F	1	0.0	0.0	0.0	100.0	(100.0)	0.0	0.0
F	1	0.0	0.0	0.0	100.0	(100.0)	0.0	0.0
F	2	22.2	11.1	66.7	0.0	(66.7)	0.0	0.0
F	2	0.0	0.0	10.0	90.0	(100.0)	0.0	0.0
F	3	27.3	18.2	0.0	54.5	(54.5)	0.0	0.0
F	3	0.0	0.0	0.0	100.0	(100.0)	0.0	0.0
F	3	0.0	0.0	16.7	83.3	(100.0)	0.0	0.0
F	1	0.0	0.0	0.0	100.0	(100.0)	0.0	0.0
F	1	20.0	20.0	0.0	60.0	(60.0)	0.0	0.0
F	1	0.0	0.0	0.0	100.0	(100.0)	0.0	0.0
F	3	30.0	0.0	0.0	70.0	(70.0)	0.0	0.0
Wtd Avg	47	11.5	3.5	4.3	79.6	(83.9)	0.0	1.1
(mmf)		11.6	3.6	4.4	80.5	(84.8)		

Table A2.13f. Compositional summary of coaly shales (CS) and pyrite (PY) layers, Glace Bay W seam section - compiled from manual data.

LITHO- TYPE	mm	VITRINITE	LIPTINITE	LOW INERTINITE	HIGH INERTINITE	(TOTAL INERTINITE)	OTHER MIN. MAT.	PYRITE
CS	70	45.1	4.6	3.4	10.2	(13.6)	25.9	10.8
CS	130	34.8	6.9	0.0	0.0	(0.0)	55.7	2.6
CS	30	41.3	2.7	2.7	3.3	(6.0)	44.7	5.3
Wtd Avg	230	38.8	5.7	1.4	3.5	(4.9)	45.1	5.5
PY	2	30.0	20.0	0.0	20.0	(20.0)	0.0	30.0

mmf - calculated on a mineral matter free basis

Table A2.13g. Weighted average composition for all lithotypes; Glace Bay W seam section - compiled from manual data.

LITHO- TYPE	mm	n=	Vol %		VITRINITE	LIPTINITE	LOW INERTINITE	HIGH INERTINITE	TOTAL INERTINITE	MINERAL MATTE	
			1	2						PYRITE	OTHER
BB	146	7	10.0	11.9	77.9	8.4	2.4	8.1	(10.5)	1.9	1.3
B	614	11	42.3	50.2	76.4	8.1	2.7	9.7	(12.4)	2.0	1.0
DB	350	10	24.1	28.6	55.1	15.0	8.5	15.2	(23.7)	2.4	3.7
D	64	2	4.4	5.2	34.4	11.9	2.4	22.8	(25.2)	13.8	14.8
F	47	24	3.2	3.8	11.5	3.5	4.3	79.6	(83.9)	1.1	0.0
PY	2	1	0.1	0.2	30.0	20.0	0.0	20.0	(20.0)	30.0	0.0
CS	230	2	15.8		38.8	5.7	1.4	3.5	(4.9)	5.5	45.1

1. Volume % of lithotype in seam (including CS) - 1453 mm

2. Volume % of lithotype in seam (excluding CS) - 1223 mm

Table A2.13h. Group maceral composition of lithotype intervals, Glace Bay W seam section (E'); compiled from manual data.

SEAM INTERVAL	mm	VITRINITE	LIPTINITE	LOW INERTINITE	HIGH INERTINITE	TOTAL INERTINITE	OTHER MIN MAT	PYRITE
IX	71.0	44.4	4.6	3.4	11.5	(14.8)	25.6	10.7
VIII	83.0	49.1	5.4	1.0	12.7	(13.7)	6.9	0.8
(VII)	not present					()		
VI	339.0	66.2	6.7	5.8	17.6	(23.4)	2.4	1.3
V	20.0	24.2	26.4	4.4	41.8	(46.2)	3.3	0.0
IV	181.0	65.8	17.4	2.8	6.5	(9.3)	2.2	5.2
III	130.0	34.8	6.9	---	---	(---)	55.7	2.6
II	194.0	64.1	16.3	3.4	15.7	(19.1)	--	0.5
I	435.0	69.5	6.8	4.8	13.0	(17.8)	3.5	2.3

Table A2.14. Summary of lithotype composition (weighted average) for each seam section; Sydney Mines (B); Victoria Mines (C); Glace Bay W (E-IBAS; E'-manual).

SECTION	LITHO-TYPE	Vol %		VITRINITE	LIPTINITE	LOW INERTINITE	HIGH INERTINITE	(TOTAL INERTINITE)	MINERAL MATTER	
		1	2						PYRITE	OTHER
B	BR	0.4	0.5	89.72	2.94	6.60	0.47	(7.08)	0.26	nm
C	BR	0.0	0.0	---	---	---	---	---	---	---
E	BR	0.0	0.0	---	---	---	---	---	---	---
E'	BR	0.0	0.0	---	---	---	---	---	---	---
B	BB	13.8	15.0	88.65	5.38	5.02	0.64	(5.67)	0.30	nm
C	BB	22.4	24.9	86.27	6.69	5.04	1.30	(6.34)	0.70	nm
E	BB	9.9	11.8	88.66	5.98	4.28	0.77	(5.05)	0.31	nm
E'	BB	10.0	11.9	77.9	8.4	2.4	8.1	(10.5)	1.9	1.3
B	B	51.3	55.9	80.38	10.89	7.16	1.03	(8.19)	0.53	nm
C	B	40.7	45.2	81.88	8.84	6.41	1.85	(8.26)	1.02	nm
E	B	41.8	49.9	83.50	7.66	6.71	1.46	(8.17)	0.68	nm
E'	B	42.3	50.2	76.4	8.1	2.7	9.7	(12.4)	2.0	1.0
B	DB	21.8	23.8	61.60	17.80	17.52	2.45	(19.97)	0.63	nm
C	DB	16.9	18.7	63.98	8.14	19.46	5.71	(25.17)	2.71	nm
E	DB	24.5	29.3	67.79	13.60	15.26	2.56	(17.83)	0.78	nm
E'	DB	24.1	28.6	55.1	15.0	8.5	15.2	(23.7)	2.4	3.7
B	D	1.9	2.0	34.36	24.71	37.90	2.36	(40.26)	0.57	nm
C	D	5.0	5.5	48.29	11.78	33.49	4.55	(38.04)	1.89	nm
E	D	4.3	5.1	39.99	23.06	25.13	9.79	(34.92)	2.03	nm
E'	D	4.4	5.2	34.4	11.9	2.4	22.8	(25.2)	13.8	14.8
B	F	2.5	2.7	30.41	16.97	40.53	10.39	(50.91)	1.70	nm
C	F	2.5	2.8	36.31	22.60	33.54	5.28	(38.82)	2.27	nm
E	F	3.1	3.7	24.76	40.46	21.64	11.13	(32.76)	2.02	nm
E'	F	3.2	3.8	11.5	3.5	4.3	79.6	(83.9)	1.1	0.0
B	CS	8.3	0.0	na	na	na	na	na	na	nm
C	CS	10.0	0.0	na	na	na	na	na	na	nm
E	CS	16.2	0.0	na	na	na	na	na	na	nm
E'	CS	15.8	0.0	38.8	5.7	1.4	3.5	(4.9)	5.5	45.1
B	PY	0.0	0.0	---	---	---	---	---	---	nm
C	PY	2.6	2.9	43.05	7.30	22.28	18.08	(40.36)	9.29	nm
E	PY	0.2	0.2	53.26	13.52	16.70	10.40	(27.10)	6.11	nm
E'	PY	0.1	0.2	30.0	20.0	0.0	20.0	(20.0)	30.0	0.0

--- not present

na lithotype present but not analysed

nm not measured by the analytical technique

Vol % 1. Volume % including CS

Vol % 2. Volume % excluding CS

Microlithotype composition of
Glance Bay W seam section (manual data)

Abbreviations for the Tables to follow:

MICROLITHOTYPES:

Monomaceral:

V - Vitrite (> 95% vitrinite)
 L - Liptite (> 95% liptinite)
 I - Inertite (> 95% inertinite)

Bimaceral:

V+L - Clarite (vitrinite, liptinite)
 I+L - Durite (inertinite, liptinite)
 V+I - Vitrinertite (vitrinite, inertinite)

Trimaceral:

V>I+L - Duroclarite (VITRINITE, liptinite, inertinite)
 I>V+L - Clarodurite (INERTINITE, vitrinite, liptinite)
 L>V+I - Vitrinertoliptite (LIPTINITE, vitrinite, inertinite)

Carbominerite:

Car - Carbaergilite (20 - 60% clays)
 Can - Carbankerite (20 - 60% carbonates)
 Csi - Carbosilicate (20 - 60% quartz)
 Cpy - Carbopyrite (5 - 20% pyrite)
 Coth- Other minerals present in quantities ranging from 20 - 60%

Mineral Matter:

Ar - Argilite (>60% clays)
 An - Ankerite (> 60% carbonates)
 Si - Silicate (> 60% quartz)
 Py - Pyrite (> 20% pyrite)
 Oth- Other minerals present in quantities greater than 60%

Note: Capital letters indicates predominant maceral in trimaceral microlithotypes

Table A2.15a. Microlithotype composition of lithotypes, Glace Bay W seam section - compiled from manual data.

LITHO- TYPE	mm	MONO			BI			TRI			
		V	L	I	V+L	I+L	V+I	V>I+L	I>V+L	L>V+I	
CS	F	30	15.1	---	2.2	7.4	---	15.4	9.3	---	---
	F	1	---	---	100.0	---	---	---	---	---	---
	F	40	15.1	---	2.2	7.4	---	15.4	9.3	---	---
	BB	13	41.7	---	---	5.0	---	15.0	3.3	---	---
	D	44	13.9	---	2.9	5.8	---	4.3	6.7	---	0.5
B	DB	26	18.9	---	6.6	14.8	---	5.7	7.4	---	---
	F	11	38.1	---	3.6	17.6	---	14.8	16.0	1.0	0.6
	F	1	---	---	100.0	---	---	---	---	---	---
	F	90	38.1	---	3.6	17.6	---	14.8	16.0	1.0	0.6
	F	3	---	---	70.0	10.0	---	20.0	---	---	---
	F	49	38.1	---	3.6	17.6	---	14.8	16.0	1.0	0.6
	F	5	---	---	90.0	---	---	---	---	---	---
	DB	120	24.7	---	24.0	10.3	4.7	11.3	15.7	4.3	0.3
	B	60	35.0	---	10.0	22.0	0.3	12.0	15.0	0.3	0.3
	D	20	4.4	---	26.4	5.5	17.6	2.2	23.1	---	14.3
	DB	16	22.7	---	4.0	18.7	5.3	6.7	24.0	6.7	10.7
	B	9	40.9	---	---	20.5	---	11.4	18.2	---	2.3
	DB	18	11.4	---	5.7	20.5	2.3	3.4	38.6	1.1	2.3
	BB	15	61.4	---	---	15.7	---	2.9	10.0	---	---
	DB	15	17.6	---	5.4	18.9	14.9	---	14.9	13.5	2.7
B	F	13	36.2	1.1	1.8	32.1	---	3.3	9.6	---	---
	F	1	20.0	---	60.0	---	---	20.0	---	---	---
	F	42	36.2	1.1	1.8	32.1	---	3.3	9.6	---	---
	DB	52	24.7	---	1.2	31.5	---	1.6	16.7	---	0.8
	CS	130	12.0	---	---	4.6	---	---	---	---	---
	F	1	---	---	40.0	20.0	---	40.0	---	---	---
	B	17	29.3	1.2	4.9	24.4	---	3.7	34.1	---	---
	F	2	---	---	62.5	25.0	---	---	12.5	---	---
	BB	17	30.6	---	2.4	27.1	---	9.4	27.1	---	---
	F	5	---	---	81.0	4.8	---	4.8	9.5	---	---
DB	F	5	25.4	---	2.3	22.0	4.6	5.2	28.9	2.3	8.1
	F	2	---	---	50.0	---	---	50.0	---	---	---
	F	30	25.4	---	2.3	22.0	4.6	5.2	28.9	2.3	8.1
	BB	13	54.7	---	1.6	18.8	---	6.3	14.1	---	---
	B	14	28.6	1.4	1.4	31.4	---	4.3	31.4	---	---
	F	2	10.0	---	60.0	---	---	0.0	0.0	30.0	---
	BB	19	35.9	---	---	21.7	---	4.3	31.5	1.1	4.3
	F	21	27.9	---	2.8	31.6	1.4	7.4	27.0	---	0.5
B	F	1	---	---	80.0	20.0	---	---	---	---	---
	F	23	27.9	---	2.8	31.6	1.4	7.4	27.0	---	0.5

Table A2.15a. Microlithotype composition of lithotypes, Glace Bay W seam section - compiled from manual data (con't).

LITHO- TYPE	mm	MONO			BI			TRI		
		V	L	I	V+L	I+L	V+I	V>I+L	I>V+L	L>V+I
DB	21	19.0	---	8.6	17.1	1.9	2.9	29.5	9.5	6.7
F	1	---	---	60.0	---	---	40.0	---	---	---
B	22	37.9	---	2.1	16.3	0.4	14.4	23.5	0.6	0.6
	PY	2	---	---	30.0	---	10.0	---	---	---
B	14	37.9	---	2.1	16.3	0.4	14.4	23.5	0.6	0.6
	F	1	---	---	66.7	---	33.3	---	---	---
B	61	37.9	---	2.1	16.3	0.4	14.4	23.5	0.6	0.6
	F	1	---	---	100.0	---	---	---	---	---
BB	19	39.9	0.9	1.4	10.3	---	15.0	29.6	---	---
	F	1	---	---	100.0	---	---	---	---	---
B	24	39.9	0.9	1.4	10.3	---	15.0	29.6	---	---
	F	7	39.3	---	3.6	10.0	---	18.8	24.6	0.2
B	F	2	---	---	55.6	---	22.2	22.2	---	---
	F	4	39.3	---	3.6	10.0	---	18.8	24.6	0.2
B	F	2	---	---	100.0	---	---	---	---	---
	F	10	39.3	---	3.6	10.0	---	18.8	24.6	0.2
B	F	3	---	---	54.5	---	18.2	---	---	27.3
	F	9	39.3	---	3.6	10.0	---	18.8	24.6	0.2
B	F	3	---	---	100.0	---	---	---	---	---
	F	57	39.3	---	3.6	10.0	---	18.8	24.6	0.2
B	F	3	---	---	91.7	---	8.3	---	---	---
	F	3	39.3	---	3.6	10.0	---	18.8	24.6	0.2
B	F	1	---	---	100.0	---	---	---	---	---
	F	22	39.3	---	3.6	10.0	---	18.8	24.6	0.2
DB	27	18.0	---	11.3	6.0	---	33.8	24.8	2.3	---
BB	26	39.7	0.8	---	11.9	---	25.4	15.1	---	---
B	B	18	37.5	---	2.3	8.0	---	13.6	20.5	---
	F	7	20.2	---	3.0	10.1	---	37.4	18.2	---
DB	F	1	20.0	---	60.0	---	---	20.0	---	---
	F	13	20.2	---	3.0	10.1	---	37.4	18.2	---
B	F	31	54.1	---	3.8	9.8	---	17.5	8.7	---
	F	1	---	---	100.0	---	---	---	---	---
B	F	3	54.1	---	3.8	9.8	---	17.5	8.7	---
	F	3	20.0	---	60.0	---	---	10.0	---	---
B	F	4	54.1	---	3.8	9.8	---	17.5	8.7	---
	CS	30	26.0	0.7	2.7	7.3	---	4.0	2.7	0.7
Wtd avg	1.	28.5	0.1	7.1	14.6	1.1	10.7	16.3	1.1	1.0
	2.	30.9	0.1	8.6	16.2	1.3	11.7	18.7	1.2	1.2

1. Weighted average including CS

2. Weighted average excluding CS

Table A2.15b. Microlithotype composition of lithotypes, Glace Bay W seam section - compiled from manual data.

LITHO- TYPE	mm	CARBOMINERITE					MINERAL MATTER					
		Car	Can	Csi	Cpy	Coth	Ar	An	Si	Py	Oth	
CS	F	30	13.6	---	1.2	9.0	---	18.5	1.5	0.6	6.2	---
		1	---	---	---	---	---	---	---	---	---	
	40	13.6	---	1.2	9.0	---	18.5	1.5	0.6	6.2	---	
	BB	13	11.6	---	---	10.0	---	10.0	1.7	---	1.7	---
	D	44	22.6	---	0.5	13.9	---	11.5	---	---	17.3	---
B	DB	26	24.6	0.8	2.5	5.7	---	11.4	---	---	1.6	---
	F	11	1.5	0.1	1.1	2.6	---	1.2	---	0.4	1.2	---
		1	---	---	---	---	---	---	---	---	---	---
	F	90	1.5	0.1	1.1	2.6	---	1.2	---	0.4	1.2	---
	F	3	---	---	---	---	---	---	---	---	---	---
	F	49	1.5	0.1	1.1	2.6	---	1.2	---	0.4	1.2	---
	F	5	---	---	---	---	---	---	---	---	10.0	---
	DB	120	2.0	---	1.0	1.7	---	---	---	---	---	---
	B	60	0.3	0.3	0.7	3.3	---	---	---	---	0.3	---
	D	20	2.2	---	---	2.2	---	2.2	---	---	---	---
	DB	16	---	---	---	1.3	---	---	---	---	---	---
	B	9	4.5	---	2.3	---	---	---	---	---	---	---
	DB	18	4.5	---	---	4.5	---	2.3	---	---	3.4	---
	BB	15	---	---	---	5.7	---	---	---	---	4.3	---
	DB	15	---	---	---	10.8	---	---	---	---	1.4	---
B	F	13	0.4	---	1.5	10.3	---	---	---	---	3.7	---
		1	---	---	---	---	---	---	---	---	---	---
	42	0.4	---	1.5	10.3	---	---	---	---	3.7	---	
DB	52	7.2	---	---	10.8	---	2.4	---	---	3.2	---	
CS	130	25.7	---	---	---	---	57.1	---	---	0.6	---	
F	1	---	---	---	---	---	---	---	---	---	---	
B	17	---	---	---	2.4	---	---	---	---	---	---	
F	2	---	---	---	---	---	---	---	---	---	---	
BB	17	---	---	---	3.5	---	---	---	---	---	---	
F	5	---	---	---	---	---	---	---	---	---	---	
DB	F	5	---	---	---	1.2	---	---	---	---	---	---
		2	---	---	---	---	---	---	---	---	---	---
	30	---	---	---	1.2	---	---	---	---	---	---	
	BB	13	---	---	---	3.1	---	---	---	---	1.6	---
	B	14	---	---	---	---	---	---	---	---	1.4	---
F	2	---	---	---	---	---	---	---	---	---	---	
BB	19	---	---	---	1.1	---	---	---	---	---	---	
B	F	21	---	---	---	0.9	---	---	---	---	0.5	---
		1	---	---	---	---	---	---	---	---	---	---
		23	---	---	---	0.9	---	---	---	---	0.5	---

Table A2.15b. Microlithotype composition of lithotypes, Glace Bay W seam section -
compiled from manual data (con't).

LITHO- TYPE	mm	CARBONIFEROUS					MINERAL MATTER				
		Car	Can	Csi	Cpy	Coth	Ar	An	Si	Py	Oth
DB	21	---	---	---	2.9	---	---	---	---	1.9	---
F	1	---	---	---	---	---	---	---	---	---	---
	22	---	---	---	2.9	---	---	---	---	1.3	---
PY	2	---	---	---	40.0	---	---	---	---	20.0	---
B	14	---	---	---	2.9	---	---	---	---	1.3	---
F	1	---	---	---	---	---	---	---	---	---	---
	61	---	---	---	2.9	---	---	---	---	1.3	---
F	1	---	---	---	---	---	---	---	---	---	---
BB	19	---	---	---	1.9	---	---	---	0.5	0.5	---
F	1	---	---	---	---	---	---	---	---	---	---
	24	---	---	---	1.9	---	---	---	0.5	0.5	---
	7	---	---	0.4	2.4	---	---	---	0.2	0.6	---
F	2	---	---	---	---	---	---	---	---	---	---
	4	---	---	0.4	2.4	---	---	---	0.2	0.6	---
F	2	---	---	---	---	---	---	---	---	---	---
	10	---	---	0.4	2.4	---	---	---	0.2	0.6	---
F	3	---	---	---	---	---	---	---	---	---	---
B	9	---	---	0.4	2.4	---	---	---	0.2	0.6	---
F	3	---	---	---	---	---	---	---	---	---	---
	57	---	---	0.4	2.4	---	---	---	0.2	0.6	---
F	3	---	---	---	---	---	---	---	---	---	---
	3	---	---	0.4	2.4	---	---	---	0.2	0.6	---
F	1	---	---	---	---	---	---	---	---	---	---
	22	---	---	0.4	2.4	---	---	---	0.2	0.6	---
DB	27	1.5	---	0.8	0.8	---	---	---	---	---	---
BB	26	---	---	---	7.1	---	---	---	---	---	---
B	18	---	---	1.1	13.6	---	---	---	---	3.4	---
	7	---	---	2.0	8.1	---	---	---	---	1.0	---
DB	1	---	---	---	---	---	---	---	---	---	---
	13	---	---	2.0	8.1	---	---	---	---	1.0	---
	31	---	---	---	5.5	---	---	---	---	0.5	---
F	1	---	---	---	---	---	---	---	---	---	---
B	3	---	---	---	5.5	---	---	---	---	0.5	---
F	3	---	---	---	---	---	---	---	---	10.0	---
	4	---	---	---	5.5	---	---	---	---	0.5	---
CS	30	6.7	---	---	6.7	---	38.0	---	---	4.0	---
Wtd avg:	1.	5.1	0.1	0.5	4.0	---	7.8	0.1	0.1	1.8	---
	2.	2.4	0.1	0.5	4.1	---	1.1	---	0.1	1.7	---

1. Weighted average including CS

2. Weighted average excluding CS

Table A2.16d. Microlithotype summary of dull (D) lithotypes, Glace Bay W seam section - compiled from manual data.

LITHOTYPE:		D	D	Wtd Avg
MICRO-				
LITHOTYPE	mm	44	20	64
	V	13.9	4.4	11.0
MONO	L	0.0	0.0	0.0
	I	2.9	26.4	10.2
	V+L	5.8	5.5	5.7
BI	I+L	0.0	17.6	5.5
	V+I	4.3	2.2	3.7
	V>I+L	6.7	23.1	11.8
TRI	I>V+L	0.0	0.0	0.0
	L>V+I	0.5	14.3	4.8
	Car	22.6	2.2	16.3
	Can	0.0	0.0	0.0
CARBO-	Csi	0.5	0.0	0.3
MINERITE	Cpy	13.9	2.2	10.3
	Coth	0.0	0.0	0.0
	Ar	11.5	2.2	8.6
	An	0.0	0.0	0.0
MINERAL	Si	0.0	0.0	0.0
MATTER	Py	17.3	0.0	11.9
	Oth	0.0	0.0	0.0

Table A2.16f. Microlithotype summary of coaly shales (CS) and pyrite (PY) layers, Glace Bay W seam section - compiled from manual data.

LITHOTYPE:		CS	CS	CS	Wtd Avg	PY
MICRO-						
LITHOTYPE	mm	70	130	30	230	2
	V	15.1	12.0	26.0	14.8	0.0
MONO	L	0.0	0.0	0.7	0.1	0.0
	I	2.2	0.0	2.7	1.0	0.0
	V+L	7.4	4.6	7.3	5.8	30.0
BI	I+L	0.0	0.0	0.0	0.0	0.0
	V+I	15.4	0.0	4.0	5.2	10.0
	V>I+L	9.3	0.0	2.7	3.2	0.0
TRI	I>V+L	0.0	0.0	0.7	0.1	0.0
	L>V+I	0.0	0.0	0.7	0.1	0.0
	Car	13.6	25.7	6.7	19.5	0.0
	Can	0.0	0.0	0.0	0.0	0.0
CARBO-	Csi	1.2	0.0	0.0	0.4	0.0
MINERITE	Cpy	9.0	0.0	6.7	3.6	40.0
	Coth	0.0	0.0	0.0	0.0	0.0
	Ar	18.5	57.1	38.0	42.9	0.0
	An	1.5	0.0	0.0	0.5	0.0
MINERAL	Si	0.6	0.0	0.0	0.2	0.0
MATTER	Py	6.2	0.6	4.0	2.8	20.0
	Oth	0.0	0.0	0.0	0.0	0.0

APPENDIX 3

Backpit Roof Unit -
Sample Collection and Analysis

A3. Contents	Page
A3.1. Sample Collection - Analysis	239
A3.2. Ash and Sulphur Analyses	239
A3.3. Microscopy	
A3.3.1. Thin section Petrography	241
A3.3.2. Maceral/Mineral Composition	241
A3.4. Rock-Eval Pyrolysis	241
A3.5. Fossil Concentration	242

List of Figures

Figure A3.1. Flow chart for Backpit roof unit (BRU) analyses.	240
Figure A3.2. Schematic of a pyrogram illustrating the evolution of S_1 , S_2 , S_3 and T_{max} values through time.	243

List of Tables

Table A3.1. Compositional estimates of the BRU from core C-136, based on thin section analyses.	246
Table A3.2. Compositional estimates of the BRU from core C-137, based on thin section analyses.	247
Table A3.3. Detailed maceral analysis, BRU - Sydney Mines section.	248
Table A3.4. Detailed maceral analysis (mineral matter free), BRU - Sydney Mines section.	249
Table A3.5. Detailed maceral analysis, BRU - Glace Bay West section.	250
Table A3.6. Detailed maceral analysis (mineral matter free), BRU - Glace Bay West section.	251
Table A3.7. Parameters measured directly by Rock-Eval pyrolysis.	252
Table A3.8. Parameters calculated from Rock-Eval pyrolysis.	252

Table A3.9. Rock-Eval data for each BRU outcrop sample and the calculated weighted average for each coastal section studied.	253
Table A3.10. Rock-Eval data - BRU from core C-136 and the weighted average for the section.	254
Table A3.11. Rock-Eval data - BRU from core C-137 and the weighted average for the section.	255
Table A3.12. Duplicate Rock-Eval analyses - BRU.	256
Table A3.13. A review of some fossil fauna reported in the Morien Group.	257

A3.1. Sample Collection - Analysis

The Backpit roof unit (BRU) was sampled in detail at the following locations (refer to Fig. 1.2 in text):

- A. Bras d'Or
- B. Sydney Mines
- C. Victoria Mines
- E. Glace Bay West
- G. Donkin West
- H. Donkin East
- J. Longbeach
- *. CBDC core C-136
- x. CBDC core C-137

Oriented samples were collected from each coastal section and provide a complete vertical record of this unit across the study area. Each sample was slabbed and a detailed facies analysis completed (refer to '1' in Figure A3.1). The roof strata from two Cape Breton Development Corporation (CBDC) cores (C-136 and C-137) were also slabbed and facies described (Plates 6 and 7). Vertical compositional variations were documented using thin section petrography. Subsamples were taken for ash, sulphur and Rock-Eval pyrolysis (refer to '2' in Fig. A3.1).

Two kilogram bulk channel samples were also collected from 1 to 30 cm thick vertical intervals at each coastal section. These samples were analysed as outlined in '3', Figure A3.1. Subsamples were pulverized and analysed for ash, sulphur and Rock-Eval pyrolysis. Detailed microfossil content of a series of vertical intervals was determined for the Sydney Mines (B) and Glace Bay West (E) roof sections. The maceral composition of the roof strata was also determined from these intervals.

A3.2. Ash and Sulphur Analyses

Ash and sulphur analyses were completed at the CBDC Coal Laboratory in Sydney, Nova Scotia, following the

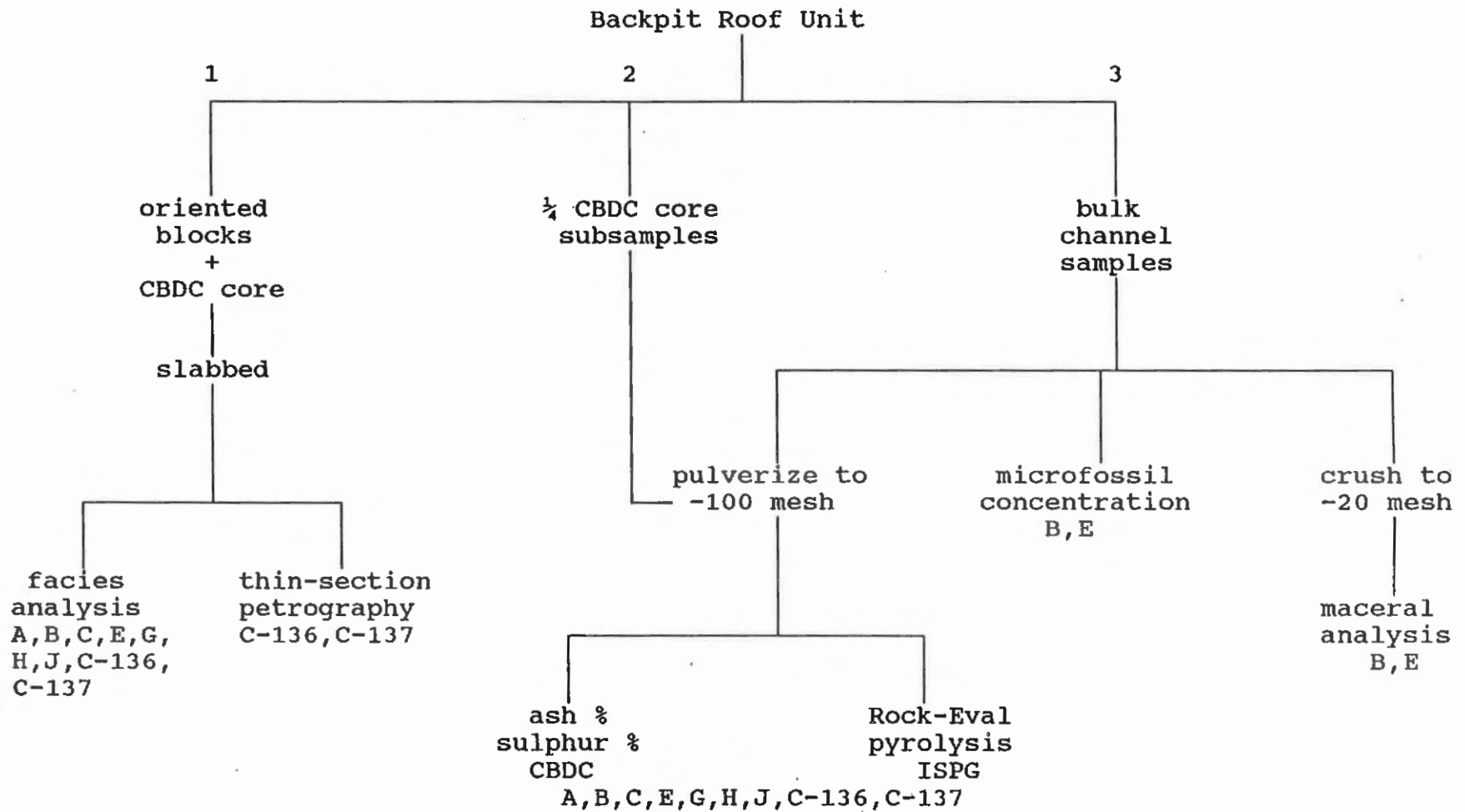


Figure A3.1. Flow chart for Backpit roof unit (BRU) analyses. A-Bras d'Or; B-Sydney Mines; C-Victoria Mines; E-Glace Bay West; G-Donkin West; H-Donkin East; J-Longbeach; C-136 and C-137 - offshore cores; CBDC-Cape Breton Development Corporation; ISPG-Institute of Sedimentary and Petroleum Geology.

procedure outlined in Appendix A2.2. Results are found in Table A2.1a.

A3.3. Microscopy

A3.3.1. Thin section Petrography

Thin sections were prepared from microfacies in the CBDC cores (refer to Plates 6 and 7) by Mr. Gordon Brown, Dalhousie University. Observations were made under plane- and cross-polarized light using a Leitz microscope. Compositional estimates of fossil groups, calcite and other grains were made according to the outline in Table A3.1. This method was favoured over point counting due to the finely interbedded nature of many samples and the abundance of bioclastic material (see Plate 9). Table A3.1 and A3.2 contain results of these estimates in tabular format.

A3.3.2. Maceral/Mineral Composition

Polished grain mount pellets were prepared from Backpit roof intervals from the Sydney Mines (B) and Glace Bay West (E) sections following the procedure outlined in Appendix A2.4.1. Maceral and mineral point count analyses were completed using both white and fluorescent light illumination on a Zeiss Universal petrographic microscope. A total of 300 points were counted from each sample with a stepping distance of 1 mm. Tables A3.3 to A3.6 contain compositional data from the samples analysed.

A3.4. Rock-Eval Pyrolysis

Variations in organic content of the BRU and its source rock potential were characterized by Rock-Eval pyrolysis. Pulverized samples were analysed using a Rock-Eval II pyrolysis instrument at the Institute of Sedimentary and Petroleum Geology in Calgary. Approximately 100 mg of sample was pyrolyzed in an inert atmosphere and a pyrogram was produced. Sample size was decreased for organic-rich

samples. The sample was heated from room temperature to 390 °C in four minutes, followed by programmed pyrolysis at 25 °C/minute to 600 °C.

Table A3.7 contains a list of parameters measured directly by this technique and their significance. Calculated parameters are contained in Table A3.8. Figure A3.2 is a schematic of a typical Rock-Eval pyrogram.

Each sample was analysed in duplicate and average parameters for coastal sections are reported in Table A3.9. Tables A3.10 and A3.11 contain detailed Rock-Eval data from CBDC core C-136 and C-137, respectively. Standards of known quality were analysed at set intervals to check the calibration of the instrument. In addition, several "unknown" duplicates were dispersed among the sample batch and the results are reported in Table A3.12. Total organic carbon content (TOC weight %) and Tmax (°C) values were highly reproducible (within 2%). Hydrocarbons (S₁, S₂ in mg HC/g rock) and carbon dioxide (S₃ in mg CO₂/g rock) were more variable, especially between subsamples (i.e. 1 and 2, Table A3.6). These values were generally reproducible within 10%.

A3.5. Fossil Concentration

Fossils were extracted from samples collected from specific vertical intervals from the Sydney Mines (B) and Glace Bay West (E) Backpit roof sections. Eight bulk samples were analysed by Mr. W.G. Parkins, Brock University, St. Catherines, Ontario by the following method. Approximately 2 kg of each sample was broken into 2 to 4 cm fragments and placed in a nylon screen bag. The bag was suspended in a bucket containing 10 l of 10 % acetic acid and left for one week. The solution in the bucket was then washed through a 150 mesh sieve and the residue was air dried at room temperature. The residue was then examined under a low powered microscope and any fossil remains were

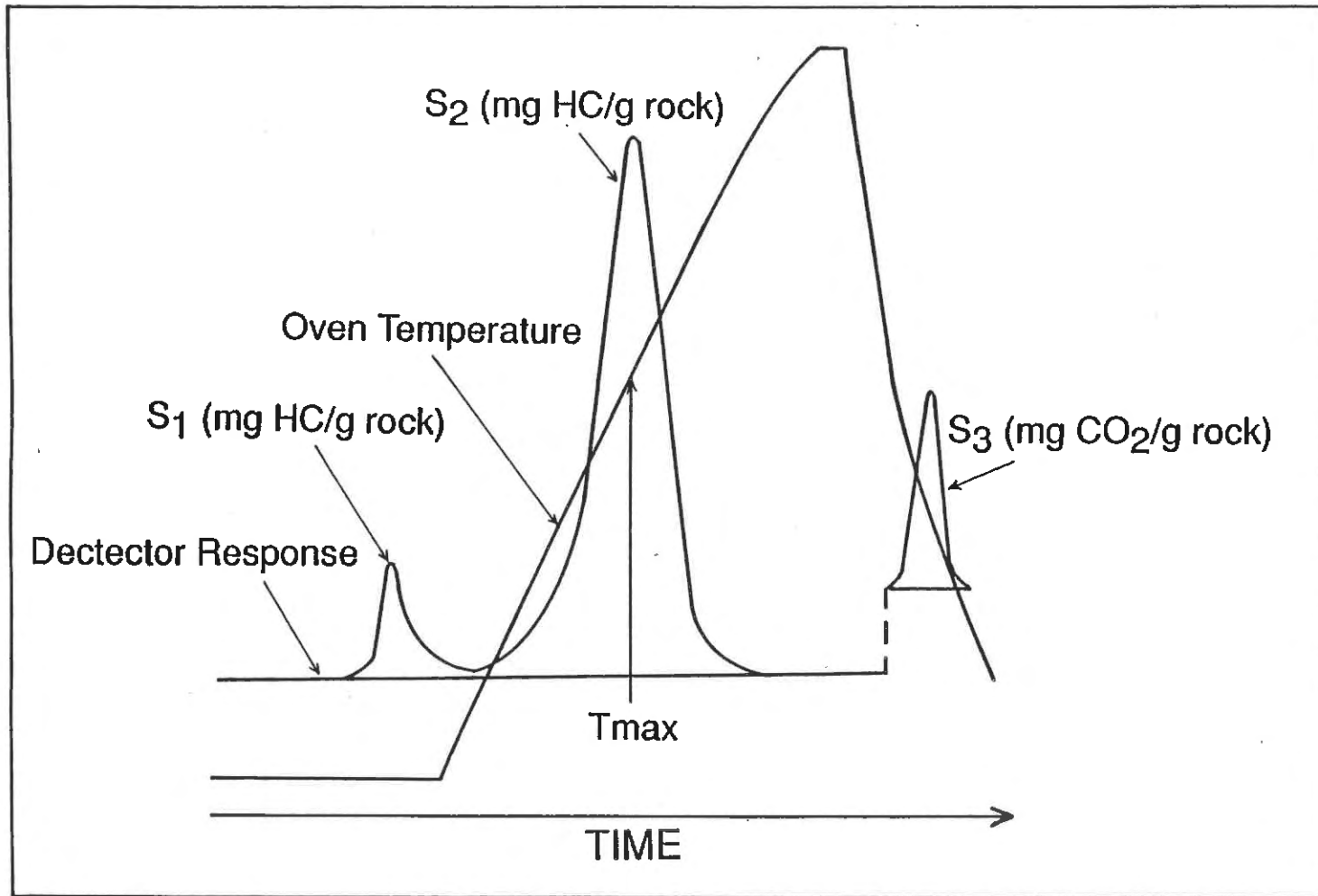


Figure A3.2. Schematic of a pyrogram illustrating the evolution of S_1 , S_2 , S_3 and T_{max} values through time (from Peters, 1986).

removed and documented. The undissolved rock was returned to the bucket with fresh acetic acid and the process was repeated until all the rock was dissolved or the remaining rock no longer reacted with the acid solution. Shale samples did not break down easily using acetic acid and alternate methods were attempted. The sample was placed in a solution of Quaternary "O" and boiled for eight hours. This was unsuccessful and the sample was then placed in a 25 % solution of hydrogen peroxide. It was then boiled in a 10 % solution of potassium hydroxide for four hours. Neither of these techniques were able to break down the shale completely. The resistant material was split into thin pieces and examined under a low power microscope for micro- and macrofossils. Table 4.2 and 4.3 (in text) contain a list of the fossils identified from each sample, with percentages based on a 1 kg sample. Table A.13 outlines fossil fauna reported from the Morien Group by previous workers compared with this study.

Appendix 3
Data Tables

Table A3.1. Compositional estimates* of the BRU from core C-136, based on thin section analyses.

SAMPLE NO.	FOSSILS			CALCITE			OTHER COMPONENTS						
	Biv.	Ostr.	Vert.	Pel.	Mic.	Spar.	Org. Cl.	Cl.	Qtz.	Cht.	Pyr.	Sid.	Phos. Grn.
C136.l	C	R	C	---	---	---	A	---	C	C	---	---	C
C136.k	C	C	---	---	---	---	A	---	U	---	U	---	C
C136.j	---	---	---	---	A	---	C	A	---	---	---	---	---
C136.i	A	A	U	---	---	---	A	---	U	U	---	---	U
C136.h	C	A	U	C	C	U	C	A	U	R	R	---	U
C136.g	C	A	U	C	C	U	C	A	U	U	U	U	U
C136.f	A	C	U	---	C	R	A	---	---	---	R	U	C
C136.e	A	C	C	---	U	C	A	R	U	U	U	---	U
C136.d	A	C	C	---	U	C	A	R	U	U	U	---	U
C136.c	A	A	C	U	C	U	C	C	U	U	C	U	U
C136.b	A	A	R	---	---	R	A	---	U	U	C	U	C
C136.a	NA	NA	NA	NA	NA	NA	NA	NA	NA	NA	NA	NA	NA

* Where: A = abundant, present in all fields of view
 C = common, present in many fields of view
 U = uncommon, found with searching
 R = rare, found with intensive searching
 --- = not observed
 NA = not analysed

Biv. = Bivalves
 Ostr. = Ostracods
 Vert. = Vertebrate fragments
 Pel. = Pellets
 Mic. = Micrite
 Spar. = Sparite
 Org. Cl = Organic-rich Clays (gyttja)
 Cl = Clays
 Qtz. = Quartz
 Cht. = Chert
 Pyr. = Pyrite
 Sid. = Siderite
 Phos. Grn. = Phosphatic grains

Table A3.2. Compositional estimates* of the BRU from core C-137, based on thin section analyses.

SAMPLE NO.	FOSSILS			CALCITE			OTHER COMPONENTS						
	Biv.	Ostr.	Vert.	Pel.	Mic.	Spar.	Org. Cl.	Cl.	Qtz.	Cht.	Pyr.	Sid.	Phos. Grn.
C137.p	U	---	---	---	---	---	A	---	---	---	---	---	---
C137.o	NA	NA	NA	NA	NA	NA	NA	NA	NA	NA	NA	NA	NA
C137.n	C	---	U	---	---	---	A	---	C	---	---	---	C
C137.m	C	C	U	---	---	---	A	---	C	C	---	---	C
C137.l	NA	NA	NA	NA	NA	NA	NA	NA	NA	NA	NA	NA	NA
C137.k	A	A	U	---	C	U	A	---	C	U	R	---	C
C137.j	C	A	U	A	A	U	C	C	U	---	U	---	U
C137.i	C	A	U	U	A	U	C	C	U	U	C	---	U
C137.h	NA	NA	NA	NA	NA	NA	NA	NA	NA	NA	NA	NA	NA
C137.g	C	A	R	C	C	U	C	A	U	U	C	---	U
C137.f	C	A	U	U	U	U	A	C	C	U	C	---	C
C137.e	A	C	U	---	---	U	A	R	U	C	R	R	C
C137.d	A	C	C	---	---	R	A	---	R	C	U	---	C
C137.c	A	A	A	---	---	R	A	---	R	C	C	R	C
C137.b	A	A	C	---	C	U	A	R	C	U	C	U	C
C137.a	NA	NA	NA	NA	NA	NA	NA	NA	NA	NA	NA	NA	NA

* See Table A3.1 for abbreviations

Table A3.3. Detailed maceral analysis, BRU - Sydney Mines section (B).

MACERAL GROUP	MACERAL	No. mm	JW-90-B40		JW-90-B41		JW-90-B42	
			12		18		7	
VITRINITE	Telinite	T	0.0		0.0		0.0	
	Telocollinite	TC	0.0		0.0		0.0	
	Desmocollinite	DC	0.0		0.0		0.0	
	Corpocollinite	CC	0.0		0.0		0.0	
	Gelocollinite	GC	0.0		0.0		0.0	
	Vitrodetrinite	VD	2.5	2.5	0.0	0.0	0.5	0.5
LIPTINITE	Macrosporinite	Mg	0.0		0.0		0.0	
	Sporangium	Sp	0.0		0.0		0.0	
	Microsporinite	Ms						
	Crassisporinite	C	0.5		0.0		0.0	
	Tenuisporinite	T	1.0		3.5		1.5	
	Cutinite	Cu						
	Crassicutinite	C	0.0		0.0		0.0	
	Tenuicutinite	T	0.0		0.0		1.0	
	Exsudatinite	Ex	0.0		0.0		0.0	
	Resinite	Re						
	Bodies	B	0.0		0.0		0.0	
	Wisps	W	0.0		0.0		0.0	
	Alginite	Al						
Telalginite	T	0.0		0.0		0.0		
Lamalginite	L	0.0		0.0		0.0		
Liptodetrinite	Ld	1.0	2.5	0.0	3.5	0.0	2.5	
INERTINITE	Semifusinite	SF	0.5		0.5		0.0	
	Semimacrinite	SM	0.0		0.0		0.0	
	Pyrofusinite	PF						
	Empty cells	E	0.0		0.0		0.0	
	Filled cells	F	0.0		0.0		0.0	
	Bogen structure	B	0.0		0.0		0.0	
	Degradofusinite	DF	0.0		0.0		0.0	
	Macrinite	Ma	0.0		0.0		0.0	
	Micrinite	Mi	0.0		0.0		0.0	
	Scretion Sclerotinite	Sc	0.0		0.0		0.0	
Inertodetrinite	Id	0.5	1.0	0.0	0.5	0.0	0.0	
MINERAL MATTER	Clays	Cl	31.5		79.5		85.5	
	Carbonates	Ca	54.5		16.0		11.5	
	Quartz	Qt	0.5		0.5		0.0	
	Other minerals	Oth	0.0		0.0		0.0	
	Pyrite	Py	7.5	94.0	0.0	96.0	0.0	97.0

Table A3.4. Detailed maceral analysis (mmf), BRU - Sydney Mines section (B).

MACERAL GROUP	MACERAL	No. mm	JW-90-B40 12	JW-90-B41 18	JW-90-B42 7
VITRINITE	Telinite	T	0.0	0.0	0.0
	Telocollinite	TC	0.0	0.0	0.0
	Desmocollinite	DC	0.0	0.0	0.0
	Corpocollinite	CC	0.0	0.0	0.0
	Gelocollinite	GC	0.0	0.0	0.0
	Vitrodetrinite	VD	41.7 41.7	0.0 0.0	16.7 16.7
LIPTINITE	Macrosporinite	Mg	0.0	0.0	0.0
	Sporangium	Sp	0.0	0.0	0.0
	Microsporinite	Ms			
	Crassisporinite	C	8.3	0.0	0.0
	Tenuisporinite	T	16.7	87.5	50.0
	Cutinite	Cu			
	Crassicutinite	C	0.0	0.0	0.0
	Tenuicutinite	T	0.0	0.0	33.3
	Exsudatinite	Ex	0.0	0.0	0.0
	Resinite	Re			
	Bodies	B	0.0	0.0	0.0
	Wisps	W	0.0	0.0	0.0
	Alginite	Al			
	Telalginite	T	0.0	0.0	0.0
Lamalginite	L	0.0	0.0	0.0	
Liptodetrinite	Ld	16.7 41.7	0.0 87.5	0.0 83.3	
INERTINITE	Semifusinite	SF	8.3	12.5	0.0
	Semimacrinite	SM	0.0	0.0	0.0
	Pyrofusinite	PF			
	Empty cells	E	0.0	0.0	0.0
	Filled cells	F	0.0	0.0	0.0
	Bogen structure	B	0.0	0.0	0.0
	Degradofusinite	DF	0.0	0.0	0.0
	Macrinite	Ma	0.0	0.0	0.0
	Micrinite	Mi	0.0	0.0	0.0
	Secretion Sclerotinite	Sc	0.0	0.0	0.0
	Inertodetrinite	Id	8.3 16.6	0.0 12.5	0.0 0.0

(mmf) - mineral matter free

Table A3.5. Detailed maceral analysis, BRU - Glace Bay West section (E).

MACERAL GROUP	MACERAL	No. mm	JW-90-E40 1	JW-90-E41 10	JW-90-E42 15	JW-90-E43 12	JW-90-E44 15				
VITRINITE	Telinite	T	0.0	0.0	0.0	0.0	0.0				
	Telocollinite	TC	2.7	0.0	0.0	0.0	0.0				
	Desmocollinite	DC	0.0	0.0	0.0	0.0	0.0				
	Corpocollinite	CC	0.0	0.0	0.0	0.0	0.0				
	Gelocollinite	GC	0.0	0.0	0.0	0.0	0.0				
	Vitrodetrinite	VD	2.3	5.0	1.5	1.5	0.5	0.5	0.0	0.0	2.5
LIPTINITE	Macrosporinite	Mg	0.0	0.0	0.0	0.0	0.0	0.0			
	Sporangium	Sp	0.0	0.0	0.0	0.0	0.0				
	Microsporinite	Ms									
	Crassisporinite	C	0.0	0.0	0.0	0.0	0.0				
	Tenuisporinite	T	4.7	4.5	1.5	0.5	6.0				
	Cutinite	Cu									
	Crassicutinite	C	0.0	0.0	0.0	0.0	0.0				
	Tenuicutinite	T	0.0	0.0	0.0	0.0	0.0				
	Exsudatinite	Ex	0.0	0.0	0.0	0.0	0.0				
	Resinite	Re									
	Bodies	B	0.0	0.0	0.0	0.0	0.0				
	Wisps	W	0.0	0.0	0.0	0.0	0.0				
	Alginite	Al									
Telalginite	T	0.0	0.0	0.0	0.0	0.0					
Lamalginite	L	0.0	3.5	2.5	0.5	4.5					
Liptodetrinite	Ld	1.7	6.3	2.5	10.5	1.0	5.0	1.0	2.0	4.0	14.5
INERTINITE	Semifusinite	SF	0.0	0.0	0.0	0.0	0.0				
	Semimacrinite	SM	0.0	0.0	0.0	0.0	0.0				
	Pyrofusinite	PF									
	Empty cells	E	0.7	0.0	0.0	0.0	0.0				
	Filled cells	F	0.7	0.0	0.0	0.0	0.0				
	Bogen structure	B	0.0	0.0	0.0	0.0	0.0				
	Degradofusinite	DF	0.0	0.0	0.0	0.0	0.0				
	Macrinite	Ma	0.3	1.0	0.0	0.0	0.0				
	Micrinite	Mi	0.3	0.0	0.0	0.0	0.0				
	Scretion Sclerotinite	Sc	0.3	0.0	0.0	0.0	0.0				
Inertodetrinite	Id	3.3	5.7	1.5	2.5	1.0	1.0	0.5	0.5	1.5	1.5
MINERAL MATTER	Clays	Cl	14.0	62.5	22.5	16.0	78.0				
	Carbonates	Ca	57.7	20.0	69.5	79.5	1.5				
	Quartz	Qt	0.0	1.0	0.0	0.0	1.0				
	Other minerals	Oth	0.0	0.0	0.0	0.0	0.0				
	Pyrite	Py	11.3	83.0	2.0	85.5	1.5	93.5	2.0	97.5	1.0

Table A3.6. Detailed maceral analysis (mmf), BRU - Glace Bay West section (E).

MACERAL GROUP	MACERAL	No. mm	JW-90-E40 1	JW-90-E41 10	JW-90-E42 15	JW-90-E43 12	JW-90-E44 15
VITRINITE	Telinite	T	0.0	0.0	0.0	0.0	0.0
	Telocollinite	TC	15.9	0.0	0.0	0.0	0.0
	Desmocollinite	DC	0.0	0.0	0.0	0.0	0.0
	Corpocollinite	CC	0.0	0.0	0.0	0.0	0.0
	Gelocollinite	GC	0.0	0.0	0.0	0.0	0.0
	Vitrodetrinite	VD	13.7 29.5	10.3 10.3	7.7 7.7	0.0 0.0	13.5 13.5
LIPTINITE	Macrosporinite	Mg	0.0	0.0	0.0	0.0	0.0
	Sporangium	Sp	0.0	0.0	0.0	0.0	0.0
	Microsporinite	Ms					
	Crassisporinite	C	0.0	0.0	0.0	0.0	0.0
	Tenuisporinite	T	27.4	31.0	23.1	20.0	32.4
	Cutinite	Cu					
	Crassicutinite	C	0.0	0.0	0.0	0.0	0.0
	Tenuicutinite	T	0.0	0.0	0.0	0.0	0.0
	Exsudatinite	Ex	0.0	0.0	0.0	0.0	0.0
	Resinite	Re					
	Bodies	B	0.0	0.0	0.0	0.0	0.0
	Wisps	W	0.0	0.0	0.0	0.0	0.0
	Alginite	AL					
	Telalginite	T	0.0	0.0	0.0	0.0	0.0
Lamalginitite	L	0.0	24.1	38.5	20.0	24.3	
Liptodetrinite	Ld	9.8 37.2	17.2 72.4	15.4 76.9	40.0 80.0	21.6 78.4	
INERTINITE	Semifusinite	SF	0.0	0.0	0.0	0.0	0.0
	Semimacrinite	SM	0.0	0.0	0.0	0.0	0.0
	Pyrofusinite	PF					
	Empty cells	E	3.9	0.0	0.0	0.0	0.0
	Filled cells	F	3.9	0.0	0.0	0.0	0.0
	Bogen structure	B	0.0	0.0	0.0	0.0	0.0
	Degradofusinite	DF	0.0	0.0	0.0	0.0	0.0
	Macrinite	Ma	2.0	6.9	0.0	0.0	0.0
	Micrinite	Mi	2.0	0.0	0.0	0.0	0.0
	Secretion Sclerotinite	Sc	2.0	0.0	0.0	0.0	0.0
Inertodetrinite	Id	19.6 33.3	10.3 17.2	15.4 15.4	20.0 20.0	8.1 8.1	

(mmf) - mineral matter free

Table A3.7. Parameters measured directly by Rock-Eval pyrolysis.

Parameter	Unit	Description	Source Rock Indicator
S1	mg HC/g rock	free hydrocarbons	quantity
S2	mg HC/g rock	<u>in situ</u> hydrocarbons released upon heating	quantity
S3	mg CO ₂ /g rock	carbon dioxide released upon heating (< 390 °C)	quantity
TOC	weight %	total organic carbon	quantity
Tmax	°C	temperature at which the maximum amount of S2 hydrocarbons are generated during pyrolysis	maturity

Table A3.8. Parameters calculated from Rock-Eval pyrolysis.

Parameter	Unit/Calc.	Description	Source Rock Indicator
HI	mg HC/g Corg $((S2/TOC)*100)$	Hydrogen Index; the quantity of pyrolyzable hydrocarbons from S2 relative to the total organic carbon content of a sample.	organic type/ quality
OI	mg CO ₂ /g Corg $((S3/TOC)*100)$	Oxygen Index; the quantity of CO ₂ from S3 relative to the total organic carbon content of a sample.	organic type/ quality
PI	--- $(S1/(S1 + S2))$	Production Index; ratio of free hydrocarbons to total hydrocarbons in a sample	maturity
PC	weight % $K*((S1 + S2)/10)$	Pyrolyzed Carbon; represents the quantity of hydrocarbons in a sample. K = 0.83	quantity
PP	mg HC/g rock $(S1 + S2)$	Petroleum Potential; the maximum quantity of extractable hydrocarbons in a sample.	quantity

Table A3.9. Rock-Eval data for each BRU outcrop sample and the calculated weighted average for each coastal section studied.

Section	No.	cm	Tmax	S1	S2	S3	TOC	PI	PP	PC	HI	OI
Bras	A45*	20	438	0.29	12.92	0.60	3.59	0.02	13.20	1.10	360	17
d'Or	A44	8	440	0.44	16.90	0.80	3.47	0.03	17.33	1.44	488	23
	A43	6	436	0.39	6.26	0.51	4.02	0.06	6.64	0.55	156	13
Wtd. Avg. A		34	438	0.34	12.68	0.63	3.63	0.03	13.02	1.08	354	17
Sydney	B42	7	438	0.05	2.10	1.87	2.71	0.02	2.15	0.18	78	69
Mines	B41	18	440	0.20	10.88	0.39	3.33	0.02	11.07	0.92	327	12
	B40*	12	443	0.16	4.77	0.52	3.19	0.03	4.93	0.41	150	16
Wtd. Avg. B		37	441	0.16	7.24	0.71	3.17	0.02	7.39	0.61	222	24
Victoria	C43	24	439	0.04	0.87	0.58	0.99	0.04	0.91	0.08	88	59
Mines	C42	25.5	438	0.15	5.22	0.41	2.44	0.03	5.37	0.45	214	17
	C41	8	438	0.62	21.02	0.46	5.25	0.03	21.64	1.80	400	9
Wtd. Avg. C		57.5	438	0.17	5.60	0.49	2.23	0.03	5.77	0.48	187	33
Glace	E44	15	445	0.93	17.01	0.80	5.25	0.05	17.94	1.49	324	15
Bay	E43	12	446	0.13	3.30	0.44	1.48	0.04	3.43	0.28	223	29
West	E42*	15	444	0.09	0.91	0.86	1.61	0.09	1.00	0.08	56	53
	E41	10	434	0.44	8.41	0.79	4.03	0.05	8.85	0.74	209	20
	E40	1	443	1.35	34.99	0.75	11.27	0.04	36.34	3.03	311	7
Wtd. Avg. E		53	442	0.42	8.06	0.73	3.25	0.06	8.49	0.70	203	30
Donkin	G41	14	442	0.10	3.67	0.25	2.15	0.03	3.77	0.31	171	11
West	G42	6.5	442	0.30	10.57	0.38	3.60	0.03	10.87	0.90	294	11
	G43	12	438	0.45	15.93	0.46	4.57	0.03	16.38	1.36	349	10
	G44	8	443	0.16	1.32	0.44	3.53	0.11	1.47	0.12	37	12
Wtd. Avg. G		40.5	441	0.24	7.94	0.37	3.37	0.04	8.19	0.68	217	11
Donkin	H55	20	441	0.62	14.38	0.90	5.22	0.04	15.00	1.25	275	17
East	H54	6	575	0.05	0.88	0.40	1.85	0.05	0.93	0.08	48	21
	H53	6	557	0.02	1.27	0.21	0.77	0.02	1.29	0.11	165	27
Wtd. Avg. H		32	487	0.40	9.39	0.68	3.75	0.04	9.79	0.81	212	20
Long-	J57	30	437	0.29	9.54	0.61	3.64	0.03	9.82	0.82	262	17
beach	J56	20	440	0.15	5.42	0.73	2.83	0.03	5.57	0.46	192	26
	J58	25	441	0.08	4.37	1.03	3.91	0.02	4.45	0.46	112	26
Wtd. Avg. J		75	439	0.18	6.72	0.78	3.51	0.02	6.89	0.60	193	22

* based on the average of four analyses, results in Table A3.12;
all other data based on the average of duplicate analyses.

Table A3.10. Rock-Eval data, BRU - core C-136 and the weighted average for the section.

Sample No.	cm	Tmax	S1	S2	S3	TOC	PI	PP	PC	HI	OI
C136.m	5.3	450	0.05	0.13	0.20	0.41	0.30	0.18	0.01	32	48
C136.l	5.2	444	0.68	7.14	0.37	3.70	0.09	7.82	0.65	193	10
C136.k	4.0	438	1.21	12.56	0.97	5.80	0.09	13.77	1.14	216	17
C136.j	0.3	437	1.12	11.03	1.41	5.19	0.09	12.15	1.01	212	27
C136.i	2.7	443	1.60	21.11	0.48	5.88	0.07	22.71	1.88	359	8
C136.h	3.0	445	0.73	7.30	0.54	3.23	0.09	8.03	0.67	226	17
C136.g*	9.5	441	0.48	5.75	0.79	2.61	0.08	6.23	0.52	221	30
C136.f	5.0	443	0.51	4.84	0.54	2.32	0.09	5.34	0.44	209	23
C136.e	6.5	440	0.86	8.38	0.71	3.78	0.09	9.24	0.77	222	19
C136.d	2.1	448	2.89	36.60	1.23	12.94	0.07	39.49	3.28	283	9
C136.c	3.0	440	1.26	7.93	0.65	5.80	0.14	9.19	0.76	137	11
C136.b	4.3	435	3.24	22.31	2.23	14.33	0.13	25.54	2.12	156	16
C136.a	2.0	443	6.01	38.69	1.00	19.98	0.13	44.70	3.71	194	5
Wtd											
Avg C136	52.9	442	1.21	10.92	0.78	5.27	0.11	12.12	1.01	197	21

* based on the average of four analyses, results in Table A3.12;
all other data based on the average of duplicate analyses.

Table A3.11. Rock-Eval data, BRU - core C-137 and the weighted average for the section.

Sample No.	cm	Tmax	S1	S2	S3	TOC	PI	PP	PC	HI	OI
c137.q	5.0	504	0.04	0.36	0.07	0.44	0.09	0.39	0.03	80	15
c137.p	4.0	445	0.12	1.45	0.20	1.39	0.07	1.56	0.13	104	14
c137.o	6.0	444	0.12	1.34	0.25	1.08	0.08	1.46	0.12	124	23
c137.n*	7.6	446	0.72	9.19	0.33	3.94	0.07	9.91	0.82	233	8
c137.m	3.0	448	1.36	19.45	0.53	6.51	0.06	20.81	1.73	299	8
c137.l	0.7	438	0.54	7.26	2.00	3.81	0.07	7.80	0.65	191	52
c137.k	3.4	451	0.87	14.75	0.61	4.52	0.06	15.62	1.30	327	14
c137.j	4.0	446	0.26	4.78	0.57	2.48	0.05	5.03	0.42	193	23
c137.i	2.7	446	0.20	3.89	0.54	1.95	0.05	4.09	0.34	199	27
c137.h	0.8	443	0.35	6.50	0.83	2.99	0.05	6.85	0.57	218	28
c137.g	3.2	443	0.29	4.35	0.59	1.93	0.06	4.64	0.38	226	31
c137.f	3.7	445	1.53	18.19	0.72	6.63	0.08	19.72	1.64	274	11
c137.e*	5.9	441	1.04	9.74	0.68	4.65	0.10	10.78	0.89	209	15
c137.d	4.6	444	1.40	13.96	0.35	5.12	0.09	15.36	1.27	274	7
c137.c	2.5	448	3.56	40.47	1.45	12.38	0.08	44.03	3.65	327	12
c137.b	4.2	442	1.62	11.62	0.72	5.39	0.12	13.24	1.10	220	13
c137.a	5.5	440	3.66	27.58	1.13	15.78	0.12	31.24	2.59	175	7
Wtd											
Avg C137	66.8	449	1.06	11.05	0.56	4.81	0.08	12.12	1.01	208	15

* based on the average of four analyses, results in Table A3.12;
all other data based on the average of duplicate analyses.

Table A3.12. Duplicate Rock-Eval analyses - BRU.

Sample No.	Tmax	S1	S2	S3	TOC	PI	PP	PC	HI	OI
A45-1	439	0.27	12.14	0.66	3.51	0.02	12.41	1.03	346	19
	438	0.29	12.90	0.71	3.52	0.02	13.19	1.09	366	20
A45-2	435	0.32	13.33	0.49	3.63	0.02	13.65	1.13	367	13
	441	0.26	13.30	0.53	3.69	0.02	13.56	1.13	360	14
AVG A45	438	0.29	12.92	0.60	3.59	0.02	13.20	1.10	360	17
STD	1	0.02	0.32	0.06	0.05	0.00	0.33	0.03	6	2
B40-1	441	0.16	5.15	0.54	3.21	0.03	5.31	0.44	160	17
	444	0.16	4.50	0.45	3.20	0.03	4.66	0.38	141	14
B40-2	443	0.16	4.61	0.51	3.25	0.03	4.77	0.39	142	16
	443	0.16	4.83	0.59	3.10	0.03	4.99	0.41	156	19
AVG B40	443	0.16	4.77	0.52	3.19	0.03	4.93	0.41	150	16
STD	1	0.00	0.17	0.03	0.04	0.00	0.17	0.02	6	1
E42-1	440	0.09	0.89	0.85	1.63	0.09	0.98	0.08	55	52
	438	0.11	1.05	0.88	1.63	0.09	1.16	0.09	64	54
E42-2	440	0.07	0.63	0.89	1.60	0.10	0.70	0.05	39	56
	456	0.09	1.06	0.81	1.58	0.08	1.15	0.09	67	51
AVG E42	444	0.09	0.91	0.86	1.61	0.09	1.00	0.08	56	53
STD	5	0.01	0.12	0.02	0.01	0.01	0.12	0.01	7	1
C136.g-1	441	0.45	5.90	0.78	2.67	0.07	6.35	0.53	221	29
	441	0.45	5.78	0.79	2.60	0.07	6.23	0.52	222	30
C136.g-2	442	0.50	5.68	0.86	2.54	0.08	6.18	0.51	224	34
	441	0.50	5.65	0.74	2.61	0.08	6.15	0.51	216	28
AVG C136.g	441	0.48	5.75	0.79	2.61	0.08	6.23	0.52	221	30
STD	0	0.02	0.07	0.03	0.03	0.00	0.05	0.00	2	1
C137.n-1	445	0.70	9.19	0.35	3.96	0.07	9.89	0.82	232	9
	446	0.73	9.34	0.37	3.95	0.07	10.07	0.84	236	9
C137.n-2	446	0.72	9.15	0.30	3.94	0.07	9.87	0.82	232	8
	446	0.72	9.07	0.30	3.89	0.07	9.79	0.81	233	8
AVG C137.n	446	0.72	9.19	0.33	3.94	0.07	9.91	0.82	233	8
STD	0	0.01	0.07	0.02	0.02	0.00	0.07	0.01	1	0
C137.e-1	440	1.08	10.53	0.77	4.73	0.09	11.61	0.96	223	16
	441	1.10	10.10	0.70	4.59	0.10	11.20	0.93	220	15
C137.e-2	441	0.95	8.85	0.66	4.67	0.10	9.80	0.81	190	14
	442	1.01	9.48	0.60	4.61	0.10	10.49	0.87	206	13
AVG C137.e	441	1.04	9.74	0.68	4.65	0.10	10.78	0.89	209	15
STD	0	0.04	0.42	0.04	0.04	0.00	0.46	0.04	9	1

Table A3.13. A review of some fossil fauna reported in the Morien Group (numbers correspond to reference list at end):

- Phylum:** Sarcodina
Class: Rhizopoda
Order: Foraminiferida (21)
Genus: Ammobaculites (22)
Ammotium (22)
Rheophax (22)
Trochammina (22)
- Class:** Reticularia
Order: Arcellinida
 (undetermined thecamoebians, 21, 22)
- Phylum:** Annelida
Class: Polychaetia
Order: Sedentarida
Genus: Spirorbis sp.
 (3,4,8,15,16,18,19,20,23)
- Phylum:** Mollusca
Class: Bivalvia (14,17)
Subclass: Pteriomorphia
Order: Mytiloida
Genus, species: Anthracomya sp. (6,7 later =
Anthraconauta sp.)
Anthraconauta phillipsii
 (10,15,16,19,23)
A. c.f. A. phillipsii (23)
A. tenuis (15,16,19)
A. wrighti s.l. (15,19)
A. caliver (15,19)
Anthraconaia arenacea s.l.
 (15,16,19)
A. c.f. A. arenacea (23)
A. sp. c.f. A. pulchella (15)
A. sp. aff. A. speciosa (15)
Naiadites sp. (3,4,18,20)
- Subclass:** Palaeoheterodonta
Order: Unionoida
Genus: Carbonicola sp. (8)
- Class:** Gastropoda (14,17,18,20)
 (unspecified)

- Phylum: Arthropoda**
 Class: Crustacea
 Order: Ostracoda (6,17)
 Genus, species: Cytherea sp. (3,4,5)
 Carbonita inflata
 (11,14,18,19,20,23)
 C. scalpellus (11,14,18,20,23)
 C. fabulina (23)
 C. evelinae (15,16,19)
 C. secans (15,19)
 C. elongata (15,19)
 C. salteriana (15,19)
 C. bairdoides (15,19)
 C. humilis (15,19)
 C. pungens (15,19)
 Candona salteriana (15,19,23)
- Order: Conchostraca
 Genus: Leaia spp. (7,8,15,16,19,23)
 Estheria sp. (8)
 Lioestheria sp. (16)
- Class: Arachnoidea
 Order: Xiphosura
 Genus, species: Euproops amiae (11)
- Class: Diplopoda
 Order: Eurysterna
 Genus: Xylobuis sp. (12)
- Class: Insecta
 Order: Blattaria (10,11)
 Genus: (unspecified insects)
- Phylum: Chordata**
 Class: Chondrichthyes (14)
 Subclass: Elasmobranchii (18,20,23)
 Order: Ctenacanthiforme
 Suborder: Hybodontoides (18,20,23)
 Order: Xenacanthidia (18,20,23)
 Genus: Orthcanthus sp. (18,20,23)
- Class: Agnatha
 Subclass: Pteraspidomorphi
 Order: Heterostraci (coelolepid tentatively identified, 23?)
- Class: Acanthodia (14,18,20,23?)
 (unspecified)

- Phylum: Chordata (con't)**
Class: Ostheichthyes
Subclass: Actinopterygii
Order: Palaeoniscoform
Suborder Palaeoniscoidea (14,20,23)
Genus: Gyrolepir sp. (1)
Amblypterus sp. (1)
Palaeoniscus sp. (1)
Rhadinichthys sp. (15,19)
Elonichthys sp. (15,19)
- Subclass: Sarcopterygii**
Order: Crossopterygii (17,23)
Suborder: Rhipidistia
Genus: Holoptychius sp. (1)
Rhizodopsis sp. (15,19)
Megalichthyes sp. (1)
- Suborder: Onychodontiforme**
Genus: Rhabdoderma sp. (19)
- Order: Dipnoi**
Genus, species: Ctenodus murchisoni (9)
Monongahela stenodonta
(18,20,23)
Sagenodus sp. (18,20)
- Class: Reptilia**
Subclass: Anapsida
Order: Captorhinida
Suborder: Captorhinomorpha
Genus, species: Limnoscelidae relictus
(13)
- Order: ?**
Genus, species: Sauropus sydnensis (2)
- Class: Amphibia**
Subclass: Labyrinthodontia (13)

References (by number, from oldest to most recent):

1. Brown (1850)
2. Brown (in Dawson, 1868)
3. Dawson (1868)
4. Robb (1876)
5. DeWolfe (1904)
6. Hyde (1913)
7. Hayes and Bell (1923)
8. Bell (1938)
9. Sternberg (1941)
10. Bell (1944)
11. Copland (1957)
12. Baird (1958)
13. Carroll (1967)
14. Masson and Rust (1983)
15. Vasey (1983)
16. Vasey and Zodrow (1983)
17. Best (1984)
18. Masson and Rust (1984)
19. Vasey (1984)
20. Masson (1986)
21. Thibaudeau and Mediolli (1986)
22. Wightman *et al.* (1992)
23. This study

REFERENCES

- Allen, J.R.L., 1963. The classification of cross-stratified units with notes on their origin. *Sedimentology*, v. 2, pp. 93-114.
- Allen, J.R.L., 1964. Studies in fluviatile sedimentation: six cyclothems from the Lower Old Red Sandstone, Anglo-Welsh Basin. *Sedimentology*, v. 3, pp. 163-198.
- Allen, J.R.L., 1965. A review of the origin and characteristics of recent alluvial sediments. *Sedimentology*, v. 5, pp. 89-191.
- Allen, J.R.L., 1970. A quantitative model of grain size and sedimentary structures in lateral deposits. *Geological Journal*, v. 7, pp. 129-146.
- Allen, J.R.L., 1973. Compressional structures (patterned ground) in Devonian pedogenic limestones. *Nature*, v. 243, pp. 84-86.
- Allen, J.R.L., 1974. Studies in fluviatile sedimentation, implications of pedogenic carbonate units, Lower Old Red Sandstone, Anglo-Welsh outcrop. *Geological Journal*, v. 9, pp. 181-208.
- Allen, J.R.L., 1986. Pedogenic calcretes in the Old Red Sandstone facies (Late Silurian-Early Carboniferous) of the Anglo-Welsh area, southern Britain. *In* V.P. Wright (editor), *Paleosols: Their Recognition and Interpretation*, Blackwell Scientific Publications, New Jersey, pp. 58-86.
- Arthaud, F. and Matte, P., 1977. Late Paleozoic strike-slip faulting in southern Europe and Northern Africa: Result of a right-lateral shear zone between the Appalachians and the Urals. *Geological Society of America Bulletin*, v. 88, pp. 1305-1320.
- Ashley, G.M., 1990. Classification of large scale subaqueous bedforms: a new look at an old problem. *Journal of Sedimentary Petrology*, v. 60, pp. 160-172.
- Austen, D.E.G., Ingram, D.J.B., Given, P.H., Binder, C.R. and Hill, L.W., 1966. Electron spin resonance study of pure macerals. *In* R.F. Gould (editor), *Coal Science*. American Chemical Society, *Advances in Chemistry Series*, v. 55, pp. 344-362.

- Avery, M.P. and Bell, J.S., 1985. Vitrinite reflectance measurements from the South Whale Basin, Grand Banks, Eastern Canada and implications for hydrocarbon exploration. In Current Research, Part B, Geological Survey of Canada, Paper 85-1B, pp. 51-57.
- Baird, D., 1958. New records of Paleozoic Diplopod Myriapoda. *Journal of Paleontology*, v. 32, n. 1, pp. 239-241.
- Baird, D., 1978. Studies on Carboniferous freshwater fishes. *American Museum Novitates*, n. 2641, pp. 1-22.
- Barss, M.S. and Hacquebard, P.A., 1967. Age and stratigraphy of the Pictou Group in the Maritime Provinces as revealed by fossil spores. In E.R. Neale and H. Williams (editors), *Geology of the Atlantic Region*, Geological Association of Canada, Special Paper 4, pp. 267-282.
- Beerbower, J.R., 1961. Origin of cyclothems of the Dunkard Group (Upper Pennsylvanian-Lower Permian) in Pennsylvania, West Virginia and Ohio. *Geological Society of America Bulletin*, v. 72, pp. 1029-1050.
- Beerbower, J.R., 1964. Cyclothems and cyclic depositional mechanisms in alluvial plain sedimentation. In F.D. Merriam (editor), *Symposium of Cyclic Sedimentation*, Kansas Geological Survey, Bulletin 169, pp. 31-42.
- Beerbower, J.R., 1969. Interpretation of cyclic Permo-Carboniferous deposition in alluvial plain sediments in West Virginia. *Geological Society of America Bulletin*, v. 80, pp. 1843-1848.
- Bell, W.A., 1927. Outline of Carboniferous stratigraphy and geological history of the Maritime Provinces of Canada. *Transactions, Royal Society of Canada*, v. 31, pp. 75-111.
- Bell, W.A., 1928. Discussion of paper by F.W. Gray. *Proceedings, 2nd Empire Mining and Metallurgy Congress*, Montreal, pp. 159-165.
- Bell, W.A., 1938. Fossil flora of the Sydney Coalfield, Nova Scotia. *Geological Survey of Canada, Memoir* 215, n. 2439, pp. 1-19.
- Bell, W.A., 1944. Use of some fossil floras in Canadian stratigraphy. *Transactions, Royal Society of Canada*, v. 38, pp. 1-13.

- Bell, W.A. and Goranson, E.A., 1938. Sydney Map Sheet (west half), Cape Breton and Victoria Counties. Map Sheet 360A, Department of Mines and Resources.
- Besly, B.M. and Turner, P., 1983. Origin of red beds in a moist tropical climate (Etruria Formation, Upper Carboniferous, U.K.). In R.C.L. Wilson (editor), Residual Deposits: Surface Related Weathering Processes and Materials. Geological Society of London, Blackwell Scientific Publications, Oxford, London, Edinburgh, Boston, Melbourne, pp. 131-147.
- Best, M.A., 1984. Detailed stratigraphy of part of the Upper Morien Group (Upper Carboniferous), North Sydney, Cape Breton Island, Nova Scotia. Unpublished M.Sc. thesis, University of Ottawa, Ottawa, Ontario, 214 p.
- Bird, D.J., 1987. The depositional environment of the Late Carboniferous coal-bearing Sydney Mines Formation, Point Aconi area, Cape Breton Island, Nova Scotia. Unpublished M.Sc. thesis, Dalhousie University, Halifax, Nova Scotia, 343 p.
- Birk, D., Pilgrim, J.C. and Zodrow, E.L., 1986. Trace element content of coals and associated rocks of the Sydney Basin, Nova Scotia. ACI-85-158, Unpublished report for Geological Survey of Canada, 100 p.
- Birkeland, P.W., 1984. Soils and Geomorphology. Oxford University Press, New York, 372 p.
- Bless, M.J.M. and Pollard, J.E., 1972. Paleocology and ostracode faunas of Westphalian ostracode bands from Limburg, the Netherlands and Lancashire, Great Britain. Mededelingen Rijks Geologische Dienst, Nieuwe serie, v. 24, pp. 21-53.
- Boardman, D.R. and Heckel, P.H., 1989. Glacial-eustatic sea-level curve for early Late Pennsylvanian sequence in north-central Texas and biostratigraphic correlation with curve for midcontinent North America. Geology, v. 7, pp. 802-805.
- Boehner, R.C., 1985. Carboniferous basin studies, salt, potash, celestite and barite - New exploration potential in the Sydney Basin, Cape Breton Island. Nova Scotia Department of Mines and Energy, Report of Activities 85-1, pp. 153-164.
- Boehner, R.C. and Giles, P.S., 1986. Geological map of the Sydney Basin, Cape Breton Island, Nova Scotia. Nova Scotia Department of Mines and Energy, Map 86-1.

- Bown, T.M. and Kraus, M.J., 1981. Lower Eocene alluvial paleosols (Willwood Formation, northwest Wyoming, U.S.A.) and their significance for paleoecology, paleoclimatology and basin analysis. *Paleogeography, Paleoclimatology, Paleoecology*, v. 34, pp. 1-30.
- Bradley, D.C., 1983. Tectonics of the Acadian Orogeny in New England and adjacent Canada. *Journal of Geology*, v. 91, pp. 381-400.
- Brown, R., 1850. Section of the Lower Coal Measures of the Sydney Coalfield in the Isle of Cape Breton. *Geological Society of London Quarterly Journal*, n. 6, pp. 115-133.
- Brown, R., 1871. The coalfields and coal trade of the Island of Cape Breton. *Geological Society of London Quarterly Journal*, n. 7, pp. 1-166.
- Burchette, T.P. and Riding, R., 1977. Attached vermiform gastropods in Carboniferous marginal marine stromatolites and biostromes. *Lethaia*, v. 10, pp. 17-28.
- Bustin, R.M., Cameron, A.R., Grieve, D.A. and Kalkreuth, W.D., 1983. Coal Petrology - Its Principles, Methods and Applications. *Geological Association of Canada, Short Course Notes*, v. 3, 230 p.
- Buurman, P., 1980. Paleosols in the Reading Beds (Paleocene) of Alum Bay, Isle of Wight, U.K. *Sedimentology*, v. 27, pp. 593-606.
- Calder, J.H., Gibling, M.R. and Mukhopadhyay, P.K., 1991. Peat formation in a Westphalian B peidmont setting, Cumberland Basin, Nova Scotia: Implications for the maceral-based interpretation of rheotrophic and raised paleomires. *Society Geology France Bulletin*, v. 162, n. 2, pp. 283-298.
- Calver, M.A., 1968a. Distribution of Westphalian marine faunas in Northern England and adjoining areas. *Proceedings, Yorkshire Geological Society*, v. 37, pp. 1-72.
- Calver, M.A., 1968b. Coal Measure invertebrate faunas. In D. Murchison and T.S. Westoll (editors), *Coal and Coal-bearing Strata*, Oliver and Boyd, Edinburgh, pp. 147-177.

- Cameron, A.R., 1978. Megascopeic description of coal with particular reference to seams in southern Illinois. In R.R. Dutcher (editor), *Field Descriptions of Coal*, ASTM STP 661, pp. 9-32.
- Cant, D.J., 1978. Development of a facies model for sandy braided river sedimentation: Comparison of the South Saskatchewan River and the Battery Point Formation. *Canadian Society of Petroleum Geologists, Memoir 5*, pp. 627-639.
- Carroll, R.L., 1967. A limnoscelid reptile from the Middle Pennsylvanian. *Journal of Paleontology*, v. 41, n. 5, pp. 1256-1261.
- Carroll, R.L., 1988. *Vetrbrate Paleontology and Evolution*. W.H. Freeman and Co., New York, 698 p.
- Casagrande, D.J., Berschinski, C. and Sutton, N., 1977. Sulphur in peat-forming systems of the Okefenokee Swamp and Florida Everglades: Origin of sulphur in coals. *Geochim et Cosmochim Acta*, v. 41, pp. 161-167.
- Cecil, C.B., Stanton, R.W., Neuzil, S.G., Dulong, F.T., Ruppert, L.F. and Pierce, B.S., 1985. Paleoclimate controls on Late Paleozoic sedimentation and peat formation in the central Appalachian Basin (U.S.A.). *International Journal of Coal Geology*, v. 5, pp. 195-230.
- Chao, E.C.T., Minkin, J.A. and Thompson, C.L., 1982. Application of automated image analysis to coal petrography. *International Journal of Coal Geology*, v. 2, pp. 113-150.
- Chesnut, D.R. and Cobb, J.C., 1989. Comment and reply on "Origin of the Pennsylvanian coal-bearing cyclothem of North America". *Geology*, v. 17, pp. 871-872.
- Cohen, A.D. and Spackman, W., 1980. Phytogenic organic sediments and sedimentary environments in the Everglades - mangrove complex, Part III: Decomposition of plant tissues and the origin of coal macerals. *Palaeontographica B*, v. 172, pp. 125-149.
- Cohen, A.D., Spackman, W. and Raymond, R. Jr., 1987. Interpreting the characteristics of coal seams from chemical, physical and petrographic studies of peat deposits. In A.C. Scott (editor), *Coal and Coal-bearing Strata: Recent Advances*. Blackwell, Oxford, Geological Society, Special Publication 32, pp. 107-125.

- Coleman, J.M., 1966. Ecological changes in a marine fresh-water clay sequence. Transactions, Gulf Coast Association of Geological Societies, v. 16, pp. 159-174.
- Cope, M.J. and Chaloner, W.G., 1980. Fossil charcoal as evidence of past atmospheric composition. Nature (London), v. 283, pp. 647-649.
- Cope, M.J. and Chaloner, W.G., 1985. Wildfire: an interaction of biological and physical processes. In B.H. Tiffoney (editor), Geological Factors and the Evolution of Plants. Yale University Press, New Haven, pp. 257-277.
- Copeland, M.J., 1957. The Arthropod fauna of the Upper Carboniferous rocks of the Maritime Provinces. Geological Survey of Canada, Memoir 236, n. 2530, pp. 1-13.
- Crelling, J.C., 1982. Automated petrographic characterization of coal lithotypes. International Journal of Coal Geology, v. 1, pp. 347-359.
- Curtis, C., 1987. Mineralogical consequences of organic matter degradation in sediments: Inorganic/organic diagenesis. In J.K. Leggett and G.G. Zuffa (editors), Marine Clastic Sedimentology, Graham and Trotman, London, Boston, pp. 108-123.
- Cypert, E., 1972. Plant succession in burned areas in Okefenokee Swamp following the fires of 1954 and 1955. Proceedings, Tall Timbers Fire Ecology Conference, v. 12, pp. 199-217.
- Davis, A., Kuehn, K.W., Maylotte, D.H. and St. Peters, R.L., 1983. Mapping of polished coal surfaces by automated Reflectance microscopy. Journal of Microscopy, v. 132, Part 3, pp. 297-302.
- Dawson, J.W., 1868. Acadian Geology: The geological structure, organic remains and mineral resources of Nova Scotia, New Brunswick and Prince Edward Island. MacMillian and Company, London, 694 p.
- Demaison, G.J. and Moore, G.T., 1980. Anoxic marine environments and oil source bed genesis. American Association of Petroleum Geologists Bulletin, v. 64, pp. 1179-1209.

- DeWolf, L.A., 1904. The structure and succession at North Sydney and Sydney Mines, C. B. Proceedings and Transactions, Nova Scotia Institute of Science, v. 10, pp. 289-323.
- Diessel, C.F.K., 1965. Correlation of macro- and micropetrography of some New South Wales coals. In J.T. Woodcock, R.T. Madigan and R.G. Thomas (editors), Proceedings, General, Commonwealth Mineralogical and Metallurgical Congress, Melbourne, pp. 669-677.
- Diessel, C.F.K., 1982. An appraisal of coal facies based on maceral characteristics. Australian Coal Geology, v. 4, Part 2, pp. 474-484.
- Diessel, C.F.K., 1986. On the correlation between coal facies and depositional environments. Advances in the study of the Sydney Basin, Proceedings, 20th Symposium, University of Newcastle, pp. 19-22.
- Dolby, G., 1988. The palynology of the Morien Group, Sydney Basin, Cape Breton Island, Nova Scotia. Project 87/22, unpublished report prepared for Nova Scotia Department of Mines and Energy, Halifax, Nova Scotia, 25 p.
- Dolby, G., 1989. The palynology of the Morien Group, Sydney Basin, Cape Breton Island, Nova Scotia. Project 88/16, unpublished report prepared for Nova Scotia Department of Mines and Energy, Halifax, Nova Scotia, 21 p.
- Duff, P.McL.D. and Walton, E.K., 1962. Statistical basis for cyclothem: A quantitative study of the sedimentary succession in the East Pennine coalfield. Sedimentology, v. 1, pp. 211-234.
- Duff, P.McL.D. and Walton, E.K., 1973. Carboniferous sediments at Joggins, Nova Scotia. 7th International Congress, Carboniferous Stratigraphy and Geology, v. 2, pp. 365-379.
- Duff, P.McL.D., Forgeron, S., van de Poll, H.W., 1982. Upper Pennsylvanian sediment dispersal and paleochannel orientation in the western part of the Sydney coalfield, Cape Breton, Nova Scotia. Maritime Sediments and Atlantic Geology, v. 18, pp. 83-90.
- Eagar, R.M.C., 1952. Growth and variation of the non-marine lamellibranch fauna above the Sand Rock Mine of the Lancashire Millstone Grit. Geological Society of London Quarterly Journal, v. 108, pp. 339-374.

- Eagar, R.M.C., 1960. A summary of the results of recent work on the paleoecology of Carboniferous non-marine lamellibranchs. Comptu Rendu, 4th Congress de Stratigraphie et de Géologie du Carbonifère, Harlen, 1958, v. 1, pp. 137-149.
- Eagar, R.M.C. and Rayner, D.H., 1952. A non-marine shelly limestone and other faunal horizons from the Coal Measures near Wakefield. Transactions, Leeds Geological Association, v. 6, pp. 188-209.
- Edwards, W. and Stubblefield, C.J.S., 1948. Marine bands and other faunal marker horizons in relation to the sedimentary cycles of the Middle Coal Measures of Nottinghamshire and Derbyshire. Geological Society Quarterly Journal, v. 103, p. 209.
- England, B.M., Mikka, R.A. and Bagnall, E.J., 1979. Petrographic characterization of coal using automatic image analysis. Journal of Microscopy, v. 116, pp. 329-336.
- Espitalié, J., Madec, M. and Tissot, B., 1980. Role of mineral matrix in kerogen pyrolysis: Influence on petroleum generation and migration. American Association of Petroleum Geologists Bulletin, v. 64, pp. 59-66.
- Espitalié, J., Madec, M., Tissot, B., Mennig, J.J. and Leplat, P., 1977. Source rock characterization method for petroleum exploration. Proceedings, 9th Annual Offshore Technology Conference, v.3, pp. 439-448.
- Esterle, J. and Ferm, J., 1986. Relationship between petrographic and chemical properties and coal seam geometry, Hance seam, Breathitt Formation, Southeastern Kentucky. International Journal of Coal Geology, v. 6, pp. 199-214.
- Esterle, J.S., Ferm, J.C. and Yiu-Liong, T., 1989. A test for the analogy of tropical domed peat deposits to "dulling up" sequences in coal beds - Preliminary results. Organic Geochemistry, v. 14, n. 3, pp. 333-342.

- Ethridge, F.G., Jackson, T.J. and Youngberg, A.D., 1981. Floodbasin sequence of a fine-grained meander belt subsystem: The coal-bearing Lower Wasatch and Upper Fort Union Formations, Southern Powder River Basin, Wyoming. In F.G. Ethridge and R.M. Flores (editors), Recent and Ancient Nonmarine Depositional Environments: A Model for Exploration, Society of Economic Paleontology and Mineralogy, Special Publication 31, pp. 191-209.
- Farrell, K.M., 1987. Sedimentology and facies architecture of overbank deposits of the Mississippi River, False River Region, Louisiana. In F.G. Ethridge, R.M. Flores and M.D. Harvey (editors), Recent Developments in Fluvial Sedimentology, Society of Economic Paleontology and Mineralogy, Special Publication 39, pp. 111-120.
- Ferm, J.C., 1970. Allegheny deltaic deposits. In J.P. Morgan (editor), Deltaic Sedimentation, Modern and Ancient. Society of Economic Paleontology and Mineralogy, Special Publication 15, pp. 246-255.
- Ferm, J.C., 1979. Pennsylvanian cyclothems of the Appalachian Plateau, a retrospective view. In J.C. Ferm and J.C. Horne (editors), Carboniferous Depositional Environments in the Appalachian Region: Columbia, South Carolina. Carolina Coal Group, pp. 284-290.
- Fielding, C.R., 1984. Upper delta plain lacustrine and fluviolacustrine facies from the Westphalian of the Durham coalfield, NE England. *Sedimentology*, v. 31, pp. 547-567.
- Fischer, C.R., 1984. Climate rhythms recorded in strata. *Annual Review of Earth and Planetary Sciences*, v. 14, pp. 351-376.
- Flores, R.M., 1981. Coal deposition in fluvial paleoenvironments of the Paleocene Tongue River Member of the Fort Union Formation, Powder River area, Powder River Basin, Wyoming and Montana. In F.G. Ethridge and R.M. Flores (editors), Recent and Ancient Nonmarine Depositional Environments: A Model for Exploration, Society of Economic Paleontology and Mineralogy, Special Publication 31, pp. 169-190.
- Forgeron, S., MacKenzie, B., and MacPherson, K., 1986. The effects of geological features on coal mining, Sydney coalfield, Nova Scotia. *Canadian Institute of Mining Bulletin*, v. 79, n. 891, pp. 79-87.

- Galloway, W.E., 1989. Genetic stratigraphic sequences in basin analysis I: Architecture and genesis of flooding-surface bounded depositional units. *The American Association of Petroleum Geologists Bulletin*, v. 73, n. 2, pp. 125-142.
- Gayes, P.T., Scott, D.B., Collins, E.C. and Nelson, D.D., (in press). A Late Holocene sea-level fluctuation in South Carolina. *Society of Economic Paleontology and Mineralogy, Special Publication 49*.
- Ghosh, S.K., 1987. Cyclicity and facies characteristics of alluvial sediments in the Upper Paleozoic Monongahela-Dunkard Groups, Central West Virginia. In F.G. Ethridge, R.M. Flores and M.D. Harvey (editors), *Recent Developments in Fluvial Sedimentology*, Society of Economic Paleontology and Mineralogy, Special Publication 39, pp. 229-239.
- Gibling, M.R., 1992. Late Carboniferous alluvial paleovalleys in the Sydney Basin of Nova Scotia. Abstract In Geological Association of Canada-Mineralogical Association of Canada, Joint Annual Meeting, Wolfville, Nova Scotia, pp. A39-A40.
- Gibling, M.R. and Bird, D.J., (submitted). Late Carboniferous cyclothems of the Sydney Basin, Nova Scotia. submitted to the *Geological Society of America Bulletin*.
- Gibling M.R. and Kalkreuth W.D., 1991. Petrology of selected carbonaceous limestones and shales in Pennsylvanian coal basins of Atlantic Canada. *International Journal of Coal Geology*, v. 17, pp. 239-272.
- Gibling, M.R. and Rust, B.R., 1984. Channel margins in a Pennsylvanian braided fluvial deposit: the Morien Group near Sydney, Nova Scotia, Canada. *Journal of Sedimentary Petrology*, v. 54, n. 3, pp. 773-782.
- Gibling M.R. and Rust, B.R., 1987. Evolution of a mud-rich meander belt in the Carboniferous Morien Group, Nova Scotia, Canada. *Canadian Society of Petroleum Geologists Bulletin*, v. 35, n. 1, pp. 24-33.
- Gibling, M.R. and Rust, B.R., 1990a. Ribbon sandstones in the Pennsylvanian Waddens Cove Formation, Sydney Basin, Atlantic Canada: the influence of siliceous duricrusts on channel-body geometry. *Sedimentology*, v. 37, pp. 45-65.

- Gibling, M.R. and Rust, B.R., 1990b. Tectonic influence on alluvial sedimentation in the coal-bearing Sydney Basin, Nova Scotia, Canada. Abstract In 13th International Sedimentological Congress, Nottingham, England, p. 188.
- Gibling, M.R., Boehner, R.C. and Rust, B.R., 1987. The Sydney Basin of Atlantic Canada: An upper Paleozoic strike-slip basin in a collisional setting. In C. Beaumont and A.J. Tankard (editors), Sedimentary Basins and Basin-Forming Mechanisms, Canadian Society of Petroleum Geologists, Memoir 12, pp. 269-285.
- Gibling, M.R., Rust, B.R. and Aksu, A.E., 1985. Mudrocks of the Pennsylvanian Morien Group, Sydney Coalfield: Mud deposition and early diagenesis on an alluvial plain. Abstract In Geological Association of Canada, Annual Meeting, p. 21.
- Gibling, M.R., Zentilli, M., Mahony, H. and McCready, R.G.L., 1989. An isotopic evaluation of sulphur recycling from evaporites to coals in the carboniferous Sydney Basin, Nova Scotia. In Current Research, Part B, Geological Survey of Canada, Paper 86-1B, pp. 73-76.
- Gibling, M.R., Calder, J.H., Ryan, R., van de Poll, H.W. and Yeo, G.M., 1992. Late Carboniferous and Early Permian drainage patterns in Atlantic Canada. Canadian Journal of Earth Sciences, v. 29, n. 2, pp. 338-352.
- Giles, P.S., 1983. Sydney Basin Project. Nova Scotia Department of Mines and Energy, Report of Activities 83-1, pp. 57-70.
- Gluskoter, H.J. and Hopkins, M.E., 1970. Distribution of sulphur in Illinois coals. In W.H. Smith (editor), Depositional Environments in Parts of the Carbondale Formation - Western and Northern Illinois. Illinois Survey Guidebook, Series 8, pp. 89-95.
- Grant, A.C., 1992. Aspects of seismic character and extent of Permo-Carboniferous sediments, Maritimes Basin and Sydney Basin. Abstract In Geological Association of Canada-Mineralogical Association of Canada, Joint Annual Meeting, Wolfville, Nova Scotia, p. A42.
- Gray, F.W. and Gray, R.H., 1941. The Sydney Coalfield. Transactions, Canadian Institute of Mining, v. 44, pp. 289-330.

- Hacquebard, P.A., 1952. A petrographic investigation of the Tracy seam of the Sydney coalfield, Nova Scotia. 2nd Conference on the Origin and Constitution of Coal, Crystal Cliffs, Nova Scotia, Nova Scotia Department of Mines and Nova Scotia Research Foundation, Halifax, pp. 293-309.
- Hacquebard, P.A., 1983. Geological development and economic evaluation of the Sydney coal basin, Nova Scotia. In Current Research, Part A, Geological Survey of Canada, Paper 83-1A, pp. 71-81.
- Hacquebard, P.A., 1986. The Gulf of St. Lawrence Carboniferous Basin; the largest coalfield of eastern Canada. Canadian Institute of Mining Bulletin, v. 79, n. 891, pp. 67-78.
- Hacquebard, P.A. and Avery, M.P., 1982. Petrography of the Harbour seam in the Donkin Reserve area of the Sydney coalfield, Nova Scotia. Coal: Phoenix of the 80's - Proceedings, 64th CIC Coal Symposium, pp. 79-86.
- Hacquebard, P.A. and Donaldson, J.R., 1969. Carboniferous coal deposition associated with flood-plain and limnic environments in Nova Scotia. Geological Society of America, Special Paper 114, pp. 143-191.
- Hacquebard, P.A. and Donaldson, J.R., 1970. Coal metamorphism and hydrocarbon potential in the Upper Paleozoic of the Atlantic Provinces, Canada. Canadian Journal of Earth Sciences, v. 7, pp. 1139-1158.
- Hacquebard, P.A., Birmingham, T.F. and Donaldson, J.R., 1967. Petrography of Canadian coals in relation to environment of deposition. Symposium on the Science and Technology of Coal, Department of Energy, Mines and Resources, pp. 84-97.
- Hacquebard, P.A., Cameron, A.R. and Donaldson, J.R., 1964. A depositional study of the Harbour seam, Sydney coalfield, Nova Scotia. Geological Survey of Canada, Paper 65-15, 31 p.
- Haites, T.B., 1950. Report on the Harbour seam in the northern part of the Sydney Coalfield, Cape Breton Island, Nova Scotia. Geological Survey of Canada Files, 32 p.
- Haites, T.B., 1951. Some geological aspects of the Sydney coalfield with reference to their influence on mining operations. Transactions, Canadian Institute of Mining, v. 54, pp. 215-225.

- Haites, T.B., 1952. Conjectural shape and extent of the Sydney coalfield. Transactions, Canadian Institute of Mining, v. 55, pp. 202-212.
- Harms, J.C. and Fahnestock, R.K., 1965. Stratification, bedforms and flow phenomena (with an example from the Rio Grande). In G.V. Middleton (editor), Primary Sedimentary Structures and their Hydrodynamic Interpretation, Society of Economic Paleontologists and Mineralogists, Special Publication 12, pp. 84-115.
- Haszeldine, R.S., 1984. Muddy deltas in freshwater lakes and tectonism in the Upper Carboniferous Coalfield of NE England. Sedimentology, v. 31, pp. 811-822.
- Hayes, A.O. and Bell, W.A., 1923. The Southern part of the Sydney coalfield, Nova Scotia. Geological Survey of Canada, Memoir 133, n. 114, 108 p.
- Hayes, A.O., Bell, W.A. and Goranson, E.A., 1938a. Sydney Map Sheet (east half), Cape Breton County, Nova Scotia. Map Sheet 361A, Department of Mines and Resources.
- Hayes, A.O., Bell, W.A. and Goranson, E.A., 1938b. Glace Bay Map Sheet, Cape Breton County. Map Sheet 362A, Department of Mines and Resources.
- Heckel, P.H., 1977. Origin of phosphatic black shale facies in Pennsylvanian cyclothems of mid-continent North America. American Association of Petroleum Geologists Bulletin, v. 61, pp. 1045-1068.
- Heckel, P.H., 1984. Changing concepts of midcontinent Pennsylvanian cyclothems, North America. 9th Congrès International de Stratigraphie et de Geologie du Carbonifère, v. 3, Carbondale, Illinois, Southern Illinois University Press, pp. 535-553.
- Heckel, P.H., 1986. Sea-level curve for Pennsylvanian eustatic marine transgressive-regressive depositional cycles along midcontinent outcrop belt, North America. Geology, v. 14, pp. 330-334.
- Heerden, van, I.L. and Roberts, H.H., 1988. Facies development of Atchafalaya Delta, Louisiana: A modern bayhead delta. American Association of Petroleum Geologists Bulletin, v. 72, pp. 439-453.
- Heide, S. van de, 1964. Compaction as a possible factor in Upper Carboniferous rhythmic sedimentation. In F.D. Merriam (editor), Symposium of Cyclic Sedimentation, Kansas Geological Survey, Bulletin 169, pp. 38-45.

- Hess, J.C. and Lippolt, H.J., 1986. $^{40}\text{Ar}^{39}\text{Ar}$ ages of tonstein and tuff sanidines: New calibration points for the improvement of the Upper Carboniferous time scale. *Isotope Geoscience*, v. 59, pp. 143-154.
- Hind, W., 1899. A monograph of the British Carboniferous lamellibranchiata. *Palaeontological Society*, Part 4, pp. 277-360.
- Ho, C. and Coleman, J.M., 1969. Consolidation and cementation of recent sediments in the Atchafalaya Basin, *Geological Society of America Bulletin*, v. 80, pp. 183-192.
- Huddle, J.W. and Patterson, S.H., 1961. Origin of Pennsylvanian underclay and related seat rock. *Geological Society of America Bulletin*, v. 72, pp. 1643-1660.
- Hunt, J.W., 1982. Relationship between microlithotype and maceral composition of coals and geological setting of coal measures in the Permian basins of eastern Australia. *Australia Coal Geology*, v. 4, n. 2, pp. 484-502.
- Hyde, R., 1913. The Carboniferous sections on Sydney Harbour. In *Guide Book No. 1, Excursion in Eastern Quebec and the Maritime Provinces*, Part 2, *Geological Survey of Canada*, Ottawa, 407 p.
- International Committee for Coal Petrology (I.C.C.P.), 1963, 1971. *International Handbook of Coal Petrology*, 2nd edition and supplement, *Centre National de la Recherche Scientifique*, Paris.
- Jackson, R.G., 1976. Depositional model of point bars in the Lower Wabash River. *Journal of Sedimentary Petrology*, v. 46, n. 3, pp. 579-594.
- Johnson, B., 1984. The great fire of Borneo. *World Wild Life Fund*, Godalming, Surrey, U.K., 24 p.
- Kalkreuth, W. and Leckie, D.A., 1989. Sedimentological and petrographical characteristics of Cretaceous strandplain coals: A model for coal accumulation from the North American western Interior Seaway. *International Journal of Coal Geology*, v. 12, pp. 381-424.

- Keppie, J.D., 1985. The Appalachian collage. In D.G. Gee and B.A. Sturt (editors), *The Caledonide Orogen - Scandinavia and Related Areas*, John Wiley and Sons Ltd. pp. 1217-1226.
- King, L.H., 1953. Occurrence, distribution and weathering of pyrite in coals from the Sydney coalfield, Nova Scotia. *Society of Economic Geologists*, v. 48, p. 623.
- King, L.H. and MacLean, B., 1976. *Geology of the Scotian Shelf*. Geological Survey of Canada, Paper 74-31, 31 p.
- King, L.H., Fader, G.B.J., Jenkins, W.A.M. and King, E.L., 1986. Occurrence and regional geological setting of Paleozoic rocks on the Grand Banks of Newfoundland. *Canadian Journal of Earth Sciences*, v. 23, pp. 504-526.
- Klein, deV. G., 1990. Pennsylvanian time-scales and cycle period. *Geology*, v. 18, pp. 455-457.
- Klein, deV. G. and Kupperman, J.B., 1992. Pennsylvanian cyclothems: Methods of distinguishing tectonically induced changes in sea-level from climatically induced changes. *Geological Society of America Bulletin*, v. 104, n. 2, pp. 166-175.
- Klein, deV. G. and Willard, D.A., 1989. Origin of the Pennsylvanian coal-bearing cyclothems of North America. *Geology*, v. 17, pp. 152-155.
- Komarek, E.V., Sr., 1972. Ancient fires. *Proceedings, Tall Timbers Fire Ecology Conference*, v. 12, pp. 219-240.
- Kraus, M.J., 1987. Integration of channel and floodplain suites II: Vertical relations of alluvial paleosols. *Journal of Sedimentary Petrology*, v. 57, pp. 602-612.
- Krumbein, W.C. and Garrels, R.M., 1952. Origin and classification of chemical sediments in terms of pH and oxidation-reduction potential. *Journal of Geology*, v. 60, pp. 1-33.
- Lambe, L.M., 1916. Ganoid fishes from near Banff, Alberta. *Transactions, Royal Society of Canada, Series 3*, v. 10, pp. 35-44.
- Lamberson, M.N., Bustin, R.M., Kalkreuth, W. and Pratt, K.C., 1990. Lithotype characteristics and variation in selected coal seams of the Gates Formation, Northeastern British Columbia. *British Columbia Ministry of Energy, Mines and Petroleum Resources*, 20 p.

- Lamberson, M.N., Bustin, R.M. and Kalkreuth, W.D., 1991. Lithotype (maceral) composition and variation as correlated with paleo-wetland environments, Gates Formation, northeastern British Columbia, Canada. *International Journal of Coal Geology*, v. 18, pp. 87-124.
- Lee, J.B., 1985. Analysis of coal blends by automated microscopy. *Journal of Microscopy*, v. 137, Part 2, pp. 137-144.
- Leeder, M.R., 1973a. Sedimentology and paleogeography of the Upper Old Red Sandstone in the Scottish Border Basin. *Scottish Journal of Geology*, v. 9, pp. 117-144.
- Leeder, M.R., 1973b. Fluvial fining-upwards cycles and the magnitude of paleochannels. *Geological Magazine*, v. 110, pp. 265-276.
- Leeder, M.R., 1975. Pedogenic carbonates and floodplain sediment accretion rates: A quantitative model for alluvial arid-zone lithofacies. *Geological Magazine*, v. 112, pp. 257-270.
- Leeder, M.R., 1988. Recent developments in Carboniferous geology: A critical review with implications for the British Isles and NW Europe. *Proceedings, Geologists Association*, v. 99, pp. 73-100.
- Leeder, M.R. and Strudwick, A.E., 1987. Delta-marine interactions: A discussion of sedimentary models for Yoredale-type cyclicity in the Dinantian of Northern England. In J. Miller, A.E. Adams and V.P. Wright (editors), *European Dinantian Environments*, Wiley, New York, pp. 115-129.
- Lippolt, H.J., Hess, J.C. and Burger, K., 1984. Isotopische Alter von pyroklastischen Sandsteinen aus Kaolin - Kohlenstein als Korrelationsmarker für das Mitteluroaische Oberkarbon. *Forschfirst Geologisches, Rheinland und Westfalen*, v. 32, pp. 119-150.
- Loncarevic, B.D., Barr, S.M., Raeside, R.P., Keen, C.E. and Marillier, F., 1989. Northeastern extension and crustal expression of terranes from Cape Breton Island, Nova Scotia, based on geophysical data. *Canadian Journal of Earth Sciences*, v. 26, pp. 2255-2267.

- Lyons, P.C., Finkelman, R.B., Thompson, C.L., Brown, F.W. and Hatcher, P.G., 1982. Properties, origin and nomenclature of rodlets of the inertinite maceral group in coals of the central Appalachian Basin, U.S.A. *International Journal of Coal Geology*, v. 1, pp. 313-346.
- Marchioni, D.L., 1980. Petrography and depositional environment of the Liddell seam, Upper Hunter Valley, New South Wales. *International Journal of Coal Geology*, v. 1, pp. 35-61.
- Marchioni, D. and Kalkreuth, W., 1991. Coal facies interpretation based on lithotype and maceral variations in lower Cretaceous (Gates Formation) coals of Western Canada. *International Journal of Coal Geology*, v. 18, pp. 125-162.
- Marshall, C.E., 1954. Introduction to a study of the nature and origin of fusain (fusinite). *Fuel (London)*, v. 33, pp. 134-144.
- Masson, A.G., 1986. The sedimentology of the Upper Morien Group (Pennsylvanian) in the Sydney Basin east of Sydney Harbour, Cape Breton, Nova Scotia. Unpublished Ph.D. thesis, University of Ottawa, 349 p.
- Masson, A.G. and Rust, B.R., 1983. Lacustrine stromatolites and algal laminites in a Pennsylvanian coal-bearing succession, near Sydney, Nova Scotia, Canada. *Canadian Journal of Earth Sciences*, v. 20, n. 7, pp. 1111-1118.
- Masson, A.G. and Rust, B.R., 1984. Freshwater shark teeth as paleoenvironmental indicators in the Upper Pennsylvanian Morien Group of the Sydney Basin, Nova Scotia. *Canadian Journal of Earth Sciences*, v. 21, pp. 1151-1155.
- Masson, A.G. and Rust, B.R., 1990. Alluvial plain sedimentation in the Pennsylvanian Sydney Mines Formation, eastern Sydney Basin, Nova Scotia. *Canadian Society of Petroleum Geologists Bulletin*, v. 38, n. 1, pp. 89-105.
- Mastalerz, M. and Smyth, M., 1988. Petrography and depositional conditions of the 64/65 coal seam in the Intrasudetic Basin, S.W. Poland. *International Journal of Coal Geology*, v. 10, pp. 309-336.

- McCabe, P.J., 1984. Depositional environments of coal and coal-bearing strata. In R.A. Rahmani and R.M. Flores (editors), *Sedimentology of Coal and Coal-bearing Sequences*, International Association of Sedimentology, Special Publication, v. 7, pp. 13-42.
- McPherson, J.G., 1979. Calcrete paleosols in fluvial redbeds of the Aztec Siltstone (Upper Devonian), Southern Victoria Land, Antarctica. *Sedimentary Geology*, v. 22, pp. 267-285.
- Miall, A.D., 1985. Architectural-element analysis: A new method of facies analysis applied to fluvial deposits. *Earth Sciences Review*, v. 22, pp. 261-308.
- Misra, B.K., Singh, B.D. and Navale, G.K.B., 1990. Resino-inertinites of Indian Permian coals - their origin, genesis and classification. *International Journal of Coal Geology*, v. 14, pp. 277-293.
- Moody-Stuart, M., 1966. High- and low-sinuosity stream deposits, with examples from the Devonian of Spitsbergen. *Journal of Sedimentary Petrology*, v. 36, pp. 1102-1117.
- Moore, P.D., 1987. Ecological and hydrological aspects of peat formation. In A.C. Scott (editor), *Coal and Coal-bearing Strata*, Geological Society, Special Publication 32, pp. 7-15.
- Moore, R.C., 1929. Environment of Pennsylvanian life in North America. *American Association of Petroleum Geologists Bulletin*, v. 13, n. 5, pp. 459-487.
- Moore, R.C., 1936. Stratigraphic classification of the Pennsylvanian rocks of Kansas. *Kansas Geological Survey Bulletin*, v. 22, 265 p.
- Moore, R.C., 1950. Late Pennsylvanian cyclic sedimentation in central United States. 18th International Geological Congress, Proceedings, Part IV, pp. 5-16.
- Moy-Thomas, J.A., 1971. *Palaeozoic Fishes*. W.B. Saunders Company, Philadelphia, Toronto, 259 p.
- Neavel, R.C., 1981. Origin, petrography and classification of coal. In M.A. Elliot (editor), *Chemistry of Coal Utilization*, 2nd supplementary volume, John Wiley, New York, N.Y., pp. 91-158.

- Newman, W.R., 1934. Microscopic features of the Phalen seam, Sydney coalfield, N. S. Canadian Journal of Research, v. 12, pp. 533-553.
- Osvald, H., 1937. Myrar och myrodling (Peatlands and their cultivation). Stockholm, Sweeden, Kooperativa Förbundels Bokforlag, 407 p.
- Parnell, J., 1983. Ancient duricrusts and related rocks in perspective: A contribution from the Old Red Sandstone, In R.C.L. Wilson (editor), Residual Deposits: Surface Related Weathering Processes and Materials, Geological Society of London, Blackwell Scientific Publications, Oxford, London, Edinburgh, Boston, Melbourne, pp. 197-209.
- Penland, S., Boyd, R. and Suter, J.R., 1988. Transgressive depositional systems of the Mississippi delta plain: A model for barrier shoreline and shelf sand development. Journal of Sedimentary Petrology, v. 58, pp. 932-949.
- Peters, K.E., 1986. Guidelines for evaluating petroleum source rock using programmed pyrolysis. American Association of Petroleum Geologists Bulletin, v. 70, n. 3, pp. 318-329.
- Pilgrim, J.C., 1983. The mode and occurrence of pyrite in the Sydney coalfield, Cape Breton, Nova Scotia. Unpublished BSc. Thesis, Acadia University, Wolfville, Nova Scotia, 68 p.
- Poll, van de, H.W., 1973. Stratigraphy, sediment dispersal and facies analysis of the Pennsylvanian Pictou Group in New Brunswick. Maritime Sediments, v. 9, pp. 72-77.
- Poll, van de, H.W. and Forbes, W.H., 1984. On the lithostratigraphy, sedimentology, structure and paleobotany of the Stephanian-Permian redbeds of Prince Edward Island. 9th International Congress of Carboniferous Stratigraphy and Geology, Compte Rendu, v. 3, pp. 271-283.
- Poole, W.H., 1967. Tectonic evolution of the Appalachian region of Canada. In E.R.W. Neale and H. Williams (editors), Geology of the Atlantic Region, Geological Association of Canada, Special Paper n. 4, pp. 9-51.

- Posamentier, H.W., Jervey, M.T. and Vail, P.R., 1988. Eustatic controls on clastic deposition I - Conceptual framework. In C.K. Wilgus, B.S. Hastings, C.G.St.C. Kendall, H.W. Posamentier, C.A. Ross and J.C. van Wagoner (editors), Sea-level Changes - An Integrated Approach, Society of Economic Paleontologists and Mineralogists, Special Publication 42, pp. 109-124.
- Pratt, K.C., 1989. The use of automated image analysis to determine conventional coal petrographic parameters - an example from southeastern British Columbia. In Contributions to Canadian Coal Geoscience, Geological Survey of Canada, Paper 89-8, pp. 137-145.
- Pye, K., Dickson, J.A.D., Scheavon, N., Coleman, M.L. and Cox, M., 1990. Formation of siderite - Mg-calcite-iron sulphide concretions in intertidal marsh and sandflat sediments, north Norfolk, England. *Sedimentology*, v. 37, pp. 325-343.
- Ramsbottom, W.H.C., 1977. Major cycles of transgression and regression (mesothems) in the Namurian. *Proceedings, Yorkshire Geological Society*, v. 41, pp. 261-291.
- Ramsbottom, W.H.C., 1978. Carboniferous. In W.S. McKerrow (editor), *The Ecology of Fossils*, The MIT Press, Cambridge, Massachusetts, pp. 146-183.
- Retallack, G.J., 1988. Field recognition of paleosols. In J. Reinhard and W.R. Sigleo (editors), *Paleosols and Weathering through Geologic Time: Principles and Applications*, Geological Society of America, Special Paper 216, pp. 1-20.
- Reynolds, P.H., Elias, P., Muecke, G.K. and Grist, A.M., 1987. Thermal history of the southwestern Meguma zone, Nova Scotia, from an $^{40}\text{Ar}/^{39}\text{Ar}$ and fission track dating study of intrusive rocks. *Canadian Journal of Earth Sciences*, v. 24, pp. 1952-1965.
- Riepe, W. and Steller, M., 1984. Characterization of coal and coal blends by automatic image analysis: Use of the Leitz texture analysis system. *Fuel*, v. 63, pp. 313-317.
- Rippon, J.H., 1984. The Clowne Seam, marine band, and overlying sediments in the Coal Measures (Westphalian B) of north Derbyshire. *Proceedings, Yorkshire Geological Society*, v. 45, Parts 1 and 2, pp. 27-43.

- Robb, C., 1876. Report on exploration and surveys in Cape Breton Island, Nova Scotia. In Report of Progress for 1874-1875, Geological Survey of Canada, pp. 166-266.
- Romer, A.S., 1945. Vertebrate Paleontology. University of Chicago Press, Chicago, 687 p.
- Rosenberg, R., 1977. Benthic macrofaunal dynamics, production and dispersion in an oxygen deficient estuary of West Sweden. *Journal of Experimental Marine Biology and Ecology*, v. 26, pp. 107-133.
- Russel, R.J., 1942. Flotant. *Geographical Review*, v. 32, n. 1, pp. 74-98.
- Rust, B.R. and Gibling, M.R., 1990. Braidplain evolution in the Pennsylvanian South Bar Formation, Sydney Basin, Nova Scotia, Canada. *Journal of Sedimentary Petrology*, v. 60, n. 1, pp. 59-72.
- Rust, B.R., Masson, A.G., Dilles, S.J. and Gibling, M.R., 1983. Sedimentological studies in the Sydney Basin, 1982. In Mines and Mineral Branch Report of Activities, Nova Scotia Department of Mines and Energy, Report 83-1, pp. 85-95.
- Rust, B.R., Gibling, M.R., Best, M.A., Dilles, S.J. and Masson, A.G., 1987. A sedimentological overview of coal-bearing Morien Group (Pennsylvanian), Sydney Basin, Nova Scotia, Canada. *Canadian Journal of Earth Sciences*, v. 24, pp. 1869-1885.
- Ryan, R.J., Boehner, R.C. and Calder, J.H., 1991. Lithostratigraphic revision of the Upper Carboniferous to Lower Permian strata in the Cumberland Basin, Nova Scotia and the regional implications for the Maritimes Basin in Atlantic Canada. *Canadian Society of Petroleum Geologists Bulletin*, v. 39, n. 4, pp. 289-314.
- Ryer, T.A. and Langer, A.W., 1980. Thickness change involved in the peat to coal transformation for a bituminous coal of Cretaceous age in Central Utah. *Journal of Sedimentary Petrology*, v. 50, n. 3, pp. 987-992.
- Saunders W.B., and Ramsbottom, W.H.C., 1986. The mid-Carboniferous eustatic event. *Geology*, v. 14, pp. 208-212.

- Schenk, P.E., 1967. Facies and phases of the Altamont Limestone and megacyclothem (Pennsylvanian), Iowa to Oklahoma. Geological Society of America Bulletin, v. 78, pp. 1369-1384.
- Schenk, P.E., 1978. Synthesis of the Canadian Appalachians. Geological Survey of Canada, Paper 78-13, pp. 111-136.
- Schenk, P.E., 1981. The Meguma Zone of Nova Scotia - A remnant of Western Europe, South America or Africa? In J.M. Kerr and A.J. Ferguson (editors), Geology of the North Atlantic Borderlands, Canadian Society of Petroleum Geologists, Memoir 7, pp. 119-148.
- Scholl, D.W., 1969. Modern coastal mangrove swamp stratigraphy and the ideal cyclothem. In E.C. Dapples and M.E. Hopkins (editors), Environments of Coal Deposition, Geological Society of America, Special Paper 114, pp. 37-61.
- Schopf, J.M., 1975. Modes of fossil preservation. Review of Palaeobotany and Palynology, v. 20, pp. 27-53.
- Scotese, C.R. and McKerrow, W.S., 1990. Revised world maps and introduction. In W.S. McKerrow and C.R. Scotese (editors) Palaeozoic Palaeogeography and Biogeography. Geological Society of London, Memoir 12, pp. 1-21.
- Scott, A.C., 1989. Observations on the nature and origin of fusain. International Journal of Coal Geology, v. 12, pp. 443-475.
- Scott, A.C. and Jones, T.P., 1992. The influence of fire in Carboniferous ecosystems. Abstract In Geological Association of Canada-Mineralogical Association of Canada, Joint Annual Meeting, Wolfville, Nova Scotia, p. A99.
- Scott, D.B., Suter, J.R. and Kusters, E.C., 1991. Marsh foraminifera and arcellaceans of the lower Mississippi Delta: Controls on spatial distributions. Micropaleontology, v. 37, n. 4, pp. 373-392.
- Shibaoka, M. and Smyth, M., 1975. Coal petrology and the formation of coal seams in some Australian sedimentary basins. Economic Geology, v. 70, pp. 1463-1473.
- Slingerland, R. and Furlong, K.P., 1989. Geodynamic and geomorphic evolution of the Permo-Triassic Appalachian Mountains. Geomorphology, v. 2, pp. 23-27.

- Sloss, L.L., 1963. Sequences in the cratonic interior of North America. *Geological Society of America Bulletin*, v. 74, pp. 93-114.
- Smith, A.H.V., 1962. The palaeoecology of Carboniferous peats based on the miospores and petrography of bituminous coals. *Proceedings, Yorkshire Geological Society*, v. 19, pp. 423-473.
- Smith, A.H.V., 1968. Seam profiles and seam characters. In D.G. Murchison and T.S. Westoll (editors), *Coal and Coal-bearing Strata*. Oliver and Boyd, Edinburgh, pp. 31-40.
- Smith, D.G., 1983. Anastomosed fluvial deposits: Modern examples from Western Canada. *International Association of Sedimentology, Special Publication 6*, pp. 155-168.
- Smith, D.G., 1986. Anastomosing river deposits, sedimentation rates and basin subsidence, Magdalena River, Northwestern Colombia, South America. *Sedimentary Geology*, v. 46, pp. 177-196.
- Stach, E., 1955. Crassidurite - a means of seam correlation in the Carboniferous coal measures of the Rhur. *Fuel*, 34, pp. 95-118.
- Stach, E., Mackowsky, M.-TH., Teichmüller, M., Taylor, G.H., Chandra, D. and Teichmüller, R., 1982. *Stach's Textbook of Coal Petrology*. Gebrüder Borntraeger, Berlin - Stuttgart, 535 p.
- Staub, J.R. and Cohen, A.D., 1979. The Snuggedy Swamp of South Carolina: A back-barrier estuarine coal-forming environment. *Journal of Sedimentary Petrology*, v. 49, n. 1, pp. 133-144.
- Stear, W.M., 1983. Morphological characteristics of ephemeral stream channel and overbank splay sandstone bodies in the Permian Lower Beauford Group, Karoo Basin, South Africa. In J.D. Collinson and J. Lewin (editors), *Modern and Ancient Systems*, International Association of Sedimentologists, Special Publication 6, pp. 405-420.
- Sternberg, R.M., 1941. Carboniferous dipnoans from Nova Scotia. *American Journal of Science*, v. 239, pp. 836-838.
- Stopes, M.C., 1935. On the petrology of banded bituminous coal. *Fuel (London)*, v. 14, pp. 4-13.

- Strehlau, K., 1990. Facies and genesis of Carboniferous coal seams of Northwest Germany. *International Journal of Coal Geology*, v. 15, pp. 245-292.
- Styan, W.B. and Bustin, R.M., 1984. Sedimentology of Fraser River Delta peat deposits: A modern analogue for some deltaic coals. In R.A. Rahmani and R.M. Flores (editors), *Sedimentology of Coal and Coal-bearing Sequences*, International Association of Sedimentologists, Special Publication 7, pp. 241-271.
- Tankard, A.J., 1986. Depositional response to foreland deformation in the Carboniferous of Eastern Kentucky. *American Association of Petroleum Geologists Bulletin*, v. 70, n. 7, pp. 853-868.
- Tasch, K.H., 1960. Die Möglichkeiten der Flözgleichstellung unter Zuhilfenahme von Flözbildungsdiagrammen, *Bergbau Rdsch.*, v. 1 pp. 153-157.
- Taylor, G. and Woodyer, K.D., 1978. Bank deposition in suspended-load streams. *Canadian Society of Petroleum Geologists, Memoir* 5, pp. 257-275.
- Teichmüller, M., 1950. Zum petrographischen Aufbau und Werdegang der Weichbraunkohle (mit Berücksichtigung genetischer Fragen der Steinkohlenpetrographie). *Geologische Jahrbuch*, v. 64, pp. 429-488.
- Teichmüller, M., 1989. The genesis of coal from the viewpoint of coal petrology. *International Journal of Coal Geology*, v. 12, pp. 1-87.
- Teichmüller, M. and Teichmüller, R., 1982. Fundamentals of coal petrology. In E. Stach, M.Th. Mackowsky, M. Teichmüller, G.H. Taylor, D. Chandra and R. Teichmüller (editors), *Textbook of Coal Petrology*, Gebrüder Borntraeger, Berlin - Stuttgart, pp. 5-86.
- Teichmüller, M. and Thompson, P.W., 1958. Vergleichende mikroskopische und schematische Untersuchungen der wichtigsten Fazies-Typen im Hauptflotz der niederrheinischen Braunkohle *Fortschr. Geologische Rheinld*, Band 2, pp. 573-598.
- Thibaudeau, S.A. and Medioli, F.S., 1986. Carboniferous thecamoebians and marsh foraminifera: New stratigraphic tools for ancient paralic deposits. Abstract In *Geological Society of America, Annual Meeting*, San Antonio, p. 771.

- Thibaudeau, S.A., Medioli, F.S. and Scott, D.B., 1987. Carboniferous marginal marine rhizopods: A morphological comparison with recent correspondents. Abstract In Geological Society of America, Annual Meeting, Phoenix, Arizona, p. 866.
- Thomas, R.G., Smith, D.G., Wood, J.M., Visser, J., Calverley-Range, E.A. and Koster, E.H., 1987. Inclined heterolithic stratification - terminology, description, interpretation and significance. *Sedimentary Geology*, v. 53, pp. 123-179.
- Thompson, C.L., Lyons, P.C., Finkleman, R.B., Brown, F.W. and Hatcher, P.G., 1983. Microscopy of sclerotinites in the coal beds of the central part of the Appalachian coalfield, U.S.A. *Journal of Microscopy*, v. 132, pp. 267-277.
- Trueman, A.E., 1942. Supposed commensalism of Carboniferous spirorbids and certain non-marine lamellibranchs. *Geological Magazine*, v. 79, n. 6, pp. 312-319.
- Trueman, A.E., 1946. Stratigraphical problems in the coal measures of Europe and North America. Anniversary Address of President, Geological Society of London *Quarterly Journal*, v. 102, pp. 1c-xciii.
- Trueman, A.E., 1954. *The Coalfields of Great Britain.* Edward Arnold, London, 396 p.
- Trueman, A.E. and Weir, J., 1946. A monograph of British Carboniferous non-marine lamellibranchia, Part 1. Monograph, Palaeontological Society of London.
- Tye, R.S. and Coleman, J.M., 1989. Depositional processes and stratigraphy of fluvial dominated lacustrine deltas: Mississippi Delta plain. *Journal of Sedimentary Petrology*, v. 59, n. 6, pp. 973-996.
- Udden, J.A., 1912. Geology and mineral resources of the Peoria Quadrangle, Illinois. *United States Geological Survey Bulletin* 506, pp. 1-103.
- Vasey, G.M., 1983. The nonmarine fauna of the Sydney Coalfield (Morien Group), Canada: Palaeoecology and correlation. 10th International Congress, Stratigraphy and Carboniferous Geology, Madrid, pp. 477-490.
- Vasey, G.M., 1984. Westphalian macrofaunas in Nova Scotia: Paleoecology and correlation. Unpublished Phd. thesis, Strathclyde University, Glasgow, 389 p.

- Vasey, G.M. and Zodrow, E.L., 1983. Environmental and correlative significance of a non-marine algal limestone (Westphalian D), Sydney Coalfield, Cape Breton Island, Nova Scotia. *Maritime Sediments and Atlantic Geology*, v. 19, n. 1, pp. 1-10.
- Veevers, J.J. and Powell, C.McA., 1987. Late Paleozoic glacial episodes in Gondwanaland reflected in transgressive depositional sequences in Euramerica. *Geological Society of America Bulletin*, v. 98, pp. 475-487.
- Walker, R.G. and Cant, D.J., 1976. Sandy fluvial systems. In R.G. Walker (editor), *Facies Models*, Geoscience Canada Special Publication 3, pp. 101-109.
- Wanless, H.R. and Shepard, F.P., 1936. Sea level and climatic changes related to Late Paleozoic cycles. *Geological Society of America Bulletin*, v. 47, pp. 1177-1206.
- Wanless, H.R. and Weller, J.M., 1932. Correlation and extent of Pennsylvanian cyclothems. *Geological Society of America Bulletin*, v. 43, pp. 1003-1016.
- Wanless, H.R., Tubb, J.B.Jr., Gednetz, D.E. and Weiner, J.L., 1963. Mapping sedimentary environments of Pennsylvanian cycles. *Geological Society of America Bulletin*, v. 74, pp. 437-486.
- Warwick, P.D. and Stanton, R.W., 1988. Depositional models for two Tertiary coal-bearing sequences in the Powder River Basin, Wyoming, U.S.A. *Geological Society of London*, v. 145, pp. 613-620.
- Webb, G.A., 1969. Paleozoic wrench faults in the Canadian Appalachians. *American Association of Petroleum Geologists, Memoir 12*, pp. 754-786.
- Weedon, M.J., 1990. Shell structure and affinity of vermiform 'gastropods'. *Lethaia*, v. 23, pp. 297-309.
- Weir, J., 1960. A monograph of British Carboniferous non-marine lamellibranchia, Part 10. *Monograph, Palaeontological Society of London*.
- Weller, J.M., 1930. Cyclic sedimentation of the Pennsylvanian period and its significance. *Journal of Geology*, v. 38, pp. 97-135.

- Weller, J.M., 1956. Argument for diastrophic control of Late Paleozoic cyclothems. *American Association of Petroleum Geologists Bulletin*, v. 40, pp. 17-50.
- Weller, J.M., 1957. Palaeoecology of the Pennsylvanian period in Illinois and adjacent states. *In* H.S. Ladd (editor), *Treatise on Marine Ecology and Palaeoecology*, Geological Society of America, Memoir 67, v. 2, pp. 325-364.
- Weller, J.M., 1964. Development of the concept and interpretation of cyclic sedimentation. *In* D.F. Merriam (editor), *Symposium on Cyclic Sedimentation*, Kansas Geological Survey, Bulletin 169, pp. 607-621.
- Westoll, T.S., 1968. Sedimentary rhythms in coal-bearing strata. *In* D. Murchison and T.S. Westoll (editors), *Coal and Coal-bearing Strata*, American Elsevier, New York, pp. 71-103.
- White, D., 1914. Resins in Palaeozoic plants and coals of high rank. U.S. Geological Survey Professional Paper 85-E, pp. 65-83.
- White, D., 1933. Role of water condition in the formation and differentiation of common (banded) coals. *Economic Geology*, v. 28, pp. 556-570.
- White, J.C. and Birk, D., 1989. The influence of sandstone channels on coals from the Sydney Basin: Mineralogy, chemistry, petrography, rheology and thermal characteristics. ACI-88-268 unpublished report for Cape Breton Development Corporation and Department of Energy, Mines and Resources.
- Wightman, W.G., Scott, D.B. and Gibling, M.R., 1992. Upper Pennsylvanian agglutinated foraminifers from the Cape Breton Coalfield, Nova Scotia: Their use in the determination of brackish-marine depositional environments. *Abstract In Geological Association of Canada-Mineralogical Association of Canada, Joint Annual Meeting*, Wolfville, Nova Scotia, p. A117.
- Williams, E.G. and Keith, M.L., 1963. Relationship between sulphur in coals and the occurrence of marine roof beds. *Economic Geology*, v. 58, pp. 720-729.
- Woodroffe, C.D., Thom, B.G. and Chappell, J., 1985. Development of widespread mangrove swamps in mid-Holocene times in northern Australia. *Nature*, v. 317, n. 24, pp. 711-713.

- Zangerl, R. and Richardson, E.S.Jr., 1963. The paleoecological history of two Pennsylvanian black shales. Chicago Natural History Museum, Fieldiana, Geological Memoirs, v. 4, 352 p.
- Ziegler, A.M., 1981. Paleozoic paleogeography. In M.W. McElhinny and D.A. Valencio (editors), Paleoenvironment of the continents, Geodynamics Series, v. 2, pp 31-37.
- Zodrow, E.L. and Cleal, C.J., 1985. Phyto- and chronostratigraphical correlations between the Late Pennsylvanian Morien Group (Sydney, Nova Scotia) and the Silesian Pennant Measures (South Wales). Canadian Journal of Earth Sciences, v. 22, n. 10, pp. 1465-1473.
- Zodrow, E.L. and McCandlish, K., 1978. Distribution of Linopteris obliqua in the Sydney coalfield of Cape Breton, Nova Scotia. Palaeontographica, v. 16, pp. 17-22.
- Zodrow, E.L. and McCandlish, K., 1980. Upper Carboniferous fossil flora of Nova Scotia. Nova Scotia Museum collections, Halifax, 275 p.

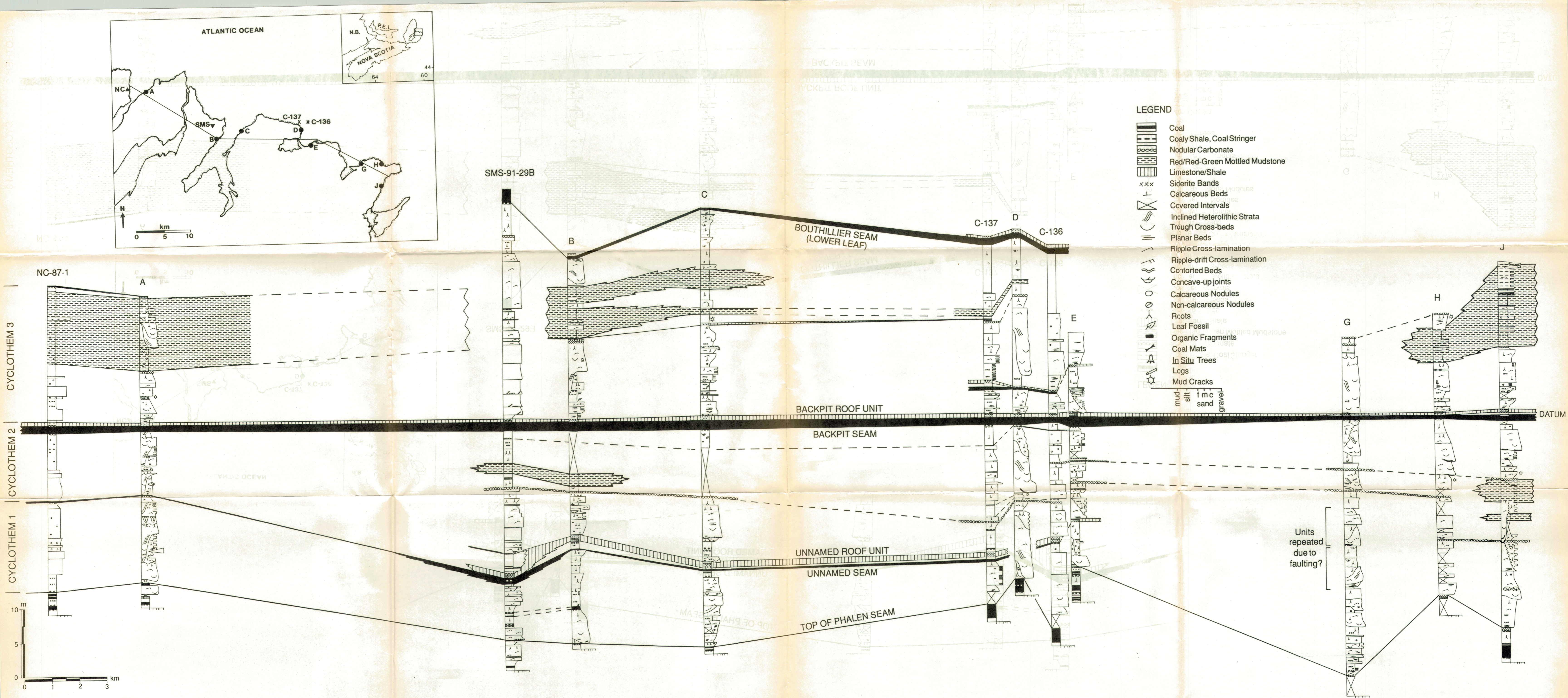


Figure 2.1. Detailed cross-section of coastal sections and core.